JAERI-Review
2003-023

NUCLEAR ENERGY SYSTEM DEPARTMENT ANNUAL REPORT
(APRIL 1, 2002-MARCH 31, 2003)

September 2003

Department of Nuclear Energy System

日本原子力研究所
Japan Atomic Energy Research Institute

本レポートは，日本原子力研究所が不定期に公刊している研究報告書です。
入手の問合わせは，日本原子力研究所研究情報部研究情報課（〒319-1195 茨城県那珂郡東海村）あて，お申し越しください。なお，このほかに財団法人原子力弘済会資料センター（〒319-1195 茨城県那珂郡東海村日本原子力研究所内）で複写による実費頒布をおこなっております。

This report is issued irregularly.
Inquiries about availability of the reports should be addressed to Research Information Division, Department of Intellectual Resources, Japan Atomic Energy Research Institute, Tokai-mura, Naka-gun, Ibarakiken 319-1195, Japan.

編集兼発行　日本原子力研究所

Nuclear Energy System Department Annual Report

(April 1, 2002 – March 31, 2003)

Department of Nuclear Energy System

Tokai Research Establishment
Japan Atomic Energy Research Institute
Tokai-mura, Naka-gun, Ibaraki-ken

(Received July 18,2003)

This report summarizes the research and development activities in the Department of Nuclear Energy System during the fiscal year of 2002 (April 1, 2002 – March 31, 2003).

The Department has carried out researches and developments (R&Ds) of innovative nuclear energy system and their related fundamental technologies to ensure the long-term energy supply in Japan. The report deals with the R&Ds of an innovative water reactor, called Reduced-Moderation Water Reactor (RMWR), which has the capability of multiple recycling and breeding of plutonium using light water reactor technologies. In addition, as basic studies and fundamental researches of nuclear energy system in general, described are intensive researches in the fields of reactor physics, thermal-hydraulics, nuclear data, nuclear fuels, and materials. These activities are essential not only for the R&Ds of innovative nuclear energy systems but also for the improvement of safety and reliability of current nuclear energy systems. The maintenance and operation of reactor engineering facilities belonging to the Department support experimental activities.

The activities of the research committees to which the Department takes a role of secretariat are also summarized.

Keywords: Nuclear Energy System Department, Annual Report, Innovative Nuclear Energy System, RMWR, Reactor Physics, Thermal-hydraulics, Nuclear Data, Nuclear Fuels, Materials

---

平成14年度エネルギーシステム研究部年報

日本原子力研究所東海研究所
エネルギーシステム研究部

(2003年7月18日受理)

本報告書は、平成14年度におけるエネルギーシステム研究部の研究・開発状況を纏めたものである。

エネルギーシステム研究部では、我が国におけるエネルギーの長期安定供給を確保するため、革新的原子力エネルギーシステム及び関連する基盤技術の研究・開発を実施している。軽水炉技術に立脚しながら、プルトニウムの有効利用の可能な革新的水冷却炉（低減速軽水炉）の研究・開発の現状を報告する。また、本報告書には、原子力エネルギーシステムの基礎基盤として重要な炉物理、熱流動、核データ、燃料、材料等の研究活動も掲載されている。これらの基礎基盤研究は、革新的原子力システムの開発や現行システムの安全性・信頼性の向上に不可欠なものである。炉工学施設の維持・管理は、実験的研究を支えるものである。

本報告では、エネルギーシステム研究部が運営を担当する研究委員会の活動状況も取り纏められている。

東海研究所：〒319-1195　茨城県那珂郡東海村白方白根2-4

Contents

Preface

The research activities of the Department of Nuclear Energy System, Japan Atomic Energy Research Institute, during the fiscal year (FY) 2002 (April 1, 2002 – March 31, 2003) are presented in this report. The Department is expected to develop an innovative nuclear energy system and to establish the related fundamental technologies for the system. The researches and developments (R&Ds) were carried out of reduced-moderation water reactor as well as fundamental researches in the fields of reactor physics, thermal-hydraulics, material science, advanced fuel and nuclear data.

The total number of permanent staff working in the Department as of March 31, 2003 was 106 including the clerical service staff. The Department was funded from JAERI expenditure amounting to 1,607 million yen for FY 2002, excluding nuclear fuel cost and personnel expense. About 1,174 million yen was provided by the research contracts with external organizations: Ministry of Education, Culture, Sports, Science and Technology (MEXT) for development of a key technology for innovative small reactors, development of active non-destructive assay technique by photon interrogation for uranium bearing waste and development of fuel assembly for very high burn-up water-cooled breeding reactor; Ministry of Economy, Trade and Industry (METI) for research on management technologies for corrosive equipment materials; Japan Nuclear Cycle Development Institute (JNC) for improvement of evaluated nuclear data for FP nuclides; the University of Tokyo for research on interactions between core materials and super-critical water under heavy irradiation; the Institute of Applied Energy (IAE) for R&D on reduced-moderation water reactor with passive safety features; the Institute of Research and Innovation (IRI) for research on IASCC data preparation for maintenance rule of aging BWR plants; Japan Power Engineering and Inspection Corporation (JAPEIC), Tokyo Electric Power Company, Inc. (TEPCO) and Tohoku Electric Power Company, Inc. for investigations on cracking incidents of the BWR core shroud and primary loop recirculation piping; Mitsubishi Research Institute, Inc. (MRI) for development of new cladding materials for advanced MOX fuels; Japan Nuclear Fuel Limited (JNFL) for research on corrosion behavior of reprocessing materials under heat flux control; Central Research Institute of Electric Power Industry (CRIEPI) for development of nuclear characteristics evaluation technique for reflector-controlled reactor cores.

The research activities have been conducted in nine research groups with the support of one division.

Research Group for Energy System Assessment

In the assessment of nuclear energy systems, studies were made on the technical possibility of multiple plutonium recycling with conventional light water reactors, and on future scenarios of spent fuel reprocessing in Japan. In the study on the role of nuclear energy, an analysis was made on Japan's long-term energy demand and supply scenarios as a part of the comprehensive study on nuclear energy vision in 2050 being promoted by the Japan Atomic Energy Industry Forum.

Research Group for Advanced Reactor System

Main research activities of the group are R&Ds for reduced-moderation water reactor (RMWR), which include reactor core and fuel design, nuclear and thermal-hydraulic analysis, analysis of MOX-fuel irradiation behavior, and safety analysis. The present efforts are focused on establishing the concept of a test reactor to demonstrate the key technologies and performance of RMWR.

Research Group of Small Reactor for Dispersive Energy Supply System

Small reactor concepts for dispersive energy supply have been studied aiming at increasing utilization of nuclear energy in an untapped field besides the large-scale nuclear power plant for electricity generation, such as for small grid electricity supply and district heating, by taking over the results of the nuclear ship research activities. Reactor cores with a thermal power of 300 or 100 MW are designed for a long life cycle of operation –5 years– until refueling. A concept of reactor siting in a pit filled with water at seaside has been studied. An in-vessel type control drive mechanism, a key technology for the reactor, has been developed.

Research Group for Reactor Physics

Research field of this group covers very wide range of fundamental studies on reactor physics. Main areas are development of calculation code systems, reactor physics experiments using critical assemblies FCA and TCA and non-destructive assay of TRU content in radioactive waste package. The code development work has been continued for high speed and high accuracy Monte Carlo codes and nodal codes to construct a comprehensive code system for reactor core design including thermal-hydraulics, core management and kinetics. The experimental studies have been concentrated on the

reduced-moderation water reactors and accelerator-driven sub-critical systems.

Research Group for Thermal and Fluid Engineering

The thermal hydraulic behaviors such as critical heat flux (CHF), pressure drop, and void fraction were investigated for the design of the reduced moderation water reactor. CHF experiments in a double humped tight-lattice rod bundle were performed using a 7-rod bundle test apparatus. A 37-rod bundle test apparatus was constructed in order to investigate the scale effect on CHF. Numerical simulations of two-phase flow were also performed to understand the boiling transition phenomenon in a fuel assembly mechanically.

Research Group for Reactor Structural Materials

This research group carries out the study of irradiation assisted stress corrosion cracking (IASCC) and development of material performance database. The group has aimed at clarifying the IASCC mechanism in in-core structural materials like stainless steels, at developing the method of evaluation and prediction of IASCC behavior, and at developing the countermeasures to IASCC. The group has also aimed at constructing the material database networking system. In addition, the failure analysis of reactor materials is another important mission of the group.

Research Group for Compatible Materials

The development program for pressure boundary materials applied to the advanced nuclear equipment has been carried out. One is a MOX fuel cladding material used in the advanced LWRs that are aiming at the ultra-high burn-up (>100GWd/t), the high Pu conversion ratio and super critical water control. The other is the new structural material with the high corrosion resistance against nitric acid solutions in reprocessing equipment. The overall development program is composed of the basic study on degradation mechanisms, development of new materials, fundamental experiments for establishing data base system and mock-up tests of miniaturized structure components for evaluating the reliability to the practical application.

Research Group for Advanced Fuel

Activities of the research group are focused on R&D on advanced fuels containing transuranium elements, which could contribute to realize flexible fuel cycle systems in future.

Rock-like oxide fuel has been developed for burning excess plutonium by use of existing LWRs, followed by direct disposal of spent fuel as a short-term subject. As a long-term subject, nitride and metallic fuels have been developed for transmutation of long-lived minor actinides and fast reactors, being coupled with pyrochemical reprocessing based on molten salt electrorefining.

Nuclear Data Center

Research activities for nuclear data evaluations are devoted to the developments of JENDL (Japanese Evaluated Nuclear Data Libraries, including Special Purpose Files as well as General Purpose File) needed in nuclear energy applications, radiation applications, medical applications, and/or fundamental researches. The latest version of JENDL-3.3 has been released and an associated CD-ROM was also published in FY2002. It contains 337-nuclide data for general use. The data are on WEB site at JAERI Nuclear Data Center (http://wwwndc.tokai.jaeri.go.jp). Now, efforts are focused on JENDL-4 developments. We also released a special purpose file (α,n) reaction data file requested from back-end applications.

Our center acts as a National Data Center by disseminating the nuclear data to Japanese customers, contacting foreign or international centers to exchange the nuclear data information, and coordinating international collaborations to enhance R&Ds of nuclear data. To coordinate the development of JENDL, this center also acts as a secretariat of Japanese Nuclear Data Committee (JNDC).

Reactor Engineering Facility Operation Division

This division operated three large-scale engineering facilities; FCA, TCA and Heat Transfer Fluid Flow Test Facilities in accordance with each experimental program and maintained them in the monthly or the annual inspection. Consequently safety operations of these facilities were achieved and the division contributed sufficiently to the execution of each experimental study. Furthermore, the maintenance work and decommissioning for VHTRC were carried out.

The Department is also involved in the following project-oriented program in JAERI:

Design Studies of Advanced Reactors.

The activities of the Department in FY 2002 have contributed to the essential progress in the field of engineering.

Takamichi IWAMURA
Director
Department of Nuclear Energy System
July 1st, 2003

1. Energy System Analysis and Assessment

Development of analytical tools and application studies have been made in order to analyze the role of nuclear energy in Japan's future energy systems and to make assessment of innovative nuclear technologies and systems from such viewpoints as reducing uranium resource utilization, improving economics, or decreasing environment risks. Major activities during the fiscal year 2002 are summarized below.

In the development of analytical tools, a nuclear fuel cycle simulation model NUSCOPE was developed in order to make a detailed study on long-term nuclear fuel cycle systems of Japan. NUSCOPE is almost equivalent with JALTES-II in the formulation of fuel material balances. But, it incorporates explicitly spent fuel reprocessing processes. In addition, it has a simple table of nuclear decay scheme, and reduction of fissile plutonium is evaluated by calculating the decay of Pu-241 when plutonium is outside reactors. With these additional capabilities, it provides precise balances of fissile plutonium demand and supply even when interim storage of spent fuel is included in fuel cycle scenarios.

In the study on power reactors and nuclear fuel cycle systems, analysis was made on the technical possibility of multiple plutonium recycling with conventional light water rectors, and on future scenarios of spent fuel reprocessing in Japan. In the former, the effect of blending UO_2 and MOX fuel was analyzed for PWRs or BWRs using MOX fuel in their entire reactor core. The results indicated that plutonium recycling is not possible at all either when fuel burn-up is 70GWd/t or minor actinides (MA) is recycled together with plutonium. The results also indicated that possible recycling times are larger in PWRs than in BWRs, and up to 4 times-recycling can be made when blending ratio of MOX and UO2 is 1:9, and fuel burn-up is 55GWe.

In the study on energy systems, analysis was made on preliminary scenarios of Japan's long-term energy demand and supply as a part of the comprehensive study on nuclear energy vision in 2050 being promoted by the Japan Atomic Energy Industry Forum. Four scenarios with different nuclear energy utilization and CO_2 emission reduction targets were defined for each of high and low energy demand cases. Energy demand and supply, and costs of energy supply systems were compared among these scenarios. Based on the results of this preliminary analysis, the assumptions are now being examined in order to develop refined scenarios of energy demand and supply.

1.1 Development of a Nuclear Fuel Cycle Simulation Model NUSCOPE

K. Tatematsu and O. Sato
(*E-mail* : ktate@ruby.tokai.jaeri.go.jp)

Analytical studies on Japan's long-term nuclear fuel cycle systems have so far been made in this laboratory by using JALTES-II. JALTES-II, a linear optimization model, is convenient in determining optimum capacity mix of future nuclear power systems. But, it has disadvantages in simulating fuel cycle systems. It assumes that all spent fuel is reprocessed after a certain cooling time without respect to reprocessing capacity. It has no consideration on the decay of Pu-241 when plutonium is outside reactors. These are serious drawbacks particularly when we analyze back-end systems of fuel cycle. Therefore, a new model, NUSCOPE, was developed for the detailed simulation analysis on fuel cycle systems.

The NUSCOPE model is almost equivalent with JALTES-II in the formulation of fuel material balances. But, it incorporates explicitly spent fuel reprocessing processes. In addition, it has a simple table of nuclear decay scheme, and reduction of fissile plutonium is evaluated by calculating the decay of Pu-241 when plutonium is outside reactors. With these additional capabilities, it provides precise balances of fissile plutonium demand and supply even when interim storage of spent fuel is included in fuel cycle scenarios.

Actual reprocessing facilities will be uniquely designed based on the characteristics of spent fuel to be treated such as average discharge burn-up or plutonium contents. The NUSCOPE model can incorporate an arbitrary number of reprocessing process depending on the configuration of nuclear fuel cycle systems given by users. A specific reprocessing process might be allocated either to each reactor type, or to a group of reactor types, or to a group of fuel types. Therefore, users must define linkage between reactor types (or fuel types) and reprocessing processes. In addition, linkage must also be defined between reprocessing processes (as producers of plutonium) and reactor types that consume plutonium. An example of such linkage is shown in Fig.1.1.1.

Spent fuel discharged from each reactor type/fuel type is sent to temporary storage of a reprocessing process specified for it. It is noted that each reprocessing process can accept spent fuel from more than one reactor types/fuel types, but spent fuel from a reactor type/fuel type can only be sent to one specified reprocessing process. In temporary storage all vintage information of spent fuel is lost, and the only information managed is the amount of uranium and plutonium isotopes ready for reprocessing.

There are two optional operation modes of reprocessing processes, full capacity operation and demand-based operation. When users select full capacity operation, each

reprocessing process is operated either at its full capacity, or at the capacity determined by the stock of spent fuel if it is not sufficient for full capacity, and plutonium is recovered regardless of its demand. When users select demand-based operation, operation levels of reprocessing processes are subject to the capacity of reactor types using plutonium and priorities in allocating plutonium for each reactor types as described below.

Each reactor type which utilizes plutonium has its own priority among reactor types in using plutonium. Also, priority is defined for each of reprocessing processes that provide plutonium to a specific reactor type. Once the installed capacity of reactor types is determined, demand for plutonium is calculated following the above priorities. If the selection of model users is full capacity operation, balances of plutonium are calculated. If it is demand-based operation, activity of each reprocessing process is determined considering both the demand for plutonium and the stock of spent fuel.

The NUSCOPE model can be used on the Microsoft Windows, and with a user support system of a GUI type, a series of operation including data input, execution of simulation, graphical representation of results are possible.

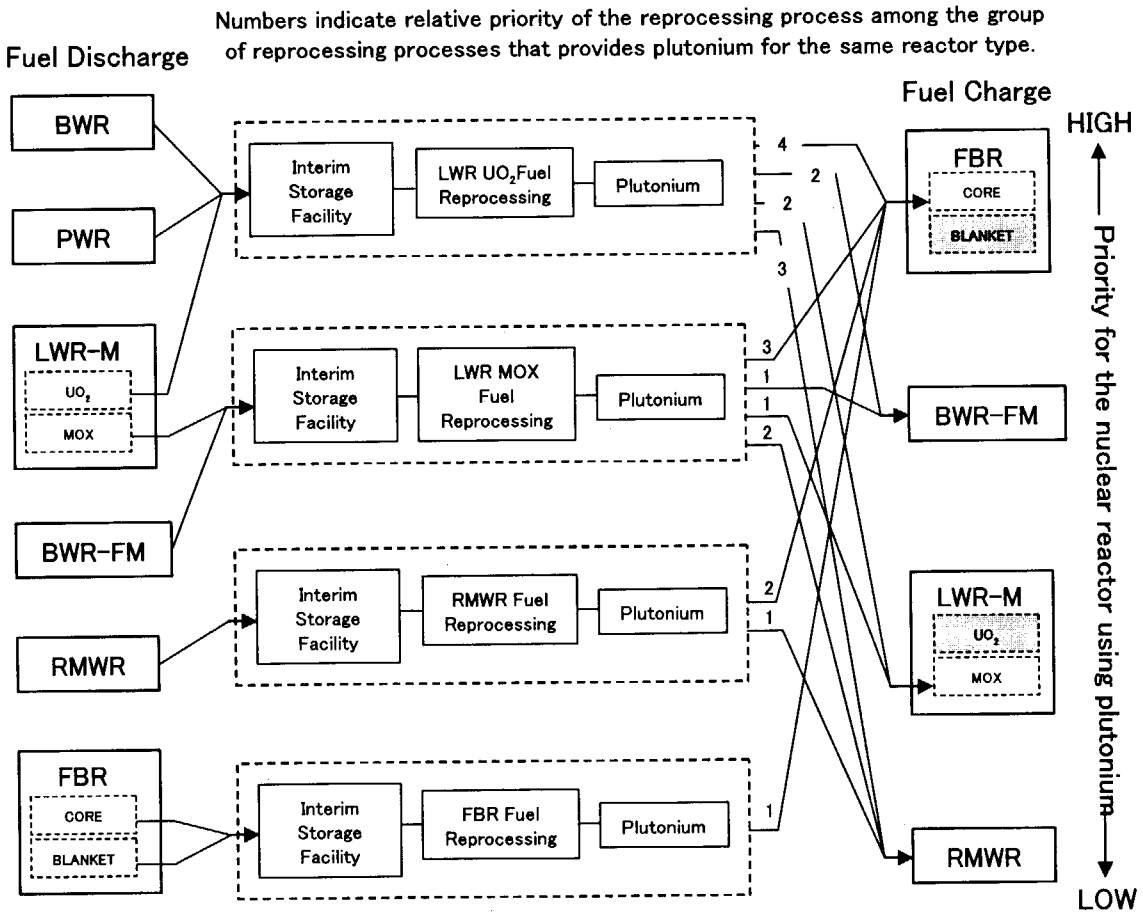

Fig. 1.1.1 Fuel material flow chart (Example)

1.2 A Study on Multiple Plutonium Recycling and Future Scenarios of Reprocessing

K. Otaki and O. Sato
(*E-mail*: k_ootaki@ruby.tokai.jaeri.go.jp)

Multiple Plutonium Recycling in LWRs

It is well known that plutonium recycling in LWRs has a certain limit of recycling times because of increasing buildup of higher plutonium isotopes. But if plutonium recovered from MOX fuel is blended with that from UO2 fuel, the reduction of fissile plutonium ratio will be controlled, and thus the limit of recycling times might be alleviated.

In this study, the effect of blending was analyzed for PWRs or BWRs using MOX fuel in their entire reactor core. For each step of recycling burn-up calculations were made by using the SRAC code with a pin-cell model, and isotopic composition, average enrichment of plutonium, and void reactivity coefficients were evaluated. Keeping negative values of the coefficient is a necessary condition for the feasibility of recycling. It was assumed that spent fuel will be reprocessed with a cooling time of one year, and recovered plutonium will be charged to reactors after one year for fabrication.

The analytical cases and the results are summarized in Table 1.2.1. As shown in the results of PWRs, plutonium recycling is not possible at all either when fuel burn-up is 70GWd/t or minor actinides (MA) is recycled together with plutonium. The results also indicated that possible recycling times are larger in PWRs than in BWRs, and up to 4 times recycling can be made when blending ratio of MOX and UO2 is 1:9, and fuel burn-up is 55GWe.

In addition, it was also confirmed by simplified calculations that, if plutonium is loaded into only one third of reactor core, void reactivity coefficients can be kept negative in all the above cases where plutonium recycling was judged impossible.

Table 1.2.1 Analytical cases and results

Case	Reactor Type	Blending Ratio MOX:UO2	Max. Burn-up (GWd/t)	Recycling of MA	Possible Recycling Times
1	PWR	1:4	55	No	2
2		1:9			4
3		1:4		Yes	0
4		1:9			0
5		1:4	70	No	0
6		1:9			0
7		1:4		Yes	0
8		1:9			0
9	BWR	1:4	55	No	1
10		1:9			2

Future Scenarios of Reprocessing

The first commercial reprocessing facility in Rokkasho-mura is planned to start its operation in 2005. This will open the era of plutonium recycling in Japan, however, currently there is no plan for reprocessing facilities thereafter.

In this study future scenarios of spent fuel reprocessing, particularly the scale and configuration of the second reprocessing facility, were analyzed based on the estimates of annual spent fuel discharge in different strategies of nuclear power development by considering technical requirements in the reprocessing of spent MOX fuel.

Reactor types considered in this study are LWRs, partially MOX fueled LWRs (P-MOX), fully MOX fueled LWRs (F-MOX), RMWRs, and FBRs. It was assumed that the lifetime of the Rokkasho facility is 40 years, and the second reprocessing facility to be introduced after decommissioning of the Rokkasho facility employs the Purex process.

As a result of the analysis on the reprocessing of spent MOX fuel from LWRs, it was found that the Rokkasho facility requires some modification in order to accept spent MOX fuel in addition to UO2 fuel. This is because that spent MOX fuel has higher fissile plutonium contents, more neutron emissions, and larger decay heat than UO2.

In the analysis on the reprocessing scenario for the case where RMWRs with a conversion ratio 1.06 are introduced from the year 2020, installed capacity of nuclear power stations with different reactor types was projected as shown in the top of Fig. 1.2.1.

If the second reprocessing facility is assumed to accept all types of spent fuel, its necessary scale will be 1600 ton/y as shown in the bottom of Fig. 1.2.1. However, this assumption is not economically realistic since the whole facility should be designed to meet most serious conditions among different types of spent fuel, and therefore construction costs will be quite large.

The better option will be to introduce two separate facilities, 1400 ton/y for UO2 fuel and 600 ton/y for MOX fuel. These sum up 2000 ton/y as indicated with a thick solid line in the figure. Considering that the two facilities will not operate fully during their lifetime in this option, however, it might be further economically efficient option to install smaller facilities such as 1200 ton/y for UO2 and 400 ton/y for MOX, although the amount of plutonium recovered will be less and capacity buildup of RMWRs will be a little delayed.

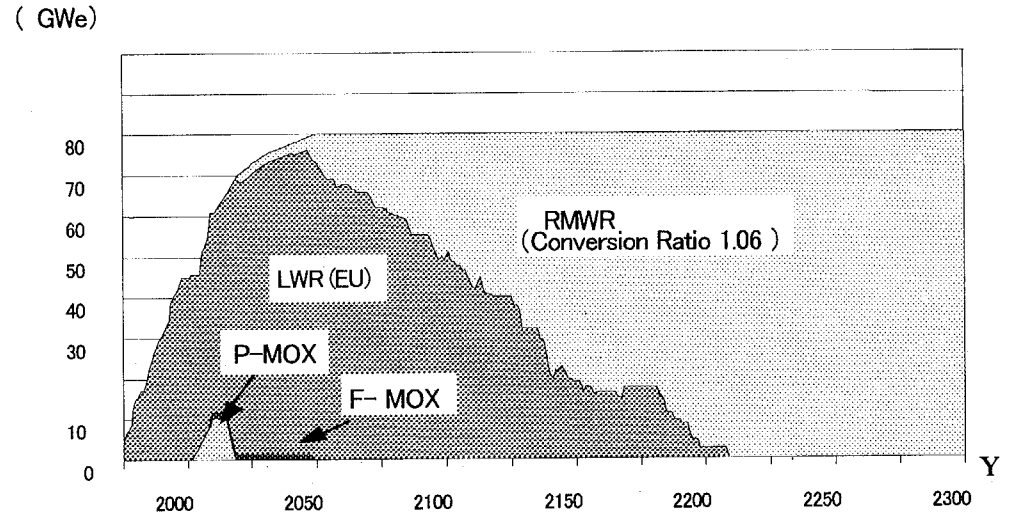

(a) Installed capacity of nuclear power plants with different reactor types

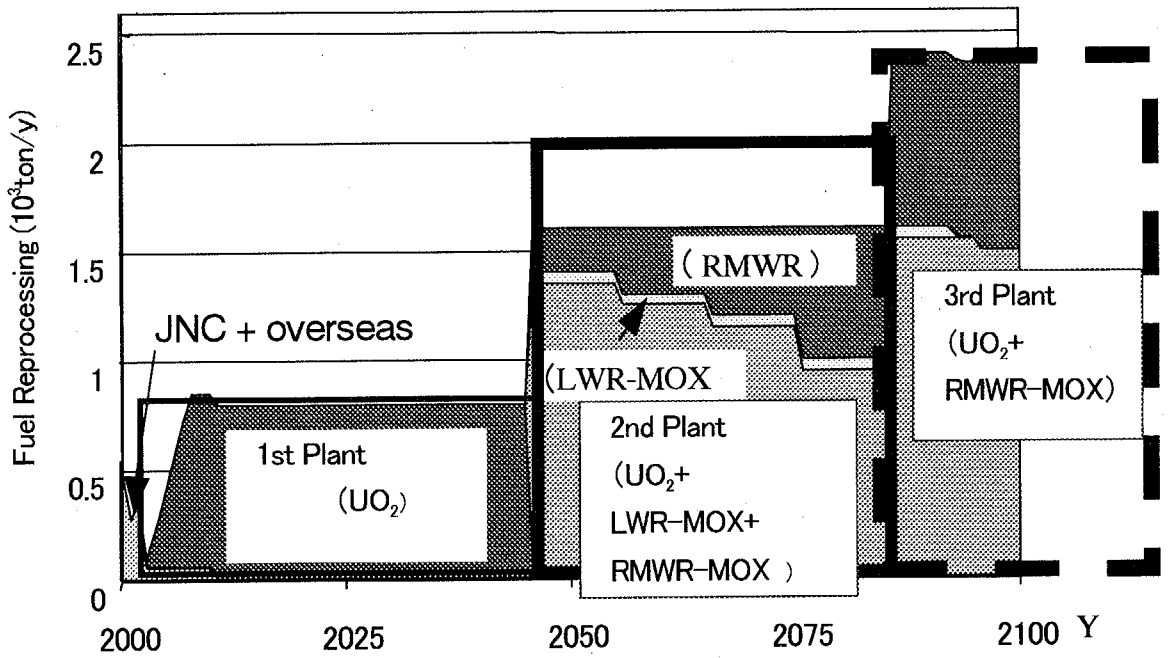

(b) Reprocessing scenario of spent fuel

Fig.1.2.1 Future reprocessing scenario for the case with RMWRs

1.3 Long-term Energy Scenarios and the Role of Nuclear Energy

O. Sato
(*E-mail*: sato@ruby.tokai.jaeri.go.jp)

A study is being made in a committee of the Japan Atomic Energy Forum on Japan's long-term prospects of nuclear energy utilization and on future strategies of research, development, and utilization. In order to inform this committee a set of analyses was made on the energy demand and supply through the year 2050, and on the role of nuclear energy.

During the year 2002, several preliminary scenarios were developed by using the MARKAL model. The procedures are as follows. First, future demand for energy services was projected. Combining high and low estimation on both GDP and population, two demand cases were defined as shown in Fig. 1.3.1. Then, energy demand and supply scenarios were developed for the four cases with different assumptions on nuclear energy utilization and CO_2 emission constraints as listed in Table 1.3.1. It is noted that CO_2 emissions can be reduced blow 1990 levels in all the scenarios, so that emission constraint 0 in the table implies actually no constraint on emissions.

The preliminary scenarios are compared in Fig. 1.3.2 to Fig.1.3.5. In primary energy supply, dependence on oil decreases substantially in 2050 in all the scenarios. But, alternative energy depends on the scenarios. In scenario A0 with no emission constraint and nuclear energy limited steam coal is used most. In scenario A1 with strict emission control and nuclear energy limited natural gas becomes a most important energy source. While, in scenarios B0 and B1 where nuclear energy is expanded, the share of nuclear energy is around 40% in 2050.

Nuclear energy contributes substantially to electric power generation as shown in Fig. 1.3.3. In scenarios B0 and B1, it generates more than 60% of electricity in 2050. Even in scenarios A0 and A1 with nuclear energy limited, its share is around 40% in a high demand case. The role of other energy sources is not more than a complimentary one. Renewable energy contributes about 30% of total generation only in scenario A1 where optimistic assumptions were made on the use of renewable energy in order to meet strict emission reduction targets.

In final energy, hydrogen becomes an important energy carrier contributing about 10% of total in 2050. Hydrogen is produced mainly by steam reforming of natural gas. Heat of this reaction is provided either from the combustion of natural gas (A0 and A1) or from nuclear energy (B0 and B1).

Finally, annual costs are compared in Fig. 1.3.5. In the scenario A1, the total cost becomes quite large in a high demand case in order to achieve emission targets by using expensive renewable technologies and a CO_2 disposal option. The difference between A1 and B1 is as large as about 5 trillion yen. However, in a low demand case the difference becomes much smaller.

Based on the results of this preliminary analysis, the assumptions are being examined in order to refine energy demand and supply scenarios.

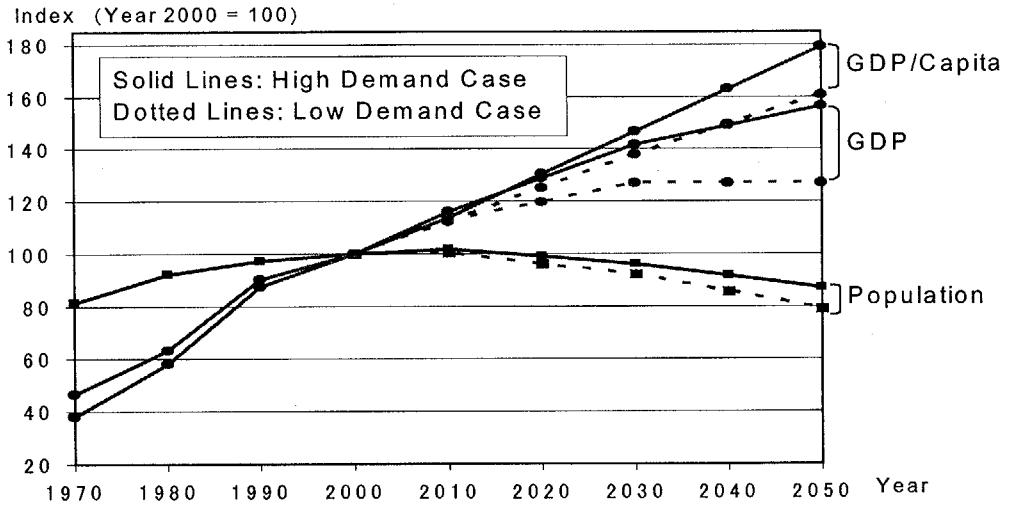

Fig. 1.3.1 Assumptions on population and GDP growth

Table 1.3.1 Analytical cases

Nuclear Energy / CO_2 Emissions	A (Limited) Power Generation: 70GWe after 2020 Hydrogen: None	B (Expanded) Power Generation: 120GWe (High Demand) 100GWe (Low Demand) Hydrogen: Available from 2020 Depending on Demand
Constraint 0 (Stabilization at 1990 Levels)	A0	B0
Constraint 1 (2050 Emissions Limited to 50% of 2010 Levels)	A1	B1

Note 1. The above 4 scenarios are analyzed for the both high demand and low demand cases.
2. It was assumed that CO2 removal-disposal is possible in the scenario A1.
3. The amounts of nuclear capacity describe above are given as upper limits.

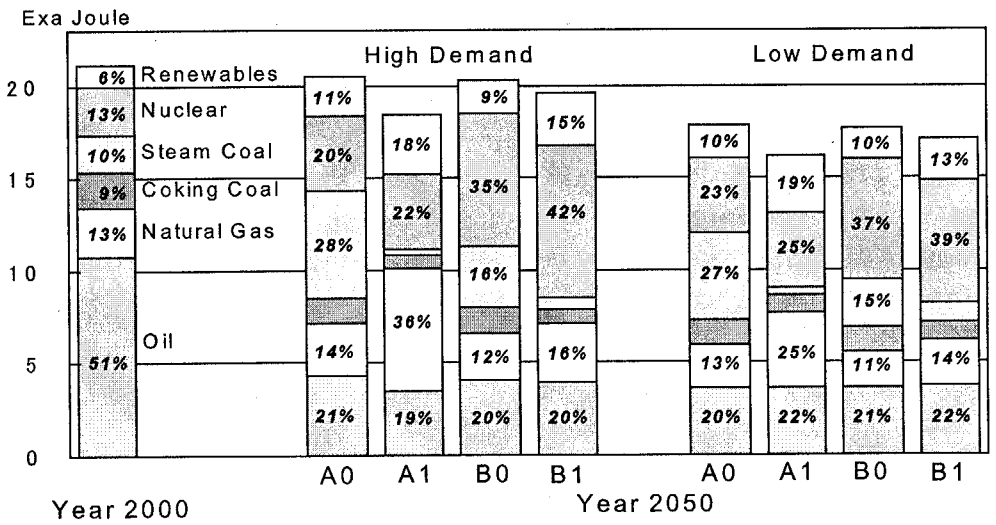

Fig. 1.3.2 Primary energy supply

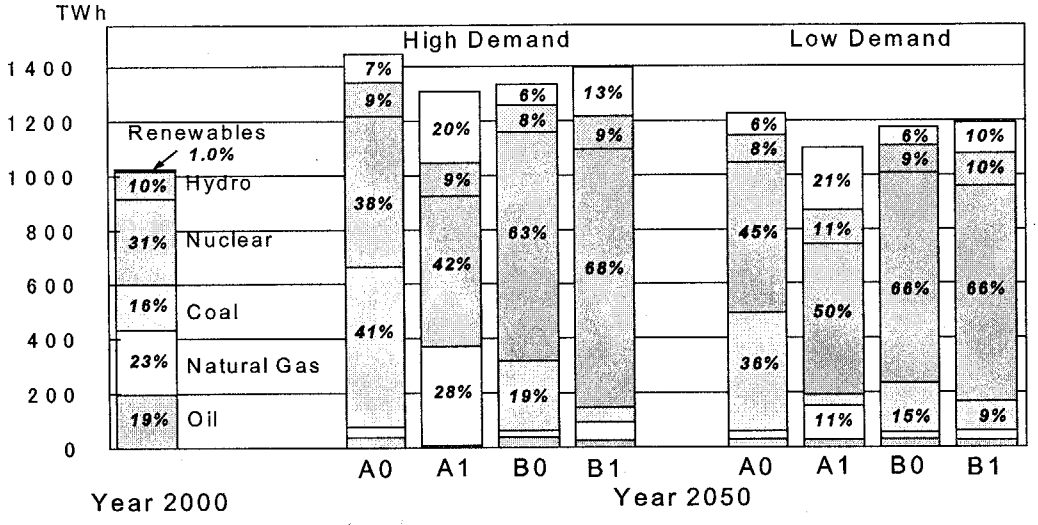

Fig. 1.3.3 Electric power generation

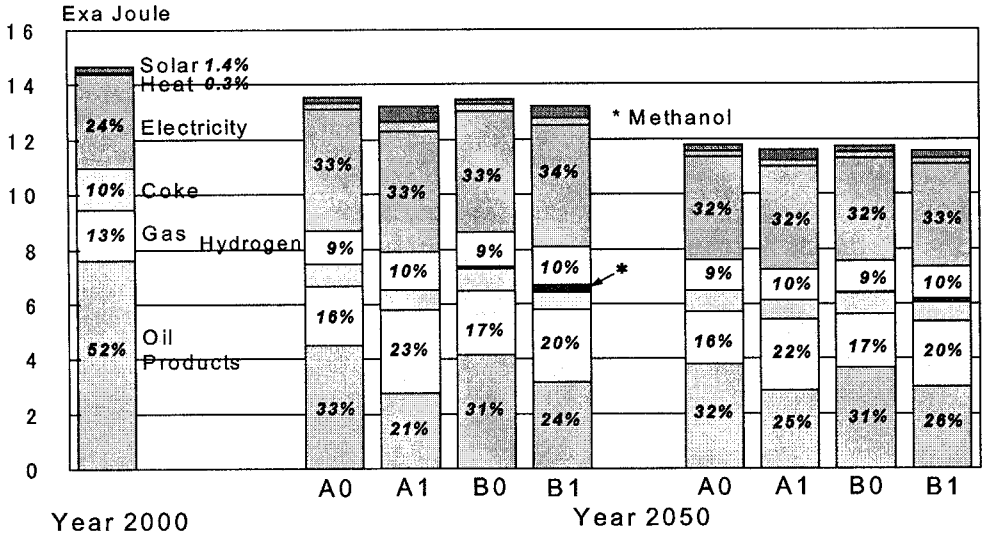

Fig. 1.3.4 Final energy consumption

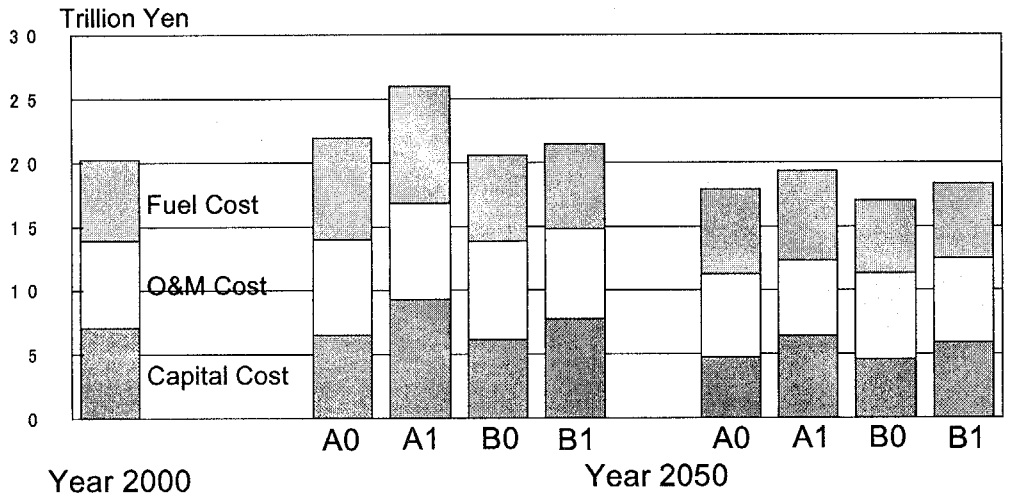

Fig. 1.3.5 Annual costs of energy supply

2. Advanced Reactor System Studies

The conceptual design study of Reduced-Moderation Water Reactor (RMWR) is being conducted. Design studies of three types of RMWR were performed. 1) *Large Scale BWR type RMWR*: The core average burn-up of 65GWd/t has been attained by optimization of the axial core configurations. 2) *Small scale RMWR*: A design study on 300MWe class RMWR has been carried out. Simplification of the system has been made to minimize the construction cost overcoming "the scale demerit". 3) *Demonstration reactor for RMWR*: Neutronic design calculation of RMWR core with thermal output of 180MW, which is intended to be a demonstration reactor, has been performed to find suitable design parameters. Attainable core performance has been clarified from the calculation results. Other topics related to the RMWRs are as followings: For the PWR-type RMWR with seed-blanket fuel assembly, the investigation on the use of metal fuel and thorium oxide fuel has been done and clarified the effect on the core performance. The channel, core and regional stabilities of the BWR type small size RMWR core under natural circulation condition were investigated. The sufficiently stable characteristics were confirmed. The recriticality accident for RMWR is studied by using MELCOR code and MVP code. Analysis results reveal that recriticality is not likely to occur at least before the debris bed is melted again. The thermal and mechanical analysis of MOX fuel rod of RMWR was performed with the MOX fuel performance analysis code FEMAXI-RM. The integrity of the fuel rod was confirmed by the analysis.

As the reactor relevant studies, the process inherent ultimate safety (PIUS) type heavy water fast reactor (ISFR) was proposed. Characteristics of ISFR was evaluated with THYDE-NEU code. The analysis of a BWR turbine trip benchmark problem was performed with the entire plant modeling by using THYDE-NEU code.

As another research area concerning to the development of anomaly detection system of nuclear power plants, the Artificial Neural Network On-line Monitoring (ANNOMA) system has been tested at the Borssele nuclear power plant in Netherlands. The test results showed the effectiveness of the developed system. A new methodology for constructing distributed computing system was proposed targeting the nuclear power plant monitoring systems.

2.1 Study on High Burn-up Core Design for High Conversion Ratio BWR Type RMWR Core

T.Okubo, R.Takeda*[1], T.Yamauchi*[2] and H.Okada*[3]
(*E-mail:* okubo@hems.jaeri.go.jp)

A detailed design study on the BWR type reduced-moderation water reactor (RMWR) with the high conversion ratio has been performed in order to attain higher core burn-up than in the reference design [1]. A schematic of the reference core design is shown in Fig. 2.1.1. This design concept has been established achieving the *Puf* conversion ratio of 1.05, the negative void reactivity coefficients and the core average discharge burn-up of 60GWd/t excluding the upper and the lower blanket regions. The total burn-up including the upper and the lower blanket regions is 45GWd/t. In the present study, increase in the burn-up was intended and the target values were set at 65 and 50GWd/t for the core and the total, respectively.

In the RMWR core design, the higher burn-up tends to increase the void reactivity coefficient, which has been known as what is called "the trade-off relation". Therefore, the length of the upper blanket is generally reduced to decrease the void coefficient. However, this, in turn, results in decrease in the conversion ratio. Then, it would be good to increase the internal blanket in order to compensate the conversion ratio. This also has the tendency to decrease the void coefficient and to increase the burn-up. Therefore, the promising basic design approach to increase the burn-up seems to increase the length of the internal blanket, and hence, this approach was adopted in the present study.

Also in the present study, the core characteristics under the equilibrium situation of multiple recycling of plutonium (Pu) have been investigated, assuming under the JAERI's simplified PUREX reprocessing scheme [2] with a little low decontamination factors (DFs) for fission products (FPs) and minor actinides (MAs). Also, the control rod operation was taken into account in the analyses. The procedures in the present analyses for the multiple recycling and the control rod operation are basically the same as these in the previous study performed last year [3].

*1 Hitachi, Ltd., *2 The Japan Atomic Power Company, *3 Tokyo Electric Power Company

As the results, the intended increases in the burn-up have been achieved as shown in Table 2.1.1, which summarizes the major core dimensions and characteristics under the equilibrium situation of Pu multiple recycling. In this high burn-up design, the length of the internal blanket is 400mm, in comparison with 295mm in the reference design. However, the *Puf* conversion ratio and the operation cycle length are decreased to 1.04 and 15 months from 1.05 and 24 months in the reference design, respectively. Although the length of the upper and lower blanket is almost the same as in the reference design, the length of the MOX is increased by about 10 % in this design. Therefore, the total height of the core including the upper and the lower blankets becomes 1,255mm in the present design, in comparison with 1,105mm in the reference design. Additionally, the fissile Pu content in the equilibrium situation of Pu multiple recycling is 58 % and the content of Pu-239 is 53 % in the present design.

References

1) T. Okubo, *et al.* : "3.1 Conceptual Designing of Reduced-Moderation Water Reactor (1) − Study on High Conversion Ratio BWR Type Core −", *Nuclear Energy System Department Annual Report (April 1, 2000 – March 31, 2001)*, JAERI-Review 2002-005, pp.46-48 (2002).

2) H. Mineo, *et al.* : "3.9 Study on Economical Reprocessing Process Relevant for RMWR", *Nuclear Energy System Department Annual Report (April 1, 2001 – March 31, 2002)*, JAERI-Review 2003-004, pp.69-71 (2003).

3) T. Okubo, *et al.* : "3.1 Study on High Conversion Ratio BWR Type RMWR Core", *Nuclear Energy System Department Annual Report (April 1, 2001 – March 31, 2002)*, JAERI-Review 2003-004, pp.45-47 (2003).

Table 2.1.1 Major dimensions and characteristics of core

Item		High burn-up	Reference
Electric power output	(MWe)	1,356	1,356
Discharge burn-up for core part	(GWd/t)	65	60
Core height	(m)	0.855	0.695
Core average void fraction	(%)	70	70
Core average fissile Pu content	(%)	9.6	10.4
Loaded fissile Pu	(t)	16.1	14.1
Fissile Pu conversion ratio	(−)	1.04	1.05
Void reactivity coefficient	($10^{-4}\Delta$k/k／%void)	-0.5	-0.5
Operation cycle length	(EFPM)	15	24
Core axial fissile Pu enrichment distribution		DU 220 mm 18 225 mm DU 400 mm 18 230 mm DU 180 mm	DU 220 mm 18 195 mm DU 295 mm 18 205 mm DU 190 mm

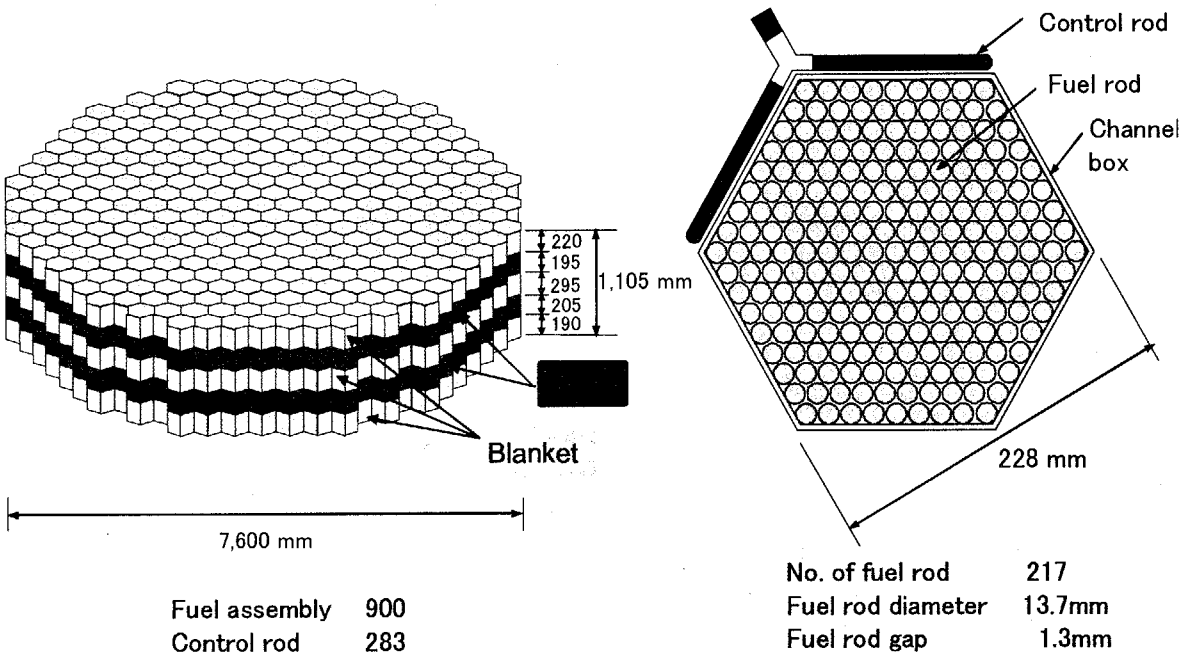

Fig. 2.1.1 Schematic of high conversion BWR type RMWR core and fuel assembly for reference design

2.2 Design Study on Small Scale RMWR

T.Okubo, R.Takeda*[1], K.Moriya*[1], T.Iwamura, T.Yamauchi*[2] and M.Aritomi*[3]
(*E-mail:* okubo@hems.jaeri.go.jp)

As the nuclear power generation, it is expected that light water reactors (LWR) will be utilized also in the future. However, for the sustainable nuclear energy supply, the multiple recycling of Pu is necessary. From this point of view, the Reduced-Moderation Water Reactor (RMWR) is under investigation in JAERI as a reactor concept to achieve the Pu multiple recycling based on the LWR technologies. On the other hand, reduction of the initial capital cost is necessary in the competition with other electric power generations, and studies on the small and/or medium size nuclear power plants have been performed. Therefore, as a reactor concept to answer these two needs, a design study on a 300MWe class small scale RMWR has been performed.

As the core design targets, the core can be cooled by the natural circulation and can achieve a conversion ratio over 1.0, a negative void reactivity coefficient, a core average burn-up over 60GWd/t and a cycle length of 2 years. The system is intended to be simplified as much as possible by introducing the passive safety components, in order to reduce the construction cost per electric power output overcoming "the scale demerit" for a small reactor comparing with the large one.

The BWR type high conversion ratio RMWR core, which is described in the previous section, is adopted to achieve the natural circulation core cooling. The core design is shown in Fig 2.2.1, and the major dimensions and characteristics of the core are summarized in Table 2.2.1. The design specifications under the equilibrium situation for the Pu multiple recycling have achieved the conversion ratio of 1.03, a negative void reactivity coefficient, a core average burn-up of 65GWd/t and a cycle length of 25 months. As the fuel reprocessing process, JAERI's simplified PUREX reprocessing scheme [1)] with a little low decontamination factors (DFs) for fission products (FPs) and minor actinides (MAs) is assumed.

As the system design concept, simplification of the system utilizing the passive safety components has been conducted in order to overcome "the scale demerit". From this point

*1 Hitachi, Ltd., *2 The Japan Atomic Power Company, *3 Tokyo Institute of Technology

of view, a hybrid safety system concept adequately combining the passive and the active components has been introduced as shown in Fig. 2.2.2 to minimize the construction cost. Also both in the reactor system and the turbine system, simplification of the system is performed. The results of the plant cost estimation show a 1.35 times higher construction unit cost per kWe than for the ABWR case, although the 0.6～0.75-th power scale law of the power ratio suggests 1.8 times higher value at the maximum. However, there are other cost reduction possibilities for the small scale reactors when the effects such as the mass production are taken into account, and this suggests the possibility of a lower construction unit cost than for the ABWR case.

The present study was supported by the governmental funding from the innovative and viable nuclear energy technology (IVNET) development project operated by the Institute of Applied Energy (IAE).

Reference

1) H. Mineo, *et al.* : "3.9 Study on Economical Reprocessing Process Relevant for RMWR", *Nuclear Energy System Department Annual Report (April 1, 2001 – March 31, 2002)*, JAERI-Review 2003-004, pp.69-71 (2003).

Table 2.2.1 Major dimensions and characteristics of core

Item	Unit	Design value
Electric power output	MWe	330
Core circumscribed radius	m	2.07
Core average burn-up	GWd/t	65
Core effective height	m	0.88
Core void fraction	%	70
Core pressure drop	MPa	0.04
Average Puf enrichment	%	9.8
Conversion ratio	—	1.03
Max. power density	kW/m	39
MCPR	—	1.3
Void reactivity coefficient	$10^{-4}\Delta$ k/k/%void	-0.5
Fuel cycle length	month	25

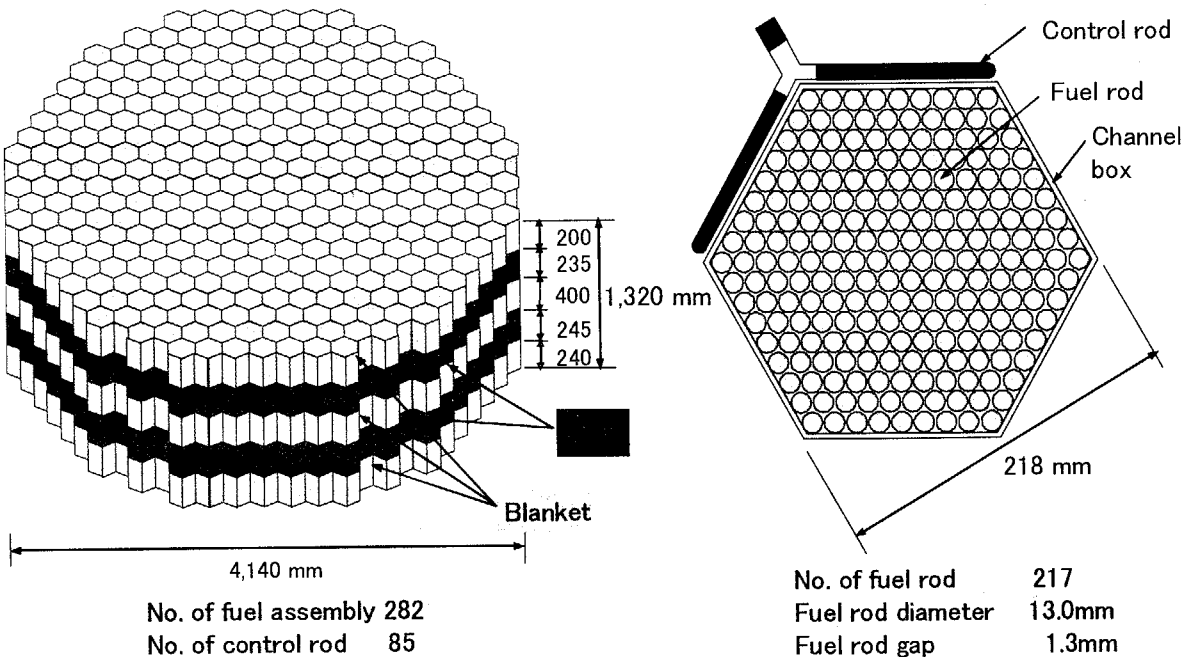

Fig. 2.2.1 Schematic of core and fuel assembly

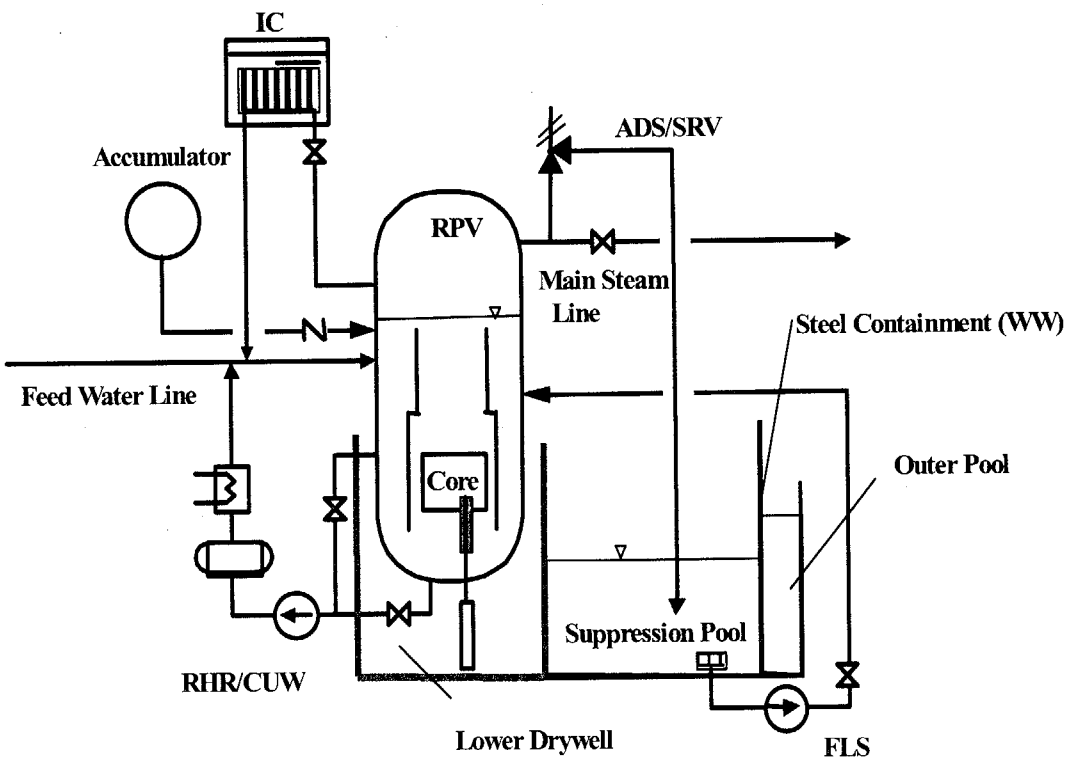

Fig. 2.2.2 Concept of hybrid safety system

2.3 Neutronic Design Study on a Demonstration Reactor for RMWR

Y. Nakano and T. Okubo
(*E-mail*: nakayosi@popsvr.tokai.jaeri.go.jp)

Neutronic calculations have been performed to find suitable design values of a RMWR core with thermal output of 180MW, which is intended to be a kind of test reactor. Figures. 2.3.1 and 2.3.2 are horizontal cross sections of the core and fuel assemblies. The core consists of 85 fuel assemblies and 36 radial reflector elements. The reflector is made of stainless steel and is used to remove moderator from the vicinity of peripheral fuel assemblies. The fuel rod axially consists of two MOX regions and three blanket regions as shown in Fig. 2.3.3. Channel boxes, fuel clad tubes and control rod follower tubes are made of stainless steel.

The SRAC code system[1] was used for the calculations. Many parametric survey calculations were done with changing plutonium enrichment, clad thickness, pellet diameter, fuel length, reactor operation cycle and so on.

Burnup dependent homogenized cross sections of the fuel assembly were generated with the PIJ routine, which is based on the collision probability method, and a cell burnup module in the SRAC. All fuel rods in the assembly were calculated at once with a hexagonal geometry and a 107-group neutron energy structure. A neutron cross section library based on JENDL-3.3[2] was used. Calculations were done on each material and void region of the assembly. An axial distribution of coolant void fraction used is also shown in Fig. 2.3.3.

Core burnup calculations were done with the COREBN diffusion calculation module in the SRAC. The core was modeled in R-Z geometry. The number of energy group was 14. The Out-In refueling method was used in the calculations. Void reactivity coefficients were evaluated from the difference in two reactivities between a nominal operation condition and a flow rate decreased condition, in which coolant density was 0.9 times of the nominal condition.

Major parameters and calculated results of typical cases are listed in Table 2.3.1. All cases meet two design targets. The first is a negative void reactivity and the other is a conversion ratio larger than unity. In the case 1, average discharge burnup of 65 GWd/t in the MOX region can be achieved with 3.5-batch refueling and 20-month cycle length.

References

1) K. Okumura, K. Kaneko and K. Tsuchihashi: "SRAC95; General Purpose Neutronics Code System", JAERI-Data/Code 96-015 (1996). (in Japanese)

2) K. Shibata, et al. : "Japanese Evaluated Nuclear Data Library Version 3 Revision-3: JENDL-3.3", J. Nucl. Sci. Technol., 39, 1125 (2002).

Table 2.3.1 Calculation parameters and results

Calculation Case		1	2	3
Thermal Power (MW)		180		
Assembly Number in Core		85		
Fuel Rod Number in Assembly		127		
Fissile Pu Enrichment in MOX (wt%)		18		
Fuel Rod Pitch (cm)		1.43		
Fuel Rod Diameter (cm)		1.3		
Clad thickness (cm)		0.055		
Pellet Diameter (cm)		1.16		
Internal Blanket Height (cm)		30	40	40
Cycle Length (month)		20	16	11
Refueling Batch Number (-)		3.5	3.5	7
Discharged Burnup (Gwd/t)	MOX Region	64.8	48.4	62.4
	Whole Assembly	26.0	19.0	24.9
Void Reactivity (dk/k/%void)	BOC	-7.0×10^{-5}	-1.9×10^{-4}	-1.1×10^{-4}
	EOC	-2.7×10^{-5}	-1.5×10^{-4}	-9.9×10^{-5}
Instantaneous Conversion Ratio	BOC	1.04	1.06	1.08
	EOC	1.06	1.09	1.09

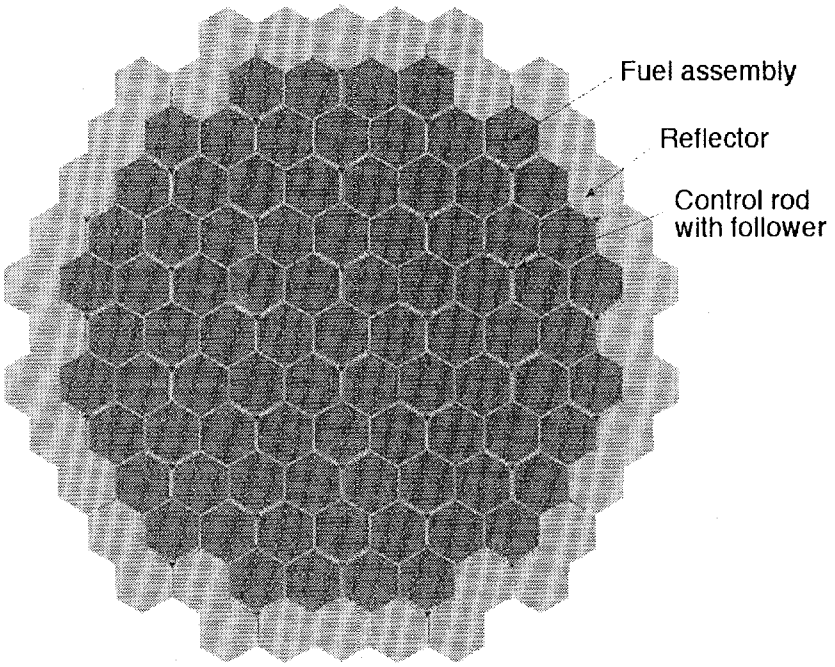

Fig. 2.3.1 Horizontal cross section of the core

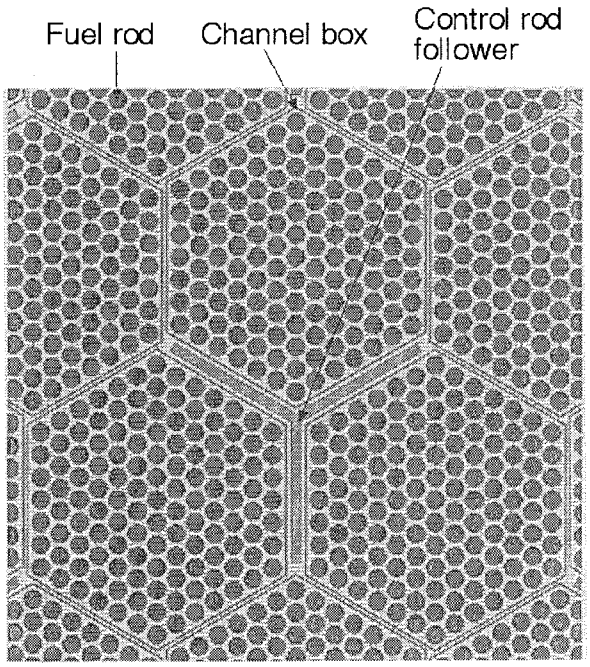

Fig. 2.3.2 Cross section of fuel assemblies and control rod follower

Height (cm)	Material	Void fraction (%)
35.0	Upper Blanket	87
27.0	Upper MOX	82
30.0 or 40.0	Internal Blanket	75
13.5	Lower MOX	65
13.5		42
10.0	Lower Blanket	6
20.0		0

Fig. 2.3.3 Vertical region height, material and coolant void fraction of fuel rod

2.4 Investigation on Effects of Metal Fuel and Thorium Based Oxide Fuel for RMWR Fuel Assembly

A. Shelley, S. Shimada[1], T. Kugo, T. Okubo and T. Iwamura
(*E-mail:* shelley@popsvr.tokai.jaeri.go.jp)

Parametric studies have been done by using metal (Pu+U+Zr) fuel and thorium based oxide fuel in a PWR-type reduced-moderation water reactor (RMWR) with the seed-blanket fuel assembly, to achieve a high conversion ratio, negative void reactivity coefficient and a high burnup. A fuel assembly with MOX as the seed and with UO_2 as the blanket is considered for the reference case[1)].

The height of the seed is considered to be 100cm x2, the axial blanket is 40cm x2 and the internal blanket is 15 cm as shown in Fig. 2.4.1 as the reference for parametric survey. The pitch for seed and blanket fuel rods is 1.3 cm, the rod diameter is 1.2 cm, and the pellet diameter is 1.048 cm. The gap between seed and blanket fuel rods is 1.0 mm. In burnup calculation, the thermal power of the assembly is adjusted to achieve the average linear heat rate of the seed is 20 kW/m. As the seed of the metal fuel, the combination of (Pu + depleted U + 10% Zr) is considered, in which density is 16.36 gm/cm^3. As the blanket of metal fuel, the combination of (depleted U + 10% Zr) is considered, in which density is 15.96 gm/cm^3. As the thorium based oxide fuel, the seed is considered to be (PuO_2+ThO_2: T-MOX) and the blanket is ThO_2. The composition of Pu is set to be $^{238}Pu/^{239}Pu/^{240}Pu/^{241}Pu/^{242}Pu/^{241}Am$ = 2.7/47.9/30.3/9.6/8.5/1.0 wt%. For a nominal case, the temperature of fuel pellet is set to be 889 K, clad is 626 K and moderator is 580 K. For void coefficient calculation, void fraction is changed from 0% to 99%. Excess reactivity of 1% Δk/k at the EOC is considered as a margin, due to the present simplified assembly-based calculation modelling uncertainty neglecting the radial neutron leakage effect in the core geometry. Survey calculations have been done by the MVP-BURN code with 70,000 histories, in which 10,000 particles times' 70 batches; plus initial 20 batches skipped from the tally. The cross section libraries are based on JENDL-3.2.

---

1 Engineering Development Co. Ltd.

Table 2.4.1 shows the burnup characteristics of the metal fuel and the thorium based oxide fuel. The burnup characteristics of these fuels are compared with the uranium based oxide fuel (reference fuel). The enrichment of fissile Pu is adjusted to achieve the average burnup of 45 GWd/t at EOL in (Seed + Internal Blanket + Outer Blanket) region, as shown in Fig. 2.4.1 by dotted line. In the reference case, the conversion ratio is less than 1.0 and void coefficient is positive as shown in Table 2.4.1. Therefore, in order to improve these core performance parameters the present survey was performed with the metal or the thorium oxide fuel.

To improve the conversion ratio, the possibility of the metal fuel is studied. Table 2.4.1 shows that, the conversion ratio increases largely by using the metal fuel. But a change in the void coefficient is large in positive value, which will be problem to use the metal fuel in a practical reactor. To improve the void coefficient of the metal fuelled seed-blanket assembly, the height of seed is decreased from 100cm x 2 to 50cm x 2. It is expected that the axial leakage of neutron will improve the void coefficient. After adjusting the enrichment of fissile Pu, it is seen that the void coefficient is still large in positive due to increase in the enrichment of fissile Pu as shown in Table 2.4.1.

To improve the void coefficient, ThO_2 is used instead of UO_2 as the axial blanket, the internal blanket and in the seed, respectively. It is seen that the conversion ratio as well as the void coefficient does not change when ThO_2 is used as the axial blanket. But when ThO_2 is used as the internal blanket, the conversion ratio increases significantly, however the height of internal blanket should be over 20cm. When ThO_2 is used in the seed i.e. T-MOX, the void coefficient is improved significantly, but the conversion ratio is significantly decreased compared to the reference fuel. Even the combination of T-MOX as the seed and ThO_2 as the internal blanket does not improve the conversion ratio.

As a conclusion from these calculations, it is possible to improve the conversion ratio of seed-blanket fuel assembly by using metal fuel, but makes the void coefficient worse. On the other hand, the T-MOX as seed is improved the void coefficient of the seed-blanket fuel assembly, however, the conversion ratio decreases.

Reference

1) A. Shelley, S. Shimada, T. Kugo, T. Okubo and T. Iwamura: "Optimization a Seed-blanket Type RMWR Fuel Assembly", JAERI-Review 2003-004, pp.57- 59 (2003).

Table2.4.1: Burnup properties of different fuels

Seed-blanket fuel assembly	Fissile Pu wt%	Cycle length in Month	Burnup in (Seed+Int.B +OB) GWD/t	Int-C.R. at EOL	Void coefficient Pcm/%void
Reference case (MOX as Seed, UO_2 as Blanket)	14.62	18.60	45.0	0.95	+31.58
Metal fuel	9.98	34.5	45.0	1.07	+126.00
Metal fuel Seed Height: 50cmx2	11.30	35.57	45.0	1.09	+116.12
ThO_2 as Axial Blanket	14.65	18.13	45.0	0.95	+31.85
ThO_2 as Internal Blanket	14.60	18.70	45.0	0.95	+27.47
ThO_2 as Internal Blanket (20cm)	14.90	19.24	45.0	1.05	+28.53
ThO_2 as Internal Blanket (30cm)	15.25	20.09	45.0	1.05	+30.96
PuO_2+ThO_2: T-MOX as Seed	16.22	18.23	45.0	0.90	+6.30
T-MOX as Seed, ThO_2 as Internal Blanket (20cm)	16.35	18.33	45.0	0.90	+0.66

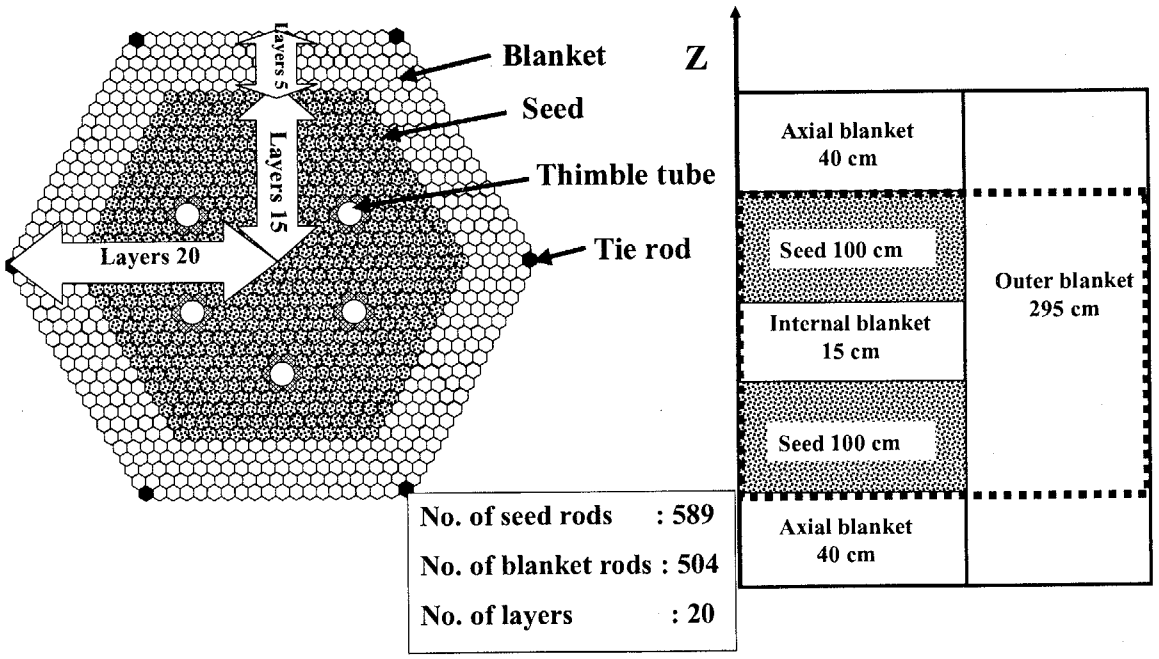

Fig. 2.4.1 Horizontal and vertical cross sectional views of seed-blanket fuel assembly

2.5 Investigation on Stability of RMWR under Natural Circulation Condition

N. Ishikawa, T. Nakatsuka, T. Okubo and T. Iwamura

(*E-mail:* ishikawa@clsu3a0.tokai.jaeri.go.jp)

The Reduced-Moderation Water Reactor (RMWR) has specific features such as tight lattice core, and being operated at low flow rate and high void fraction condition to improve the conversion ratio. To confirm the stability of RMWR, the analysis of channel and core stabilities for BWR type small size RMWR (330MWe) under natural circulation condition was performed utilizing the transient analysis code TRAC-BF1[2]. The stability under forced circulation condition has been previously investigated. The natural circulation condition is attained by extending the flow channel above the core region to gain the driving force for the coolant circulation in the reactor vessel. This extending flow channel is called as chimney. Extending the channel about 6[m] from the forced circulation setting, the natural circulation condition has been attained.

The channel stability was evaluated by the channel model of fuel bundle with the channel extension as shown in Fig.2.5.1. The length of heated part of the fuel bundle is 1.30[m], which consists of MOX region and blanket region. The total length of the fuel bundle is set to 2.92[m] including the channel box extension for the control rod follower guide. Further 5[m] channel extension is made to simulate the divided chimney. The channel of fuel bundle and extension part was modeled by CHAN component of TRAC-BF1 code. The pressure boundary condition was introduced by setting the BREAK components at the top and bottom of the CHAN component. The channel stability was evaluated by channel flow response against the pressure disturbance induced at the bottom BREAK component. The amplitude of the pressure disturbance is 5% of the pressure drop between inlet and outlet of the channel. The response of the channel flow is shown in Fig.2.5.2. Although the settling time of the response is about 10[sec], which is identical to the transit time of the channel flow, no oscillatory responses are observed.

To investigate the core stability, we have obtained the geometry inside the reactor vessel as shown in Fig.2.5.3, which attained natural circulation condition by channel extension for simulating the divided chimney. The core stability was evaluated from the core power response against the reactivity disturbance. Figure 2.5.4 shows the response of core

power when the reactivity disturbance of 5[cents] was added. The little fluctuation was observed in the core power response due to the core flow response perturbation in the natural circulation case, however, the response settled stably because of the small absolute value of the void reactivity coefficient of RMWR core. The core flow response is also depicted in Fig.2.5.5. It is confirmed that the RMWR core under natural circulation condition shows the stable characteristics within these analysis results.

The present study was supported by the governmental funding from the innovative and viable nuclear energy technology (IVNET) development project.

References

1) R. Takeda, et al.: "Conceptual Designing of Reduced-Moderation Water Reactor –Design of Small Core with Natural Circulation-- ", 2002 Annual Meeting of the Atomic Energy Society Japan, G23 (2002) [in Japanese].

2) J. A. Borkowski, et al.: "TRAC-BF1/MOD1: An Advanced Best-Estimate Computer Program for BWR Accident Analysis", NP-1850-CCM, NUREG/CR-4356 (1992).

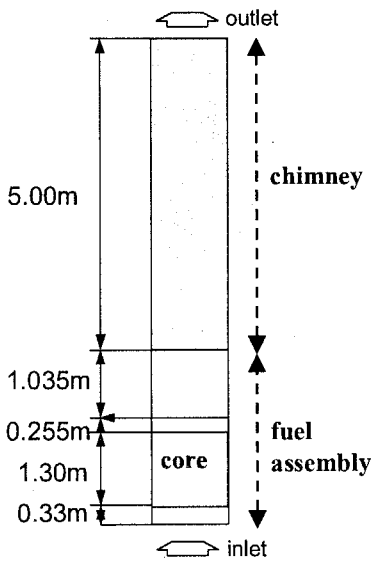

Fig.2.5.1 Channel model

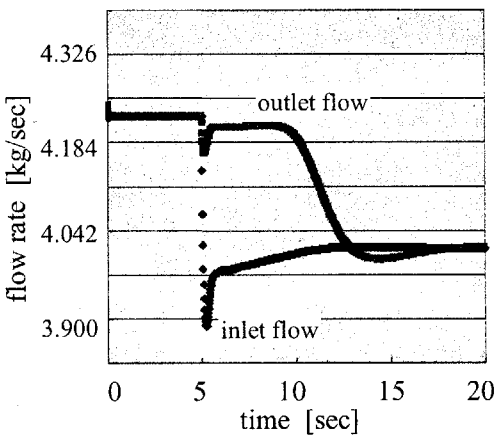

Fig.2.5.2 Channel flow response

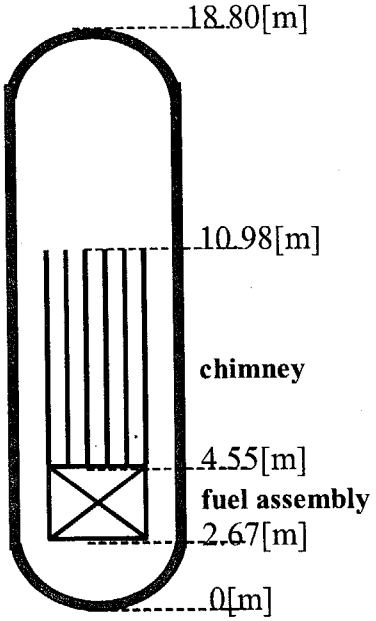

Fig.2.5.3 Geometry inside the reactor vessel

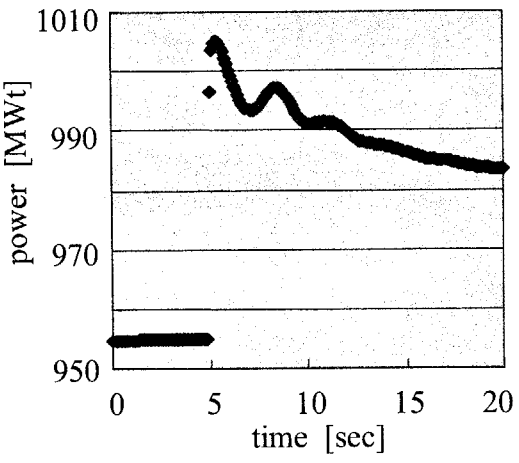

Fig.2.5.4 Reactor power response

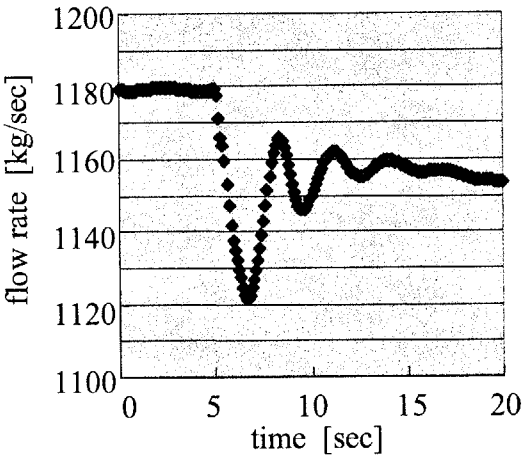

Fig.2.5.5 Core flow response

2.6 Regional Instability Evaluation of Small-Scale RMWR with TRAC-BF1/MLK3D

T. Nakatsuka, N. Ishikawa, T. Okubo and T. Iwamura
(*E-mail*: nakatuka@popsvr.tokai.jaeri.go.jp)

The high conversion ratio BWR type Reduced-Moderation Water Reactors (RMWRs) possess short and double-piled flat cores. Diameter and height of the cores are designed to be 7.6 m and 0.695 m for large-scale core and 4.14m and 0.76m for small-scale core, respectively[1]. Regional stability of such flat cores has been a major concern in the design study. Ishikawa et al. assessed dynamical response characteristics of the RMWRs using the thermal hydraulic transient analysis code[2, 3]. From the viewpoint of channel and core stabilities, they pointed out that the core shows the stable response characteristics against the perturbation.

According to the knowledge base of the current BWRs' stability, in case the core dynamics characteristics show both channel and core stabilities, the core also retains regional stability. In the present study, to investigate whether the trend is also true for the RMWR, analysis was performed for the small-scaled RMWR with a time domain analysis code TRAC-BF1/MLK3D which is a coupling system of plant thermal hydraulic analysis code TRAC-BF1[4] and three-dimensional neutron

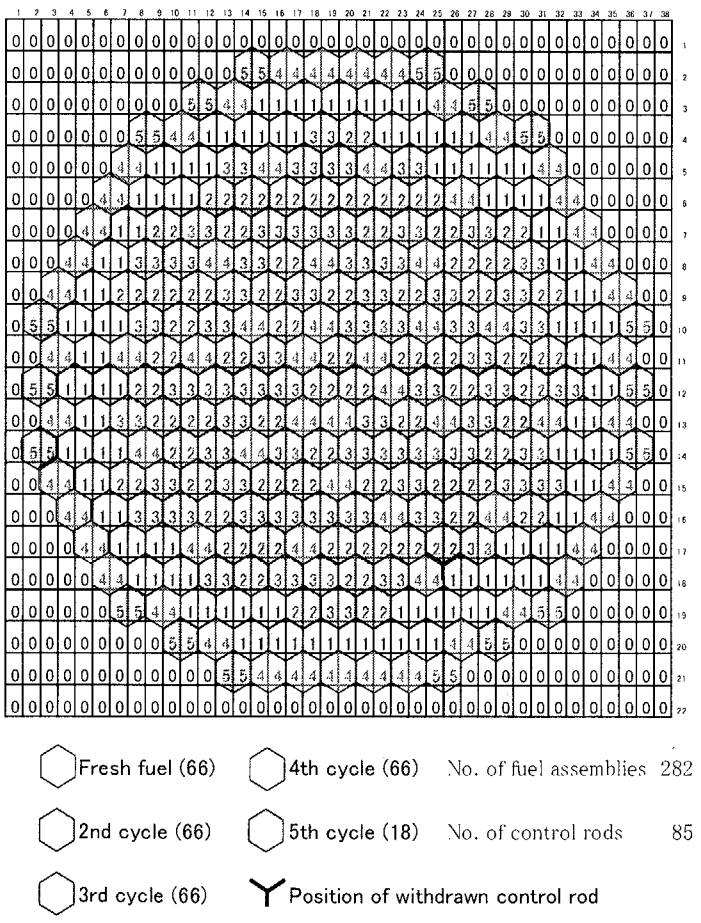

Fig. 2.6.1 Regional stability analysis model for MLK

diffusion calculation code MOSRA-Light for Kinetics (MLK)[5].

The MLK cannot directly treat the hexagonal assemblies like those of RMWRs, since it is assumed that the shape of fuel assemblies is rectangle. Therefore, in the present analysis, to apply MLK to the RMWR, a hexagonal assembly was divided into two equivalent rectangle cell models (Fig.2.6.1).

For TRAC-BF1, a hexagonal assembly is modeled as a CHANNEL component. Fig.2.6.2 shows the component noding inside the reactor vessel for TRAC-BF1 input data.

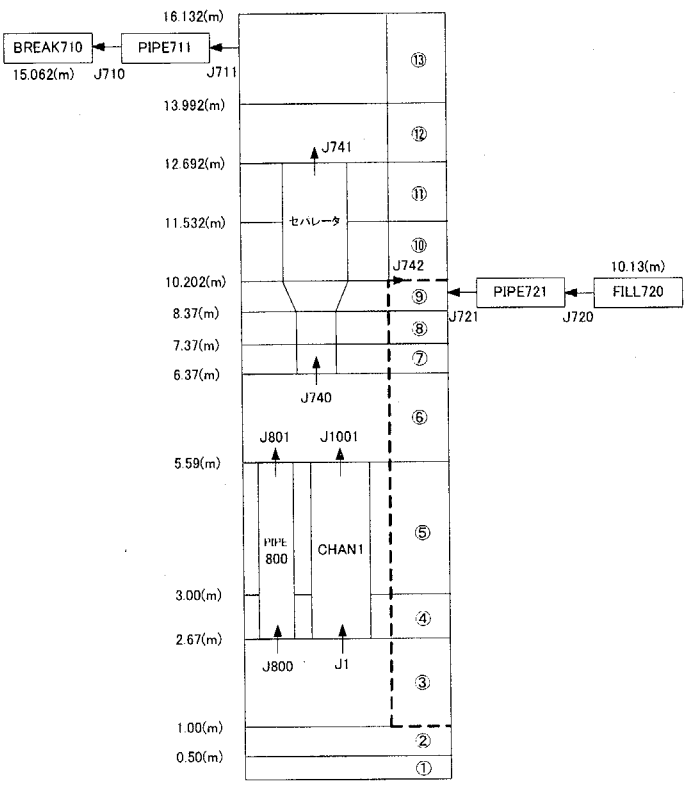

Fig.2.6.2 Reactor vessel model for TRAC-BF1

First, steady state calculation was performed. Power density distribution in upper and lower MOX parts are shown in Fig.2.6.3.

Then transient calculation for 30 seconds was performed on condition that one control rod depicted in Fig.2.6.1 was withdrawn. The corresponding power density distributions are shown in Fig.2.6.4. No significant oscillation or divergence is observed in the power density distribution. It is confirmed that the RMWR core shows the regional stability against the perturbation within the results of the present analysis.

The present study was supported by the governmental funding from the innovative and viable nuclear energy technology (IVNET) development project operated by the Institute of Applied Energy (IAE).

References

1) T. Iwamura, et al.: "Development of Reduced-Moderation Water Reactor (RMWR) for Sustainable Energy Supply", Proc. of The 13th Pacific Basin Nuclear Conference (PBNC 2002), pp. 1631-1637

(2002).

2) N. Ishikawa, F. Araya and T. Iwamura: "Sensitivity Analyses on Channel and Core Stability for High Conversion Ratio BWR Type RMWR Core", JAERI-Review 2002-005, pp. 64-66 (2002).

3) N. Ishikawa, et al.: "Study on Dynamical Response Characteristics of RMWR Core", JAERI-Review 2003-004, pp. 60-62 (2003).

4) J.A. Borkowski, et al.: "TRAC-BF1/MOD1: An Advanced Best-Estimate Computer Program for BWR Accident Analysis", NUREG/CR-4356 (1992).

5) K. Okumura: "MOSRA-Light; High Speed Three-Dimensional Nodal Diffusion Code for Vector Computers", JAERI-Data/Code 98-025 (1998). [In Japanese]

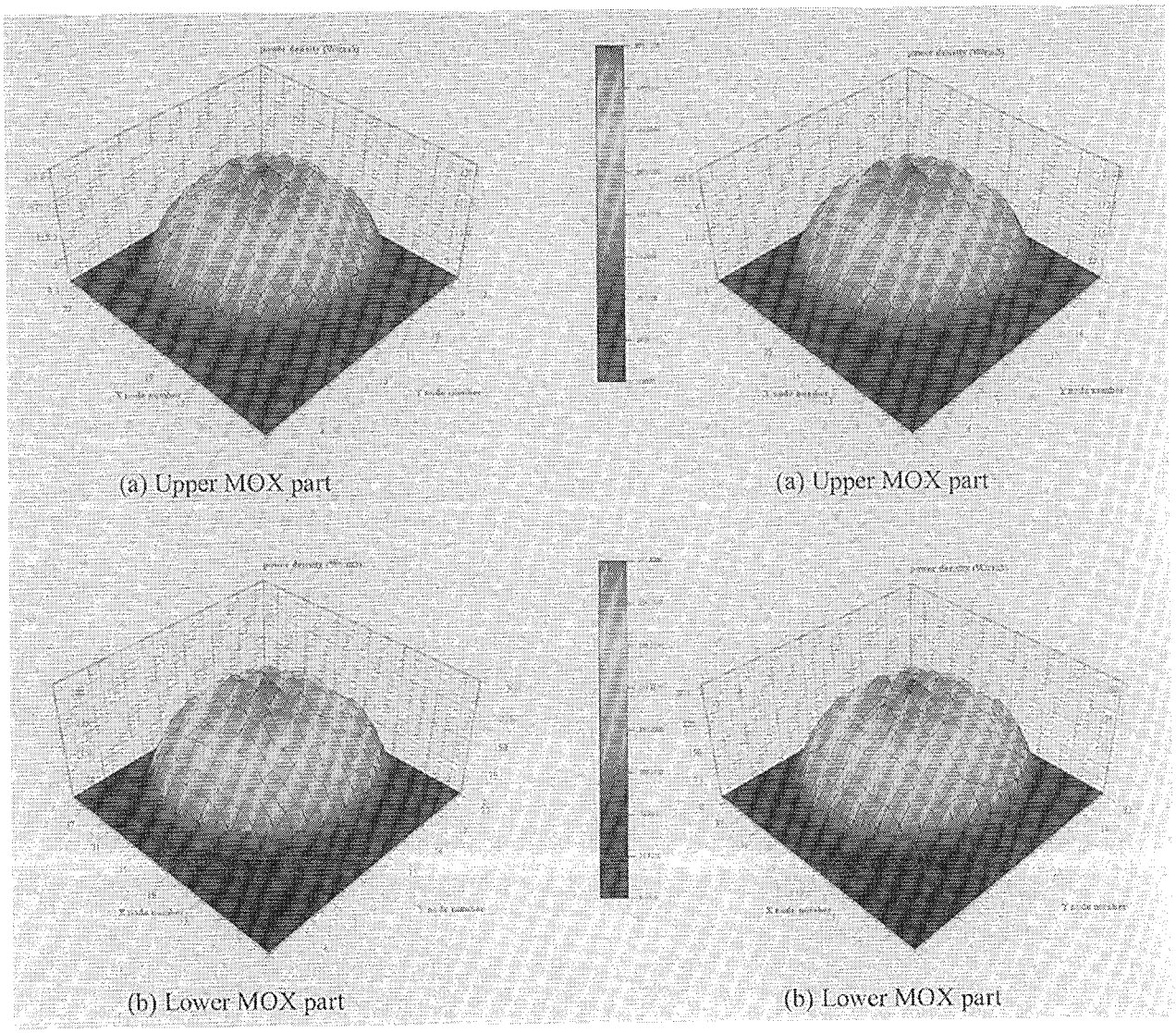

Fig.2.6.3 Power density distribution (steady state calculation)

Fig.2.6.4 Power density distribution (transient calculation: after 30 s)

2.7 Study on Recriticality Accident for RMWR

T. Yonomoto and H. Akie
(*E-mail:* yonomoto@lstf3.tokai.jaeri.go.jp)

The recriticality accident has been one of the most important safety issues for Liquid Metal FBRs that utilize highly enriched plutonium fuel. The possibility of the recriticality during a severe accident of RMWR was first shown by JNC[1], which is summarized as 1) the recriticality can occur in the core when the cladding material is melted down and separated from the fuel pellets during a severe accident, and 2) its mechanistic impacts on the structure integrity are, however, supposed to be small due to the absence of liquid-phase water in the core when it occurs. Those results, together with the core damage behavior and the possibility of the recriticality in the lower head, were investigated in 2002.

Coolant distributions in the pressure vessel during accidents were analyzed using the RELAP5/MOD3 code[2]. Two scenarios were analyzed; one represented a typical low-pressure core damage scenario initiated by a large break in the main steam line, and the other represented a typical high-pressure scenario assuming the failure of the automatic depressurization system. The results have confirmed that the liquid phase coolant does not exist in the core when the core begins to melt even for the high-pressure scenario characterized by the absence of the flashing-induced liquid level reduction.

The core damage behavior due to the excess temperature rise was analyzed using the MELCOR code[3]. The results have shown that 1) the collapse of the fuel bundles begins from the center region at ~3000 s after the initiation of the temperature excursion (see Fig.2.7.1) and propagates in the radial direction, and 2) when the molten debris jet begins to penetrate the core support plate in the center region, the peripheral core region is still intact. This calculated behavior is different from the estimated behavior for the TMI accident, where relatively large amount of molten fuel was created in the upper part of the core and was relocated to the lower plenum through the thermally-damaged core barrel. This is one of characteristic for the RMWR core having a flat geometry, which affects the debris bed formation in the lower head.

The previous studies on severe accidents have shown that debris particles are created due to the interaction between the debris jet and the surrounding steam flow, are solidified and entrained in the liquid flow, and accumulated in the bottom of the pressure vessel.

Because of this accumulation process, the enriched plutonium fuel is mixed well with the other materials in the debris bed. The recriticality of the well-mixed debris bed was analyzed using the MVP code,[4] which is a continuous energy Monte Carlo code. Calculation parameters include the amount of the fuel and cladding, the space fraction among debris particles, and the coolant void fraction in the space. The results have shown that the recriticality does not occur in the well mixed debris bed.

Those results suggest that the recriticality that may affect the pressure vessel integrity is not likely to occur at least before the debris bed is melted again.

The present study was supported by the governmental funding from the innovative and viable nuclear energy technology (IVNET) development project.

References

1) T. Mihara, et al: "FBR shisutemu gijyutsu kentousyo – heisei 12 nenndo houkoku," JNC TY9400, 2001-012, pp. 1442-1445 (2001) [in Japanese].
2) The RELAP5 Development Team: "RELAP5/MOD3 Code Manuals," NUREG/CR-5535 (1995)
3) R. O. Gauntt et al: MELCOR Code Manuals, NUREG/CR-6119 (2000).
4) T. Mori, M. Nakagawa and M. Sasaki: " Vectorization of Continuous Energy Monte Carlo Method for Neutron Transport Calculation", J. Nucl. Sci. Technol., vol.29, 325 (1992).

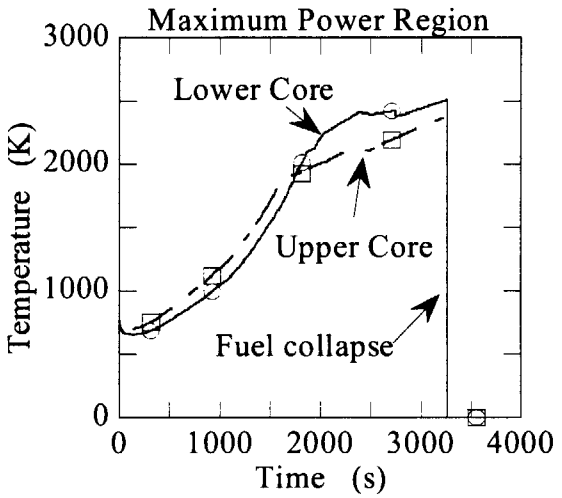

Fig. 2.7.1 Fuel temperatures during a main steam line break LOCA assuming the failures of all the safety systems by the MELCOR code

2.8 Thermal and Mechanical Analysis of MOX Fuel Behavior in RMWR by FEMAXI-RM Code

M. Suzuki, T. Okubo and T. Iwamura
(*E-mail:* motoe@popsvr.tokai.jaeri.go.jp)

To assess the thermal and mechanical feasibility of MOX fuel rod design in RMWR irradiation conditions, MOX fuel performance code FEMAXI-RM has been developed as an extended version of FEMAXI-V[1] and analysis on the thermal and mechanical behaviors of the MOX rod has been carried out. In the calculation, specifications of the rod have been input in conformity with the design of RMWR[2], and the rod is divided into 34 axial segments, in which pellet chemical composition, linear power, and fast neutron flux are designated by input to predict temperature, fission gas release, internal pressure, deformations, and PCMI.

With respect to the MOX fuel thermal conductivity, results of two cases have been compared; a conservative case with Baron model[3], and non-conservative case with MATPRO-11 model[4]. Baron model assumes considerable degradation with burnup, while the other has no burnup dependence. For fission gas release, White-Tucker-Speight model[5,6] has been adopted, and for pellet swelling, Studsvik model[7] has been adopted.

Figure 2.8.1 shows the pellet center temperatures at peak power elevation of MOX fuel. The temperature is higher with Baron model than the other. However, the highest temperature is around 2400K at 49.4 GWd/t, having a large safety margin in comparison with the melting point of 31%Pu-MOX fuel of 2950K by MATPRO-11.

Figure 2.8.2 shows internal pressure rise, which is attributed mainly to the fission gas release. It is 6.2 MPa at the maximum with Baron model and does not exceed the coolant pressure of 7.2MPa, suggesting that the cladding will not cause creep-out by overpressure.

Diameter increase of cladding induced by fuel swelling and thermal expansion has been analyzed by three different FEM geometries: the global rod-length deformation geometry "A", local ridging PCMI geometry "B", and local deformation at MOX-Blanket interface region "C". Result of "A" is shown in Fig.2.8.3, and the result of "B" is shown in Fig.2.8.4. Comparison of these results reveals that the cladding diameter increase (strain) is roughly 1% at most, calculated equivalent stresses are 40 to 80MPa, which are sufficiently lower than 400 – 600MPa yield stress of irradiated cladding. Therefore, it is expected that

these deformation cannot deteriorate fuel rod integrity. On the other hand, the analysis in the geometry "C" has given the results that axial strain of cladding at the interface region of MOX and blanket pellet reaches 3 – 4 %. However, this strain can be easily reduced to 1% level by such contrivance as tapering the MOX pellet adjacent to the blanket pellet.

In conclusion, calculated fuel center temperature of MOX fuel does not reach the melting point by a large margin, internal pressure enhanced by fission gas release is below the coolant pressure level, cladding diameter increase does not significantly exceed 1%. These results permit to predict that the MOX fuel rod integrity will be held during irradiation in RMWR, though actual behaviors of MOX pellet swelling requires to be investigated in detail.

The present study was supported by the governmental funding from the innovative and viable unclear energy technology (IVNET) development project operated by Institute of Applied Energy (IAE).

References

1) M. Suzuki: "Light Water Reactor Fuel Analysis Code FEMAXI-V(ver.1)", JAERI-Data/Code 2000-030 (2000).
2) T.Okubo, M.Suzuki, T.Iwamura, et al.: "Design of small Reduced-moderation water reactor (RMWR) with natural circulation cooling", PHYSOR 2002, Seoul, Korea (2002).
3) D.Baron and J.C.Couty: Proc. IAEA TCM on Water Reactor Fuel Element Modelling at High Burnup, Windermere, U.K. (1994).
4) D.L.Hagrman and G.A.Reyman: MATPRO-Version11, NUREG/CR-0497, TREE-1280, Rev.3. (1979).
5) R.J.White, and M.O Tucker: "A new fission gas release model", J.Nucl.Mater.,118, 1-38 (1983).
6) M.V.Speight: Nucl.Sci.Eng.37, 180 (1969).
7) D.Schrire, A.Kindlund, and P.Ekberg: "Solid Swelling of LWR UO_2 Fuel", HPR-349/22, Enlarged HPG Meeting, Lillehammer, Norway (1998).

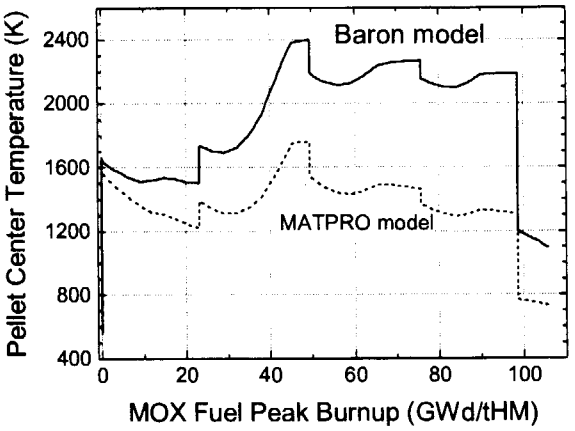

Fig.2.8.1 Calculated MOX pellet center temperatures.

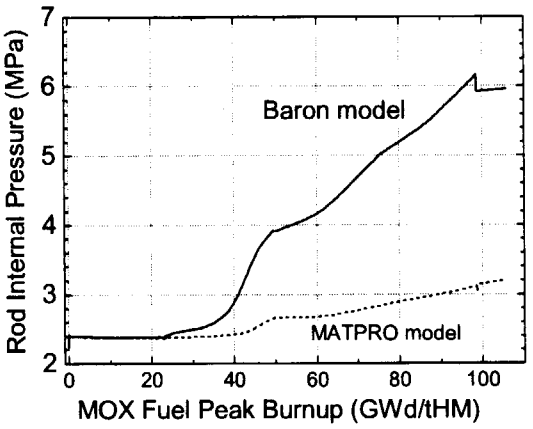

Fig.2.8.2 Calculated internal pressures.

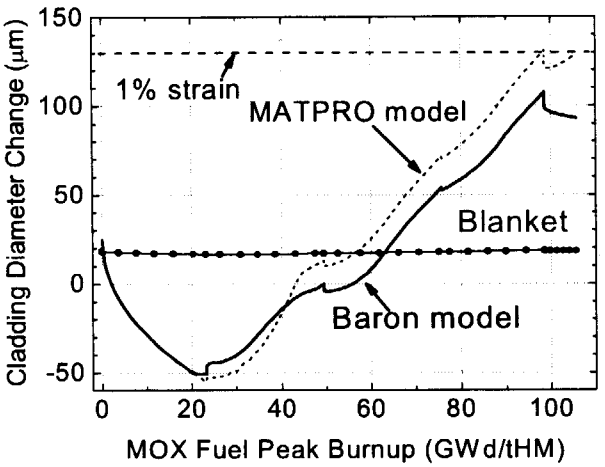

Fig.2.8.3 Calculated cladding diameter changes for MOX fuel part and blanket part in the global rod-length geometry "A".

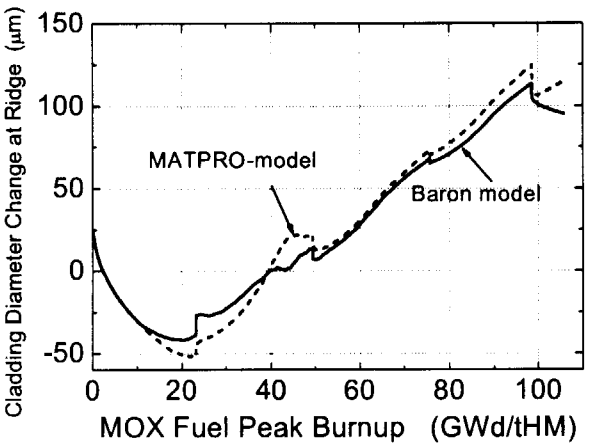

Fig.2.8.4 Calculated cladding diameter changes for MOX fuel part and blanket part in the local ridging PCMI geometry "B".

2.9 Conceptual Design of Inherently Safe Fast Reactor (ISFR)

Y. Asahi
(*E-mail* : y.asahi@popsvr.tokai.jaeri.go.jp)

ISFR is a boiling heavy water fast reactor of process inherent ultimate safety (PIUS) type[1]. ISFR may breed fuel in the core. The volume ratio of moderator to fuel V_m/V_f is 0.643, while the power density is 71 kW/L in the core. Its fuel contains MAs (minor actinides) which act not only as burnable poisons, but also as fertile materials. Heavy water is used as the coolant, since it not only produces photo-delayed neutrons[2, 3], but also has a relatively small slowing down power. Since ISFR has not only a positive void coefficient, but also voids already at a steady state, it must be carefully designed. Owing to a positive void coefficient, the application of the PIUS concept to ISFR is not straightforward. Thus, the gap conductance is small so that the time constant τ_α of the positive void feedback process is sufficiently large, while the initially-closed two-way check valves to be used as passive switches to the pumps are installed at the lower honeycombs. As a result, the passive shutdown mechanisms can come into effect sufficiently soon to suppress the positive feedback reactivity. Both large τ_α and the passive switches also help stabilize the system so that ISFR can perform a constant power operation with a simple control logic for the main coolant pump speed (Fig. 2.9.1). In a steam generator tube rupture, the reactor power was found to smoothly decrease to the decay heat level (Fig. 2.9.2). In the dynamical calculations of ISFR, the THYDE-NEU code[4] was found very useful. The feasibility of ISFR was proved only to some extent.

References

1) D. Babala et al., "Pressurized Water Reactor Inherent Core Protection by Primary System Thermohydraulics", Nucl. Sci. Eng., 90, 400 (1985)
2) Berstein et al., "Yield of Photo-Neutrons from U235 Fission Products in Heavy Water ", Phys. Rev., 71, 573 (1947)
3) G. R. Keepin et al., "Delayed Neutrons from Fissionable Isotopes of Uranium, Plutonium, and Thorium", Phys. Rev., 107, 1044 (1957)
4) Y. Asahi, THYDE-NEU : Nuclear Reactor System Analysis Code, JAERI-Data/Code 2002-002, March 2002

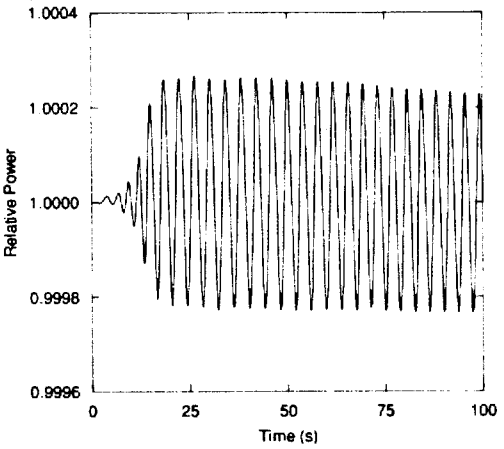

Fig. 2.9.1 Reactor power in constant power operation

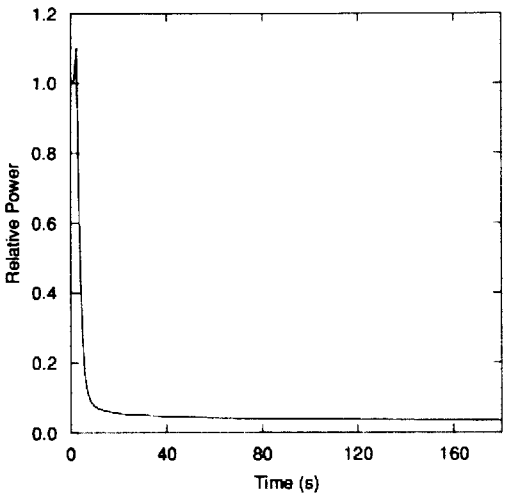

Fig. 2.9.2 Relative reactor power in SGTR

2.10 Analysis of a BWR Turbine Trip Experiment by Entire Plant Simulation with Spatial Kinetics

Y. Asahi , T. Suzudo, N. Ishikawa and T. Nakatsuka
(*E-mail* : y.asahi@popsvr.tokai.jaeri.go.jp)

OECD/NEA/NSC (Nuclear Science Committee) under the sponsorship of US Nuclear Regulatory Commission recently completed a benchmark problem[1] of a boiling water reactor turbine trip conducted at Peach Bottom-2 (a GE-designed BWR/4) Plant. The benchmark was organized by a team at the Pennsilvania State University, who provided the participants with the benchmark specifications[1] along with cross-section files. We participated in the benchmark with the THYDE-NEU code[2, 3]. What characterizes the work is that, in spatial kinetics, a notion of reactivity was not used, while, in thermal-hydraulics, the plant was treated as a closed coolant system whose pressure can be lower than the atmospheric pressure (at the condenser). At low pressures, nonlinearity of the thermal-hydraulic equation enhances and hence a thermal non-equilibrium model is required. To simulate an entire plant, it was also found necessary to have the moisture separator model and to account for a reversible pressure drop at a junction with an area change. Among parameters in THYDE-NEU is γ in the thermal non-equilibrium model in addition to C_1 and C_2 regarding the manner in which to express the coolant density used in the table look-up of cross sections. To a pair of C_1 and C_2, there may correspond a value of γ, namely, γ_C, with which it is possible to reproduce the experimental fact that the core averaged local power range monitor output R_{APRM} reached 0.95 at 0.63 s to generate the scram signal. One of the calculations with γ_C was compared to the experiment. Sensitivity calculations also were performed with respect to the temporal behavior of the bypass valve opening. The comparisons between the experiment and the calculations are shown in Figs. 2.10.1 and 2.10.2 for the core averaged local power range monitor output and the bypass valve flow rate, respectively.

References

1) J. Solis et al., "Boiling Water Reactor Turbine Trip (TT) Benchmark, Volume I : Final Specifications", USNRC, OECD/NEA, June 2001
2) Y. Asahi., "THYDE-NEU : Nuclear Reactor System Analysis Code", JAERI-DATA/CODE

2002-002, March 2002

3) Y. Asahi et al., "A Spatial Kinetics Method Ensuring Neutronic Balance with Thermal-Hydraulic Feedback and Its Application to a Main Steam Line Break", Nuclear Science and Engineering, 139,78-95(2001)

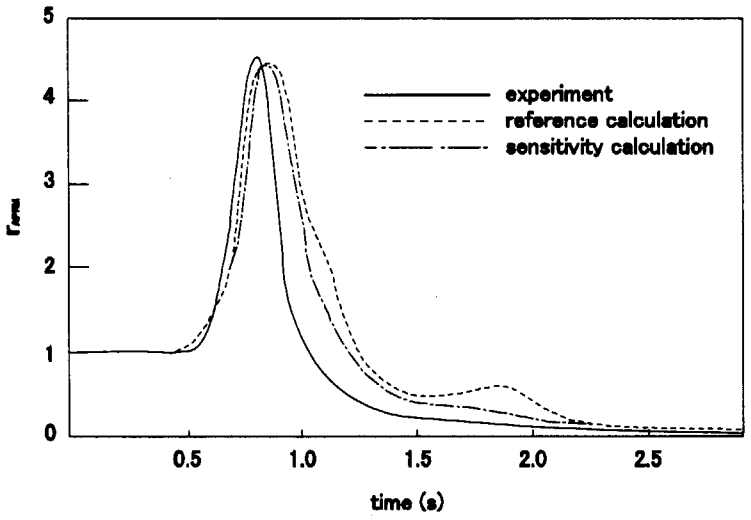

Fig. 2.10.1 Core averaged local power range monitor output (normalized to the initial value)

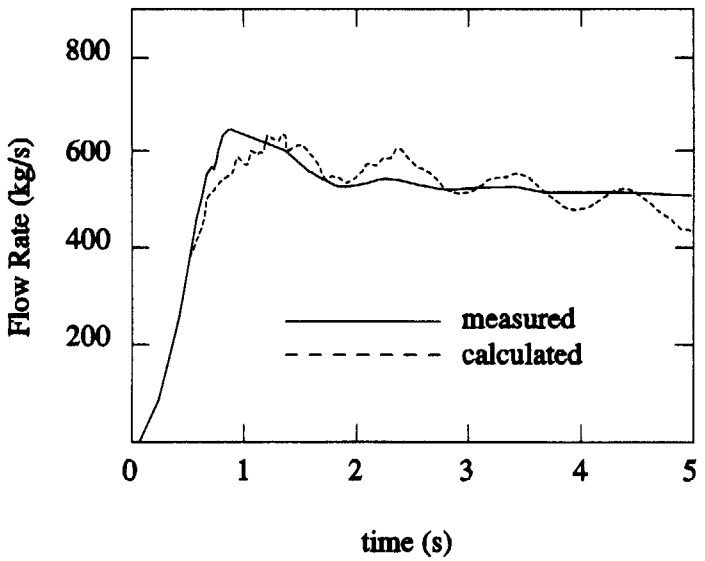

Fig. 2.10.2 Bypass valve flow rate

2.11 The Combination of Neural Networks and an Expert System for On-line Nuclear Power Plant Monitoring

K. Nabeshima, E. Ayaz*, S. Şeker*, B. Barutçu* and E. Türkcan*

(*E-mail:* nabe@clsu3a0.tokai.jaeri.go.jp)

Main purpose of on-line nuclear power plant (NPP) monitoring is to identify the current status of the operational plant using process signals. This is one of the formidable tasks from the point of view of the reactor safety and maintenance. However, there are recently several small accidents happened in NPPs, because those anomalies could not be realized by the operators at the beginning. Therefore, it must be more important to detect the symptom of small anomalies, especially at aged NPPs. In this study, we have developed Artificial Neural Network On-line Monitoring Aids (ANNOMA) system to find the symptom of small accidents earlier than the conventional alarm system.

The overview of on-line monitoring system is shown in Fig. 2.11.1. The Borssele NPP in the Netherlands is a two-loop pressurized water reactor with nominal electric power output of 477 MWe. The data acquisition system sends 72 plant signals to the monitoring system every two seconds. Out of these, 34 of most significant plant signals are selected for the inputs of neural networks; neutron flux, flow rate, pressure, temperature, electric power, etc. Recurrent and feedforward neural networks in auto-associative mode train with plant's normal operational data, then model the plant dynamics. The expert system diagnoses the plant status with the measured signals, the output of neural networks and the alarm information from the conventional alarm system. Whole monitoring system is developed on PC, and the software of data acquisition, neural networks and the expert system are programmed by Visual C and FORTRAN. The advisory displays are programmed by Visual Basic.

The feedforward neural network, Jordan[1] and Elman[2] recurrent networks were applied to the plant modeling. Those networks have three layers: input, one hidden and output layer. The numbers of input and output nodes are 34, respectively. In auto-associative networks, the output signals are supposed to be the same as the input signals at the same or next time step. The number of hidden node is selected as 25. The backpropagation algorithm is used for learning, and the sigmoidal function is selected as transfer function.

---

*Istanbul Technical University, Turkey

The patterns for the initial learning were obtained during the normal start-up operation of Borssele NPP. The electric power increased from 100 to 477 MWe within 30 hours. The number of the initial learning data is 1613 patterns, and the learning is repeated 1,000 times per each pattern. The patterns are given randomly within each learning cycle. The sums of square error by the feedforward network is always smaller than the errors by two recurrent networks, because the random order learning of feedforward network is very efficient for the error convergence. Furthermore, the learning time of the feedforward network is shorter because of the simpler component. From the above results, the feedforward network only is applied to anomaly detection in the following section.

The basic principle of the anomaly detection is to monitor the deviation between process signals measured from the actual plant and the corresponding values predicted by the plant model, i.e., the neural networks. In the actual application, the fault level during steady state operation is defined experimentally as $1.25 \cdot \varepsilon_{max}$; the maximum error ($\varepsilon_{max}$) is the largest deviation per each signal during the initial learning. On the other hand, the fault level during transient operation is defined as $1.45 \cdot \varepsilon_{max}$. If one of the deviations exceeds the fault level, the error message will be displayed on the screen. Figure 2.11.2 shows that the neural network detected a small anomaly of pressurizer level signal, which was caused by the off-normal operation.

The expert system is used as a decision agent that works on the information space of both neural networks and the conventional alarm system. By using the plant simulator, the responses of neural networks in many kinds of anomaly cases are stored in the database. It is clear that the patterns of anomaly detection channels from the discrepancy between the predicted and actual outputs depend on the kind of anomaly[3]. Furthermore, the monitoring results during steady state and transient operation showed almost same anomaly detection property. Therefore, the expert system can easily diagnose the plant status and identify the type of anomalies by using the output of neural networks and the simple "if-then" rules.

We have developed on-line plant monitoring system with the combination of neural networks and an expert system. The off-line and on-line test results at nuclear power plant in the Netherlands show that the neural networks can successfully detect the symptom of anomalies earlier than the conventional alarm system and the expert system can diagnose the plant status sufficiently. The next step will be the application of this system to the natural gas power plant in Turkey.

References

1) M. I. Jordan: "Attractor Dynamics and Parallelism in a Connectionist Sequential Machine", Proceedings of the 1986 Cognitive Science Conference, Baldonado, pp.531-546 (1986)

2) J. Elman: "Finding Structure in Time. Cognitive Science", Vol. 14, pp.179-211 (1990)

3) K. Nabeshima, et al.: "On-line Neuro-Expert Monitoring System for Borssele Nuclear Power Plant", Progress in Nuclear Energy, Vol. 43, pp.397-404 (2003)

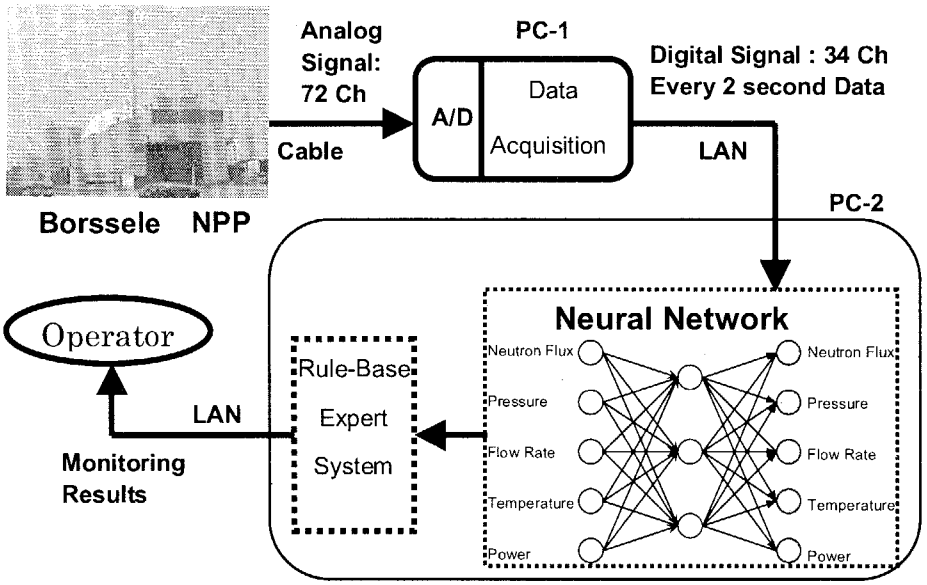

Fig. 2.11.1 ANNOMA system overview

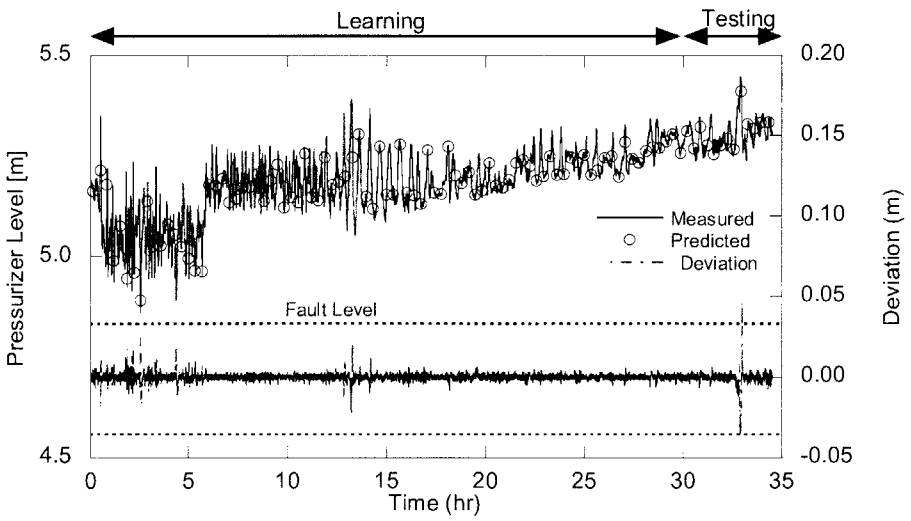

Fig.2.11.2 Monitoring result of "Pressurizer Level" during start-up operation

2.12 Object-Oriented Distributed Computing for Intelligent Monitoring Systems

T. Suzudo and K. Nabeshima
(Email: suzudo@clsu3a0.tokai.jaeri.go.jp*)*

A new methodology to construct distributed computing systems specially targeting nuclear power plant monitoring systems was proposed. In this framework, a monitoring system is composed of multiple modules and a client that administrates them. Each module was designed as a TTY-based interactive program, which reads from and writes to the standard I/O so that human can operate it. TTY-based programs have many advantages during the developing phase, which include, but are not limited to:

1. Most program languages support the standard I/O functions.
2. Standard I/O function is easy to use for most programmers.
3. Because they can be executed independently, the quality control is easy.
4. Automatic software testing is easily achieved by a script.

The communication between the client and each module is established by a TELNET communication, therefore these modules can be located at any host computer being capable of a TELNET service, see the detail in Ref. 1).

The client is programmed as it automates human operations necessary for administrating all the modules. For this purpose, we used to use a potable interpreter script language, called Tcl[2]. This language has a set of libraries for operating multiple TTY-based interactive programs, which is called Expect[3]. Although Tcl is easy to learn, it is not beneficial to make a complicated program being structured well.

In the recent additional work, we rewrote the client program using C++ with the object-oriented programming techniques: The client holds virtual modules, which are defined as a class in the meaning of object-oriented programming. Each of them works as the "agent" of a module in a remote host, that is, the virtual modules implement the commands of the corresponding modules as a form of interface in the meaning of object-oriented programming.

The neural-network-based anomaly detection system[1] was updated using the new framework. The schematic picture of this is depicted in Fig. 2.12.1. In the system are three host computers, a client host and two remote hosts for the modules. A module called "daq" is

in charge of reading plant signals, transforming them into a set of digital data and sending the data to the client on request. Its virtual module, the "daq object" is located in the client host, and the TELNET communication is established when the system is started. Similarly, the neuro module, which is in charge of diagnosing the goodness of the plant state by the analysis of the data using a neural network technology, is located in the other remote host, and get connected to its virtual module, the "neuro module". As seen in the pseudo source code of the "main" function, the client repeatedly calls the "getData()" interface of the daq module to obtain the plant data and "isNormal()" interface of the neuro module to diagnose the plant state. Because the commands in the remote modules are implemented in the virtual modules, the client program is executed as if all the processes were included only in the client host computer: The client program is therefore easily structured.

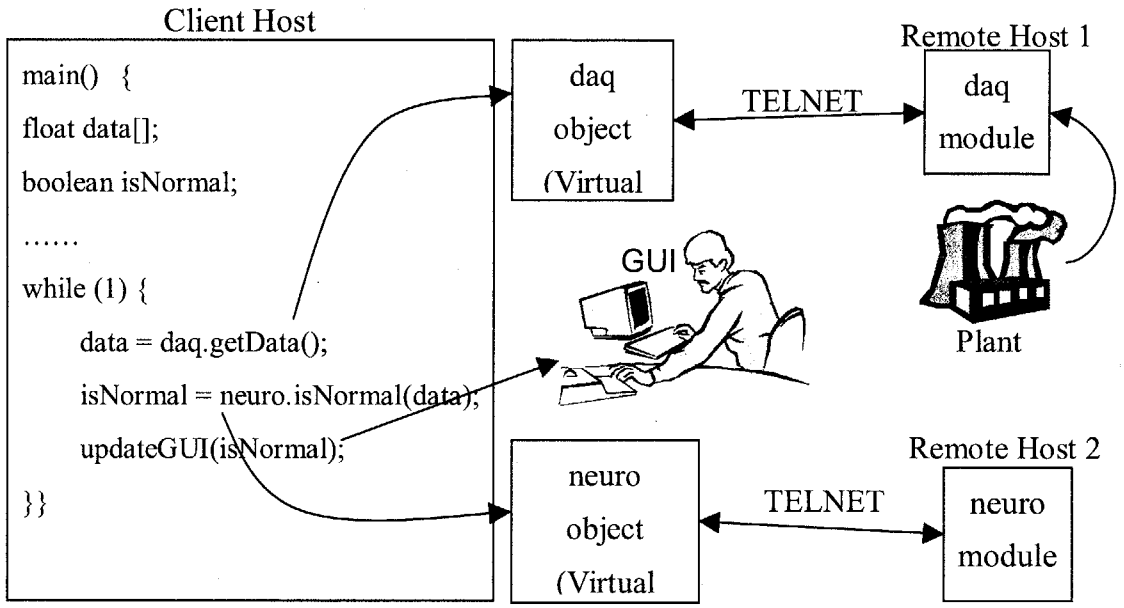

Fig. 2.12.1 Schematic picture of object-oriented distributed computing applied for neural-network-based monitoring system.

References

1) T. Suzudo, K. Nabeshima and H. Takizawa: "Software Integration for Monitoring Systems with High Flexibility", Prog. Nucl. Energy, 43, 1-4, 405(2003).
2) J. K. Ousterhout: "Tcl and Tk Toolkit", Addison-Wesley (1994).
3) D. Libes: "Exploring Expect; A Tcl-Based Toolkit for Automating Interactive Programs", O`Reilly (1995).

3. Research on Small Reactor for Dispersive Energy Supply System

Concept designs of two small-scale reactors for dispersive energy supply systems, which will be sited close to demand areas, have been studied by taking over the results of the nuclear ship research activities. Enhancements of safety and economy are focused on the design study. The one of the reactors is the MR-100G with thermal output of 100 MW exclusive for district heat supply, which has been studied from 2000, and the other is the PSRD with a thermal output of 100 to 300 MW for small grid electricity supply, which has commenced in 2001. These reactors adopt an integrated-type PWR, natural circulation and self-pressurization in the primary loop.

Regarding the district heat supply system with the MR-100G, the reactor is designed to be sited at a deep underground in depth of about 50m. Feasibility studies on construction of reactor system at the deep underground and economics of the system have been conducted and revealed to be feasible.

Upon the PSRD, the reactor core has been designed for a long life cycle –about 5 years– of operation until refueling, using the neutronics code system, SRAC95. Dynamics of reactor response to the load and postulated accidents such as a loss of coolant accident have been analyzed using RELAP5 code.

A concept of reactor siting has been studied on the PSRD; to avoid releasing the radioactive materials to the environment even if a hypothetical accident, the containment is submerged in a pit filled with seawater at a seaside. Refueling or maintenance of the reactor can be conducted using an exclusive barge instead of the reactor building.

An in-vessel type control drive mechanism (CRDM), a key technology for the reactor, has been developed for these integrated type reactors on the base of the CRDM developed for the marine reactor, MRX.

3.1 Development of In-vessel Type Control Rod Drive Mechanism for Integrated-type Reactor

T. Ishida and T. Yoritsune

(*E-mail:* tishida@popsvr.tokai.jaeri.go.jp)

The in-vessel type control rod drive mechanism, INV-CRDM, which is set inside the RPV, allows a possibility of the rod ejection accident to eliminate, both of the reactor pressure vessel and the containment to be compact, and the reactor system to be simple. The INV-CRDM, therefore, is a key technology for an integrated- type reactor. The electric motor driving type of INV-CRDN[1] developed by JAERI has a fine controllability in control rod position. It provides neither pipes penetrating the RPV nor a complicated control system, which are provided in the hydraulic driving type INV-CRDM[2].

The whole structure of the INV-CRDM is shown in Fig.3.1.1. It consists of a driving motor, a latch magnet, separator ball nuts, a driving shaft, a ball bearing and other components. These components work in a fluid of the primary loop. The INV-CRDM available to the working condition of high temperature water (583K, 12MPa) for the marine reactor (MRX), has been already developed. The condition for working in the Passive Safe Small Reactor (PSRD), however, is steam (583K, 10MPa), which is considered as more

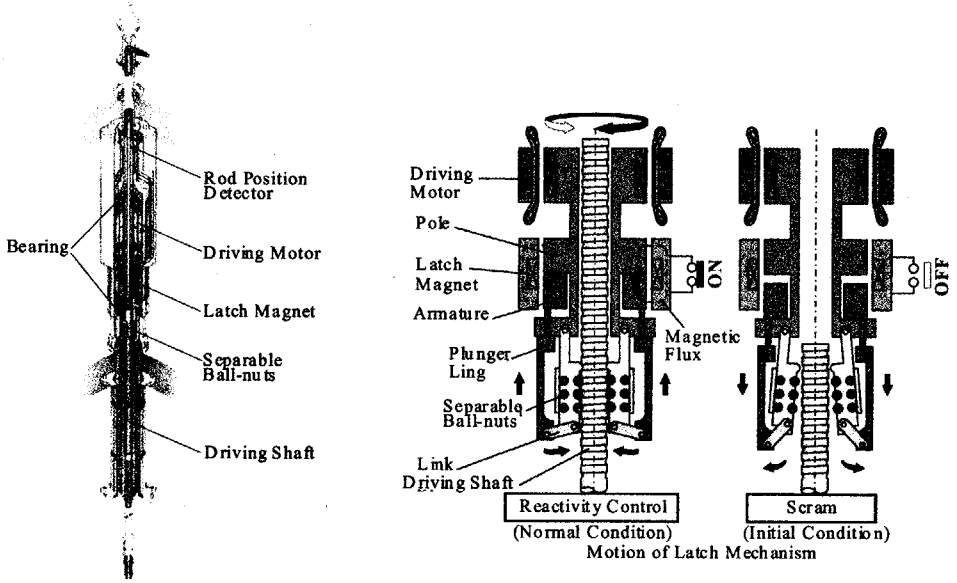

Fig.3.1.1 Concept of INV-CRDM driven by electric motor

severe. JAERI have developed the INV-CRDM for the PSRD.

Components of the INV-CRDM to be developed for the steam condition were the ball bearing and the driving motor. Others are not affected by this condition. Developments of the both components have basically completed, and the former is described in this report, as follows.

Materials of the ball bearing were surveyed by test to clarify the wear characteristics under the steam condition and find out proper materials. The test facility of an autoclave-type of small pressure-vessel, was the same as the one used for MRX bearing. Bearing test specimen consists of the ball, the flat ring, the rotating ring and the retainer. Materials of these components were the same as those of MRX bearing except one of the retainer. In the test, wears of specimens were measured after rotation with speed of 185rpm and with thrust force of 290N for 100, 150, and 200hrs, respectively. Specimen and test conditions are shown in Fig.

(a) Materials of components and test conditions of specimens

	Specimen A	Specimen B	Specimen C
Materials : Ball	Cermet (TiCN_NiCo): (—●—)	Same to left (----○----)	Same to left (·····●·····)
Flat ring	SUS316 coated by Cobalt alloy(Co-Cr-W-C) (—▲—)	Same to left (----△----)	Same to left (·····▲·····)
Rotating ring	SUS316 coated by Cobalt alloy(Co-Cr-W-C) (—■—)	Same to left (----□----)	Same to left (·····■·····)
Retainer	Graphite (C, Hs* = 80) (—◆—)	Same to left (----◇----)	C. Hs*=55 (·····◆·····)
Test condition	In hot water : 310℃, Saturated	In steam : 310℃, Sat.	In steam : 310℃, Sat.

•Hs : Shore hardness.
•Marks inside (----) indicate wears of the figure (c)

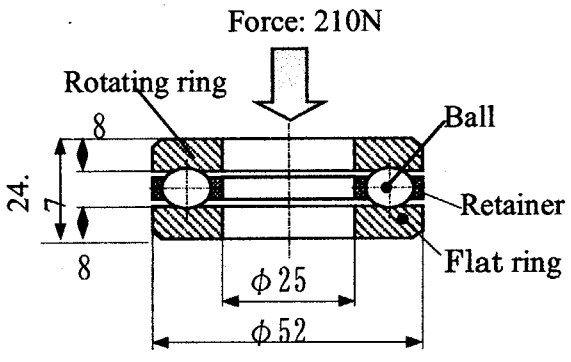

(b) Specimen for material test

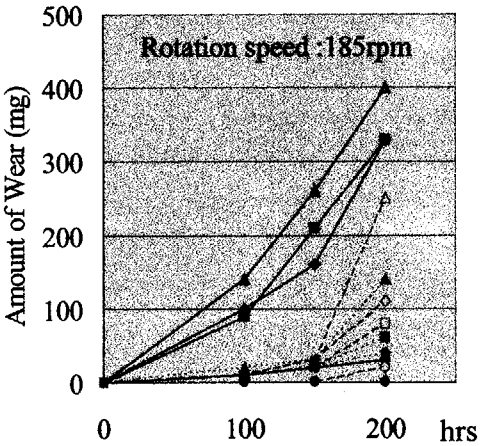

(c) Wears of components of bearing specimen

Fig. 3.1.2 Material test of bearing in CRDM of PSRD

3.1.2 (a), (b) together with the test result in (c). Materials of specimen A and specimen B were the same, but test atmospheres were different; water or steam.

Comparing wear of specimen A with that of specimen B, it was clarified that wear characteristics in the high temperature water and the steam were different: While the wear in high temperature water increased gradually according to time, the one in steam increased suddenly after about 150hrs, although being very small before that time. The reason of sudden increase was considered due to deposit of worn powder of the ball, rings and retainer on the flat ring.

Specimen C using softer graphite in the retainer showed less amount of wear than that of specimen B. This leads that softer graphite for the retainer is effective in the case of steam condition.

Acceptable maximum wear amount is 56mg for the ball, 690mg for the flat ring and 620mg for the rotating ring, respectively, which were obtained on the base of a long term durability testing with the full scale bearing of the MRX. The time required to that of the PSRD is 150hrs, which was obtained from a lifetime of 40yrs, frequencies of load follow and scram, etc, during the lifetime. This means all specimens in the test were available for the bearing of PSRD.

As a result, the materials of specimen C, for the bearing working in steam for the PSRD can be recommended as better one. The INV-CRDM developed by JAERI, therefore, can be available to the both working condition of high temperature water and steam.

References

1) T. Ishida, et al.: "Development of In-vessel Type Control Rod Drive Mechanism for Marine Reactor", J.Nucl. Scie. and Tech., 38-7, 557(2001).

2) Zheng, Yanhau, et al.: "Step Dynamic Process of the Hydraulically-driven Control Rod, (II) Theoretical Model on Step-down Process", J.Nucl. Scie. and Tech., 38-12, 1133(2001)

3.2 Design Study on Very Small Reactor for Small Grid Electricity Supply − Reactor Siting at Seaside Pit Filled with Water −

T. Ishida and K. Sawada
(*E-mail:* tishida@popsvr.tokai.jaeri.go.jp)

JAERI has been studying a Passive Safe Small Reactor (PSRD) for Distributed Energy Supply System concept. The PSRD is an integrated-type PWR with reactor thermal power of 100 to 300 MW aimed at supplying mainly electricity. In design of the PSRD, high priority is laid on enhancement of safety as well as improvement of economy. Safety is enhanced by the following means: i) Extreme reduction of pipes penetrating the reactor vessel, by limiting to only those of the steam, the feed water and the safety valves, ii) Adoption of the water filled containment and the passive safety systems with fluid driven by natural circulation force, and iii) Adoption of the in-vessel type control rod drive mechanism, accompanying a passive reactor shut-down device. For improvement of economy, simplification of the reactor system and long operation of the core over five years without refueling with low enriched UO_2 fuel rods are achieved.

The radioactive materials should not be released to the environment as possible, even if a hypothetical accident, since the PSRD will be sited close to demand areas. Regarding reactor siting, JAERI has been studying concepts of nuclear barge[1], deep underground siting for supplying district heat at a city[2], and a seaside pit siting[3] besides a normal on-ground siting. Idea and concept of seaside pit siting are as follows.

In the safety evaluation concerning the reactor site, amount of radioactive material released to the environment should be estimated on the base of the accumulated inventory of its material inside the fuel rods that is released in the containment and leak rate of the containment by assuming a hypothetical accident. The leak rate is given as function of pressure difference between the inside and the outside of the containment during transient of an accident. This leak rate can be reduced by decreasing the pressure difference. If the outside pressure of the containment is higher than the inside pressure of it, leakage cannot happen to occur. The situation can be realized by submerging the containment in the deep water, that is, with help of high water pressure.

A reactor siting using water filled pit at a seaside is shown in Fig.3.2.1. The PSRD

module reactors are set inside pits made in the bedrock at a seaside and submerged in seawater, that is, the outside of the containment vessel is filled with seawater. Water depth of about 50 to 100m will enable the radioactive material to be confined in the containment for almost transient of hypothetical accident. The pit, of reinforced concrete, can be constructed by a Pneumatic caisson method, which is used in popular for basic construction such as bridges or tunnels. The seawater will be taken through the pipe and flow out to the waterway after circulating inside the pit by natural circulation force. This means that unlimited cooling water as the final heat sink can be provided.

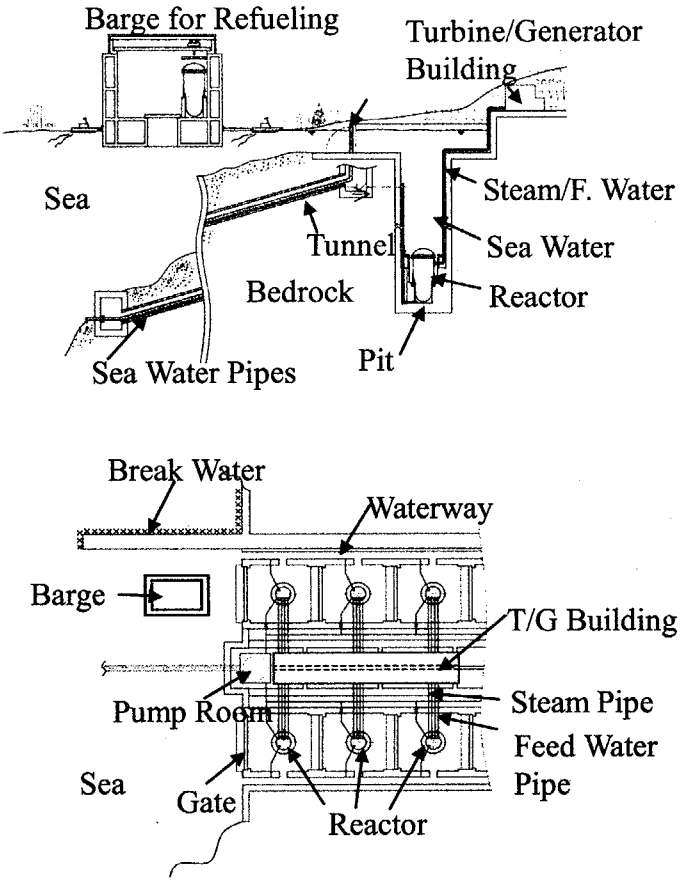

Fig.3.2.1 Reactor siting in seaside pit

Main issues to be clarified in practical use are i) corrosion of containment vessel with seawater, ii) earth quake resistance, iii) economic feasibility including pit construction cost, iv) operational procedure including refueling or maintenance. Concerning corrosion, its rate is, in general, very low at deep seawater over 10m. Lining of titanium alloy can be used in practice for undersea structures, and is said, effective over 100 years. On the earthquake, pit itself can provide enough strength and a rigid bedrock will support it. Preferably the pit in bedrock has advantages of being strong against earthquake and crash of a flying object. Pit construction cost is not so high in a preliminary cost estimation, and it will be lowered by rationalization under construction of the site.

The modular reactors are controlled at a central control station. Number of the reactors can be decided according to demand. Optimization of reactor operation can produce economical competitiveness for the system. The basic procedure of refueling is as follow.

An exclusive barge instead of the reactor building is used for refueling or periodical

maintenance of reactors. The barge is drawn to the place on the pit as shown in Fig. 3.2.2. Seawater in the pit is pumped out. The cover of containment is removed by using a crane and is placed on a bet of the barge. After removing the cover of reactor vessel together with the core internal and the INV-CRDMs, the fuel exchange facility is set on the containment. Spent fuels are withdrawn and set in the fuel cask. The spent fuels can be optionally stored inside the fuel storage coffin in the pit. New fuels carried are set in the reactor. The refueling procedure is desirable to be done by the all remote control system.

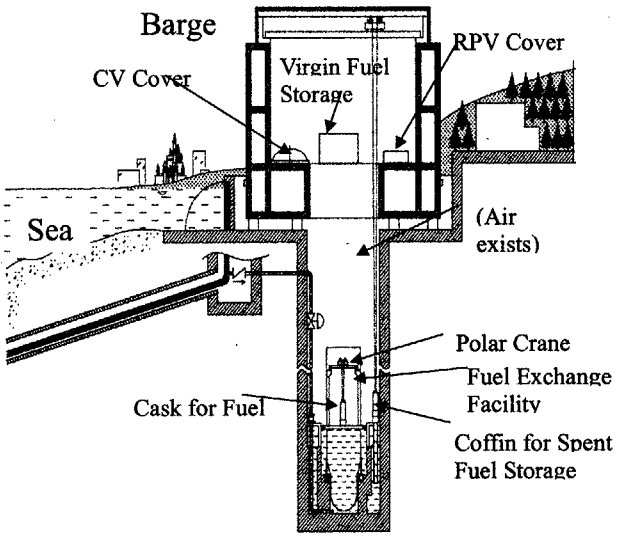

Fig.3.2.2 Concept of refueling

References

1) T. Ishida, et al.:"Proc. Int. Workshop on Utilization of Nuclear Power in Oceans", 55(2000)
2) S. Nakajima, et al.:"Proc. 7th Symposium on Power and Energy", JSME, 00-11, 225(2000) [in Japanese]
3) T. Ishida, et al.:"Proc. 17th Int. Conf. STRUCTUAL MECHNANICS in REACTOR TECHNOLOGY", SMIRT 17, Czech Republic, (2003)

4. Reactor Physics

For improvements of the calculation system, a capability of a continuous energy Monte Carlo code MVP has been enhanced and benchmark calculations for verification of nuclear data were done. The random number generator used in MVP has been upgraded by a vectorized 63-bit linear congruential generator with a period of ~9 x 10^{18}. Criticality evaluations for various light water moderated uranium fueled systems were carried out using MVP with different nuclear data files. Ratios of calculation to experiment values became smaller with the decrease of ^{235}U enrichment for each data file. Benchmark data for verification of nuclear data of fission products was obtained in the thermal critical facility TCA and calculations were done using MVP with JENDL-3.3. For a feasibility design study on an active nondestructive assay system by photon interrogation, MVP was modified to calculate the photonuclear reaction. The modified MVP code was found to have sufficient accuracy by the analysis of an experiment.

The experiments concerning reduced-moderation water reactor (RMWR), accelerator-driven subcritical reactor systems (ADS), thermal reactors and rock-like oxide (ROX) fueled cores were carried out. The mockup experiment with use of uranium fuel plates was carried out in the fast critical facility FCA for RMWR design study. Analyses were done with two different conventional systems and their results were compared. To study basic characteristics of ADS, measurements of subcriticality and fission rate distributions were carried out in FCA XXI-1 with use of tungsten to simulate accelerator target in ADS. To examine the calculation accuracy of the Doppler effects in thermal reactors, the ^{238}U Doppler effects were measured in FCA XXI-1D2. The experiments were analyzed by both the fast and thermal reactor analysis methods. The Doppler effects on resonance materials for ROX fueled cores were measured in the intermediate neutron spectrum of FCA XXI-1. Calculations agreed with the measurements for tungsten and thorium samples, while they overestimated that for an erbium sample.

Applicability of several experimental methods to subcriticality measurements was investigated. As for the inverse kinetics method, it was found that the measurement results depended on the regression model used in the Least Squares fitting when count rates were small. As for the noise experiment, the neutron detecting Feynman-α method was applicable to higher subcritical cores compared to other methods. As for the source multiplication method, the high-energy γ-ray detecting source multiplication method was found to be promising for high subcriticality measurements from a comparison of subcriticality measurements carried out in TCA with Monte Carlo calculations. In addition, the highly accurate reactivity measurement method for small samples was developed for TCA. Its error was minimized to be less than 2×10^{-6} dk/k.

4.1 Random Number Generator for MVP Version 2

Y. Nagaya and T. Mori
(*E-mail* : nagaya@mike.tokai.jaeri.go.jp)

MVP[1] has used the following 31-bit linear congruential generator (LCG) so far;

$$S_{k+1} = (32771S_k + 1234567891) \bmod 2^{31}, \quad (1)$$

where S_k is an integer and a random number in the interval [0,1) is generated by dividing S_k by 2^{31}. The multiplier and the additive constant are the same as those of the RANU2 routine in Fujitsu SSL-II library[2] and namely the same sequence of random numbers is produced as RANU2. The period of the generator is 2^{31} (~2 x 10^9) and is not long enough for today's fast computing platforms. In addition, we found that the generator fails the standard statistical tests[3] for random number generators (RNGs). Therefore, we have upgraded the MVP RNG. The new RNG is as follows;

$$S_{k+1} = (9219741426499971445S_k + 1) \bmod 2^{63}. \quad (2)$$

This is a 63-bit LCG and the period is 2^{63} (~9 x 10^{18}). This RNG is proposed by L'Ecuyer and has a good lattice structure from the viewpoint of the spectral test[4]. This RNG is also one of the RNGs for MCNP Version 5[5]. In the implementation, a vectorized algorithm has adopted and optionally preserves the random number sequence of the previous version.

TESTS FOR RNGS

The traditional MVP RNG and the new RNG have been subjected to the standard statistical tests described by Knuth[3], the DIEHARD test suite proposed by Marsaglia[6] and the spectral test. As a result, the traditional MVP RNG fails the serial and collision tests in the standard tests with L'Ecuyer's[7] and Vattulainen's[8] test parameters and fails the equidistribution, serial, poker, coupon, permutation runs-up, maximum-of-t and collision tests with Mascagni's test parameters[9]. For the results of the DIEHARD test suite, the traditional MVP RNG fails the binary rank for 32x32 matrices, bitstream, overlapping-pairs-sparse-occupancy, overlapping-quadruples-sparse-occupancy, DNA, count-the-1's on a stream of bytes tests and failures in less significant bits can be found for the birthday-spacings, binary rank for 6x8 matrices, count-the-1's for specific bytes tests. The MVP RNG also fails the

spectral test. On the other hand, the new RNG passes all the tests in the standard and DIEHARD test suites and the spectral test.

BENCHMARK CALCULATIONS

We performed benchmark calculations to verify consistency of results with the traditional and new RNGs. The calculational geometry is an infinite pin of the 2.4% UO_2 fuel for PWR[10]. Figure 4.1.1 shows the frequency of the k_{eff} values for hundred independent runs with different initial random numbers. The averaged results are listed in Table 4.1.1. The averaged k_{eff} value over hundred runs with the new RNG agrees with that of the traditional RNG within a standard deviation and no systematic difference can be found.

SUMMARY

We have upgraded the MVP RNG from a 31-bit LCG to a 63-bit LCG. We have also tested the LCGs and found that the traditional MVP RNG fails several RNG tests but the new RNG passes all the tests. We have verified that the new RNG gives consistent results with those obtained with the traditional RNG. No systematic difference can be found between the results with the traditional and new RNGs. The new RNG is to be implemented into MVP Version 2.

References

1) T. Mori, et al., JAERI-Data/Code 94-007 (1994) [in Japanese].
2) Fujitsu Ltd, Fujitsu SSL-II USER'S GUIDE, 99SP-4020-1 (1986) [in Japanese].
3) D.E. Knuth, The Art of Computer Programming – Vol. 2, pp. 1-170, Addison-Wesley (1991).
4) P. L'Ecuyer, Math. of Comp., 68, pp. 249-260 (1999).
5) F.B. Brown, et al., Trans. Am. Nucl. Soc., Vol. 87 , pp. 230-232 (2002).
6) G. S. Marsaglia, http://stat.fsu.edu/pub/diehard.
7) P. L'Ecuyer, Comm. ACM 31(6): pp. 742-749 (1988).
8) I. Vattulainen, et al., Comput. Phys. Comm. 86, 209 (1995).
9) M. Mascagni, et al., private communication (1999).
10) I. Soares, Nucl. Sci. Eng. 114, 160 (1993).

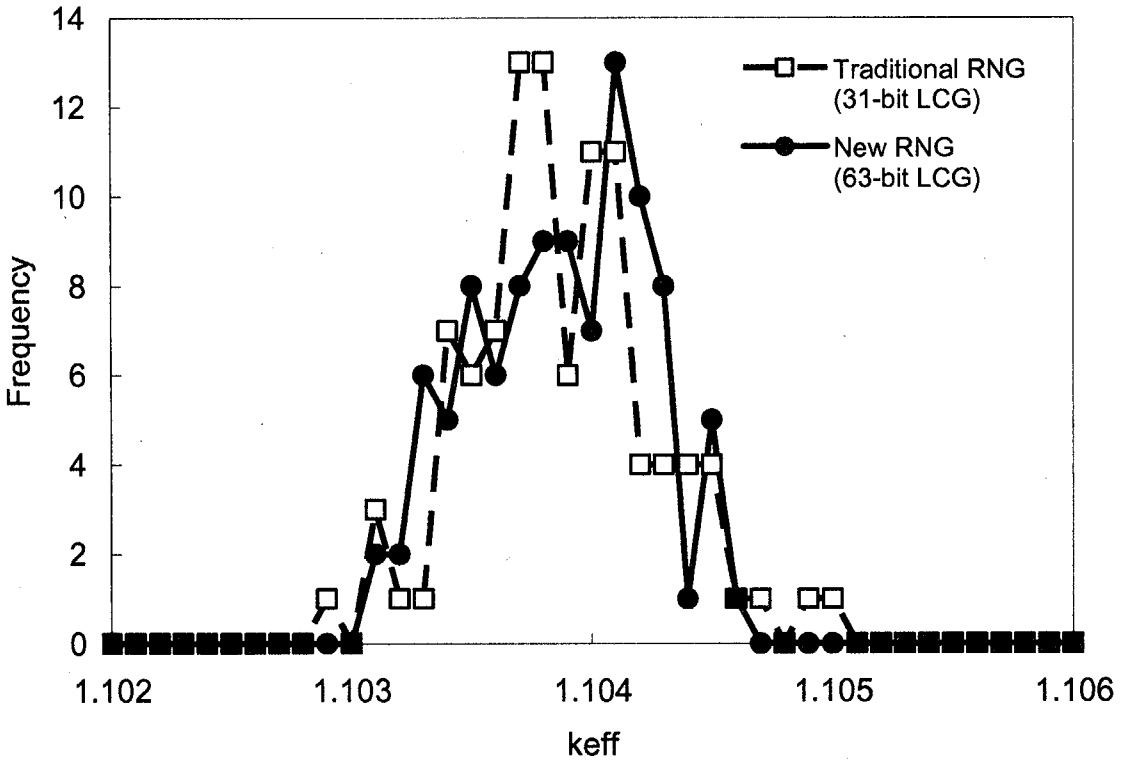

Fig. 4.1.1 Frequency of the k_{eff} values for 100 independent runs

Table 4.1.1 Averaged results for the benchmark problem

	New RNG (63-bit LCG)	Traditional RNG (31-bit LCG)
Averaged k_{eff} value over 100 runs	1.10382	1.10382
Apparent standard deviation	3.57E-04	3.60E-04

4.2 Investigation of Dependence of Criticality Evaluation Accuracy on U-235 Enrichment in Light Water Moderated Uranium Fueled Systems

K. Okumura and T. Mori
(*E-mail* : okumura@mike.tokai.jaeri.go.jp)

As a series of benchmark tests of JENDL-3.3[1], criticality benchmark calculations have been carried out for many thermal reactors[2]. In this study, the benchmark results are presented for light water moderated uranium fueled systems, aiming at investigating dependence of criticality evaluation accuracy on U-235 enrichment. Totally 39 cases of benchmark cores have been investigated as shown in Table 4.2.1. Most of them (No.1-No.26) are light water moderated uniform lattices of cylindrical UO_2 fueled pins at room temperature. Fuels of the TRX cores are exceptionally metal-uranium. Since there are a few experiments for medium or highly enriched UO_2 fueled cores, the benchmark cores are supplemented with the cores for uniform solution or plate type fueled systems moderated by hydrogen at room temperature (No.27-No.39).

All of the benchmark calculations were performed by using a continuous-energy Monte Carlo code MVP[3] and its four different nuclear data libraries generated from JENDL-3.2, JENDL-3.3, JEF-2.2 and ENDF/B-VI (R8). In each of the MVP calculations, the first 30 batches were skipped, and followed by 1,000 active batches with 10,000 particles per batch. Statistical errors (1σ) of k_{eff} values are within the range from 0.00015 to 0.00025. As far as the MISTRAL core is concerned, the MVP results are referred from the literature[4] published by NUPEC members, because detailed information to construct 3D modeling of the MISTRAL core is not opened. The JENDL-3.3 result for the MISTRAL core has not been reported yet.

As shown in Fig.4.2.1 (a), JENDL-3.3 underestimates the k_{eff} values for the cores with relatively lower U-235 enrichments, while it overestimates for the cores with highly U-235 enrichments. The deviation of the C/E values from unity is obviously depending on U-235 enrichment systematically. It should be noted that the dependence is not caused by the amount of uranium in the system but caused by the uranium enrichment, because the C/E vales hardly depend on the uranium concentration as shown in the results for the STACY experiments.

Similar dependence on U-235 enrichment is observed in Fig. 4.2.1 (b) for the results with the other nuclear data libraries. The calculated k_{eff} values in each core are generally

larger in the order of the JENDL-3.2, JEF-2.2, JENDL-3.3 and ENDF/B-VI (R8) results. Further investigation and improvement are required for the evaluation of U-238 or U-235 cross section data to dismiss the systematic dependence on U-235 enrichment in the criticality evaluation.

References

1) K. Shibata, *et al.*: "Japanese Evaluated Nuclear Data Library Version 3 Revision-3: JENDL-3.3," *J. Nucl. Sci. Technol.* **39**, 1125, (2002).
2) K. Okumura and T. Mori, "Integral Test of JENDL-3.3 for Thermal Reactors", Proc. of the 2002 Symposium on Nuclear Data, Nov. 21-22, 2002, JAERI, Tokai, Japan, pp.15-21, JAERI-Conf 2003-006 (2003).
3) T. Mori and M. Nakagawa, "MVP/GMVP: General Purpose Monte Carlo Codes for Neutron and Photon Transport Calculations based on Continuous Energy and Multigroup Methods," JAERI-Data/Code 96-018, (1996) (in Japanese).
4) T. Yamamoto *et al.*: "Core Physics Experiment of 100% MOX Core: MISTRAL," Proc. of Int. Conf. Global'97, Vol.1, 395 (1997).
5) NEA Nuclear Science Committee: "International Handbook of Evaluated Criticality Safety Benchmark Experiments," NEA/NSC/DOC(95)03, September 2002 Edition. (ICSBEP Handbook).

Table 4.2.1 List of benchmark cores

No	Core	U-235/ U	H/U	Remarks
1	TRX-1	1.3	3.3	Metal-U, Hexagonal lattice, Al clad. (11.506mmϕ)
2	TRX-2	1.3	5.6	Metal-U, Hexagonal lattice, Al clad. (11.506mmϕ)
3	KRITZ2:1	1.89	3.4	Zry-2 clad (12.25mmϕ), Boron:218ppm
4	KRITZ2:13	1.89	5.0	Zry-2 clad (12.25mmϕ), Boron:452ppm
5	B&W-XI*	2.46	5.4	Al-6061 clad (12.06mmϕ), Boron:1511ppm
6-8	TCA-1.50U*	2.6	4.3	3 cases of different loading patterns, Al clad (14.17mmϕ)

(to be continued)

Table 4.2.1 List of benchmark cores (continued)

9-13	TCA-1.83U*	2.6	5.3	5 cases of different loading patterns, Al clad (14.17mmϕ)
14-18	TCA-2.48U*	2.6	7.2	5 cases of different loading patterns, Al clad (14.17mmϕ)
19-23	TCA-3.00U*	2.6	8.6	5 cases of different loading patterns, Al clad (14.17mmϕ)
24	DIMPLE3*	3.0	3.0	SS clad (10.937mmϕ)
25	MISTRAL-C 1	3.7	5.1	By NUPEC, Zry-4 clad (9.5mmϕ), Boron:300ppm
26	DIMPLE7*	7.0	8.4	SS clad (8.324mmϕ)
27-33	STACY* 001-007	10.0	72~ 103	Nitrate solution in water reflected 600mmϕ cylindrical tank, 7 cases of different U concentrations: 310.1~225.3 gU/liter,
34	TRACY	10.0	7.2	Nitrate solution, 430g/liter, critical level:45.3cm with CR
35	JRR4-U20	20.0	-	U_3Si_2-Al dispersed fuel, minimum critical core (12 elements)
36	JRR4-U93	93.0	-	U.Al alloy, minimum critical core (12 elements)
37	KUCA-B(1:1)	5.4	9.56	EU:NU=1:1, B3/8"P33EU-NU-NU-EU(5)
38	KUCA-B(1:1)	9.6	13.4	EU:NU=2:1, B3/8"P36EU-NU-NU-EU(3)
39	KUCA-B(1:1)	93.0	9.3	EU:NU=1:0, B1/8"P80EU(2)

*Experimental data and benchmark models are taken from the ICSBEP Handbook[5)]

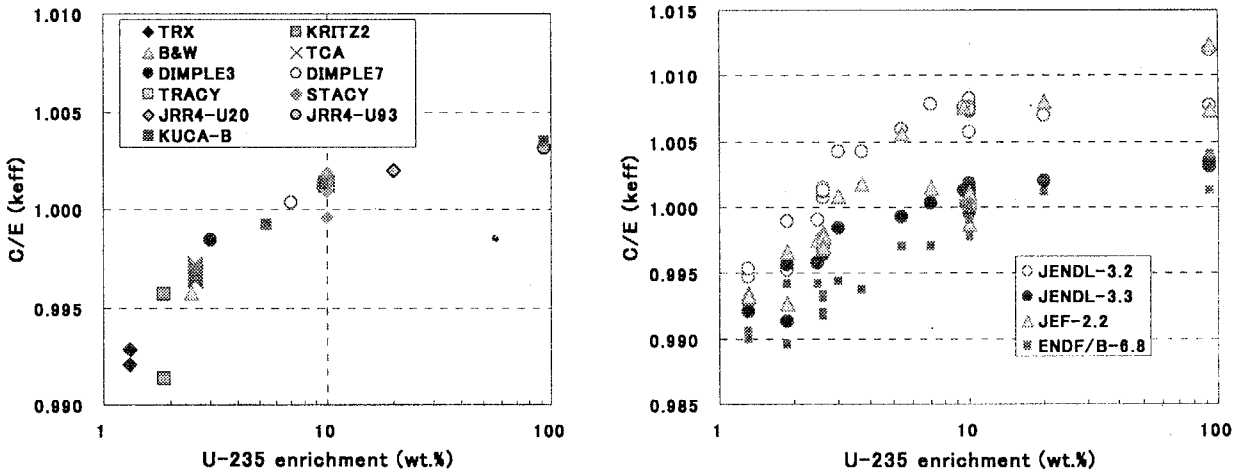

(a) (b)

Fig. 4.2.1 Dependence of C/E (*k-eff*) on U-235 enrichment

(a) JENDL-3.3 results, (b) Nuclear data library dependence

4.3 Experiments and Analyses for Evaluating Nuclear Data of FP Elements and Others

T. Suzaki, K. Okumura, K. Sugiura*, Y. Hoshi, K. Murakami, M. Kurosawa and S. Fujisaki
(*E-mail* : suzaki@mike.tokai.jaeri.go.jp)

Verification of nuclear data of fission product (FP) and minor actinide (MA) nuclides is becoming an important issue, especially for the purposes of designing higher burnup light water reactor fuel and the use of burnup credit in the criticality safety design of spent fuel storage and transportation facilities.

For obtaining the benchmark data concerning FP elements and others, a light-water-moderated 2.6%-enriched UO_2 fuel lattice core reflected by thick water reflector was constructed at the TCA, as shown in Fig. 4.3.1. The central 3x3 fuel-rods region (test region) was separated from the surrounding core region by an Al channel box of which outer dimension was 60 mm x 60 mm and the side-wall thickness was 2 mm. Into the moderator water in the test region, B, Cs, Nd, Er, Rh, Sm, Gd and Eu samples of natural isotopic compositions were solved, and the critical water level of each core was measured. The solution height was kept as 130 cm from the lower end of active fuel region of the outer rods. Since the channel box had a bottom-wall of 5 mm thickness, the lower end of active fuel region inside the channel box was higher than that of outer region by 5 mm. The total length of active fuel region of every rod was 144.2 cm. The temperatures of cores and solution samples were within 18±0.3℃ throughout this experiment. The element concentrations in solution samples and the critical water levels measured from the lower end of active fuel region of outer rods are listed in Table 4.3.1. By using the critical water levels, the reactivity effects (ρ) caused by the replacement of moderator water with the solution samples in the test region were evaluated as

$$\rho\,(\%\,\delta\,k/k) = K\beta_{eff}[(\pi/(H_0+\lambda))^2-(\pi/(H+\lambda))^2], \qquad (1)$$

where K: buckling coefficient of reactivity (4288 $\$cm^2$),[1)]

β_{eff}: effective delayed neutron fraction (0.760% δ k/k),[1)]

λ : sum of extrapolation length at the upper and the lower ends of core (12.2 cm),[1)]

H_0, H: critical water level when the test region contains pure water or solution sample.

The results are also shown in Table 4.3.1.

The k_{eff} values of the critical cores were calculated by the Monte Carlo code MVP[2)] with the latest Japanese nuclear data library JENDL3.3[3)]. The core configuration was exactly

*Nagoya University

modeled, and 20 millions neutron history was traced for every case where the standard deviation of k_{eff} value (σ) was about 0.018% δ k/k. The results of calculated k_{eff} are given in Table 4.3.1 with the differences Δk(%) from the case of pure water.

As seen in the table, the values of Δk for the cases other than B are within about 4 σ, suggesting that the nuclear data of Cs, Nd, Er, Rh, Sm, Gd and Eu in JENDL3.3 are satisfactory. As for the case of B, low solubility of boric acid in water could make some problem in the procedure to take the solution sample for chemical analysis. We are considering an additional experiment for the case of B with a proper care in solution sampling.

References:

1) T. Suzaki, et al.: "Precise Determination of β_{eff} for Water-Moderated U and Pu-U Cores by a Method Using Buckling Coefficient of Reactivity", Proc. ICNC'99, Versailles, France, p.386(1999).

2) T. Mori, et al.: "Vectorization of Continuous Energy Monte-Carlo Method for Neutron Transport Calculation", J. Nucl. Sci. Technol., 29, p.325(1992).

3) K. Shibata, et al.: "JENDL-3.3: A New Version of JENDL General-purpose Library", J. Nucl. Sci. Technol., 39, p.1125(2002).

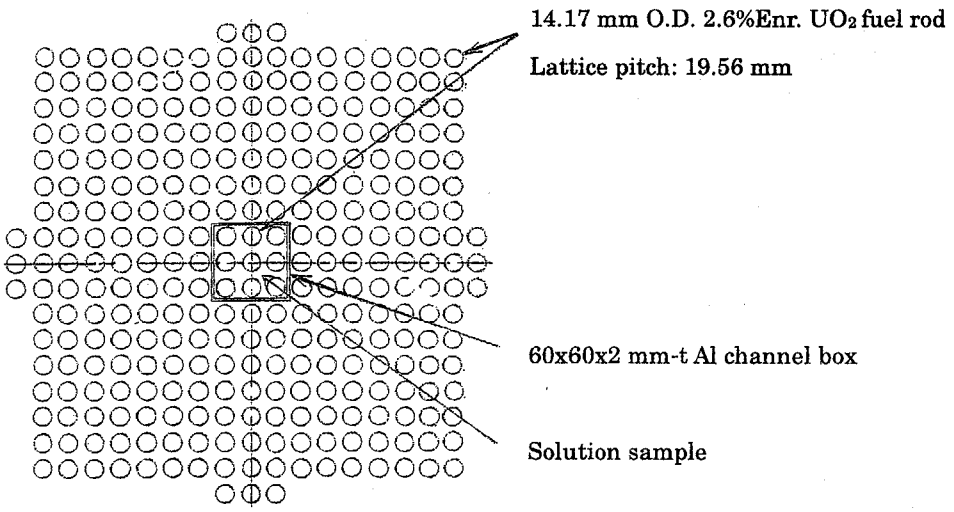

Fig. 4.3.1 Plan of experimental core

Table 4.3.1 Results of experiments and analyses

Sample	Element concentration (g/l)	Critical water level (cm)	$-\rho$ (% δ k/k)	Calculated k_{eff}	Δk(%)
H_2O	-	96.71	0	0.99689	0
H_3BO_3	0.760	122.85	0.948	1.00037	+0.348
$CsNO_3$	70.9	106.56	0.431	0.99658	-0.031
$CsNO_3$	33.4	101.45	0.222	0.99692	+0.003
$Nd(NO_3)_3$	53.0	102.91	0.284	0.99710	+0.021
$Nd(NO_3)_3$	27.9	99.49	0.133	0.99701	+0.012
$Er(NO_3)_3$	51.1	131.54	1.155	0.99644	-0.045
$Er(NO_3)_3$	24.3	112.30	0.637	0.99697	+0.008
$Rh(NO_3)_3$	13.2	106.69	0.436	0.99609	-0.080
$Sm(NO_3)_3$	1.08	117.86	0.810	0.99763	+0.074
$Gd(NO_3)_3$	0.390	118.09	0.817	0.99632	-0.057
$Eu(NO_3)_3$	2.06	111.64	0.614	0.99652	-0.037
Error:	<2%	<0.03 cm	<3%	1 σ ≒0.018%	0.025%

4.4 Development of Active Nondestructive Assay Technique by Photon Interrogation for Uranium Bearing Waste*
-(1) Development of Code System for Feasibility Design Study of Assay System-

T. Sakurai, M. Haruyama, T. Mori and K. Kosako†
(*E-mail* : sakurai@tru.tokai.jaeri.go.jp)

A feasibility design study has been carried out in JAERI on an active nondestructive assay system by photon interrogation for uranium bearing waste [1]. Figure 4.4.1 shows a schematic view of the assay system which consists of an electron Linac(7~15 MeV) with a target as the Bremsstrahlung photon source, ^{3}He neutron detectors and the waste contained in a drum of 200 liter. In this system, the waste is exposed to the photons and the uranium in the waste is detected by counting neutrons of a photonuclear reaction of uranium.

This design study needs a coupled neutron/photon transport code which can calculate the photonuclear reaction. In the present work, JAERI's continuous-energy Monte Carlo transport code MVP [2] has been modified and equipped with the function to calculate the photonuclear reaction and a resultant emission of photoneutrons. A photonuclear cross section library of more than 180 nuclides has also been prepared for this code by processing evaluated photonuclear data files of Japan, Korea, USA, Russia and China [3]. This library covers almost all the nuclides that should be taken into consideration in calculations for the present design study.

The modified code has been verified by analyzing an old experiment using an electron Linac of its energy range between 10 to 36 MeV with 'thick' targets of various materials(C, Al, Cu, Ta, Pb and U) [4]. In this experiment, total neutron yields from these targets were measured as a function of incident electron energy. All of these targets were 11.4-cm square with various thickness. The diameter of incident electron beam spot at the target was approximately 1.3 cm.

As the MVP code has no capability to calculate the transport of electrons, MCNP code[5] was used for the calculation of electron transport in the target and the photon generation by the Bremsstrahlung. The MCNP results were used as the photon source in the MVP code for the analysis of neutron yields. Figure 4.4.2 shows the geometry of target used in the present analysis. The neutron yields were calculated by tallying all the neutrons that leaked from the target.

Figure 4.4.3 presents the results of analysis based on photonuclear data file of JENDL(Japanese Evaluated Nuclear Data Library) for the uranium target. The calculated neutron yields are in good agreement with the measured ones almost within the experimental uncertainty of 15 %. The analysis has been performed also for the other targets of C, Al, Cu, Ta and Pb. Most of these calculated results agree with the measured ones within 30%. From this analysis, the modified MVP code is found to have sufficient accuracy for the present feasibility study.

*This study was conducted as the contract research from the Ministry of Education, Culture, Sports, Science and Technology.
†Sumitomo Atomic Energy Industries,Ltd.

Rcferences:

1) T. Sakurai M. Haruyama T. Mori and K. Kosako, "Development of Active Nondestructive Assay Technique by Photon Interrogation for Uranium Bearing Waste -(1) Development of Code System for Conceptual Design Study of Assay System-", to be published in JAERI Conf. [in Japanese]
2) T. Mori *et al*, "Vectorization of Continuous Energy Monte Calro Method for Neutron Transport Calculation", J. Nucl. Sci. Technol., 29, 325 (1992).
3) P. Obložinský, "Photonuclear Data", J. Nucl. Sci. Technol., Supplement 2, 31 (2002).
4) W.C. Barber and W.D. George, "Neutron Yields from Targets Bombarded by Electrons", Phys. Rev. 116(6), pp.1551-1559 (1959).
5) J.F. Briesmeister(ed), "MCNP™ - A General Monte Carlo N-Particle Transport Code Version 4C", LA-13709-M (2000).

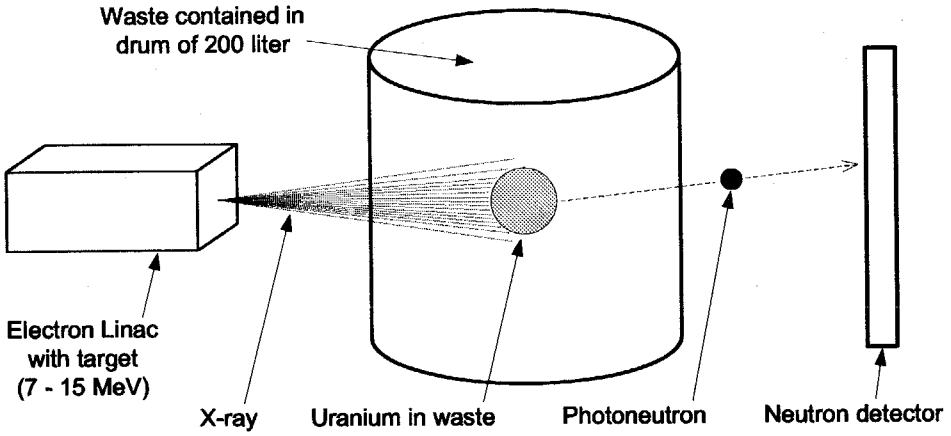

Fig.4.4.1 Schematic view of active nondestructive assay system by photon interrogation for uranium bearing waste

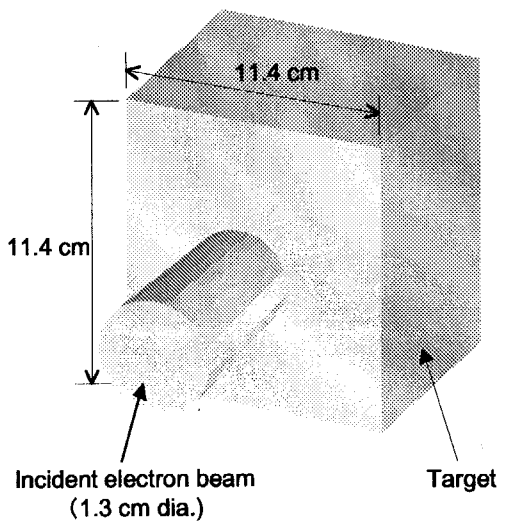

Fig.4.4.2 Geometry of target used in analysis of experiment

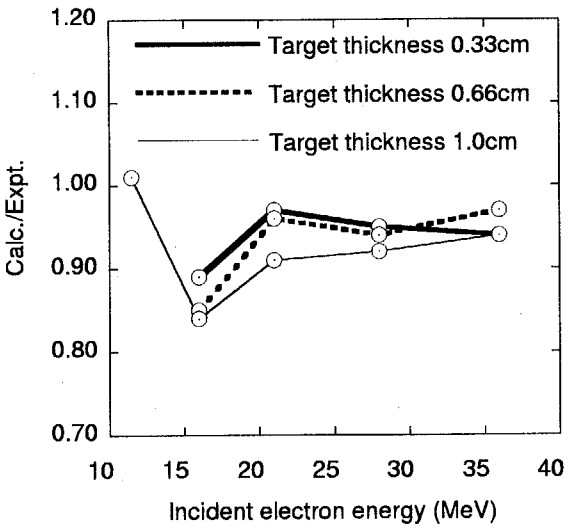

Fig.4.4.3 Results of analysis for neutron yields from uranium targets

4.5 Critical Experiment Using Uranium Fuel Plates for Design Study of Reduced-Moderation Water Reactor (RMWR) in FCA

S. Okajima, T. Yamane and M. Andoh
(*E-mail:* okajima@fca001.tokai.jaeri.go.jp)

To estimate the accuracy of prediction of core characteristics in the design study of RMWR, a program of critical experiments was planned at the fast critical facility, FCA. This program consisted of two phases; the first phase critical experiments in the mock-up core composed of uranium fuel plates and the second ones in the mock-up core composed of a combination of uranium and plutonium fuel plates to simulate MOX fuel. The principal aim of the first phase experiment is to study the basic characteristics of the RMWR core. In this paper the first phase experiments were described.

The first phase FCA-RMWR core, XXI-1D, is a coupled system of a central test zone and a driver zone. As shown in Fig. 4.5.1, the test zone is approximately represented by a rectangular prism with about 38 cm in square base and 61 cm in height. It is surrounded by the enriched U driver zone and two blanket zones; an inner blanket zone of 30cm in thickness containing a significant amount of depleted uranium oxide and sodium, and an outer blanket zone of 15cm in thickness containing only depleted uranium metal. The test zone is composed of a combination of uranium fuel plates and moderator material (foamy polystyrene) plates to simulate the neutron energy spectrum of RMWR (Fig. 4.5.2). The cell averaged fissile enrichment of the test zone is 15 atomic % of ^{235}U and the hydrogen to uranium atomic number ratio (H/U) is 0.5.

The following parameters were measured: criticality (keff value), central fission rate ratios, central sample reactivity worth and so on.

Since the nuclear reactions dominantly occur in the intermediate neutron energy range, two different conventional calculation systems were used to analyze the experiment and their results were compared; the SRAC code system[1] and a standard calculation code system for a fast reactor (FR code system).

The cell averaged effective cross sections for each cell were obtained by the collision probability calculation with a one-dimensional infinite slab model and the group constant set generated from the JENDL-3.2 library [2]. The effective cross sections in the resonance energy range were calculated by the table-look-up method of resonance shielding factors based on the narrow resonance approximation. The criticality and the forward and adjoint fluxes were obtained from the three-dimensional transport calculation code

THREEDANT[3] with P0-S8 approximation.

The typical experimental and calculated results are shown in Table 4.5.1. Both calculation code systems overestimate the criticality by about 2%. In the transport calculation, the anisotropic effect of neutron leakage caused by the plate-type fuel and materials cannot be considered. When the effect is considered, the calculated value will become about 1~2% smaller. When we compare the central fission rate ratios between the calculation and the experiment, the calculation overestimates $^{238}U/^{235}U$ and $^{237}Np/^{235}U$, and underestimates $^{239}Pu/^{235}U$. From these results, both calculation code systems have a tendency to give a harder neutron spectrum. When we compare the C/E values of $^{239}Pu/^{235}U$ between SRAC and FR systems, the latter system gives about 20% larger value than the former one. This difference comes from the smaller effective fission cross sections for ^{235}U by the FR system in comparison with those obtained by the SRAC code system.

Acknowledgement

Portion of the present study was supported by the governmental funding from the innovative and viable nuclear energy technology (IVNET) development project operated by the Institute of Applied Energy (IAE).

References

1) K. Okumura, K. Kaneko and K. Tsuchihashi: "SRAC 95 ; General Purpose Neutronics Code System", JAERI-Data/Code 96-015 (1996).
2) T. Nakagawa, et al.: J. Nucl. Sci. Technol., 32, 1259-1271 (1995).
3) R. E. Alcouffe, et al.: "DANTSYS: A Diffusion Accelerated Neutron Particle Transport Code System", LA-12969-M (1995).

Table 4.5.1 Typical results in the first phase FCA-RMWR experiment

Parameter	Experiment	Calculation*	
		SRAC	FR
Criticality (keff)	1.00267±0.00017	1.02235 (1.0196)†	1.01824 (1.0155)
Fission Rate Ratio			
$^{239}Pu/^{235}U$	1.539±4.3%	1.287 (0.836)	1.519 (0.987)
$^{238}U/^{235}U$	0.0199±5.8%	0.0218 (1.095)	0.0219 (1.101)
$^{237}Np/^{235}U$	0.145±5.4%	0.154 (1.062)	0.150 (1.034)

* Diagonal Transport Calculation with P0-S8 Approximation.

† Value in parentheses shows C/E value.

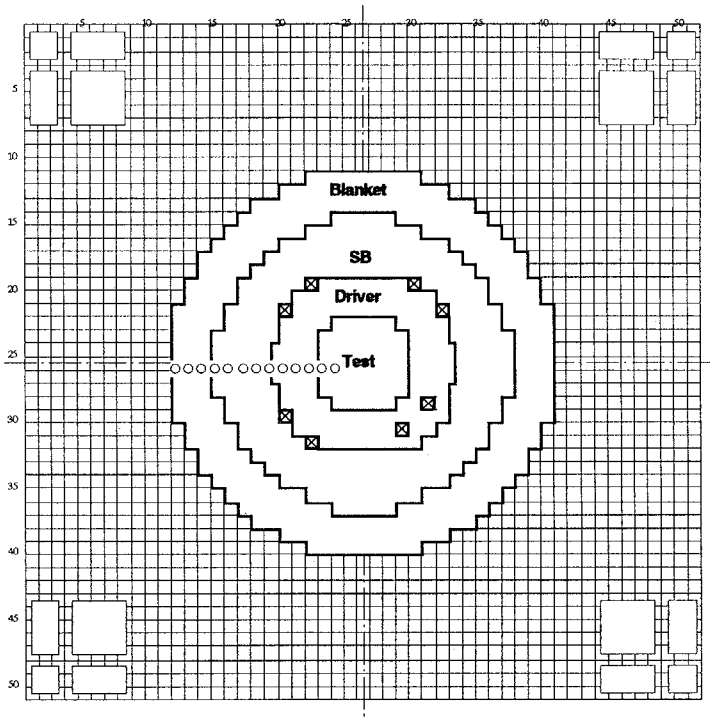

Fig. 4.5.1 Cross-section view of the first phase FCA-RMWR core

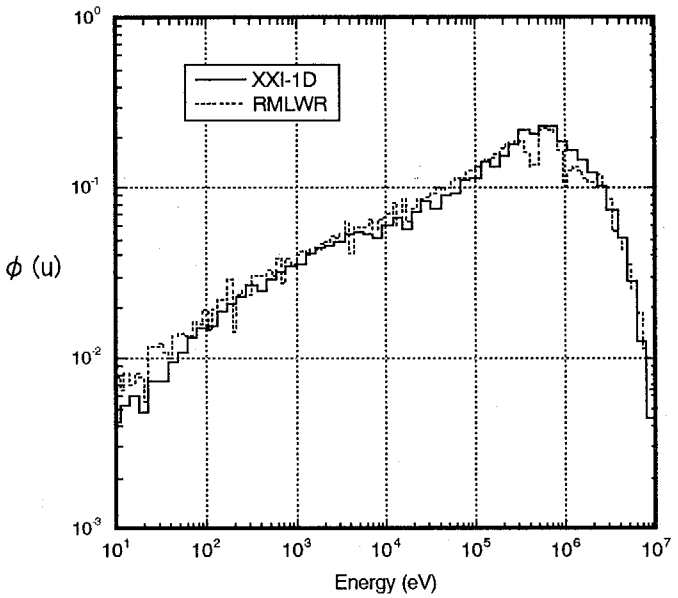

Fig. 4.5.2 Calculated neutron energy spectra

4.6 Evaluation of Doppler Effect in Thermal Reactor at FCA - (I) Experiment in a Uranium Fueled Core -

M. Andoh, K. Kawasaki and S. Okajima
(*E-mail:* andoh@fca001.tokai.jaeri.go.jp)

The Doppler effect is one of the most important feedback effects in the case of reactivity accidents. The Doppler effect has been measured in various neutron spectra and fuel composition in the developement of fast reactor, while few experimental data has been evaluated for thermal reactor cores since 1970's. To examine the calculation accuracy of the Doppler effect in thermal reactor, measurement of the ^{238}U Doppler effect aimed at lower energy region than 100eV was planned at Fast Critical Assembly (FCA). The Doppler effect is measured in a uranium fueled XXI-1D2 core and in MOX fueled XXII-1 series cores in this plan. The neutron spectra are varied adjusting the atomic number ratio between hydrogen and heavy metal nuclide (H/HM) of the fuel with the use of different void fraction of polystyrene plates as the moderator in the MOX fueled XXII-1 series cores to obtain experimental data in the different spectra. Core characteristics of the FCA cores are listed in Table 4.6.1. The neutron spectra at the center of the cores are compared amang the FCA cores in Fig. 4.6.1. Figure 4.6.1 shows that intermediate neutron spectra are formed in the FCA cores and those of the XXI-1D2 and XXII-1(65V) cores are similar. It also shows that those of the XXII-1 series cores varies in wide range depending on the void fraction of the polystyrene plates of each core.

As the first phase of this study, the Doppler effect was measured in the XXI-1D2 core. The Doppler effect was measured as the sample reactivity change between the heated and unheated samples (*i. e.,* Doppler reactivity worth). Various composition/size of cylindrical uranium samples are used to measure the Doppler effect of ^{238}U. Each Doppler sample was heated up to 1073 K by an electric heater set in the capsule at the center of the core. Table 4.6.2 shows the diameter and weight of each Doppler sample and the experimental results at 1073K. Length of all the samples is 150 mm.

The experiments were analyzed by two different calculation methods: the standard analysis method for FCA fast reactor (the FCA analysis system)[1),2)] and the standard analysis method for thermal reactor (the SRAC system)[3)]. The nuclear data library used for the calculations is JENDL-3.2 [4)]. The effective cross sections of the Doppler samples were calculated with one-dimensional cylindrical geometry using the PEACO-X code[5)] and the PEACO routine [3)] for the FCA analysis system and the SRAC system, respectively. The Doppler reactivity worths were calculated by first-order perturbation theory[6)] by replacing the

cross section of the Doppler sample at 293 K with the cross sections at the other temperatures. The C/E values of the Doppler reactivity worth (from 293 K to 1073 K) by both the analysis system are listed in Table 4.6.2. From the table, followings are pointed out :

1) There is a tendency for both the systems to overestimate the measured values by 3 to 9 %.
2) There is little dependence of the C/E values on the samples.
3) Both the analysis systems give similar C/E values.

Measurement of the Doppler effect is being continued in the MOX fueled XXII-1 series cores. In the next phase of this study, the Doppler effect is measured in the XXII-1(65V) core, where the neutron spectrum is similar to that in the XXI-1D2 core.

Acknowledgments

This experiment project was carried out under the collaboration agreement between JAPCO and JAERI.

References

1) M. Nakagawa and K. Tsuchihashi :JAERI 1294(1984).
2) T. B. Fowler, D. R. Vondy and G. W. Cummingham : "Nuclear Reactor Analysis Code; CITATION", LA-4432 (1970).
3) K. Okumura, K. Kaneko and K. Tsuchihashi : JAERI-Data/Code 96-015 (1996).
4) T. Nakagawa, et al. : "Japanese Evaluated Nuclear Data Library version 3 revision-2: JENDL-3.2", J. Nucl. Sci. and Technol., 32, 1259(1995).
5) S. Okajima, H. Oigawa and T. Mukaiyama: "Resonance Interaction Effect between Hot Sample and Cold Core in Analysis of Doppler Effect Measurement", J. Nucl. Sci. and Technol., 31, pp.1097-1104 (1994).
6) S. Iijima and S. Okajima : JAERI-Data/Code 2002-023(2002).

Table 4.6.1 Core characteristics of the XXI-1D2 and XXII-1 series cores

	U core	MOX core		
Characteristics	XXI-1D2	XXII-1(45V)	XXII-1(65V)	XXII-1(95V)
Void fraction of polystyrene	80%	45%	65%	95%
Enrichment	15% ^{235}U	16% Pu-f*	16% Pu-f	16% Pu-f
V_M/V_F**	1.7	0.6	0.6	0.6
H/HM	0.50	0.81	0.52	0.09

* : (^{239}Pu+^{241}Pu)/(U+Pu+Am)
**: Volume ratio between moderator and fuel

Table 4.6.2 Results of the measurement and analysis of the Doppler reactivity worths in the XXI-1D2 core (293 => 1073 K)

Sample	Diameter (mm)	Mass of ^{238}U (g)	Expt. ($x10^{-5}\Delta k/k$)	C/E value FCA*	C/E value SRAC**
U-metal-25	24.8	1337	-4.60±4%	1.07	1.05
U-metal-20	20.0	863	-3.22 ±5%	1.05	1.03
UO_2-25	25.0	601	-2.74 ±6%	1.09	1.07
UO_2-20	20.0	374	-1.87 ±9%	1.07	1.05

* : the FCA analysis system was used

**: the SRAC system was used

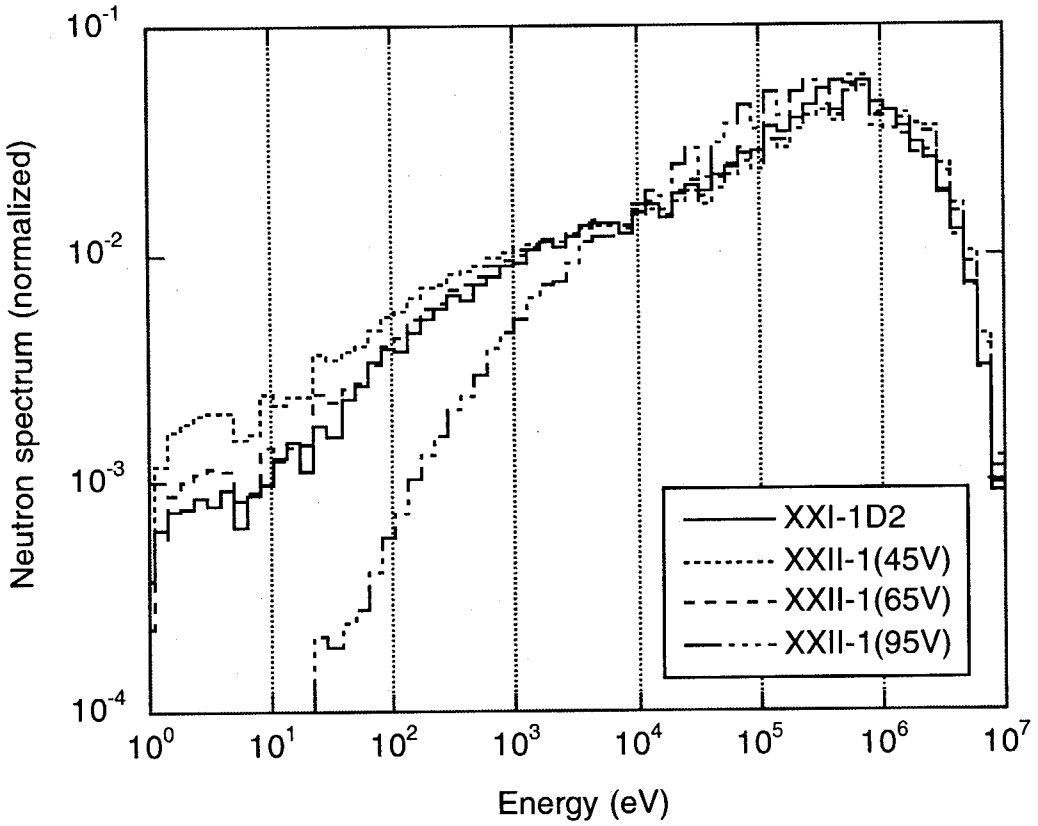

Fig. 4.6.1 Comparison of neutron spectra amang the XXI-1D2 and XXII-1 series cores

4.7 Doppler Effect Measurement on Resonance Materials for Rock Like Oxide Fuels in an Intermediate Neutron Spectrum

M. Andoh, Y. Nakano, S. Okajima and K. Kawasaki
(*E-mail:* andoh@fca001.tokai.jaeri.go.jp)

As a Rock-like oxide (ROX) fuel contains only small amounts of fertile materials, the ROX fueled Light Water Reactor (LWR) may have reactivity coefficient problems such as insufficient Doppler effect. To examine the calculation accuracy of the Doppler effect of resonance materials for ROX fuels, a series of the Doppler effect experiments on certain resonance materials has been carried out at the FCA. As the first phase of this study, the Doppler effect was measured in an FBR simulated core (FCA XX-2 core) [1], since the measurement equipment was developed for the measurements in fast reactor cores. The purpose of the present, second, phase of this study, is to obtain experimental data of the Doppler effect in softened neutron spectrum and to examine the calculation accuracy of a conventional calculation code for thermal reactor, the SRAC system [2].

The Doppler effect was measured in the FCA XXI-1 core. An intermediate neutron spectrum is formed at the center of the test zone that consists of plates of enriched uranium, natural uranium, polystyrene and stainless steel. The averaged ^{235}U enrichment of the test zone is 15%. The atomic number ratio of hydrogen to ^{235}U of the test zone is 3.3. The calculated neutron spectra in the core are compared among both the FCA cores and a typical ROX fueled LWR with weapon-grade plutonium [3] in Fig. 4.7.1. This shows that the spectrum in the core of the present phase of this study is intermediate one between those in the FBR (XX-2 core) and the ROX fueled LWR. Cylindrical Doppler samples of the resonance materials, such as erbium metal (Er), tungsten metal (W) and thorium dioxide (ThO_2), were used. The natural uranium metal and dioxide (U-metal and UO_2, respectively) samples were also used, to obtain reference data. The Doppler samples are 150 mm in stack length and 23 (25 for the uranium samples) mm in diameter. Each Doppler sample was heated up to 1073 K by an electric heater set in the capsule at the center of the FCA core. The Doppler effect was measured as the sample reactivity change between the heated and unheated samples (*i. e.*, Doppler reactivity worth). The measured Doppler reactivity worths in the XXI-1 core are listed in Table 4.7.1.

Calculations of the Doppler reactivity worth were performed using the SRAC system with a 101-group energy structure. The nuclear data library used for the calculations is JENDL-3.2 [3]. As for the Er sample, nuclear data of the JENDL-3.3 library [4] were used. The effective cross sections of the Doppler samples were calculated with one-dimensional cylindrical

geometry using PEACO, a collision probability routine with an ultra fine energy structure, to consider resonance interaction effect between the sample and the adjacent core. Neutron flux distributions with the Doppler samples at room temperature (293 K) at the core center were obtained by diffusion calculations in two-dimensional R-Z geometry using the CITATION module of the SRAC system. The Doppler reactivity worths were calculated by first-order perturbation theory by replacing the cross sections of the Doppler samples at 293 K with those at the other temperatures.

The C/E values of the Doppler reactivity worth (from 293 K to 1073 K) are listed in Table 4.7.1 together with those in the XX-2 core [1]. The calculated Doppler reactivity worth of the W and ThO_2 samples agreed with the measured values within the experimental error. There is a tendency for the C/E values for the resonance material samples in the present core to be bigger than those in the XX-2 core. The calculation overestimated the experiment for the Er sample by 12%, while it showed a good agreement with the measurement in the XX-2 core. There is a tendency that the calculations give smaller C/E values for the W sample relative to the other samples in both the cores. To investigate the result of the Er sample, the transport calculation was carried out using the TWODANT [5] code with JAERI's 70-group constant set (JFS-3-J3.2). The transport calculation gave the result that the transport effect, the ratio of the calculated Doppler reactivity worth between the transport and diffusion calculations, on the Er sample was −12.7%, while the effects on the other samples were about -7%. The C/E value of the Er sample was improved to be 0.98 with the correction of the transport effect. The transport corrected C/E value for the W sample, however, was 0.92. This means that the calculation underestimates the measured value beyond the experimental error of 5%. Tungsten has a giant resonance cross section around 6 eV. It is considered that there is a problem with the calculated effective cross section of the W sample or with the nuclear data library itself.

It has been confirmed that the calculation method using the SRAC system had good accuracy for the analysis of the experiment both for the fast and the intermediate neutron spectrum throughout the series of the experiments except for the tendency of the underestimation for the W sample in both the spectra and the overestimation for the Er sample in the intermediate neutron spectrum.

References

1) Y. Nakano, et al. : Progress in Nuclear Energy, 38, 343 (2001).
2) K. Okumura, K. Kaneko and K. Tsuchihashi, JAERI-Data/Code 96-015 (1996).
3) H. Akie, et al., : Proc. Int. Conf. on Future Nuclear Systems (Global '97), October 5-10,

1997, Yokohama, Japan, Vol. 2, 1136 (1997).

4) T. Nakagawa, et al. : J. Nucl. Sci. and Technol., 32, 1259 (1995).

5) K. Shibata, et al.: J. Nucl. Sci. and Technol., 39, 1125 (2002).

6) R. E. Alcouffe, et al : LA-12969M (1995).

Table 4.7.1 Results of the experiment and analysis of the Doppler reactivity worths (293 => 1073 K)

Sample	XXI-1		XX-2
	Expt. ($x10^{-5}\Delta k/k$)	C/E	C/E
Er	-5.07±0.17	1.12±3.3%*	0.98±6.6%
W	-3.59±0.18	0.99±5.0%	0.89±8.9%
ThO_2	-3.11±0.16	1.04±5.1%	0.99±12%
U-metal	-4.60±0.18	1.05±3.9%	1.06±6.6%
UO_2	-2.74±0.16	1.07±5.8%	1.03±11%

* Experimental error (relative error)

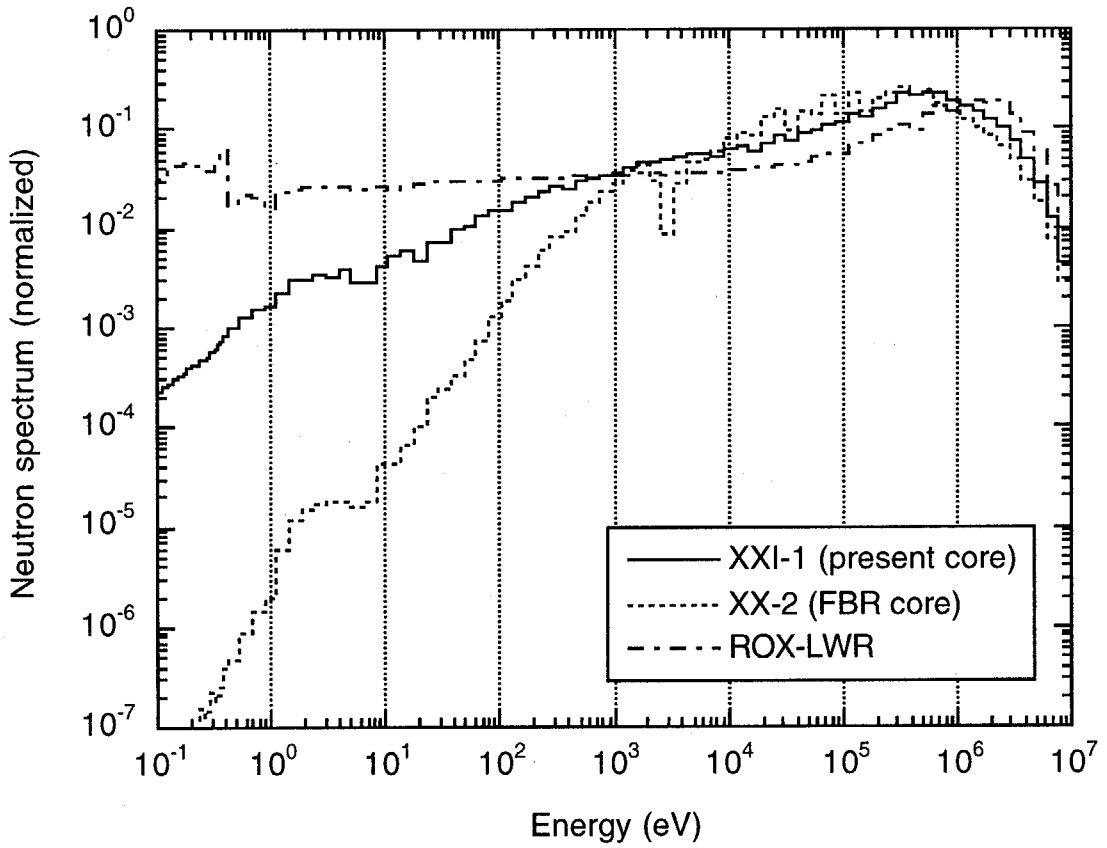

Fig. 4.7.1 Comparison of the neutron spectra amang the XXI-1, XX-2 and ROX-LWR cores

4.8 Effects of Statistical Fluctuation in Negative Reactivity Measurement by Inverse Kinetics Method

K. Iwanaga*, T. Yamane, K. Nishihara, S.Okajima, H.Sekimoto† and T. Asaoka††
(*E-mail*: iwanaga@fca001.tokai.jaeri.go.jp)

When the reactivity ρ and the source intensity S are determined by the inverse kinetic method (the IK method), the measurement errors depend on the fluctuation of count rate of the neutron detector. In this study, the effect of the fluctuation in the data processing procedures was investigated.

The experiments were performed in the core that consists of the enriched uranium (93%) and the stainless steel. The core was kept in a subcritical state. A neutron source of ^{252}Cf was put in the core. Three neutron detectors were used: two in-core monitors of ^{235}U fission chamber and one out-of-core monitor of the linear power channel for reactor operation. Figure 4.8.1 shows the positions of the neutron source and of the fission chambers. The reactivity of -5.5 dollars was inserted into the subcritical state of 0.5 dollars. The raw output data of each neutron detector after the reactivity insertion is shown in Fig. 4.8.2. From the figure it is clear that the fluctuation of output the neutron detector P1 is larger than those of the other detectors. In the data processing procedure, the following different methods were used: the Least Square method (LS) with two different regression models (LS-3 and LS-4) ‡), the Memorial Index method (MI) [1] and the Maximum Likelihood method (ML) [2].

The measurement results obtained by each neutron detector are summarized in Table 4.8.1. The results by the Source Multiplication method (SM) are also shown as the reference.

The measured results are compared among the data processing procedures. In the case of usage of detector ch5, the reactivities and the source intensities in each method agree well within 0.8% and 1.4%, respectively. In the case of detector M8, those agree with each other within 1.1% and 1.7%, respectively. On the other hand, when the detector P1 is used, the LS-4 method gives poor results. In this method, the output data $n(t_i)$ are fitted to a linear function $\rho' n(t_i) = \rho n(t_i) + \Lambda S$ and the values of ρ and S are determined so that the summation $\sum_i (\rho' n(t_i) - (\rho n(t_i) + \Lambda S))^2$ is minimized. Here the reactivity ρ' is the apparent reactivity that does not include the effect of source intensity.

---

*Fellow of Advanced Science from Tokyo Institute of Technology
† Tokyo Institute of Technology
†† Tokai University
‡ S. Tamura, "Reactivity Analysis by Inverse Kinetics Method, Effect of Signal Fluctuation", Proc. of 2001-Fall meeting of Atomic Energy Society of Japan, pp493 (2001).

In the data fitting, the statistical fluctuation of detector counts is assumed to follow the Gaussian distribution while the practical one differs from it because of small count rates. Consequently the poor result is obtained.

When we compare the results between the IK methods and the SM method, the results agree well within the experimental errors in the case of usage of the ch5 detector.

Through the experiment, it was found that the measurement results depended on the regression model used in the LS method when count rates were small.

References

1) A. Kitano, M. Itagaki and M. Narita, "Memorial-Index-Based Inverse Kinetics Method for Continuous Measurement of Reactivity and Source Strength", J. Nucl. Sci and Technol., 37, pp.53-59 (2000).

2) K. Nishihara, K. Iwanaga, T. Yamane and S. Okajima, "Determination of Reactivity and Source Intensity Based on the Maximum Likelihood Method", JAERI-Research 2002-030 (2002)[in Japanese].

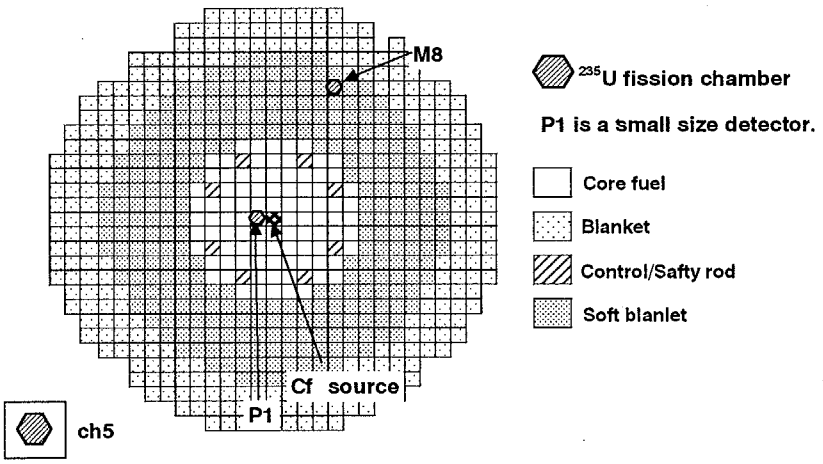

Fig.4.8.1 Cross section view of the core and detector arrangement

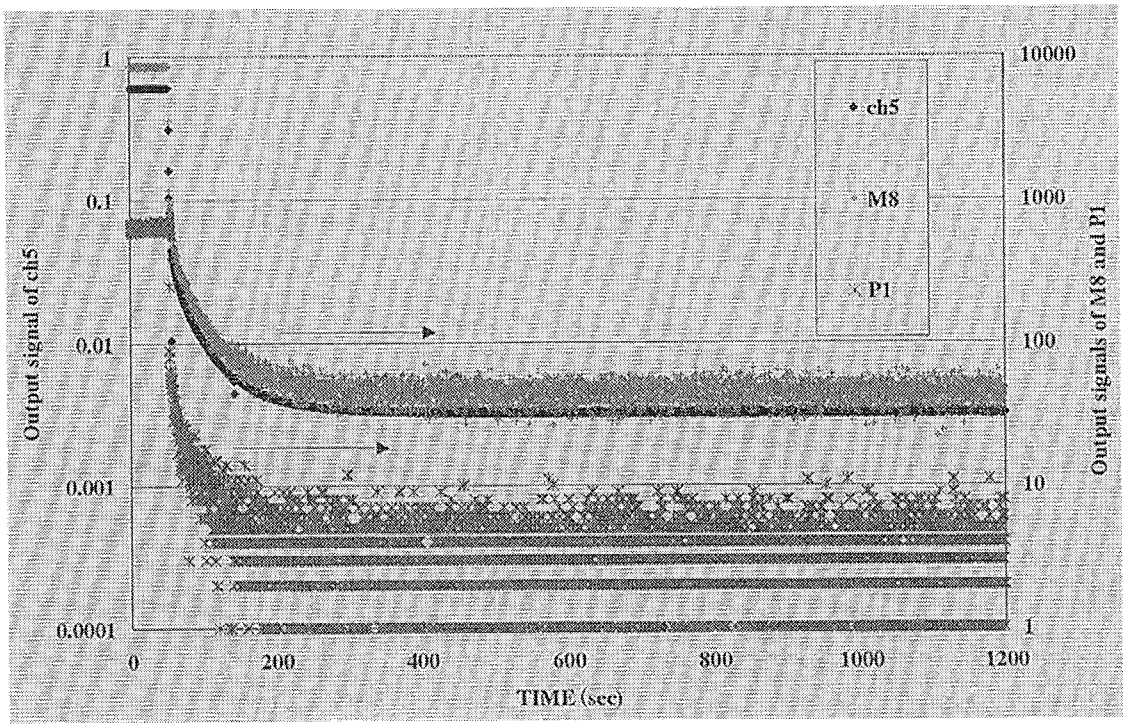

Fig.4.8.2 Experiment results

Table 4.8.1 The reactivities and the source intensities by the IK method for different detectors

	Detector Ch5		Detector M8		Detector P1	
	ρ ($)	S (n/s)	ρ ($)	S (n/s)	ρ ($)	S (n/s)
LS –3	-5.63	4.77E+08	-6.19	4.99E+08	-6.83	5.63E+08
LS –4	-5.63	4.77E+08	-6.09	4.88E+08	-0.20	0.74E+08
MI	-5.60	4.69E+08	-6.10	4.95E+08	-6.53	5.29E+08
ML	-5.55 ±0.13(%)[a]	4.64E+08 ±0.146(%)[a]	-6.04 ±1.87(%)[a]	4.80E+08 ±2.2(%)[a]	-6.55 ±6.4(%)[a]	5.27E+08 ±7.4(%)[a]
Average	-5.61 ±0.8%	4.73E+08 ±1.4%	-6.12 ±1.1%	4.91E+08 ±1.7%	-5.05 ±64%	4.26E+08 ±55%
SM method	-5.59 ±0.07%	4.69E+08 ±0.01%	-5.74 ±1.63%	4.63E+08 ±0.09%	-5.56 ±5.6%	4.44E+08 ±0.31%

a) error estimated with the confidential level of 99 % (3σ)

4.9 Measurements of Subcritical Reactivity and Fission Rate Distribution in Uranium Core FCA-XXI-1

T.Yamane and S.Okajima
(*E-mail*: yamane@vhtrc01.tokai.jaeri.go.jp)

In the design of accelerator-driven subcritical reactor systems (ADS), the subcritical reactivity of core is a key parameter to evaluate not only nuclear safety characteristics but also core performance such as neutron multiplication and power distribution. To study the basic core characteristics of subcritical multiplying system driven with an external neutron source, measurements of subcritical reactivity and fission rate distributions were carried out in a subcritical configuration constructed in a uranium-fueled core FCA XXI-1.

The FCA XXI-1 core has a simple core composition that consists of enriched uranium and stainless steel. The subcritical configuration, as shown in Fig.4.9.1, has the central test zone of 3x3 drawers (16cmx16cm) in the fixed half assembly and it is driven with an external neutron source of ^{252}Cf. In this experiment, three types of test drawers were prepared and replaced with normal fuel drawers in the test zone. The loading patterns of test drawers are shown in Fig.4.9.2. The tungsten in WSSV and WSB drawers was used to simulate accelerator target in ADS. The ^{252}Cf neutron source (~10^8 n/s) was placed on the center axis in the test zone. To examine the effect of source position on reactivity determination and power distribution, measurements were carried out at two source positions of 2.5cm(1Z) and 18cm(4Z) from the mid-plane of assembly. The subcritical reactivity was measured with the source multiplication method by using ten fission chambers: two startup channels for nuclear instrumentation in the outside of core and eight monitor channels distributed in the fixed half. The fission rate distributions were measured along the axial direction in the test zone using a miniature ^{235}U fission chamber.

Figure 4.9.3 shows typical experimental results of fission rate distribution in the case of the source position of 4Z. The reactivity in the figure is the average of measured values obtained by using the two startup channels. In the reference system where the test zone was loaded with normal fuel drawers, no effect of the external source was seen in the shallow subcritical state (-0.10$) with relatively high reactor power (2W). In the deeper subcritical state of -0.32$ with lower power of 0.15W, a hump appeared near the external source in the

observed distribution. When the normal fuel drawers in the test zone are replaced with WSSV or WSB drawers, the subcriticality went down deep to −11$ and also the reactor power decreased to 0.019W, and then a remarkable peak was observed at the external source position.

Preliminary analysis was made using a fast reactor analysis code system. The cell calculations were performed with the SLAROM code with the JFS-3 library based on a nuclear data file JENDL-3.2. In the core calculations, a two-dimensional transport code TWODANT was employed with an approximation of P_0-S_8 in R-Z geometrical model.

The results showed that the calculated reactivity worths of test drawers were extremely lower by 20~40% than experimental ones. Moreover, even at a critical state of the reference system, the calculation overestimated the effective multiplication factor more than 1%Δk. As for the fission rate distribution, some adjustment of system reactivity had to be made in calculations to reproduce a peak near the external source as observed in the measured distributions in the subcritical configurations. Detailed analysis has been continued.

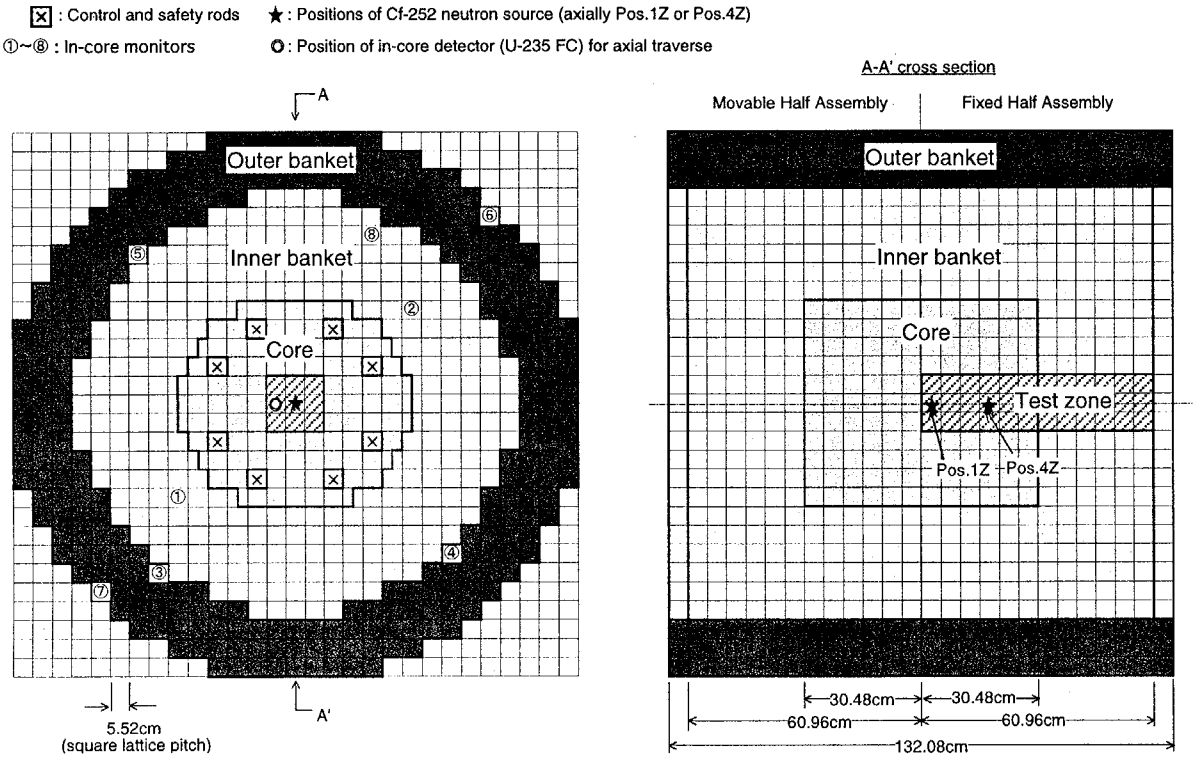

Fig.4.9.1 Subcritical configuration in FCA XXI-1 core

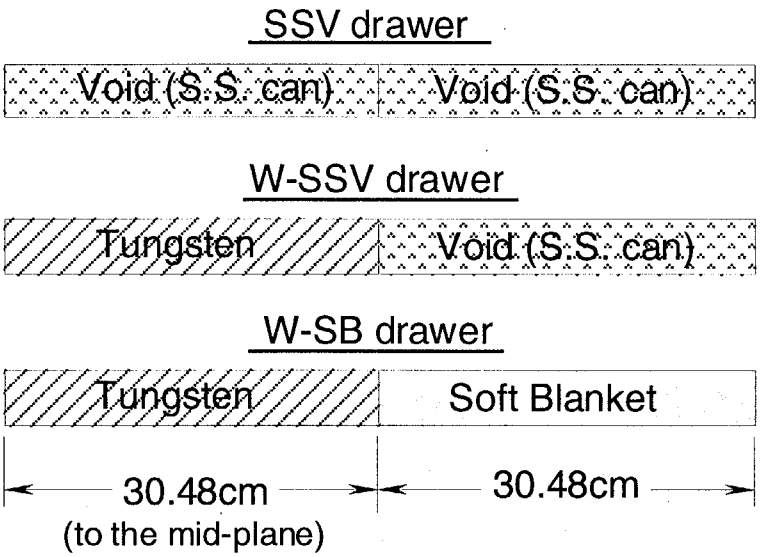

Fig.4.9.2 Drawer patterns in test zone

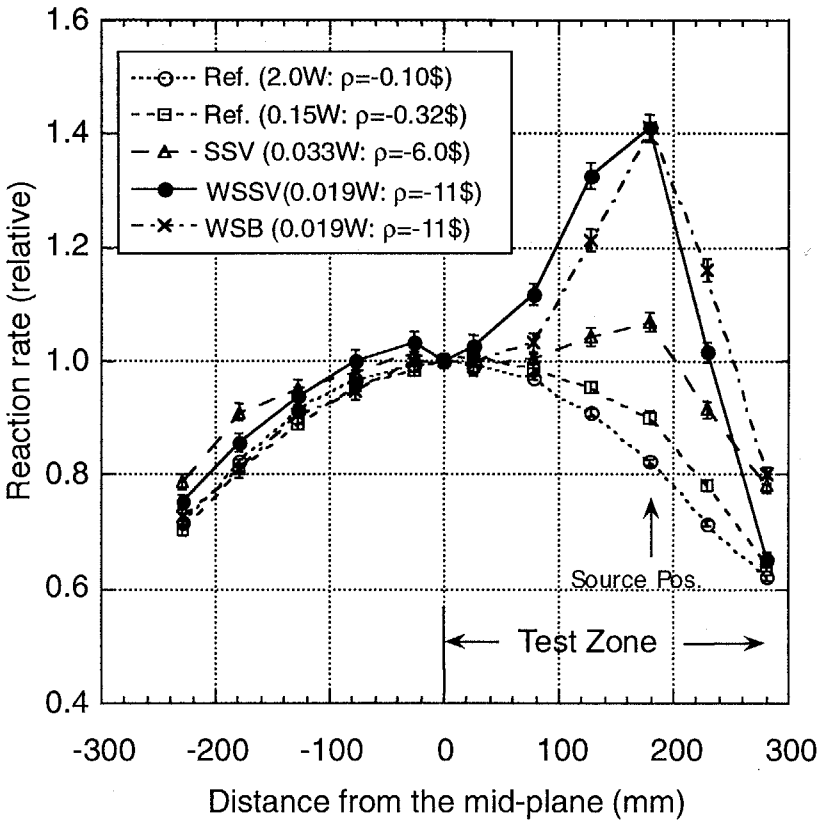

Fig.4.9.3 Typical experimental results of fission rate distribution

4.10 Subcriticality Measurement by High-Energy Gamma-Ray Detecting Source Multiplication Method

T. Suzaki, K. Tonoike, K. Murakami, M. Kurosawa, S. Fujisaki and Y. Hoshi
(*E-mail* : suzaki@mike.tokai.jaeri.go.jp)

The neutron source multiplication method is often used for measuring the subcriticality of core and the reactivity effects caused by a perturbation added to the core. In general, such an experiment in a subcritical state has an advantage in the aspects of safety and expanding the parameter range compared to that at the critical state. The method is, however, known to be not reliable without a theoretical correction especially for measuring a high subcriticality and a large reactivity effect, because the measured results vary depending on the arrangement of neutron source (S) and detector (D). Therefore, it is important in this method to select the experimental conditions such as the S-D arrangement so as to minimize the amount of theoretical correction, and then, to evaluate the correction factor for those conditions with a sufficient accuracy. For these purposes, it is considered that the detection of higher energy γ-rays than 3 MeV accompanied with fission could be used more effectively compared to the conventional neutron detection method, because the γ-rays of that energy range can be distinguished from the fission-product γ-rays as shown in Fig. 4.10.1, and their high penetration ability will give the information of source multiplication inside the whole core without depending largely on the S-D arrangement.

To investigate an applicability of the high-energy γ-ray detecting source multiplication method to high subcriticality measurement, light-water moderated and reflected N x N rods square lattices of 2.6%-enriched UO_2 fuel were constructed at the TCA, and N was changed from 17 to 5 with the lattice pitch of 19.56 mm. The water levels of those cores were fixed as 100 cm from the lower end of the active fuel region. As shown in Fig. 4.10.2, a ^{252}Cf neutron and γ-ray source was positioned at the core center with an Al tube, and a BGO γ-ray detector was located in the water reflector apart horizontally from the source by 52 cm. A typical γ-ray spectrum is shown in Fig. 4.10.3.

The reactivity ρ (=1-1/k_{eff}) of each core was determined by

$$\rho / \rho_0 = (CR_0/CR)\, f, \qquad f = f_s f_x, \tag{1}$$

where ρ_0 is the reactivity of the reference N = 17 core obtained from the difference in water level between the critical and the subcritical states, CR_0 and CR are the count rates of higher energy γ-rays than 3 MeV for the reference and the relevant cores, respectively, subtracted those of direct γ-rays from the source CR_s, and the correction factors f_s and f_x correspond to

the change in shielding effect of multiplied fission γ-rays and the change in importance of source neutrons relative to fission neutrons between the two cores, respectively. The CR_s and f_s for the N x N core were evaluated as $CR_s = A \exp(-\kappa N)$ and $f_s = \exp\{\kappa (17-N)\}$, where A is the measured count rate without fuel rods and κ the γ-ray shielding factor reported as 0.027 in Ref. 1). The f_x is defined similarly to that in the case of neutron detection,[2] and was calculated by using the fission rate distribution and the importance distribution in each core.

The results of k_{eff} and f for the cores of N = 17～5 are shown in Fig. 4.10.4 together with the calculated k_{eff}'s[3] by a Monte Carlo code KENO-IV. As seen in the figure, the change in f is very small for the present cores of different horizontal sizes, and agreements between the measured and the calculated k_{eff}'s are fairly well even for the core of which k_{eff} is about 0.6. The method presently developed was reported in a newspaper* as a promising method usable to the on-line subcriticality monitoring in such nuclear fuel cycle facilities as the fuel fabrication plant.

References:

1) T. Suzaki, et al.: Proc. PHYSOR96, Mito, Japan, L-130(1996).

2) N. Mizoo: JAERI-M 7753, (1978), [in Japanese].

3) T. Suzaki: J. Nucl. Sci. Technol., 28, 1067(1991).

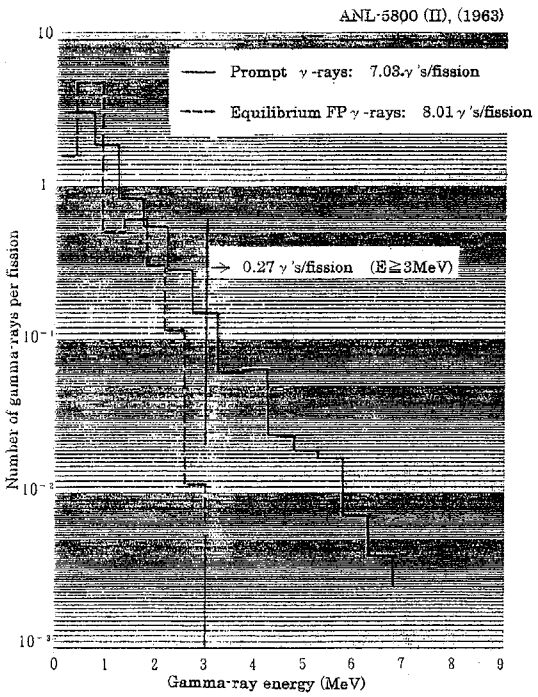

Fig. 4.10.1 γ-rays emitted by fission

*The Nikkan Kogyo Shinbun, 13 Nov. 2002.

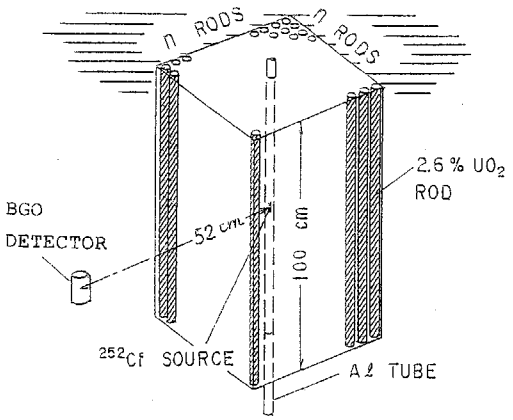

Fig. 4.10.2 Experimental arrangement

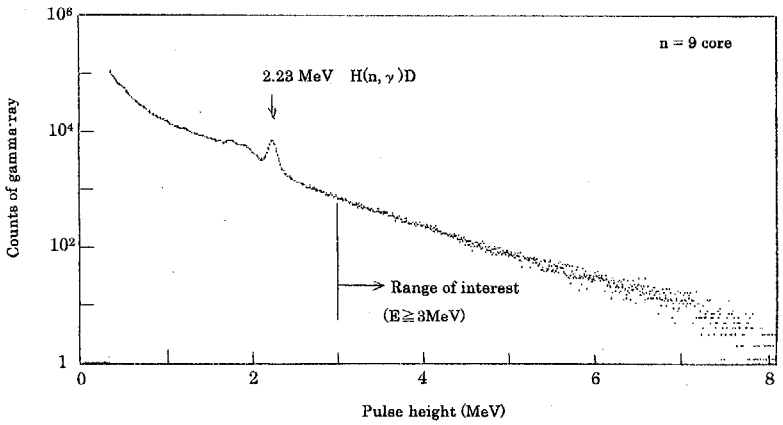

Fig. 4.10.3 Typical γ -ray spectrum

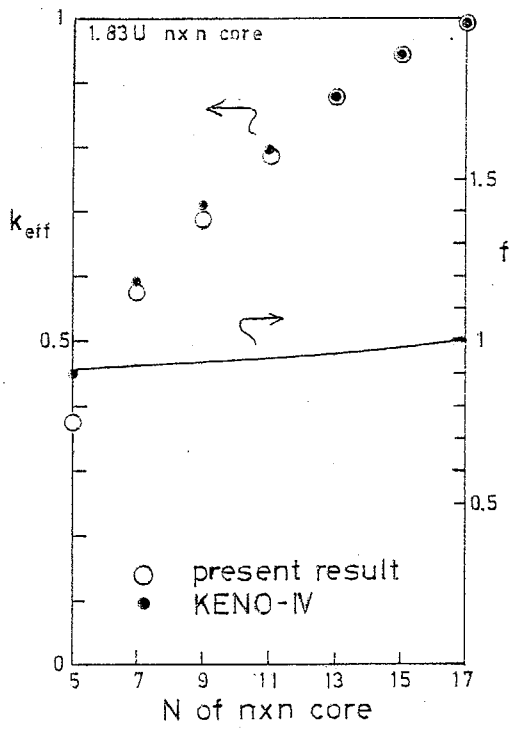

Fig. 4.10.4 Results of k_{eff} and f

4.11 Neutron and Gamma-Ray Detecting Noise Experiments at TCA

T. Suzaki and K. Tonoike
(*E-mail* : suzaki@mike.tokai.jaeri.go.jp)

Noise measurements inherently accompanied with fission chain reactions are useful in wide areas of reactor physics for determining subcriticality, reactivity effects and kinetic parameters. In a stationary core, each neutron randomly born from an extraneous source or as a delayed neutron starts a fission chain decaying with a time constant α called as the prompt neutron decay factor. Therefore, two counts from neutrons belonging to the same fission chain have a correlation characterized by α, and are distinguished from those of different chains. Similarly, prompt γ-rays emitted in the same fission chain could be used as the correlated count pairs by distinguishing randomly generated fission-product γ-rays of lower energy than 3 MeV as seen in Fig. 4.10.1 in Sec. 4.10. The Feynman-α and the Rossi-α methods are based on this property of count pairs of neutrons and γ-rays, and the on-line data processing tools have been developed* with a very high efficiency by using the recently available electronics.

For studying an applicability of the neutron and γ-ray detecting Feynman-α and Rossi-α methods to the light-water moderated and reflected cores of TCA ranging from the critical to a high subcritical states, 2.6%-enriched UO_2 fuel rods were arrayed into N x N rods square lattices with the lattice pitch of 19.56 mm, and N was changed from 17 to 5. A ^{3}He neutron detector and a NaI(Tl) γ-ray detector were positioned in the side reflector region apart from the core edge by about 6 cm at 50 cm-height from the lower end of active fuel region (origin of height measurement at the TCA). The N=17 core attained the criticality when the water level (WL) was 121.56 cm, and the noise measurements were performed at WL=120.04 and 115.68 cm under the steady states with the spontaneous fission neutrons from ^{238}U. For the other subcritical cores of N=17 (WL=80 and 60 cm) and N=15～5 (WL=100 cm), a ^{252}Cf neutron source of about 30 MBq was inserted at −15 cm-height in an Al tube located at the horizontal core center.

Typical results are shown in Fig. 4.11.1. For the Feynman-α method where the variance-to-mean ratios of radiation counts are plotted against the gate-time widths, variation of power level during the measurement affects significantly.* Therefore, the difference-filter technique[1)] was applied to the N=17 cores without the ^{252}Cf source. For both methods, the theoretical functions were fitted to the measured data, and the α-values were determined. As seen in Fig. 4.11.1, the ratio of the correlated term to the uncorrelated term of the prompt γ-ray counts is smaller than that of neutron counts. This is because the number

* K. Tonoike, et al.: Proc. Annual Mtg. of At. Ene. Soc. J., H12 and H15(2003), [in Japanese].

of γ-rays of higher energy than 3 MeV is smaller than that of neutrons emitted in one fission as seen in Fig. 4.10.1. Figures 4.11.2～4 show thus determined α-values of the N=17～5 cores together with the estimated or measured ones from the pulsed neutron source (PNS) experiment. From these figures, the following remarks could be made:

1) The neutron and γ-ray detecting Feynman-α and Rossi-α methods presently studied are applicable to the cores near the critical state of which k_{eff} is larger than 0.96 (Fig. 4.11.2).

2) For all cores, the error in the neutron detecting Feynman-α method is the smallest, and the method is applicable to higher subcritical cores compared to the other methods.

3) The α-values from noise method are systematically larger than those from PNS method for higher subcritical cores (Fig. 4.11.3). It has been noted that the horizontal neutron flux distribution differs between the time-decaying state of the PNS experiment and the steady state kept with the vertical neutron current caused by the extraneous source as the noise experiment as seen in Fig. 4.11.5.[2] Therefore, the larger values of α in the noise method could be explained by the smaller value of neutron generation time Λ in the harder neutron spectrum of the noise-measurement state, since the product $\alpha\,\Lambda(=\beta_{eff}-\rho)$ should be kept almost unchanged in both states, where ρ is the reactivity and β_{eff} the effective delayed neutron fraction.

References:

1) K. Hashimoto, et al.: J. Nucl. Sci. Technol., 36, 555(1999).

2) T. Suzaki: Proc. Int. conf. on Nucl. Criticality Safety (ICNC'91), Oxford, UK, VI-16(1991).

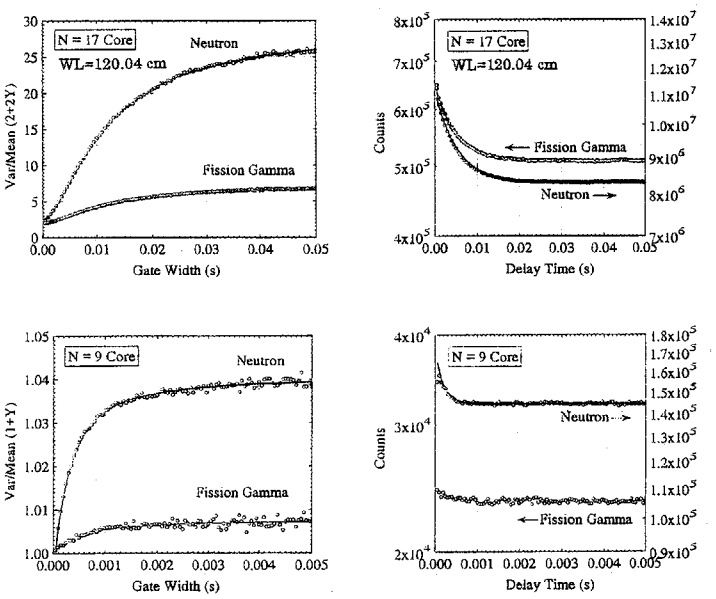

Feynman-α Rossi-α

Fig. 4.11.1 Typical results of noise experiment

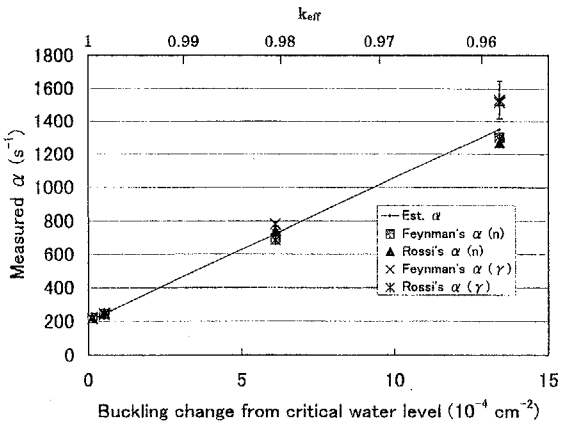

Fig. 4.11.2 Measured α for N=17 core

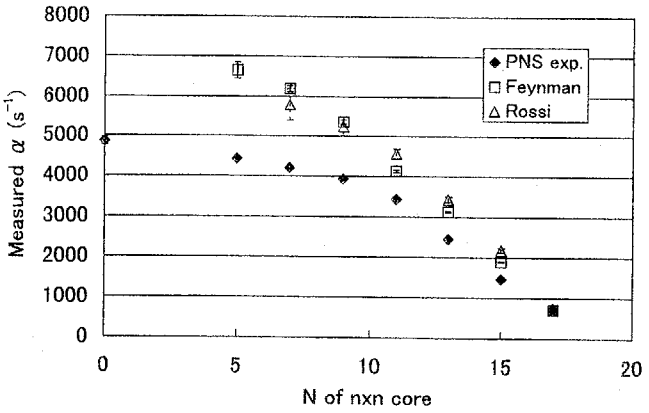

Fig. 4.11.3 Measured α from neutron detection

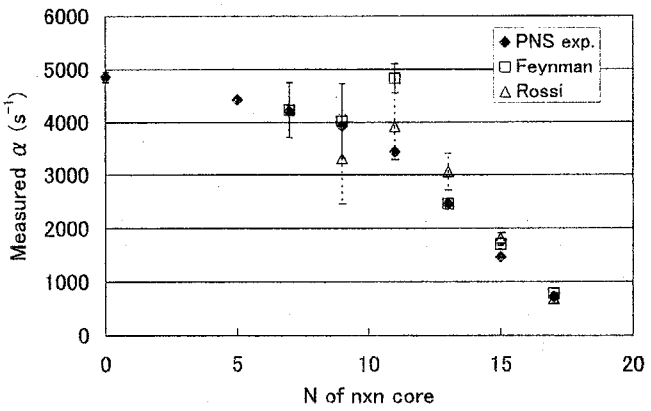

Fig. 4.11.4 Measured α from γ-ray detection

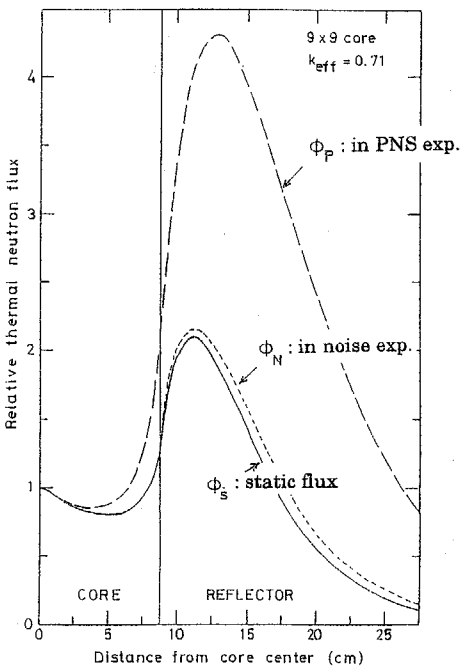

Fig. 4.11.5 Difference of horizontal neutron flux distribution

4.12 Small Reactivity Measurement at TCA

T. Suzaki, S. Fujisaki, K. Murakami, M. Kurosawa and Y. Hoshi
(*E-mail* : suzaki@mike.tokai.jaeri.go.jp)

In the reactivity measurements of small samples of fission product (FP), minor actinide (MA) nuclides etc. for verification purpose of the nuclear data of those nuclides, it is often required to determine a small reactivity with a very high accuracy. In order to develop the reactivity measurement method of high accuracy, the following experiment was carried out at the TCA.

As shown in Fig. 4.12.1, a cylindrical core of water-moderated 2.6%-enriched UO_2 fuel lattice was constructed, and small samples of a Cd piece of 10 mm x 25 mm x 0.5 mm-thick and 2 kinds of 5 UO_2 fuel pellets of 12.5 mm-diameter clad by a 14.2 mm-outer diameter x 155 mm-long x 0.76 mm-thick Al tube (Al cladding) were moved vertically in an 18 mm-outer diameter x 1 mm-thick Al tube (sample tube) positioned at the core center. One pellet-sample was natural UO_2 of 80.8 g-weight and 63.7 mm-long, and another was 2.6%-enriched UO_2 of 81.5 g-weight and 64.0 mm-long in 5 pellets total. At a position in water reflector apart 3.9 cm from the outer-most fuel rod of the core, an Al tube of 14.2 mm-outer diameter x 0.76 mm-thick was installed, and a regulating rod (3.2%-enriched UO_2 fuel rod of 11.7 mm-outer diameter x 68 cm-long) was moved in the Al tube to keep the critical state by compensating the sample reactivity. The moderator-reflector water level was kept at a height near the upper end of active fuel region of core, and the core-temperature shift was less than 0.1 ℃ during the measurement of one kind of sample. Prior to the sample worth measurement, the calibration curve of the regulating rod worth was obtained by fitting a smooth curve to a data set of the rod position and the rod worth measured with a reactivity meter of which precision was confirmed to be within 0.1 cents from comparison with the period method.

The most important thing to obtain a reactivity value of smaller error in this method is how accurately we can determine the critical state. For this purpose, the electric current signal from a UIC detector located in reflector region near the core was fed to a pico-ampere-meter, and the output voltage was suppressed by about 90% to enlarge the time change of reactor power level of about 2 W. The suppressed signal was used as the input of reactivity meter, and the output passed a low-pass filter was monitored on a recorder chart to be as close to zero as possible by controlling the regulating-rod position.

After the sample-worth measurement in the bare sample-tube, the tube was covered by a 0.5 mm-thick Cd sheet, and the similar measurements for 2 kinds of 10-pellet samples of natural and 2.6%-enriched UO_2 were performed to obtain information of resonance reactions of neutrons. The weight and length of natural UO_2 sample were 161.6 g and 122.3 mm, and

those of 2.6%-enriched one were 164.4 g and 129.2 mm, respectively. As shown in Fig. 4.12.1, a number of fuel rods were added to keep the critical water level near the upper end of active fuel region, and the calibration curve of regulating rod was measured also for this core.

The measured results of sample worths in the bare and the Cd-covered sample tubes are shown in Fig. 4.12.2 and 4.12.3, respectively. The vertical distributions of Cd-piece and Al-cladding worths lie on the theoretical curves (square of cosine function) very well as shown in Fig. 4.12.2, and the scattering of the measured data around the theoretical curve is limited within 0.03 cents. This means that the error in the present reactivity measurement method could be minimized to be less than 2×10^{-6} δ k/k.

The reactivity worths of fuel pellets in the figures were obtained by subtracting the Al-cladding worth from the sample worth. The Al-cladding worth was about -0.1 cents at maximum in the bare sample tube, while it was negligibly small in the Cd-covered tube. The vertical distributions of fuel-pellet worths shift slightly toward positive near the both ends. This phenomenon could be explained as the suppression effect of neutron streaming by the pellet sample and the effect of lower reflector for the case of 2.6%-enriched fuel. From the results of fuel-pellet worths around the core center in both figures, it is observed that the contributions of neutron reactions in the resonance and the thermal energy ranges to the reactivity are almost equally negative for the case of natural UO_2, while for the case of 2.6%-enriched UO_2, the negative reactivity by the former contribution decreases to about a half of that of natural UO_2, and the latter contribution turns positive. The amounts of these measured reactivity worths could be used as the benchmarks for verifying the nuclear data of relevant nuclides through comparison with precise perturbation calculations. Furthermore, the present results gave us a prospect to measure small reactivities such as the Doppler effect.

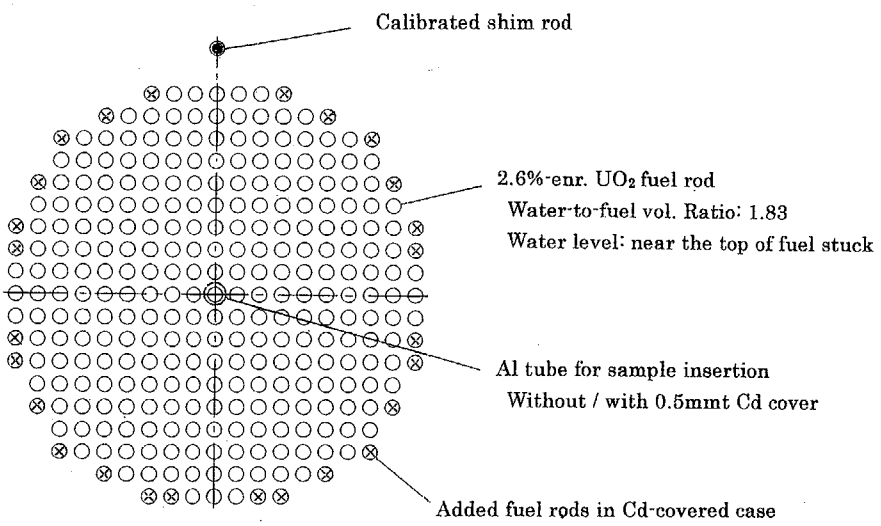

Fig. 4.12.1 Experimental arrangement for small reactivity measurement

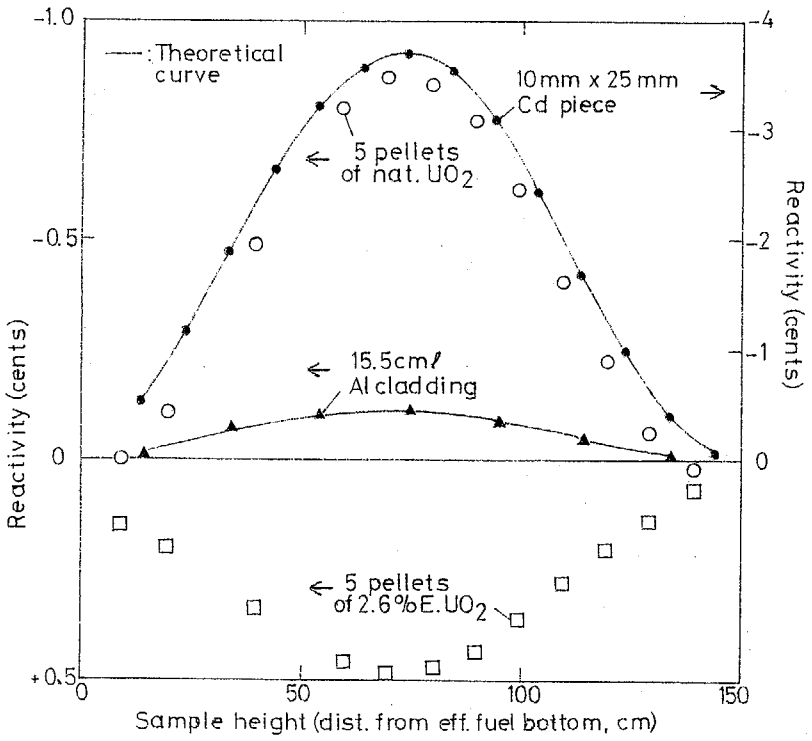

Fig. 4.12.2 Vertical distribution of reactivity worth in bare sample tube

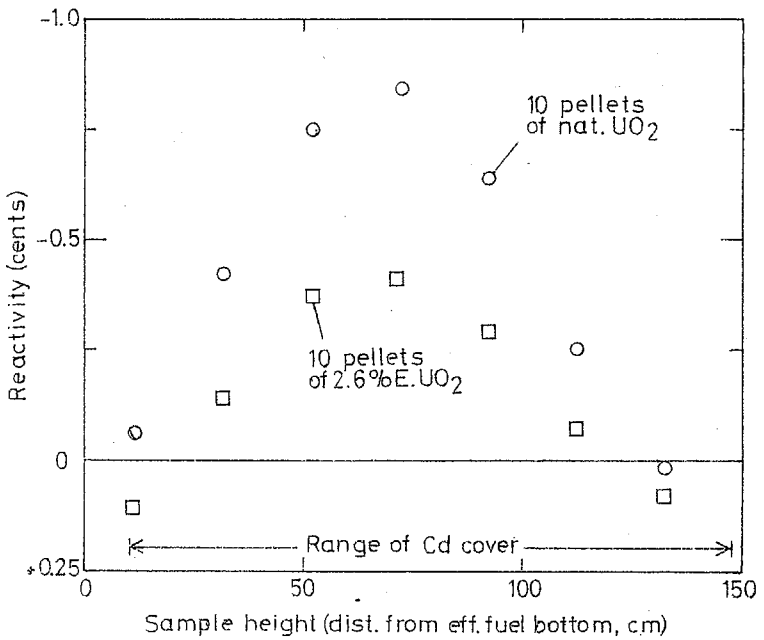

Fig. 4.12.3 Vertical distribution of reactivity worth in Cd-covered sample tube

5. Thermal and Fluid Engineering

Advanced computer programs have been developed and several tests were performed to develop thermal hydraulic analyses method in next-generation nuclear systems such as reduced moderation water reactors (RMWRs), and fusion reactor.

A critical heat flux (CHF) test for a high conversion type RMWR design was performed using the tight-lattice fuel assembly including seven heater rods arranged in the triangular array with 1.3 mm rod gap size. Measured data shows that the Arai correlation, which is used in the design work, gave reasonable predictions around nominal operation condition of the RMWR although the correlation over predicted the critical power under high mass velocity or low pressure conditions. A new critical power correlation was developed based on CHF test data performed at JAERI in Fys 2001 and 2002 and BAPL data. The pressure prop and void fraction in the tight lattice bundles have been studied to check the applicability of existing correlations to RMWRs. A test apparatus with 37 heater rods was constructed to investigate the scale effect on CHF in the tight lattice core.

An assessment study of COBRA-TF and TRAC-BF1 codes was performed for CHF tests with seven heater rods to check the applicability to the tight-lattice core. The COBRA-TF code overestimated the critical power by about 50 %, while the TRAC-BF1 code gave good prediction under a nominal operating condition of RMWR.

To predict boiling transition in the tight lattice core accurately, cross flow between subchannels and spacer effects are important. We started the development of the detailed two-phase flow simulation code with interface tracking (named TPFIT code) in FY 2000 to understand phenomena mechanistically. In FY 2002, numerical simulations of liquid film flow around grid spacer, two-phase flow mixing between subchannels have been done. These analysis results demonstrate the capability of numerical simulations on the research of detailed flow mechanisms. Visualization programs have also been developed for two-phase flow analysis results using the AVS code.

To support the experimental fusion reactor design, several analyses were performed for the ingress of coolant event and condensation characteristics of vapor in cold water.

5.1 Critical Power Experiments in a Double Humped Tight-Lattice Bundle

M. Kureta, W. Liu and H. Akimoto
Email: kureta@hflwing.tokai.jaeri.go.jp

Critical power experiment in a tight lattice bundle, with axially exerted a complicate 12-step power distribution that simulates RMWR core, has been carried out. Totally 304 data points have been obtained. Effects of mass velocity, inlet temperature, pressure, local peaking factor and axial non-uniform heated on critical power and critical quality are evaluated. Arai correlation[1)], which is the only correlation that optimized for tight lattice bundle system, is verified with the data. There shows a need for the development of a better critical power correlation for tight lattice bundle.

Critical Power Experiment

The experimental system is outlined in Fig.5.1.1. Pure water, after being pumped through flow meter, enters preheater and test section. The vapor-water two-phase flow that comes out of the test section is separated and condensed in condenser. The condensed water then flows back to pump and repeat the circulation. Mass velocity is controlled by valve VA and VB. Inlet water temperature is controlled by preheater. Pressure at the exit of the test section is adjusted by pressure controller automatically.

Fig.5.1.2 shows the schematic view of the test section. The test section is a 7-rod bundle, which consists of one

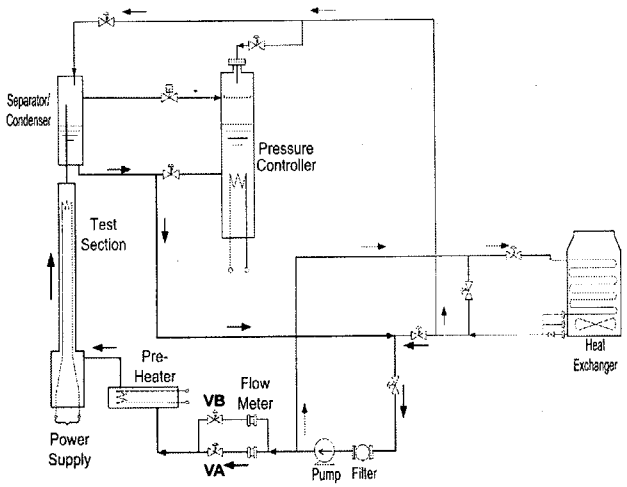

Fig.5.1.1 Outline of experimental system

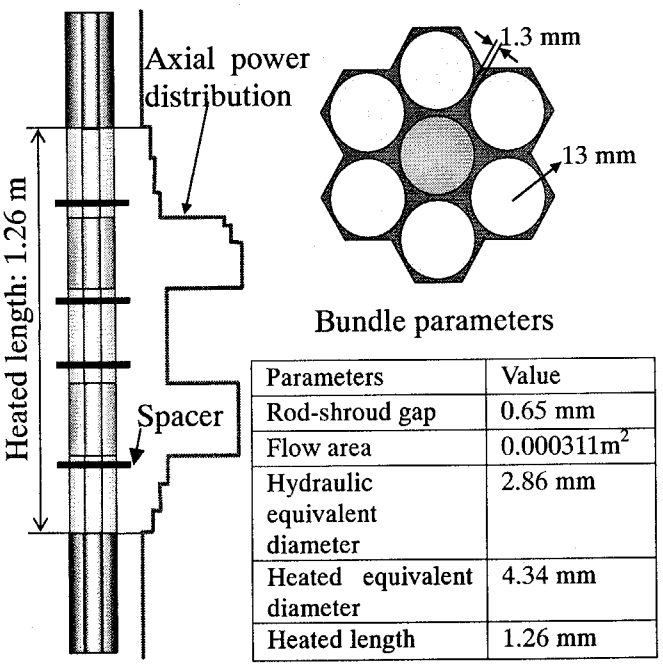

Bundle parameters

Parameters	Value
Rod-shroud gap	0.65 mm
Flow area	0.000311m^2
Hydraulic equivalent diameter	2.86 mm
Heated equivalent diameter	4.34 mm
Heated length	1.26 mm

Fig.5.1.2 Schematic view of the test section

center rod and six peripheral rods. The 7 rods are arranged on a 14.3 mm equilateral triangular pitch with a 1.3 mm rod gap. To simulate RMWR core, a 12-step power distribution is employed on axial direction (Fig.5.1.2). The axial peaking factor is 2.19 at the elevation from 760 to 850 mm. In radial direction, the center rod has a higher power distribution than that on the peripherals. Relevant bundle parameters are shown in the Fig.5.1.2.

Experimental Condition

Table 5.1.1 gives out working conditions in the experiments. The experiments are performed in an extensive working range, with the nominal working condition (P_{ex}= 7.2MPa, G= 400kg/m^{2}s, ΔT_{in} = 5K, F_r = 1.3) considered centrally.

Table 5.1.1: Experiment condition

Parameter	Range
Exit pressure, P_{ex}	1-8.5 MPa
Mass velocity, G	100. – 1381 kg/m^{2}s
Inlet subcooling, ΔT_{in}	2 - 50 K
Local peaking factor, F_r	1.04 – 1.44

Results

From the obtained data, critical power shows being an increase function of mass velocity and inlet subcooling degree. The effect of pressure on critical power, although being not very significant, is observed. The critical power firstly increases along the increase of pressure, reaches its maximum around P_{ex} = 4 – 6 MPa, and then decreases against the increase of pressure. No obvious effect of local peaking factor on critical power is observed.

To understand the effect of axial double humped non- uniform heating, critical power data derived in the present experiment and that derived in axial uniform heated condition[2] under P_{ex} = 7.2 MPa, ΔT_{in} =5 K are shown in Fig.5.1.3, together with the lines of exit perfect evaporation conditions for the two bundle systems, respectively. Under same working condition, the present axial double humped non- uniform heating gives a lower critical power than that of the axial uniform heating condition. Furthermore, compared with the uniform heated data, which maintains near to the exit perfect evaporation line and shows a mild detaching tendency with the increase of mass velocity, the axial double humped non- uniform heated data shows a sudden change of critical power – mass velocity trend at about 200 kg/m^{2}s. When mass velocity is lower than 200 kg/m^{2}s, Boiling Transition (BT) happens at nearly the exit perfect evaporation condition. While when mass velocity is higher than 200 kg/m^{2}s, BT condition departs from the exit perfect evaporation line. The trend tells us that the BT triggering mechanism changes before and after G =200 kg/m^{2}s.

Figure 5.1.4 shows critical quality data in the present experiment and in axial uniform heated condition[2]. A much faster decreasing tendency of critical quality in the

present double humped non- uniform heating is observed.

Verification of Arai Correlation

Arai correlation, which is the only correlation that optimized for tight lattice bundle system, is verified with the present critical power data. The results showed that the correlation, although being able to give reasonable critical power predictions around nominal operation condition, over-predicts at high mass velocity or low pressure conditions and under predicts at low mass velocity or high local peaking factor condition. Thereby, there shows a need for the development of a better critical power correlation for tight lattice bundle. For more detailed information about this part, those interested please refer to reference[3].

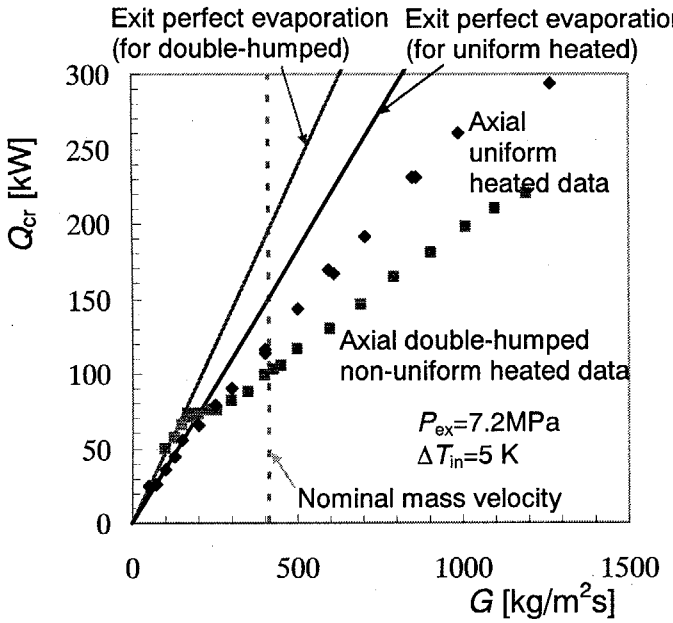

Fig.5.1.3 Critical power data for axial uniform heated and double-humped condition

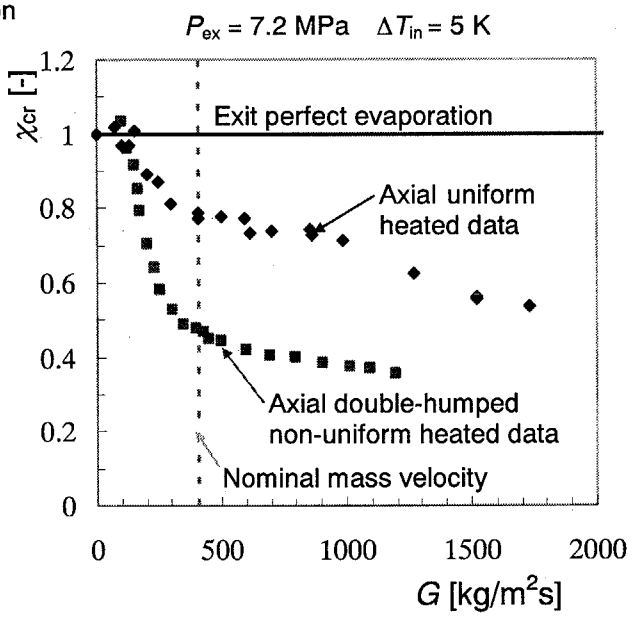

Fig.5.1.4 Critical quality data for axial uniform heated and double-humped condition

Reference

1) K. Arai et al., "Critical Power Characteristics of a High Conversion Boiling Water Reactor", IAEA Technical Committee on Technical and Economic Aspects of High Converters, (1990)

2) M. Kureta, et al, "Critical Heat Flux Experiment for Reduced-Moderation Water Reactor (RMWR)", Proc. of ICAPP-1129, Florida, USA, (2002)

3) W. Liu, et al, "Critical Power Characteristics of Tight Lattice Bundles", Proc. of ICONE11-36099, Tokyo, Japan, (2003)

5.2 Critical Power Correlation for Tight-Lattice Bundles

W. Liu, M. Kureta, T. Okubo and H. Akimoto
(*Email:* liuwei@hflwing.tokai.jaeri.go.jp)

A critical power correlation is proposed for tight lattice bundle system at low mass flow rate condition. The correlation is developed from searching the relationship between local heat flux and critical quality based on JAERI axially uniform heated data[1)] and axially non-uniform heated data[2)]. The proposed correlation is fit for the condition that mass velocity G < 2000 kg/m^{2}s, with exit pressure P_{ex} in the range from 3 MPa to 11 MPa. The correlation is verified with BAPL data[3)], JAERI axially uniform heated data and JAERI axially non-uniform heated data with good accuracy. The correlation is also confirmed being able to predict reasonable parametric trends of mass velocity, pressure, inlet temperature, equivalent heated diameter and local peaking factor on critical power.

Correlation Development

Around the Reduced-Moderation Water Reactor (RMWR) nominal operating condition, i.e., P_{ex} = 7.2 MPa, G = 400 kg/m^{2}s and inlet subcooling ΔT_{in} = 5 K, it is wide accepted that boiling transition happens due to a complete dryout of liquid film. As the dryout of liquid film is associated with a local heat flux and a quality directly, the correlation is developed from searching the relationship between local critical heat flux ($_{local}CHF$) and critical quality (χ_c). The basic steps for the correlation development are: firstly, under P_{ex} = 7.2 MPa, develop a correlation for axial uniform heated condition; secondly, expand the correlation to axial non-uniform heated condition and at last, complete the correlation by including pressure effect. The datasets used for the correlation development are JAERI 7-rod axially uniform heated data and axially double humped non-uniform heated data.

JAERI 7-rod axially uniform heated data at P_{ex} = 7.2 MPa are plotted in Fig.5.2.1. With χ_c = 0.7 as a boundary, the data can be generally divided into a low quality region and a high quality region data, respectively. In the low quality region, local critical heat flux decreases step by step with the increase of critical quality. The data generally gather to a line and can be approximated with a simple function. Around χ_c = 0.7, a significant decrease of critical local heat flux with the increase of quality is observed. The development of the correlation is carried out for the two quality regions, respectively. In the both regions, the

relation between $_{local}CHF$ and χ_c is found being little affected by mass flow rate and inlet subcooling. The correlations under P_{ex} = 7.2 MPa for axially uniform heated condition are written in:

(a) For the low quality region:

$$_{local}CHF_1 = (a_0 e^{b_0 \chi_c} + 40) \times F_r^{-0.5} \quad (5.2.1a)$$

where a_0 = 2024.3, b_0 = -1.2548. F_r is local peaking factor.

(b) For the high quality region:

$$_{local}CHF_2 = a_1 \times e^{b_1 F_r^{0.5} \chi_c} \times F_r^{0.5} / D_h^{0.5} \quad (5.2.1b)$$

where a_1=1375, b_1= -4.71 and D_h is equivalent heated diameter.

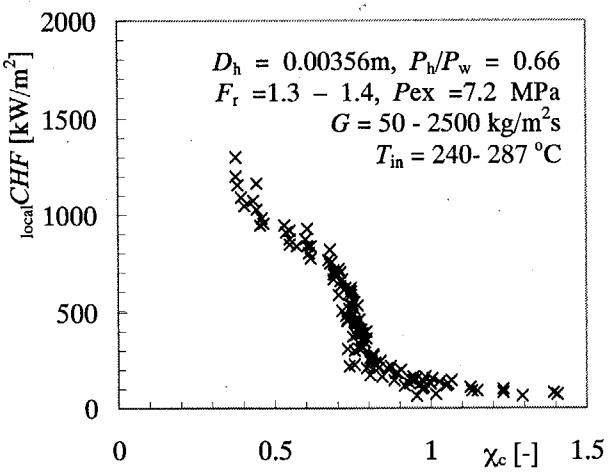

Fig.5.2.1 JAERI 7-rod axially uniform heated data

The developed correlations are then expanded to axially non-uniform heated condition. Fig. 5.2.2 shows both JAERI 7- rod axially double humped non-uniform heated data and axially uniform heated data at P_{ex} = 7.2 MPa. For axially double humped data, a much earlier decrease of critical heat flux than axially uniform heated data is observed. Local axial power distribution coefficient F_z is employed to correlate the tendency. The correlations expanded to axially non-uniform heated condition are:

(a) For the low quality region:

$$_{local}CHF_1 = (a_0 e^{b_0 F_z \chi_c} + 40) F_r^{-0.5} F_z \quad (5.2.2a)$$

(b) For the high quality region:

$$_{local}CHF_2 = a_1 F_z^{-1.5} e^{b_1 \chi_c F_r^{0.5}} F_r^{0.5} / D_h^{0.5} \quad (5.2.2b)$$

At last, the correlation is completed with including the pressure effect to the constants a_0, a_1. The developed correlations are finally written in:

$$_{local}CHF_1 = (a_0 e^{b_0 F_z' \chi_c} + 40) F_r^{-0.5} F_z' \quad (5.2.3a)$$

$$_{local}CHF_2 = a_1 F_z'^{-1.5} e^{b_1 \chi_c F_r^{0.5}} F_r^{0.5} / D_h^{0.5} \quad (5.2.3b)$$

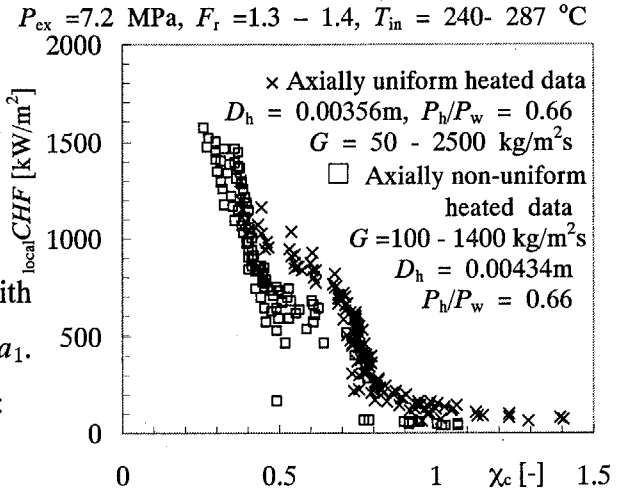

Fig.5.2.2 JAERI 7-rod axially uniform heated data and axially non-uniform heated data

where D_h is equivalent heated diameter; $a_0 = 1286 + 479 \times P_{ex} - 71 P_{ex}^2 + 2.6 P_{ex}^3$; b_0 = -1.2548

$a_1 = 509 + 223.2 \times P_{ex} - 14.3 P_{ex}^2$; b_1= -4.71; $F_z' = F_z$ when $F_z \geq 1$ and $F_z' = 1$ when $F_z < 1$

The calculated critical heat flux is: $_{local}CHF = \min(_{local}CHF_1, _{local}CHF_2)$ (5.2.4)

The units in the developed correlation are: G: [kg/m^{2}s]; P_{ex}: [MPa]; D_h [m]. The calculated local heat flux ${}_{local}CHF_1$, ${}_{local}CHF_2$ and ${}_{local}CHF$ are in [kW/m^2].

Correlation Verification

To calculate ${}_{local}CHF_1$ and ${}_{local}CHF_2$, Eqs. (5.2.3a) and (5.2.3b) need being solved together with the energy balance equation. And the lower one is taken as the calculated critical heat flux (Eq. (5.2.4)). JAERI axially uniform heated database and axially non-uniform heated database are first used for the verification. The result is shown in Fig.5.2.3. The correlation can predict JAERI axially uniform heated data and axially non-uniform heated data in an error band about ±10%. To check the expandability of the proposed correlation, BAPL database[3] is verified and the result is shown in Fig.5.2.4. The proposed correlation can predict BAPL data with good accuracy as well in a wide range of working condition. Further more, the correlation has been confirmed being able to predict reasonable parametric trends of mass velocity, pressure, inlet temperature and local peaking factor on critical power. For more detailed information about this report, those interested please refer to reference[4].

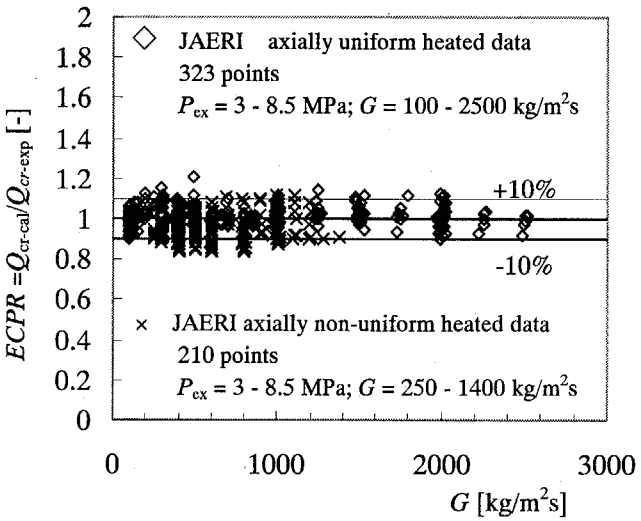

Fig.5.2.3 Verification results to JAERI axially uniform heated data and JAERI axially non-uniform heated data

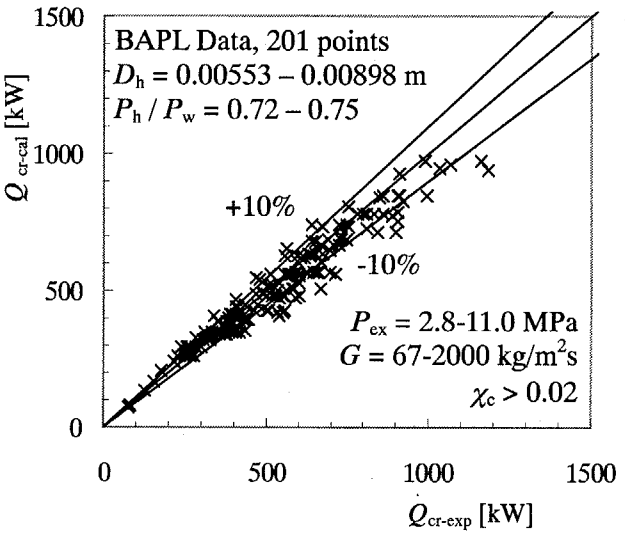

Fig.5.2.4 Verification result to BAPL data

Reference

1) M. Kureta, et al, Proc. of ICAPP-1129, Florida, USA, (2002)

2) W. Liu, et al, Proc. of ICONE11-36099, Tokyo, Japan, (2003)

3) B.W. Letourneau, et al, WAPD-TM-1013, (1975)

4) W. Liu, et al, Proc. of ICOPE-03, Kobe, Japan, (2003)

5.3 Void Distribution of Boiling Flow in a Tight-Lattice Bundle Measured by Neutron Radiography Techniques

M. Kureta, T. Sato and H. Akimoto
(*E-mail*: kureta@hflwing.tokai.jaeri.go.jp)

JAERI have developed detailed thermal-hydraulic analysis codes[1] to design the Reduced-Moderation Water Reactor (RMWR)[2]. In order to verify the code, detail flow information such as void distribution is requested. Therefore, we have developed 3D void fraction measurement system using neutron radiography and tomography techniques, named 'Neutron Tomography'. We conducted the void fraction experiments to measure the void fraction distribution of boiling flow in tight lattice bundles which simulates the RMWR core.

Figure 5.3.1 shows the neutron tomography system[3]. The system consists of neutron radiography imaging system, water circulating loop with a tight lattice test section, position control motor and camera link system for the tomography, image processing computer system and visualization computer system. JRR-3 is used as the neutron source. 3D void fraction data is calculated in the original computer program by processing the neutron radiography images. Maximum resolution of the result is 0.1mm.

Figure 5.3.2 shows the test section for the neutron tomography. The seven heater rods are installed into the flow shroud with the gap between rods of 1.0mm. The rods are directly and uniformly heated by D.C. power supplies with the heated length of 0.89m. Pure water flows upward between rods and flow shroud with mass velocity of 139 – 462 kg/m^{2}s. Inlet water temperature is set about 90°C, and exit pressure is atmospheric pressure.

Figure 5.3.3 shows the void distribution of boiling flow at the exit of the heated region. Inlet condition of Fig. 5.3.3 is similar to that of RMWR, inlet subcooling is 10K, mass velocity of 415kg/m^{2}s. L.H.S. in Fig. 5.3.3 shows the result at the exit 214mm region. Center one magnifies the lower part of the L.H.S., and R.H.S. is also magnified image of the upper side. In Fig.5.3.1, void fraction in the flow area and seven rod area are presented as the gray-scale image. White area indicates high void fraction and black area indicates low void fraction area. It was observed from the experiment that axial change of the void fraction is small, water layer tends to stay between rods and void tends to move to the center line in the Fig. 5.3.3 condition.

Basic measurement technique is established, and void distribution of boiling flow in a rod bundle could be made clear. Next step, we are planning to measure the void distribution

in a 14-rod bundle and an axial non-uniformly heated tube etc.

References

1) H. Yoshida, A. Ohnuki, K. Takase, M. Kureta, H. Akimoto, H. Okada and K. Yamamoto, "Development of Mechanistic Boiling Transition Model in Rod Bundle", Proc. of 11th Int. Conf. of Necl. Eng. (ICONE-11), 36097, Tokyo, Japan (2003).

2) T. Iwamura, T. Okubo, M. Kureta, T. Nakatsuka, R. Takeda and K. Yamamoto, "Development of Reduced-Moderation Water Reactor (RMWR) for Sustainable Energy Supply", Proc. of 13th Pacific Basin Nucl. Conf. (PBNC2002), TS-8C-6, China (2002).

3) M. Kureta, "Measurement Technique of Two-Phase Flow by Neutron Tomography", J. of Jet Flow Eng., Vol. 20, 2, (2003) (in Japanese).

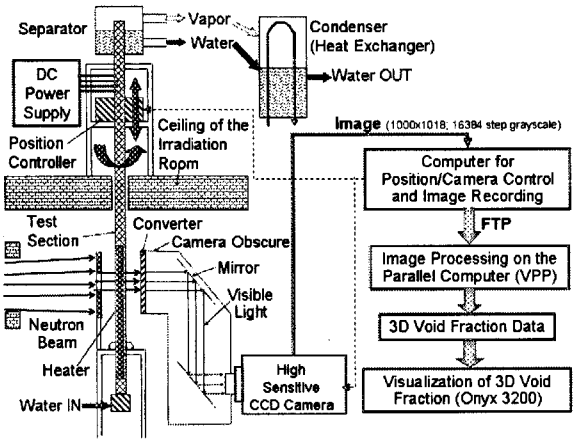

Fig. 5.3.1 Schematic diagram of the neutron tomography system

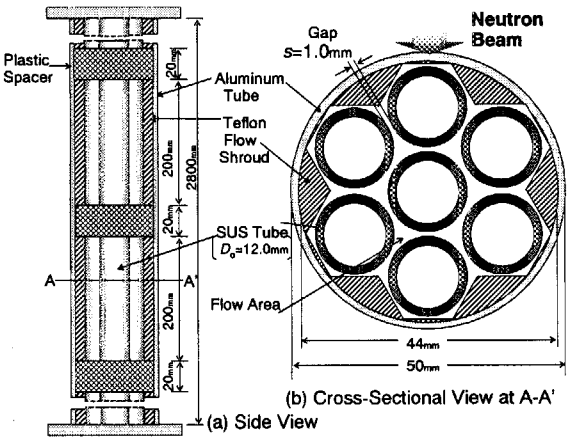

Fig. 5.3.2 Schematic view of the test section

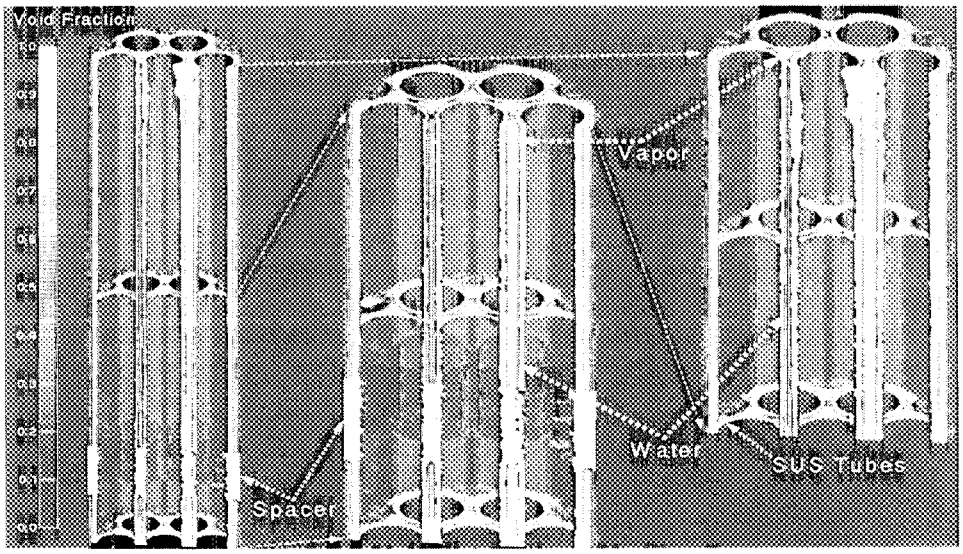

Fig. 5.3.3 Void distribution of boiling flow

5.4 Pressure Drop Characteristics in Tight-Lattice Bundle for BWR-Type Reduced Moderation Water Reactor

H. Tamai, M. Kureta and H. Akimoto.
(*E-mail:* tama@hflwing.tokai.jaeri.go.jp)

For design of the Reduced-Moderation Water Reactor core from the point of view of thermal-hydraulics, an evaluation method on pressure drop characteristics in tight-lattice rod bundles is required. The objective of this study is to investigate whether the general evaluation method proposed by Martinelli & Nelson[1] can apply to the prediction of the friction loss in the two-phase flow at the tight-lattice configuration.

As the experimental data with the triangular tight-lattice configuration, the results of 4 x 5 rod bundle experiments at the Bettis Atomic Power Laboratory(BAPL)[2] and 7-rod bundle experiments at JAERI were used. A schematic of the experimental configuration at BAPL[2] is shown in Fig.5.4.1. Two kinds of hydraulic diameters D_e were provided; 3.94 and 6.02 *mm*. The experiments were conducted under the conditions of pressure P = 2.8-13.8 *MPa* and mass velocity G = 70-5400 kg/m^2s. Only the experimental data with a uniform heat flux distribution and a boiling length beyond 30% of the heating length were selected and compared with calculated results by the Martinelli-Nelson's correlation[1]. The drift-flux model was used to evaluate axial distributions of void fraction and velocities. Distribution parameter and drift velocity in the drift-flux model were calculated by the Ishii's correlation[3]. The pressure loss at the spacer in the two-phase flow was evaluated by a sum of the local pressure losses along the spacer[4] and the homogeneous model. The friction loss calculated by the Martinelli-Nelson's correlation was compared with the experimental results in Fig.5.4.2. The Martinelli-Nelson's correlation can predict the friction loss within the error less than ±30 %, except for the loss less than about 10 *kPa*, i.e., the low flow rate condition (G < 1000 kg/m^2s).

Two schematics of seven-rod bundle experiments at JAERI are shown in Fig.5.4.3 and Fig.5.4.4. Axial power distributions were uniform and double-humped, and hydraulic diameters were 2.36 and 2.86 *mm*, respectively. The experiments were conducted under the conditions of P = 7.2 *MPa*, G = 400-2500 kg/m^2s and the inlet temperature T_{in} = 556 *K*. A local peaking factor of center rod was set on 1.3. The comparison between the experimental

and calculated friction losses is shown in Fig.5.4.5. The Martinelli-Nelson's correlation tends to overestimate the friction loss in these test facilities.

All the comparisons were plotted by the hydraulic diameter in Fig.5.4.6. This figure clearly shows that the friction loss is smaller than the calculated value by Martinelli-Nelson's correlation in case of the hydraulic diameter less than about 3 *mm*. One of the reasons is because of the effect of the small hydraulic diameter on the two-phase multiplier and the distribution parameter in the drift-flux model[5]. The other reason is the friction loss in a single-phase flow at the tight-lattice configuration. Rehme[6] carried out systematic investigations on the friction loss in a single-phase flow on about 60 types of rod bundles. He pointed out that the coefficient of the pressure loss decreases to approximately 60% of the circular tube with decreasing the ratio of a pitch to diameter in the bundles.

References

1) Martinelli, R. C. and Nelson, D. B., Trans. of the ASME, 70, 695-702 (1948).

2) LeTournean, B. W., et al., WAPD-TM-1013 (1975).

3) Ishii, M., ANL Report ANL-77-47 (1977).

4) Okubo, T., et al., JAERI-M 91-055, (1991) [in Japanese].

5) Mishima, K. and Hibiki, T., Int. J. Multiphase Flow, 22, 4, 703-712 (1996).

6) Rehme, K., Int. J. Heat Mass Transfer, 15, 2499-2517 (1972).

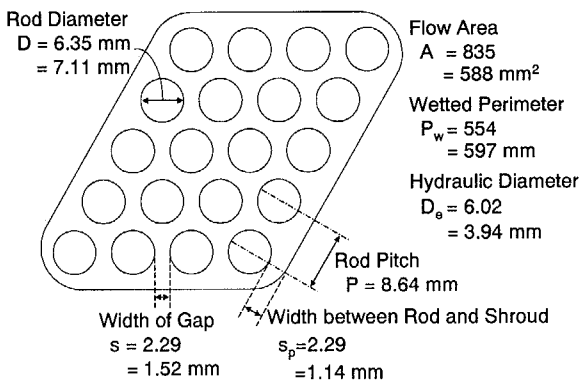

Fig, 5.4.1 Cross-section view of test section at BAPL[2]

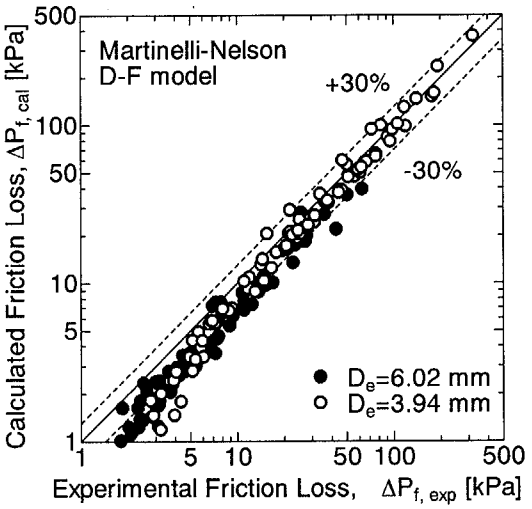

Fig.5.4.2 Comparison between experimental results at BAPL[2] and calculated results by Martinelli-Nelson

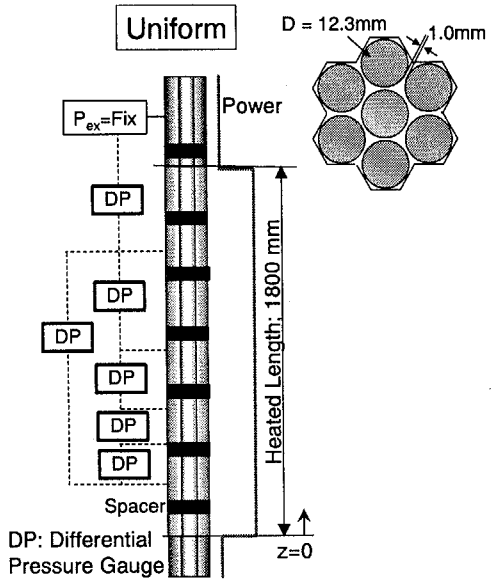

Fig.5.4.3 7-rod bundle geometry with a uniform axial power distribution

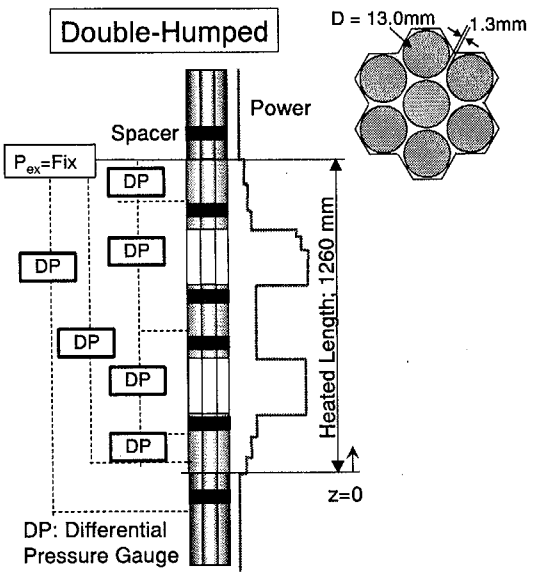

Fig.5.4.4 7-rod bundle geometry with a double-humped axial power distribution

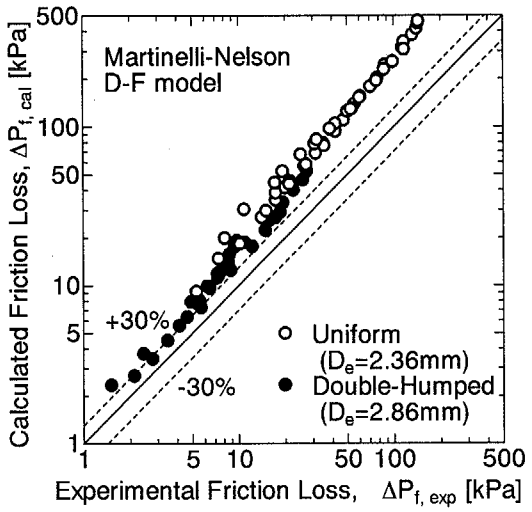

Fig.5.4.5 Comparisons between experimental and calculated friction losses for the configuration in Fig.5.4.3 and Fig.5.4.4

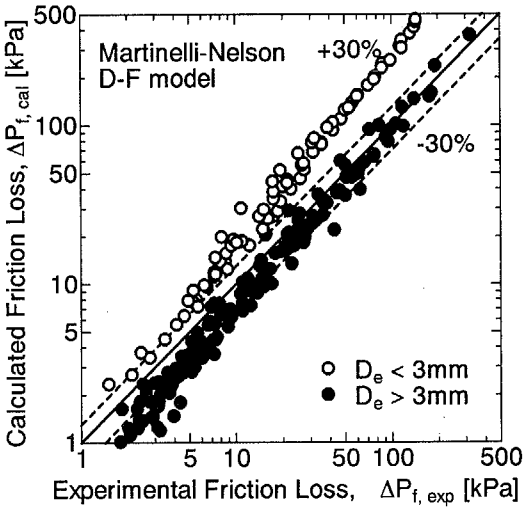

Fig.5.4.6 Comparisons between experimental and calculated friction losses for the tight-lattice configuration

5.5 Analysis of Critical Power Experiments of Tight-Lattice Bundle for BWR-Type Reduced Moderation Water Reactor

H. Tamai, T. Nakatsuka, M. Kureta and H. Akimoto
(*E-mail:* tama@hflwing.tokai.jaeri.go.jp)

Assessment of thermal margin in tight-lattice bundles is important for design of the Reduced-Moderation Water Reactor (RMWR) core. In this study, a series of tight-lattice CHF experiments performed in JAERI were analyzed with TRAC-BF1 and COBRA-TF codes to evaluate applicability of these analysis codes to the tight-lattice cores.

The test section was a 7-rod bundle with rod diameter of 13.0 mm, rod gap of 1.3 mm and heated part length of 1.26 m (Fig. 5.5.1). Axial power distribution was double-humped. The experiments were conducted under the conditions of pressure; P = 2.0-8.5 MPa, mass velocity; G = 100-1200 kg/m^2s, inlet temperature; T_{in} = 512-560 K and local peaking; R_f = 1.0-1.4. Nodings in TRAC-BF1 and COBRA-TF codes are shown in Fig. 5.5.2. The heated part was axially divided into 52 nodes in both codes. In the COBRA-TF code, a 1/6 symmetry model was adopted for simplicity, as shown in Fig. 5.5.2(b). A local pressure coefficient at a spacer was tuned with the single-phase experimental data.

The critical power calculated by TRAC-BF1 was compared with experimental data, as shown in Fig. 5.5.3. In the calculation, boiling transition (BT) was detected by critical quality correlation[1] in the code. It was found that TRAC-BF1 gives good prediction of critical power for mass velocity of around 400 kg/m^{2}s, which corresponds to a nominal operating condition of RMWR.

Figure 5.5.4 shows comparisons between the experimental data and calculated critical power by COBRA-TF. The code detected the BT as disappearance of a liquid film flow. The figure shows that COBRA-TF tends to overestimate the critical power in the tight-lattice bundle. This is because the present models for cross-flow between subchannels and pressure loss cannot apply to the tight-lattice core.

References

1) K. Arai, et al.: "Critical Power Characteristics of a High Conversion Boiling Water Reactor", IAEA, Technical Committee on Technical and Economic Aspects of High Converters, (1990).

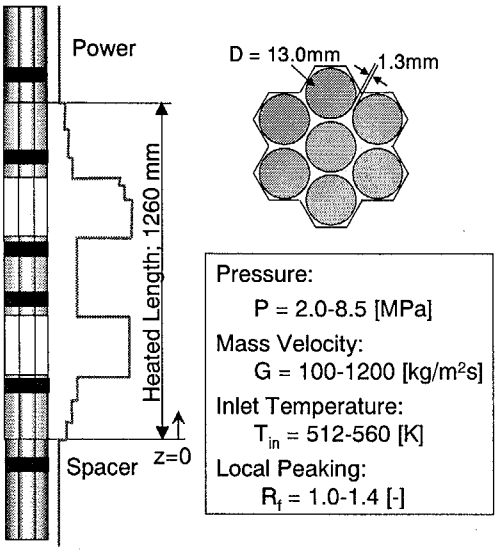

Fig.5.5.1 7-rod bundle geometry with a double-humped axial power distribution

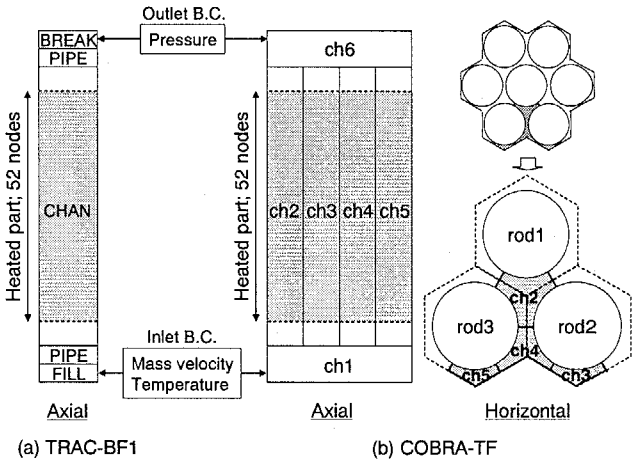

Fig, 5.5.2 Noding in analysis codes; (a) TRAC-BF1, (b) COBRA-TF

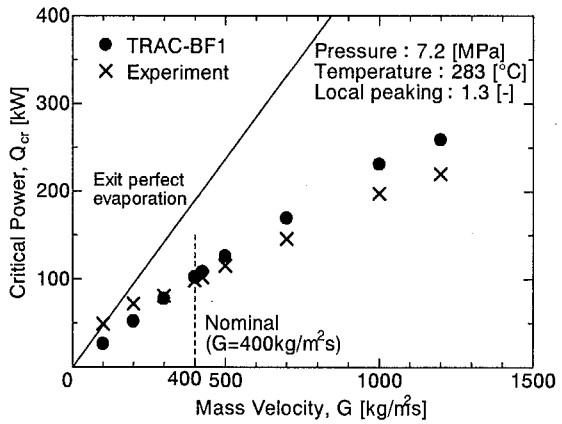

Fig. 5.5.3 Comparison between calculated critical power (TRAC-BF1) and experimental data

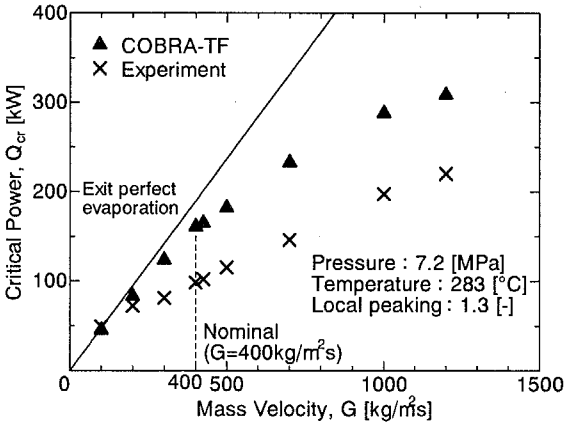

Fig. 5.5.4 Comparison between calculated critical power (COBRA-TF) and experimental data

5.6 Numerical Simulation of Liquid Film around Grid Spacer with Interface Tracking Method

H. Yoshida, Y. Ose, H. Tamai, K. Takase and H. Akimoto.
(*E-mail:* yoshida@hflwing.tokai.jaeri.go.jp)

In the RMWR core, remarkably narrow gap spacing between rods (about 1 mm) is used to reduce the moderation of the neutron (see Fig. 5.6.1). To optimize the thermal design, boiling transition (BT) in such a tight lattice core is one of most important subjects to be evaluated, but effects of the gap and spacer configuration have not been fully investigated. Then, advanced prediction method of BT is required to optimize and evaluate the thermal design of the RMWR core[1].

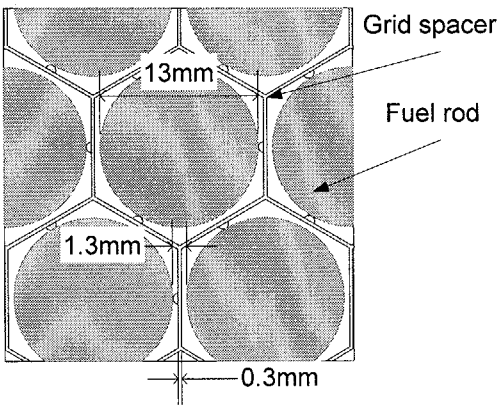

Fig. 5.6.1 Detail of RMWR fuel assembly

To predict BT in the tight lattice core accurately, cross flow between sub-channels in the fuel assemblies and spacer effects are important phenomena. Then, detailed two-phase flow simulation codes that can simulate these phenomena are necessary. Thus, we are developing the detailed two-phase flow simulation code with interface tracking method (named TPFIT).

The TPFIT code with the advanced interface tracking method applied to the air-water two-phase flow simulations in rectangle duct. Schematic of the analyzed region is shown in Fig.5.6.2. In the duct, a flat plate of the thickness of 0.3mm and length of 20.0mm exists to simulate the grid spacer of RMWR fuel assemblies. The duct height is equal to 1.8mm, and flow reduction ratio of the duct conforms to that of RMWR core. The duct width and length are set to 5.0mm and 45.0mm respectively. The grid size is 50×27×450. The grid intervals of

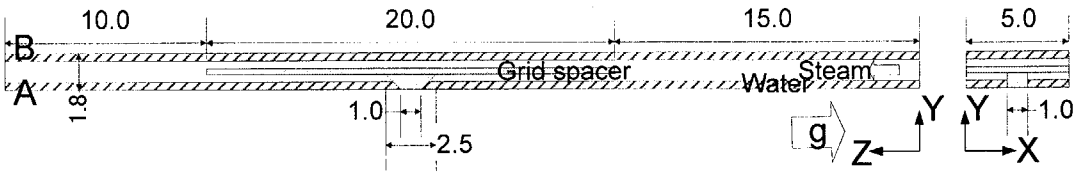

Fig.5.6.2 Flow configuration

x and z directions are equals to 0.1mm. The maximum and minimum grid intervals of y direction are set to 0.1mm and 0.0125mm respectively. Both non-slip walls of the rectangle duct are corresponding to the fuel rods surface. On the one side of non-slip wall plate ("wall A" in Fig.5.6.2), simulated fuel rod support is attached (the other face is called "wall B"). Two liquid films are configured on the "wall A" and "B" as the initial values. Initial values of liquid films thickness are set to 0.075mm. Inlet and initial values of z-direction water film velocity are set to 2.48m/s, and those of z-direction steam velocity are equal to 6.47m/s to simulate normal operating condition of RMWR reactor core.

The z-direction distributions of the average liquid film thicknesses from t=0.009 to 0.0135s are shown in Fig.5.6.3. On the "wall A", averaged liquid film thickness gradually reduces from the entrance. The liquid film thickness increases on the front face of the rod support. And liquid film thickness reduces in the wake of the rod support. On the "wall B", distributions of the averaged liquid film thicknesses have almost constant values from inlet to the spacer section. At the starting point of the spacer section, averaged liquid film thickness reduces sharply and recovers gradually after that. In the outlet section, the liquid film thickness increases sharply, and the distribution of the x direction is small in all calculated region. The fluctuation of the liquid film thickness on the "wall A" is more gradual in comparison with that on the "wall B" except near rod support region.

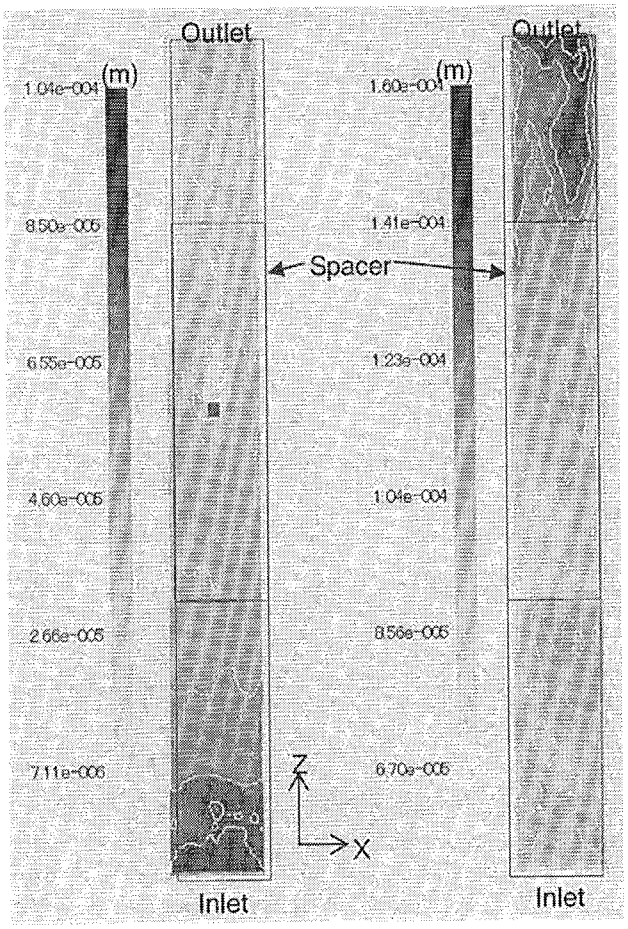

(a) side A (b) side B

Fig.5.6.3 Distribution of film thickness

References

1) H. Yoshida, et al., "Development of Mechanistic Boiling Transition Model in Rod Bundles", Proc. of ICONE11-36097, Tokyo, Japan, (2003).

5.7 Numerical Simulation of Fluid Mixing between Subchannels using Interface Tracking Method

H. Yoshida, Y. Ose, H. Tamai, K. Takase and H. Akimoto.
(*E-mail:* yoshida@hflwing.tokai.jaeri.go.jp)

To predict BT in the tight lattice core accurately, cross flow between sub-channels in the fuel assemblies is important phenomena. Thus, we are developing the detailed two-phase flow simulation code with interface tracking method (named TPFIT)[1]. The TPFIT code with the advanced interface tracking method applied to the air-water two-phase flow simulations in a rectangle duct. Schematic of the analyzed region is shown in Fig.5.7.1. The rectangle duct is divided into two channels by flat plate of the thickness of 0.5mm. At the center of the flat plate, there is a narrow slit of 50×10mm. And the channels are connected through the slot. The duct height is equal to 200mm.

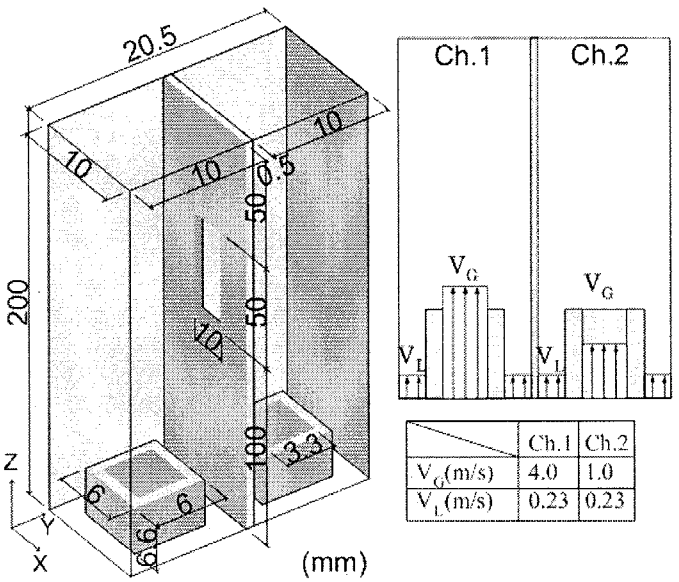

	Ch.1	Ch.2
V_G(m/s)	4.0	1.0
V_L(m/s)	0.23	0.23

Fig. 5.7.1 Flow configuration

On all walls, non-slip boundary condition is assigned, and outlet pressure is fixed at 0.103 MPa. Initial values of void fraction are set to 0.0 in all regions. From the bottom of simulated region, air and water are injected at constant velocity. Inlet flow conditions are summarized in Fig.5.7.1. The bubbly flow is formed in the Ch.2 according to the experimental result. And slug flow occurs for the flow Ch.1. The snap shots of void distribution are shown in Fig.5.7.2. In the figure, white part is air and black shows liquid phase, and the channel 1 and 2 are shown on the left and right side, respectively. According to experimental results, the slug and bubbly flow must be observed in the channel 1 and 2 respectively. The bubbles begin to flow in with time 0s and the slag bubbles of channel 1 have reached slit section. In 0.16s, a part of the slag in the channel 1 is segregated at upper part of the slit and moves to channel 2. In position "A" in figure 5.7.2, a part of the slag

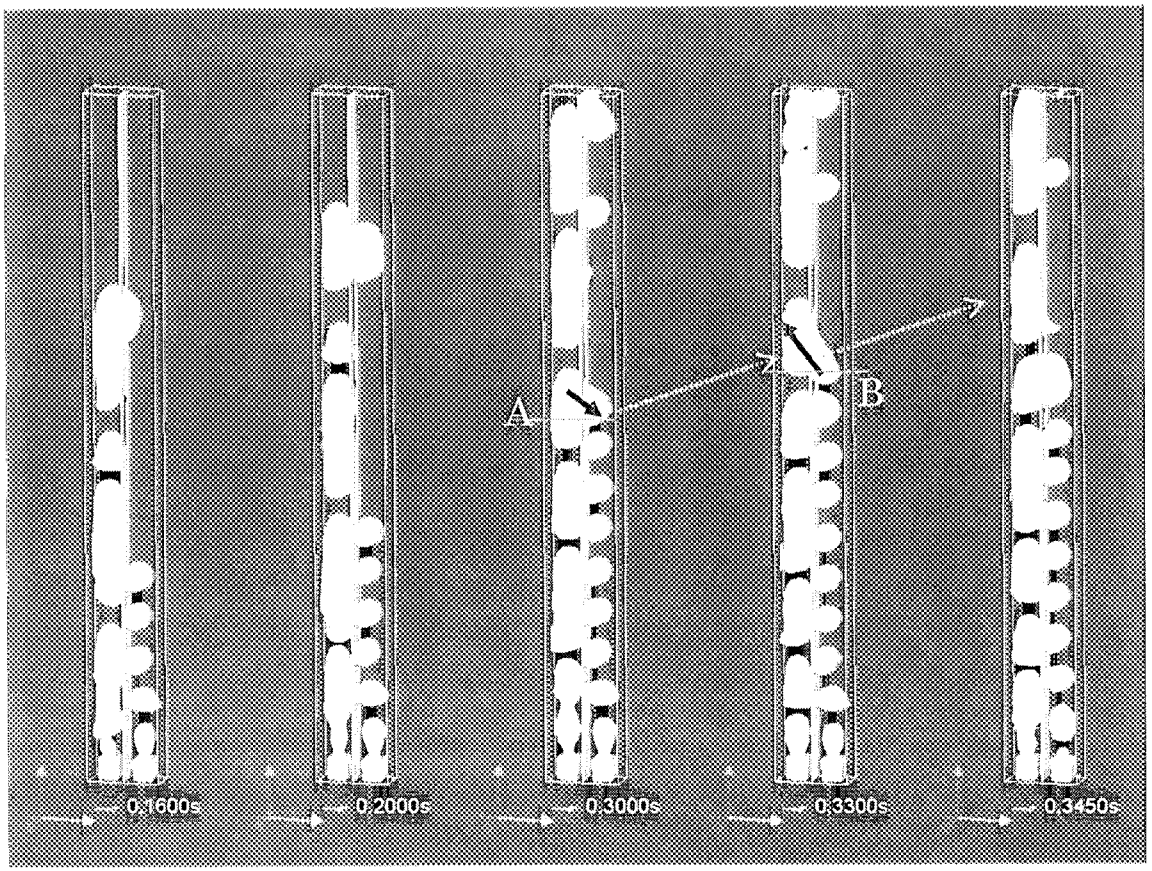

Fig.5.7.2 Void fraction distribution

bubble is move from Ch.1 to Ch.2. However, 0.33s later (position B in figure 5.7.2), the bubble comes to move to opposite direction and exist hardly in duct 2 at t=0.345s.

In the previous work[2], it is reported that the fluid mixing is affected by pressure difference between the subchannels. To check the cause of bubble movement, the horizontal pressure distributions around the bubble at position A and B are shown in Fig.5.7.3. In bubbles, pressure is almost constant and the pressure difference exists in only in the liquid

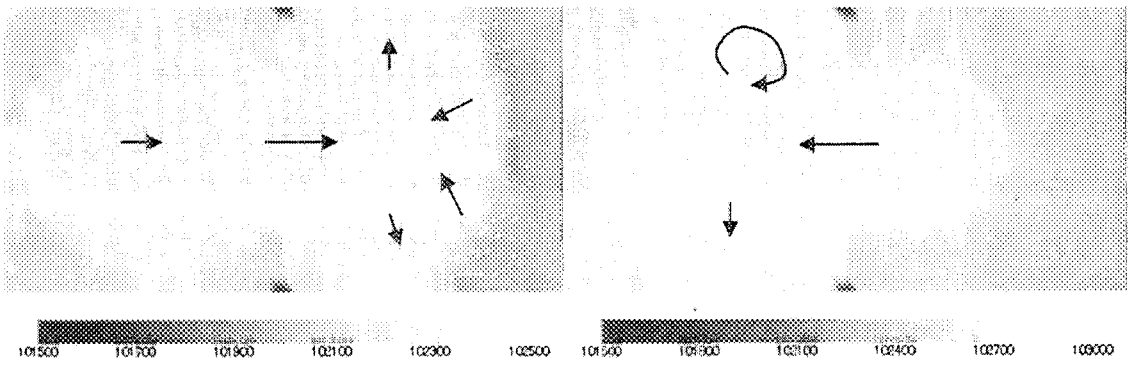

(a) Position "A" (b) Position "B"

Fig.5.7.3 Horizontal Pressure distribution

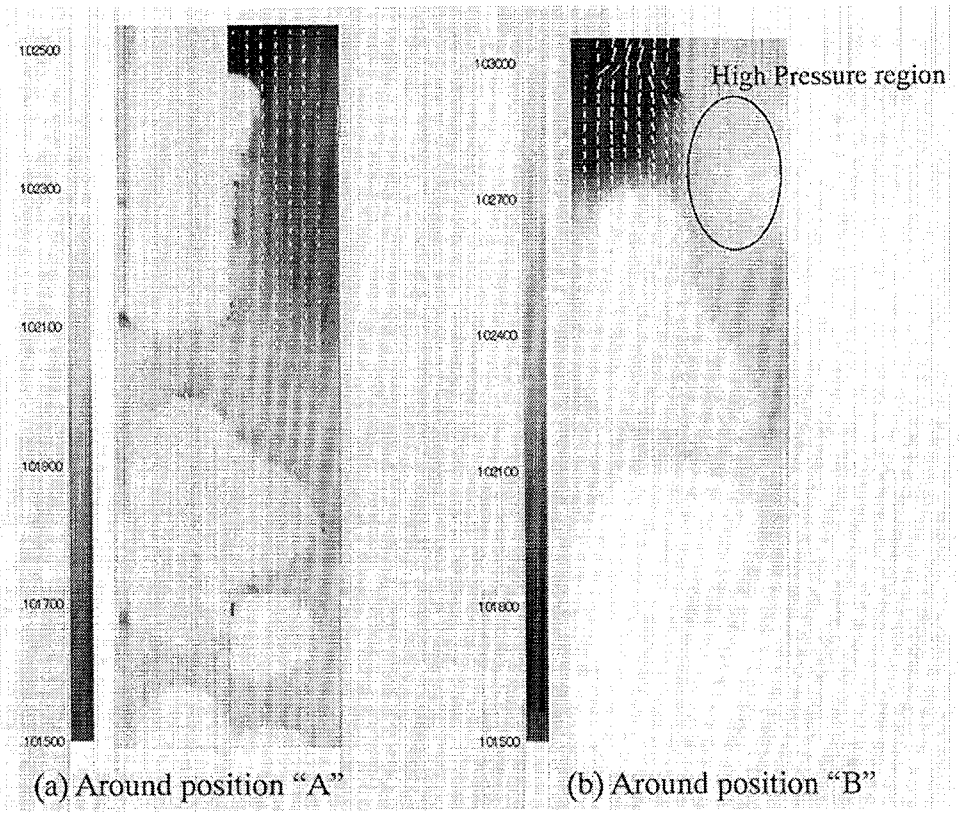

Fig.5.7.4 Pressure distribution in vertical plane

phase. Complicated velocity distributions are formed in bubbles. In Fig.5.7.3, the pressure of Ch.1 is higher in comparison with Ch.2. However, in Fig.5.7.3 (b), the bubble is moving from Ch.2 to Ch.1 against the pressure difference. Figure 5.7.4 shows the vertical pressure distributions around at position A and B. Because the high pressure range exists in the upper part of the bubble at Ch.2, the bubble considered to move from Ch.2 to Ch.1. Then, it is understood that movement of bubbles is affected by total pressure balances around the bubbles, and pressure distribution in the horizontal or vertical plane is not sufficient information to predict fluid mixing between the subchannels

Reference

1) H. Yoshida, et al, Proc. of 16th Symposium on Numerical Fluid Mechanics, D11-1, Tokyo, Japan, (2002), [in Japanese]

2) Sumida, et al., JSME Journal B, 63, 612, (1997) [in Japanese]

5.8 A Large-Scale Numerical Simulation on Liquid Film Flow Behavior around a Spacer Rib in a Narrow Fuel Channel

K. Takase, H. Yoshida, Y. Ose*, H. Tamai and H. Akimoto
(*E-mail:* takase@popsvr.tokai.jaeri.go.jp)

A reduced-moderation light water reactor (RMWR), which is studied by the Japan Atomic Energy Research Institute, needs the volume ratio of the coolant and fuel less than 0.2, in order to attain 1.1 or more high breeding ratios. The RMWR fuel assembly consists of many fuel rods with a diameter of around 10 mm with the triangular tight-lattice configuration in the horizontal direction. Here, gap spacing between fuel rods is about 1 mm. Moreover, spacers are set to keep uniformly the gap spacing for horizontally. These spacers are installed with a fixed interval to the flow direction in a reactor core. As a result, a complicated flow is formed around each spacer because of a large flow disturbance.

Many studies on the thermal-hydraulic characteristics around spacers and obstacles in narrow channels have been conducted for a field of the single-phase flow. On the other hand, as for the thermal-hydraulics in the liquid film flows inside narrow channels with spacer ribs, the flow visualization experiments and the measurements of the liquid film thickness on ribbed channels have been carried out. However, shapes and geometries of spacer ribs in cases of previous studies are different from those of the present study. Therefore, it is not appropriate from the results of the previous research to predict the two-phase flow behavior in narrow channels with spacer ribs. Then, the present study was conducted to investigate numerically the fundamental liquid film flow behavior in a narrow rectangular channel with a three-dimensional spacer rib.

The two-phase flow analysis code developed by Yoshida was used for the present study. This code can transport an interface between the liquid and gas in the time and space directions with high accuracy. The analytical model consists of a three-dimensional rectangular channel with a simplified spacer rib. Since the channel height is equal to the rib height, the flow does not overcome the spacer rib. It is thought that the fluid flow from the channel inlet separates right and left at the front of the spacer rib and then flows back. Dimensions of length and width at the channel are 81 and 27 mm and those at the spacer rib are 6 and 3 mm. The height (H) is changed in the range of 2-10 mm as a parameter. Boundary conditions are as follows: top and bottom at the channel and the surface of the spacer rib are walls; every wall has the no-slip condition; both sides at the channel are set to the symmetric boundary and free-slip conditions; and the velocity profile at the channel inlet is uniform.

---

* Yamato System Engineer

Water and vapor are used in the present analysis. The water flows near the bottom wall at the channel and the vapor flows near the top wall. In the calculations the film thickness (h), water velocity (J_l) and vapor velocity (J_g) were given to the channel inlet as initial values. The film flow behavior around the spacer rib progressing in the time direction was analyzed numerically changing the channel and spacer rib height, vapor velocity and film thickness. The calculations were carried out in the range of the following conditions: non-heated isothermal flow; h=1-7 mm; J_l=1 m/s; and J_g=1-10 m/s. Thermal properties of water and vapor were calculated using a saturation temperature 288°C at pressure 7.2 MPa. These values simulate the coolant condition at the vicinity of the RMWR core outlet.

Figure 5.8.1 shows the visualized interface behavior around a spacer rib. Each interface corresponds to the void fraction of 0.5. Calculated conditions are as follows: H=10 mm, h=3 mm, J_l=1 m/s, and J_g=5 m/s. A large flow disturbance takes place around the spacer rib with the start of the calculation (Fig.5.8.1 (a)). It is amplified with time and changes a wavy flow and then advances back (Fig.5.8.1 (b),(c)). The wavy flow disappears gradually with decreasing the flow instability (Fig.5.8.1 (d),(e)). A short separated line behind the spacer rib is seen. (Fig.5.8.1 (f))

Similarly, the visualized interface behavior around a spacer rib at H=10 mm, h=3 mm, J_l=1 m/s, and J_g=10 m/s is shown in Fig.5.8.2. The J_g is twice as high as that in Fig.5.8.1. Behavior on the flow disturbance and waving is almost the same as the case of Fig.5.8.1 (Fig.5.8.2(a),(b),(c)). Since J_g is faster than that in Fig.5.8.1, it is thought that an interface receives a strong shear stress in comparison with the case in Fig.5.8.1. Consequently, it was confirmed that a part of the interface is broken and takes off (Fig.5.8.2(d)). Along separated lines generating from the rear end of the spacer rib, a wake is formed (Fig.5.8.2(e)). In the wake region, the liquid film thickness becomes extremely thin due to a large flow disturbance and is mostly filled with vapor (Fig.5.8.2(f)). From this result, it is suggested that the spacer rib located downward will receive the effect of a wake by the spacer rib located upward if the spacer ribs are installed in a line with an arbitrary interval for the flow direction. Therefore, it is very important to consider the optimum spacer rib arrangement.

Three-dimensional computations on a liquid film flow around a simulated spacer rib under a simplified RMWR flow channel condition were carried out using a newly developed two-phase flow analysis code. A fundamental effect of a spacer rib on the liquid film flow was clarified numerically and the following conclusions were derived.

1) A wake behind the spacer rib takes place easier when the initial liquid film thickness is small and then the gas velocity is higher than the liquid velocity.
2) The liquid film thickness reduces with increasing the gas velocity and with decreasing the channel height

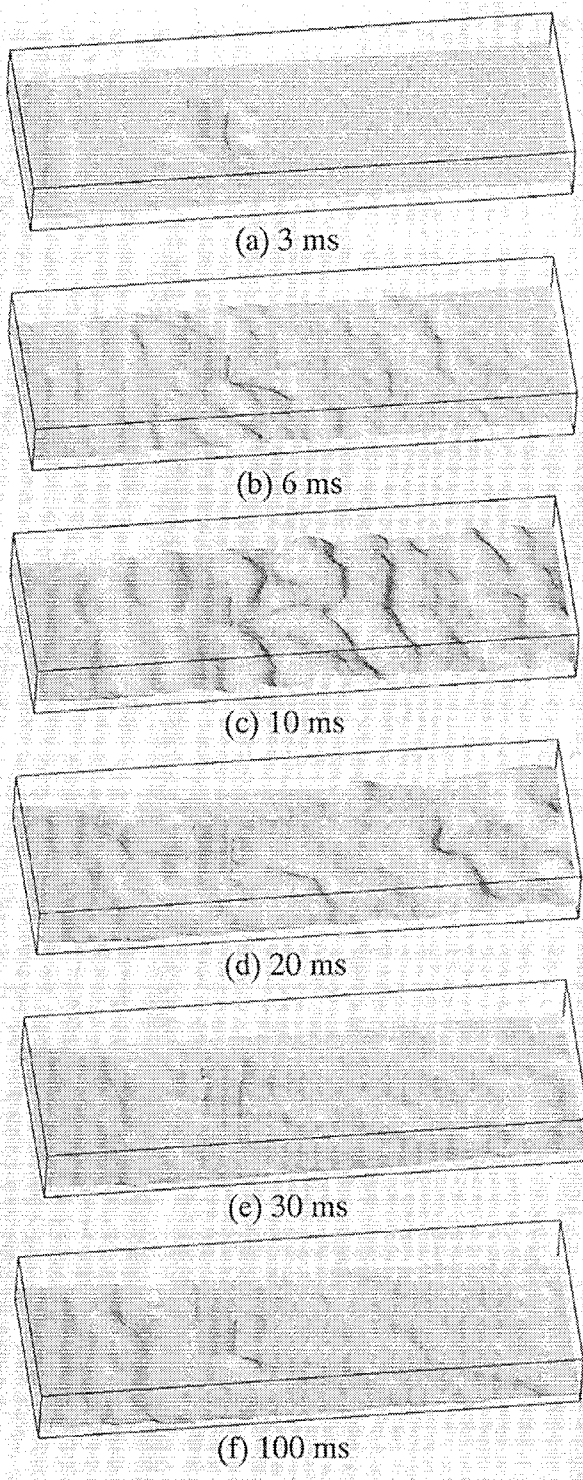

Fig.5.8.1 Predicted film flow patterns with time from the start of the calculation at H=10 mm, h=3 mm, J_l=1 m/s and J_g=5 m/s.

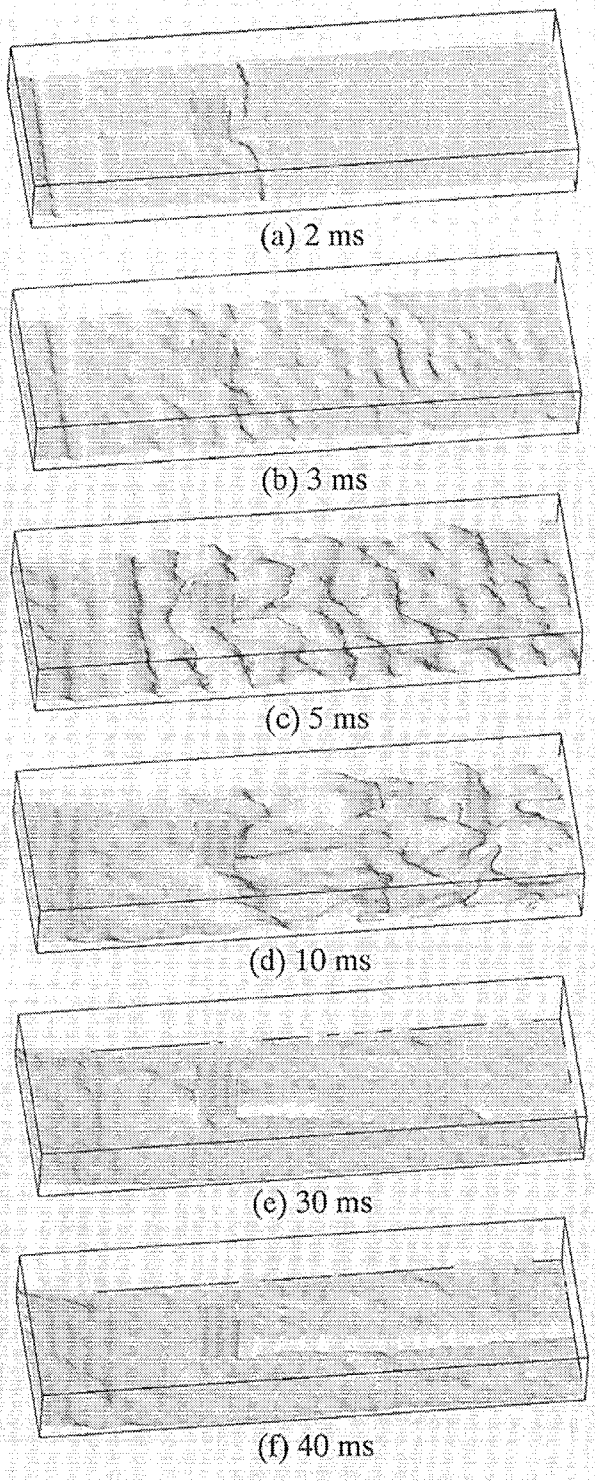

Fig.5.8.2 Predicted film flow patterns with time from the start of the calculation at H=10 mm, h=3 mm, J_l=1 m/s and J_g=10 m/s.

5.9 Experimental and Analytical Investigations on a Thermal-hydraulic Transient Issue in a Fusion Experimental Reactor

K. Takase, M. Shibata, Y. Ose*, H. Watanabe and H. Akimoto
(*E-mail:* takase@popsvr.tokai.jaeri.go.jp)

An integrated ingress-of-coolant event (ICE) test facility[1] was constructed in order to investigate whether the concept of the ITER[2] vacuum vessel pressure suppression system (VVPSS) is adequate. On the other hand, numerical analyses with the modified TRAC-PF1 code[3] were performed and its prediction accuracy was verified using the results of the integrated ICE experiments. The integrated ICE test facility simulates the current ITER VVPSS with a small-scale model of 1/1600 and mainly consists of a plasma chamber (PC), divertor, vacuum vessel (VV), relief pipes, suppression tank, drain tank and drain pipe.

Experimental conditions were as follows: water temperature and pressure in the boiler 125-150°C and 2-4 MPa; PC wall temperature 230°C; VV wall temperature 100-230°C; initial pressure inside the test facility less than 100 Pa; number of used water injection nozzles 3; injection time period of water 45 s; and number of relief pipes 1-3. The total amount of water (i.e., 0.26 m^3), which is injected into the PC by the combination of 3 water injection nozzles and 45 s injection time period, corresponds to 1/1600 of the total injected water volume (i.e., 420 m^3) in ITER during the ICE

Figure 5.9.1 shows the effect of the wall and water temperatures on the pressure rise inside the PC. Although the solid and dashed lines show almost the same pressure transients, the dotted line shows a lower value than the solid and dashed lines. From this result it was found that the pressure rise in the PC under the ICE strongly depends on the water temperature in comparison with the VV wall temperature when the PC wall temperature is constant. About this matter the following reason is considered. Since the inside of the PC gets wet as soon as the water is injected into the PC, the PC wall is cooled down by the ingress water and then the PC wall temperature is almost equal to the water temperature. As a result the PC pressure is equivalent to the saturation pressure which is determined by the water temperature.

Figure 5.9.2 shows the effect of the cross-sectional area of the relief piping on the pressure rise in the PC. The solid, dashed and dotted lines represent the measured pressure transients in the PC when the number of the used relief piping is 1, 2 and 3. The PC pressure decreases as the number of the used relief pipeing increases. That is, the pressure rise in the

---

* Yamato System Engineer

PC during the ICE depends on the cross-sectional area of the relief pipe. Because a large amount of vapor is sent to the suppression tank and condenses immediately in case that the cross-sectional area of the relief pipe is large. The one-pointed solid line shows the result under the old designed ITER VVPSS. It is evident from this result that the performance of the current designed ITER VVPSS is higher than that in the old designed ITER VVPSS.

Figure 5.9.3 shows the void fraction distributions inside the PC and VV predicted by three-dimensional computations with the modified TRAC-PF1 code. Here, (a) 0.5 s, (b) 2 s, (c) 4 s and (d) 45 s present the time from the start of the water injection. The water injected from the three nozzles into the PC hits on the opposite wall (Fig.5.9.3(a)). The water is accumulated inside the PC with time (Fig.5.9.3(b)-(d)). After the water injection into the PC, the accumulated water in the PC moves gradually to the VV through the divertor according to the pressure balance between the suppression tank and drain tank.

A series of the present experimental and analytical results are summarized as follows:

1) The ITER VVPSS is very effective to reduce the pressurization during the ICE;
2) The pressure rise characteristics strongly depend on the water temperature in comparison with the VV wall temperature when the PC wall temperature is constant;
3) The pressure decrease in the PC caused by the condensation of vapor in the suppression tank depends on the cross-sectional area of the relief piping;
4) The modified TRAC-PF1 code can predict the maximum pressure in the PC during the water injection with sufficient accuracy to the integrated ICE experimental results;
5) The present three-dimensional numerical analysis with the modified TRAC-PF1 code is very useful to clarify quantitatively the water-vapor two-phase flow behavior during the ICE.

References

1) K. Takase, et al.: "Depressurization behavior of vacuum vessel pressure suppression systems in fusion reactors at multiple first wall pipe break events", International Journal of Applied Electromagnetics and mechanics, Vol.13, pp.365-372 (2001/2002).
2) R. Aymer: "ITER R&D: Executive Summary: Design Overview", Fusion Engineering and Design, Vol. 55, pp.107-118 (2001).
3) K. Takase, et al.,: "Analysis of Pressure Rise in an ITER-Like Fusion Reactor during In-Vessel LOCA by a Modified TRAC-PF1 Code", Fusion Technology, Vol.39, pp.1050-1055 (2001).

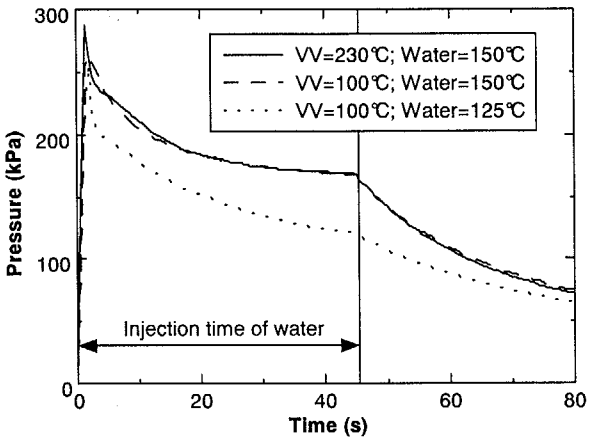

Fig.5.9.1 Effect of wall and water temperatures on pressure rise in the PC

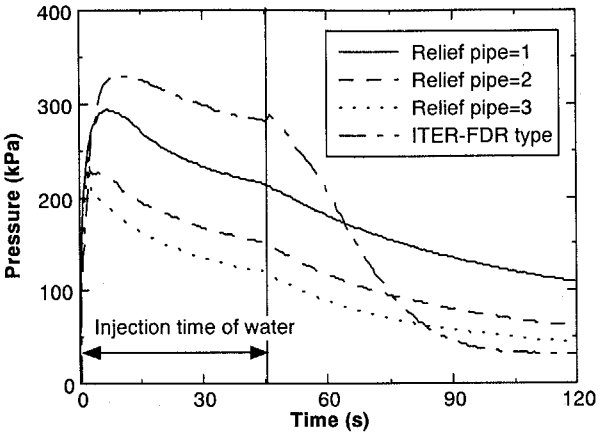

Fig.5.9.2 Effect of cross-sectional area of the relief pipe on pressure rise in the PC

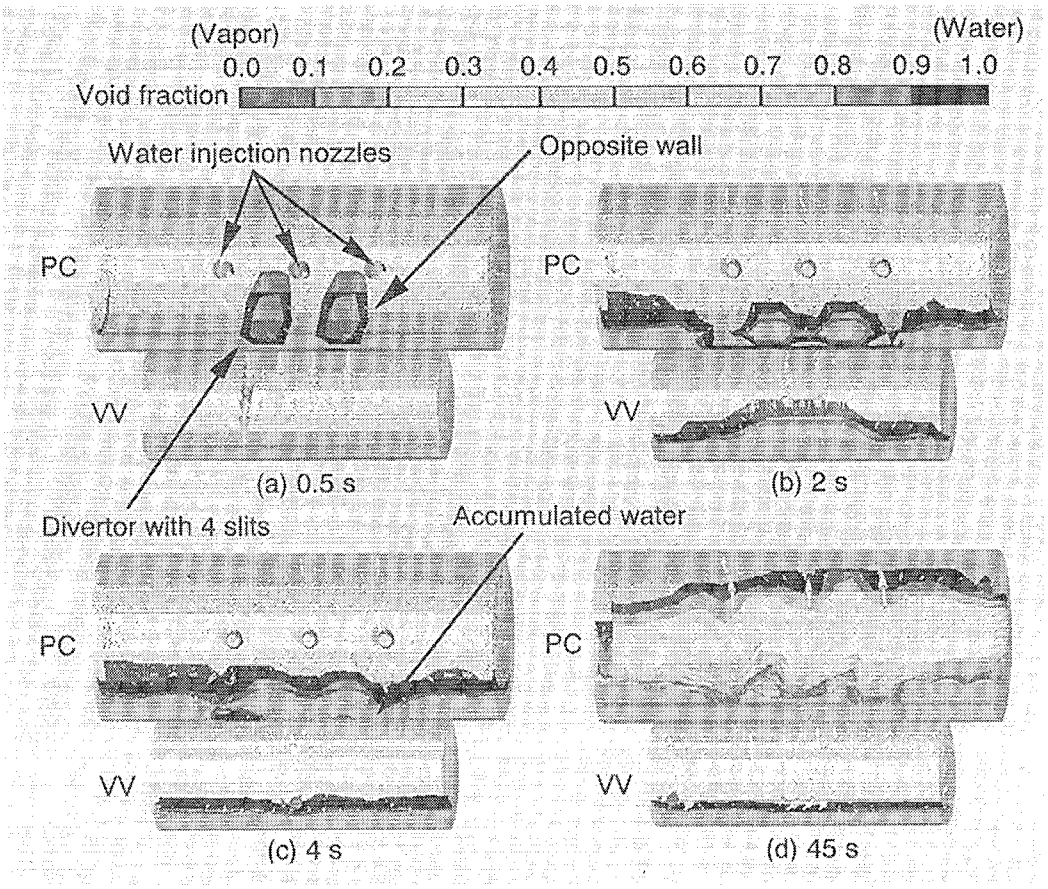

Fig.5.9.3 Void fraction distributions in the PC and VV predicted by three-dimensional computations with the modified TRAC-PF1 code

5.10 Experimental and Numerical Studies on Condensation Characteristics of Vapor in Cold Water

K. Takase, Y. Ose*, M. Shibata and H. Akimoto
(*E-mail:* takase@popsvr.tokai.jaeri.go.jp)

A pressure suppression system is considered to protect the facility components in a vacuum vessel (VV) of a fusion reactor from the rapid pressurization during an ingress of coolant event. It mainly consists of a suppression tank and relief piping. The suppression tank initially holds water under low temperature and pressure and then the vapor generated by the ICE is sent from the VV through the relief piping to the suppression tank, and is cooled down by low temperature water in the suppression tank. Finally, the pressure in the VV is decreased. Therefore, it is very important to clarify the performance of the suppression tank during the ICE from the viewpoint of the fusion reactor safety. Then, preliminary flow visualization experiments were carried out to investigate qualitatively the direct-contact condensation behavior between the water and vapor under low pressure. Furthermore, numerical analyses on a water-vapor two-phase flow were performed to predict the condensation phenomenon in the suppression tank during the ICE with high accuracy.

Figure 5.10.1 shows the experimental apparatus for the flow visualization. It simulates one organ pipe installed into the suppression tank and consists of a boiler, a simulated organ pipe with a diameter of 16 mm and an acrylic rectangular water tank with the dimensions of 600 mm in length, 600 mm in width, 1200 mm in height and 20 mm in thickness. The water tank is initially filled with water under low temperature to the level of around 1000 mm upward from the base. Experimental conditions are as follows:

- Vapor pressure and temperature are 100-130°C and 1-3 kPa;
- Initial pressure in the water tank is less than atmospheric pressure;
- Initial temperature in the water tank is less than 30°C;
- Injection time of vapor into the water tank is less than 60 s; and,
- A multi-hole duct is used as a simulated organ pipe, as can be seen in Fig.5.10.2.

Figure 5.10.3(a) and (b) show the observed flow configurations of vapor around the multi-hole duct in the water tank after 0.1 and 0.5 s from the start of the experiment. The lower end of the duct has closed and 30 holes with a diameter of 2 mm are prepared from the lower end of the duct in 10 mm pitch to the right-and-left direction (i.e., an interval of 180 degrees in the circumferential direction of the duct) toward the upper part, respectively. The position of a hole on either side shifts 5 mm in the axial direction.

---

* Yamato System Engineer

The fragmentation of bubbles is observed with promotion of condensation. That is, a large bubble is divided by some small bubbles, and changes many microbubbles. Finally, the microbubbles are condensed and changes water. Since the interfacial surface between water and vapor increases due to a large number of microbubbles, it can be prospected that high condensation efficiency is expectable under the multi-hole duct.

Figure 5.10.4(a) and (b) are the predicted temperature distributions around the multi-hole duct and correspond to the results of Fig. 5.10.3 (a) and (b). In case of the multi-hole duct, since the vapor spreads throughout the water tank in comparison with the strait duct, it can be expected that condensation is mostly promoted.

Figure 5.10.5 shows the velocity vector distributions around the multi-hole duct during the vapor injection and was obtained by the PIV technique. Here, the velocity vectors are shown for an upper half area of the multi-hole section in the duct. From this result, it was clarified that many vortexes generate in the water with the ingress of vapor and then the fluid mixture inside the water is promoted by the generated vortexes.

Direct-contact condensation behavior of vapor injected into the cold water under low pressure was investigated visually and numerically. From the present study it was found that the current numerical approach is very effective to clarify the effects of the configuration of organ piping and the arrangement of duct holes on the condensation of vapor. The present results were reflected to the optimum design of the ITER suppression system.

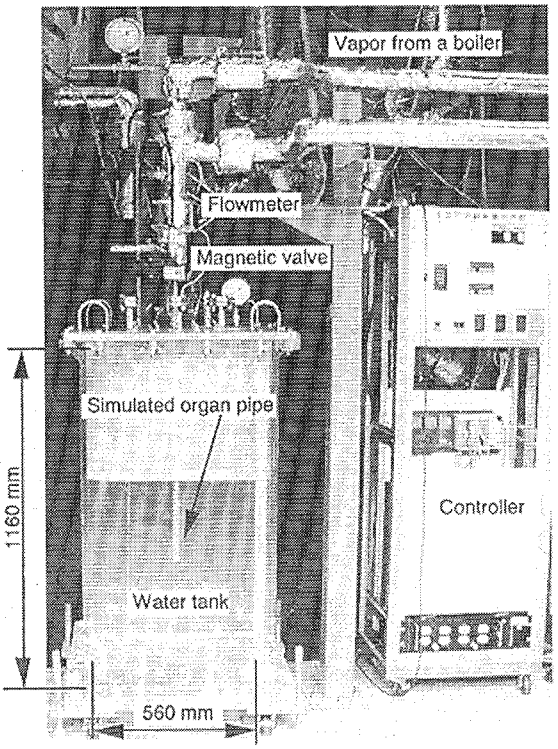

Fig.5.10.1 An experimental apparatus

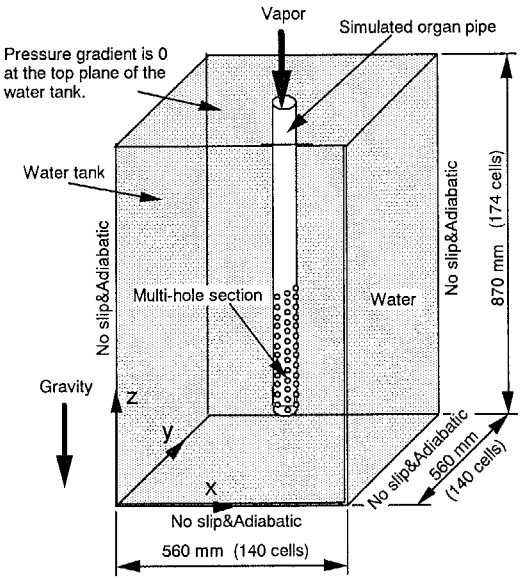

Fig.5.10.2 Analytical geometry

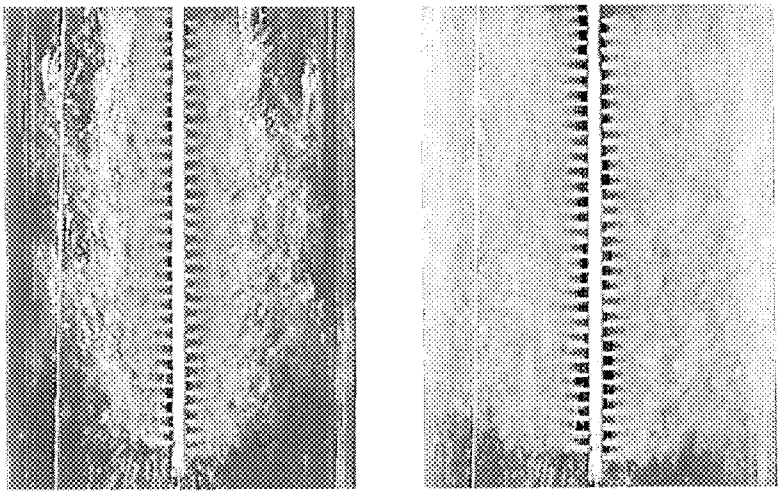

(a) After 0.1 s (b) After 0.5 s

Fig.5.10.3 Observed flow configurations of the vapor injected from the multi-hole duct

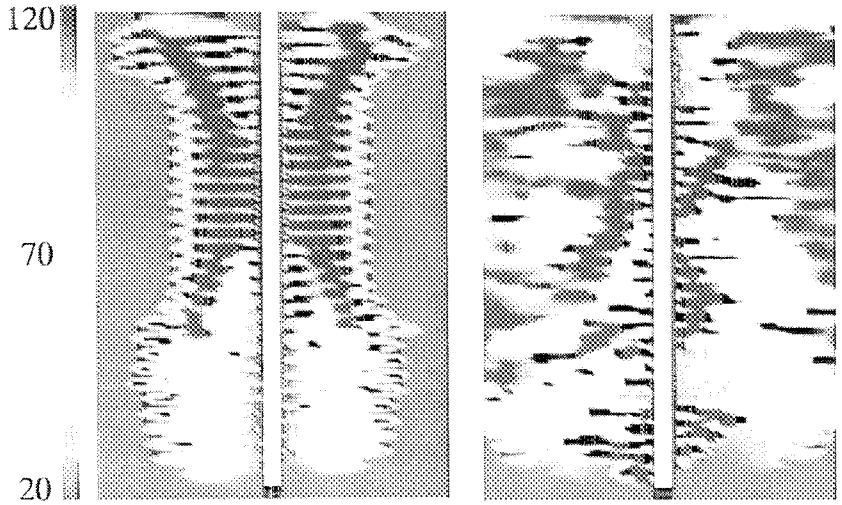

(a) After 0.1 s (b) After 0.5 s

Fig.5.10.4 Predicted temperature distributions corresponding to Fig.5.10.3(a) and (b)

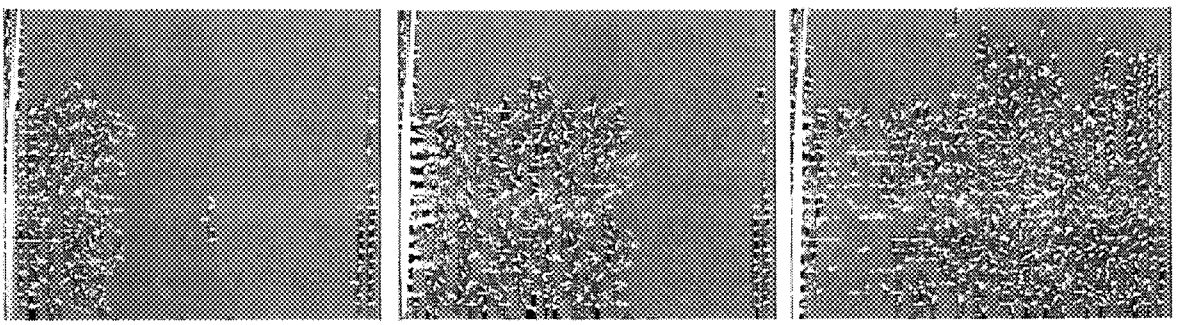

(a) After 0.1 s (b) After 0.3 s (c) After 0.5 s

Fig.5.10.5 Time change of velocity vector distributions around a multi-hole duct obtained by the PIV technique

5.11 Development of Visualization Programs for Two-Phase Flow Analysis Results using the AVS Code

K. Takase, H. Yoshida, H. Tamai, Y. Ose*, E. Kume and K. Masuko
(*E-mail:* takase@popsvr.tokai.jaeri.go.jp)

The reduced-moderation light water reactor (RMWR)[1] has been developed for the purpose of advanced use of light water reactors. In order to obtain 1.0 or more conversion ratios, it is expected from the results of the previous studies that the volume ratio of water and fuel must be decreased to about 0.25 or less. To satisfy this condition, a fuel bundle with a triangular tight-lattice arrangement is required. Here, a fuel rod outer diameter is around 13 mm and the gap spacing between each rod is around 1 mm. Although the coolant is 100% water at the core inlet, it changes water and vapor along the flow direction due to the heating by the fuel rods, and then the vapor occupies 70% or more at the core outlet. The flow rate at the actual RMWR core is reduced down to around 10 % of the water flow rate at the BWR with 8x8 fuel bundle. Therefore, the RMWR has very severe coolant condition on the viewpoint of the thermal engineering.

Authors are performing the three-dimensional computations regarding the thermal-hydraulic characteristics in a tight-lattice fuel bundle in order to conduct the thermal design of the RMWR core. Since its geometry is complicated and huge calculation memory is required, however, it takes lots of time to carry out the quantitative evaluation for the analysis results. Then, to make the quantitative evaluation easy, the visualization programs for the analytical results were developed using the visualization soft AVS/Express[2], which is one of the most sophisticated visualization tools in the world.

Figure 5.11.1 shows the analytical model. It simulates a heating section in the RMWR fuel bundle and consists of 37 fuel rods and a hexagonal flow passage which is a casing made of stainless steel. The geometry and dimensions simulate the 37-rod bundle heat transfer test facility which was constructed to obtain the critical heat flux data on triangular tight-lattice coolant channels in the RMWR core. The casing has a hexagonal cross section and a length of one hexagonal side is 51.6 mm. An axial length of the fuel bundle is 1260 mm. The water flows upward from the bottom of the fuel bundle. A flow area corresponds to a region which deducted the cross-sectional area of all fuel rods from the hexagonal flow passage. Four grid spacers are installed into the fuel bundle at the axial positions of 220, 540, 750 and 1030 mm from the bottom. The axial length of each grid spacer is 20 mm.

---

* Yamato System engineer

Figure 5.11.2 shows a drawing model of 37 fuel rods which is created by AVS/Express. Similarly, Fig.5.11.3 shows a drawing model of a casing in which the fuel rods are inserted. AVS/Express creates a network combining some modules expressed by the icon on the program. An example of a network for the present developed visualization program is shown in Fig.5.11.4. The network mainly consists of three regions: analysis result, fuel rod structure and analytical conditions.

Figure 5.11.5(a) shows the appearance of a fuel bundle which consists of a couple of drawing models of 37 fuel rods seen in Fig.5.11.2 and a casing presented in Fig.5.11.3. Figure 5.11.5(b) is a visualized example and it is created by the analytical result and Fig.5.11.5(a).

Figure 5.11.6 shows the axial velocity distributions at arbitrary flow regions in a fuel bundle. Here, (a) and (b) represent the visualized analytical results without and with a spacer. The axial velocity develops almost uniformly when there is no spacer. On the other hand, when there is a spacer, the axial velocity decreases extremely just behind a spacer.

In order to make the quantitative evaluation easy on the thermal-hydraulic analytical results of the RMWR fuel bundle, the visualization programs were developed using the AVS/Express and coordinates conversion processing. By the present study, the three-dimensional visualization on physical parameters of the predicted axial velocity, temperature, void fraction, etc. was attained.

References

1) T. Okubo et al: "Design of small reduced-moderation water reactor (RMWR) with natural circulation cooling", Proc. of International Conference on the New Frontiers of Nuclear Technology; Reactor Physics, Safety and High-Performance Computing (PHYSOR 2002), Seoul, Korea (2002).

2) For instance, "On-line AVS/Express Workbook (by Scientific Visualization Lab Exercises)", http://www.ncsc.org/training/materials/express_workbook/

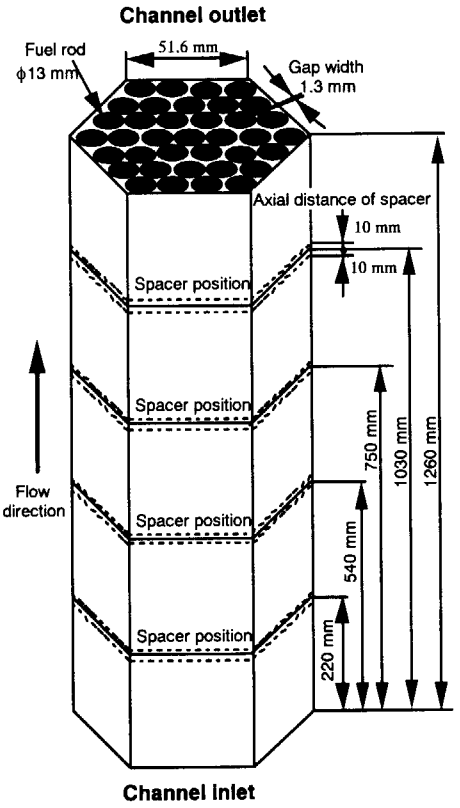

Fig.5.11.1 Analytical geometry

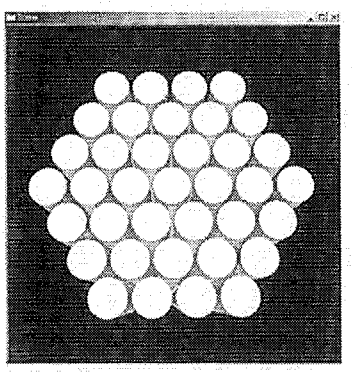

Fig.5.11.2 37 Fuel rods

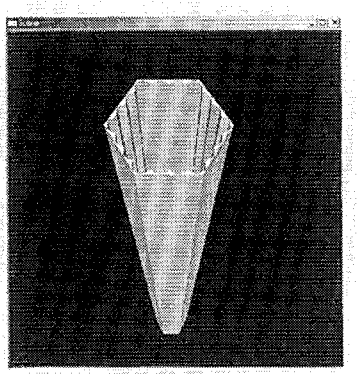

Fig.5.11.3 Casing

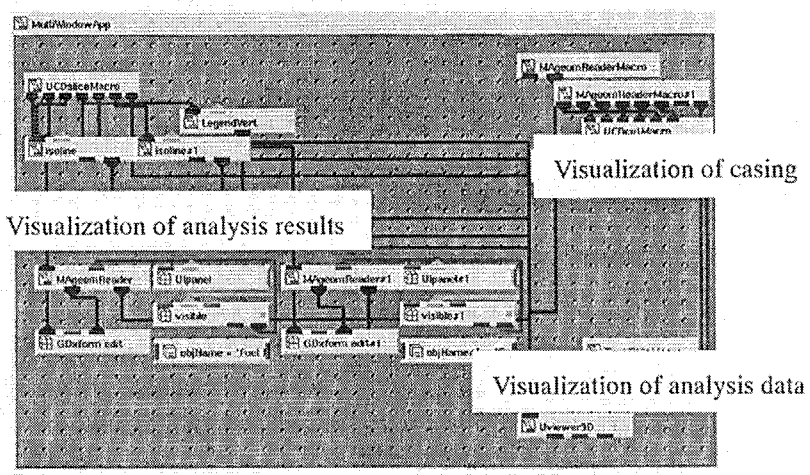

Fig.5.11.4 Block diagram of the present visualization

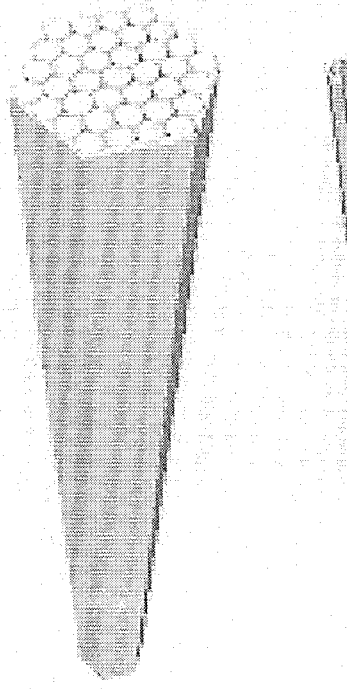

(a) Appearance of a casing and fuel rods

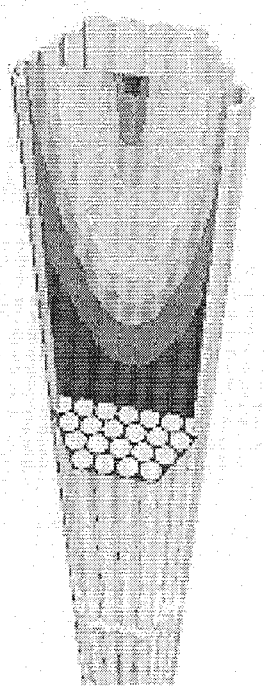

(b) Visualized result

Fig.5.11.5 Examples of visualization of numerical data

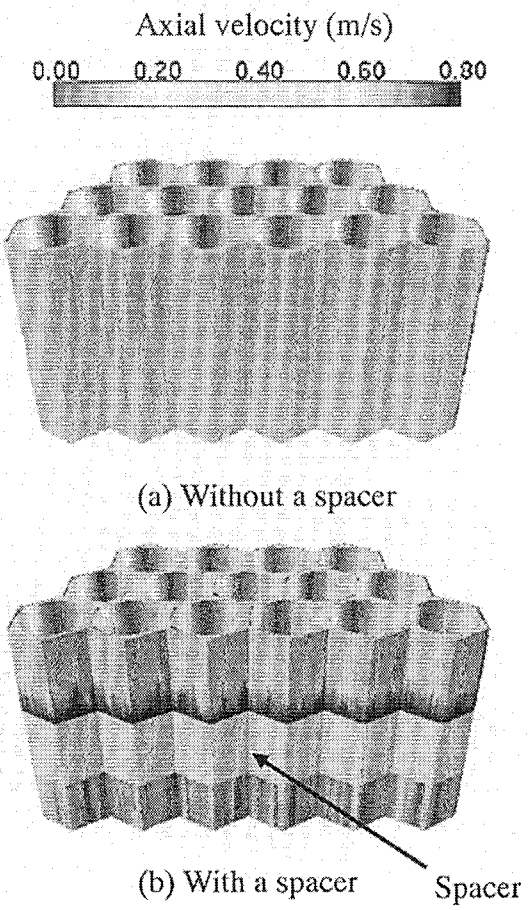

Fig.5.11.6 Visualized axial velocity distributions around fuel rods in flow regions with and without a spacer

6. Reactor Structural Materials

Structural materials used in the light water reactors (LWRs) are exposed to the high flux radiation and high temperature water, therefore stress corrosion cracking (SCC) and irradiation assisted stress corrosion cracking (IASCC) are chief concerns relating to the integrity of in-core structural materials.

In recent years, cracking incidents of BWR core shroud and primary loop recirculation (PLR) piping have increased significantly, and investigated by the electric utilities. Since October 2002, JAERI has investigated the cracking to provide JAERI's own evaluation as a third-party organization for assuring transparency of the investigations.

IASCC is known as a degradation phenomenon that is caused by synergistic effects of irradiation, stress/strain and high temperature water on the in-core materials of LWRs. Since it is essentially important to study the influence of alloying and impurity elements on IASCC behavior in order to clarify its mechanism, stress-strain behavior and susceptibility to IASCC of the neutron irradiated high purity type SS were investigated to evaluate influence of Si and Mo additions on IASCC. Effects of test temperature and strain rate on IASCC were also studied on type 316 stainless steels irradiated up to 17 dpa.

A new collaboration research has been started between JAERI and Japan Nuclear Cycle Development Institute (JNC). The objective of this research is a development of damage evaluation techniques for the irradiated and damaged structural materials of LWR and Fast Breeder Reactor (FBR). These techniques are based on the quantitative evaluation of corrosion and magnetic properties along grain boundaries in the materials

Since the synergies of radiation, stress and high temperature water cannot be reproduced outside reactor core, the in-pile IASCC testing is a key experiment to understand IASCC behavior. A high temperature water loop facility was, therefore, installed at the Japan Materials Testing Reactor (JMTR) to carry out the in-core testing. Development of techniques to perform the in-pile IASCC initiation/propagation testing has been conducted including technique to irradiate specimens under simulated BWR condition in the core of JMTR.

The JAERI Material Performance Database (JMPD) was developed with a view to utilizing material performance data efficiently. To store the irradiation condition at JMTR and experimental IASCC data, some data items and functions are added in the JMPD. The data for irradiation capsule including irradiation condition of specimens are also stored in the JMPD.

6. 1 Investigation of Stainless Steel Samples from BWR Core Shroud and Primary Loop Recirculation Piping Failed by SCC

T. Tsukada, Y. Kaji, F. Ueno, Ugachi, J. Nakano, Y. Miwa, M. Suzuki, K. Kiuchi, H. Amano, F. Kanaitsuka, T. Nishino, M. Shindo, K. Shibata and H. Nakajima
(*E-mail:* ttsukada@popsvr.tokai.jaeri.go.jp)

In recent years, cracking incidents of BWR core shroud and primary loop recirculation (PLR) piping have increased significantly. For example, at the Fukushima Dai-ni Nuclear Power Station Unit-3 of the Tokyo Electric Power Company (Boiling Water Reactor, 1100MW), cracks were found near welded joint portion of outside surface of lower ring of core shroud by the visual testing of in-core structures in 2001. The cracking has been observed near the weld lines of core shroud and pipes fabricated from low carbon austenitic stainless steels (SSs), types 304L and 316L.

Since October 2002, JAERI has investigated stainless steel samples from BWR core shrouds and PLR pipes under contracts with the Japan Power Engineering and Inspection Corporation (JAPEIC) and electric power companies. An aim of the investigations by JAERI is to provide JAERI's own evaluation as a third-party organization for assuring the transparency of investigation. Two types of investigations were conducted by JAERI. In one way, JAERI staffs examined the material samples supplied by the electric power companies at JAERI's Hot laboratories and made reports based on the data obtained by ourselves. In the other way, examinations of material samples were conducted by the electric power companies cooperating with Nippon Nuclear Fuel Development Co. Ltd. (NFD) under the observation by JAERI. Data obtained at NFD were transferred to JAERI and we made reports based on the data. Both reports of the investigation prepared separately by JAERI and electric utilities were submitted to the Nuclear and Industrial Safety Agency (NISA) and assessed by the committee opened to the public.

At JAERI, two material samples were examined at Hot laboratories which were from the core shroud of Fukushima Dai-ni Nuclear Power Station Unit-3 and from the PLR pipe of Onagawa Nuclear Power Station Unit-1 of the Tohoku Electric Company. The other six shroud and one PLR pipe samples were examined at NFD under observation by JAERI. As an example of the results of investigations, the findings obtained from the cracked region of

outer H6a welding portion of the core shroud at Fukushima Dai-ni Nuclear Power Station Unit-3 are shown as follows;

(1) Three cracks were observed at the portion 3 to 9mm apart from the weld metal and the maximum depth was about 8mm.

(2) From the result of observation of two fracture surfaces, intergranular cracking was observed in almost whole fracture surface. The transgranular cracking was partially observed within the depth of about 300μm from the surface.

(3) Hardening layer over Hv400 at maximum was found from the surface to the depth of about 500μm. The outer surface of the lower ring hardened due to the mechanical processing at its manufacturing stage.

(4) The oxides were observed in the whole inside of cracks from opening portion to the crack tip. The oxides mainly consisted of Fe-oxides.

(5) Slight fluctuations of contents of main elements in the alloys were observed, but no significant correlation was confirmed between the oxides and the cause of cracking.

Based on the examination results described above concerning presence of tensile residual stress by welding and relatively high dissolved oxygen contents in core coolant and so on, it is concluded that this crack was mainly initiated in the hardening layer of outer H6a welding portion of core shroud by transgranular stress corrosion cracking (SCC) and propagated along the grain boundaries.

Through the investigations of material samples, significant features of the cracking of core shroud and PLR pipes fabricated from low carbon SSs were known as mentioned above, but the cracking can not been explained on the basis of classical IGSCC mechanism, because no grain-boundary carbides and apparent Cr depletion at grain boundaries have observed by the transmission electron microscopy. Therefore, further investigations are required to clarify the mechanism of SCC in low carbon SSs.

6.2 Effects of Silicon and Molybdenum Additions on IASCC of Neutron Irradiated Austenitic Stainless Steels

J. Nakano, Y. Miwa, T. Tsukada and H. Tsuji
(E-mail:lantis@popsvr.tokai.jaeri.go.jp)

Irradiation assisted stress corrosion cracking (IASCC) is known as a degradation phenomenon that is caused by synergistic effects of neutron /gamma irradiation, stress/strain and high temperature water on the in-core structural materials of light water reactors (LWRs). From the view point of the life management of core components of aged LWRs, IASCC is concerned to be one of the key issues. Although it is essentially important to study the influence of alloying and impurity elements on IASCC behavior in order to clarify its mechanism, it is difficult to examine the influence using the commercial purity alloys. Therefore, by the authors, high purity type stainless steels (SSs) had been fabricated and slow strain rate testing (SSRT) for the irradiated specimens had been performed in high temperature water. In the present study, stress-strain behavior and susceptibility to IASCC of the neutron irradiated high purity type SS were investigated to evaluate influence of Si and Mo additions on IASCC behavior.

Chemical contents of high purity type 304 and 316 SSs used in this study are shown in Table 6.2.1. After solution heat treatment (1453K×30min and water quench), round bar type specimens with 24 mm in gage length and 4 mm in diameter were machined from the SSs. Specimens were irradiated to neutron fluence of 3.5×10^{25} n/m^2 (E > 1 MeV) at 513 K in the Japan Research Reactor - 3 (JRR-3). SSRT for the irradiated specimens was performed in oxygenated water (dissolved oxygen concentration = 8 ppm) at 561 K. Applied strain rate was 1.7×10^{-7} s^{-1}.

Stress-strain curves obtained from SSRT in this study and the reference[1)] were shown in Fig. 6.2.1. In the case of HP304, yield stress was increased and strain was decreased with increasing neutron fluence. SSs with Si or Mo had shown more than 20% of strain in SSRT after irradiation to 7×10^{24} n/m^2. However, the SSs irradiated up to 3.5×10^{25} n/m^2 showed high increase of stress and decrease of strain less than 10%, and no apparent effects of Si or Mo addition. It is, therefore, considered that effects of additional elements, Si or Mo, on the mechanical behavior would be saturated. At present, fracture surface on the specimens is examined using scanning electron microscope (SEM). From the results, susceptibility to IASCC of the SSs would be evaluated quantitatively.

Reference

1) T. Tsukada: "Irradiation Assisted Stress Corrosion Cracking of Austenitic Stainless Steels" , JAERI-Research 98-007 (1998).

Table 6.2.1 Chemical compositions of high purity type 304 and 316 SSs (mass%).

Alloy-ID	C	Si	Mn	P	S	Cr	Ni	Mo	Ti	Al	N	Fe
HP304	0.003	0.01	1.36	0.001	0.0014	18.17	12.27	-	0.01	0.16	0.0014	Bal.
HP304/Si	0.003	0.69	1.36	0.001	0.0014	18.01	12.24	-	<0.01	0.10	0.0014	Bal.
HP316	0.004	0.02	1.40	<0.001	0.001	17.21	13.50	2.50	0.01	0.10	0.0020	Bal.

※ Bal.=Balance

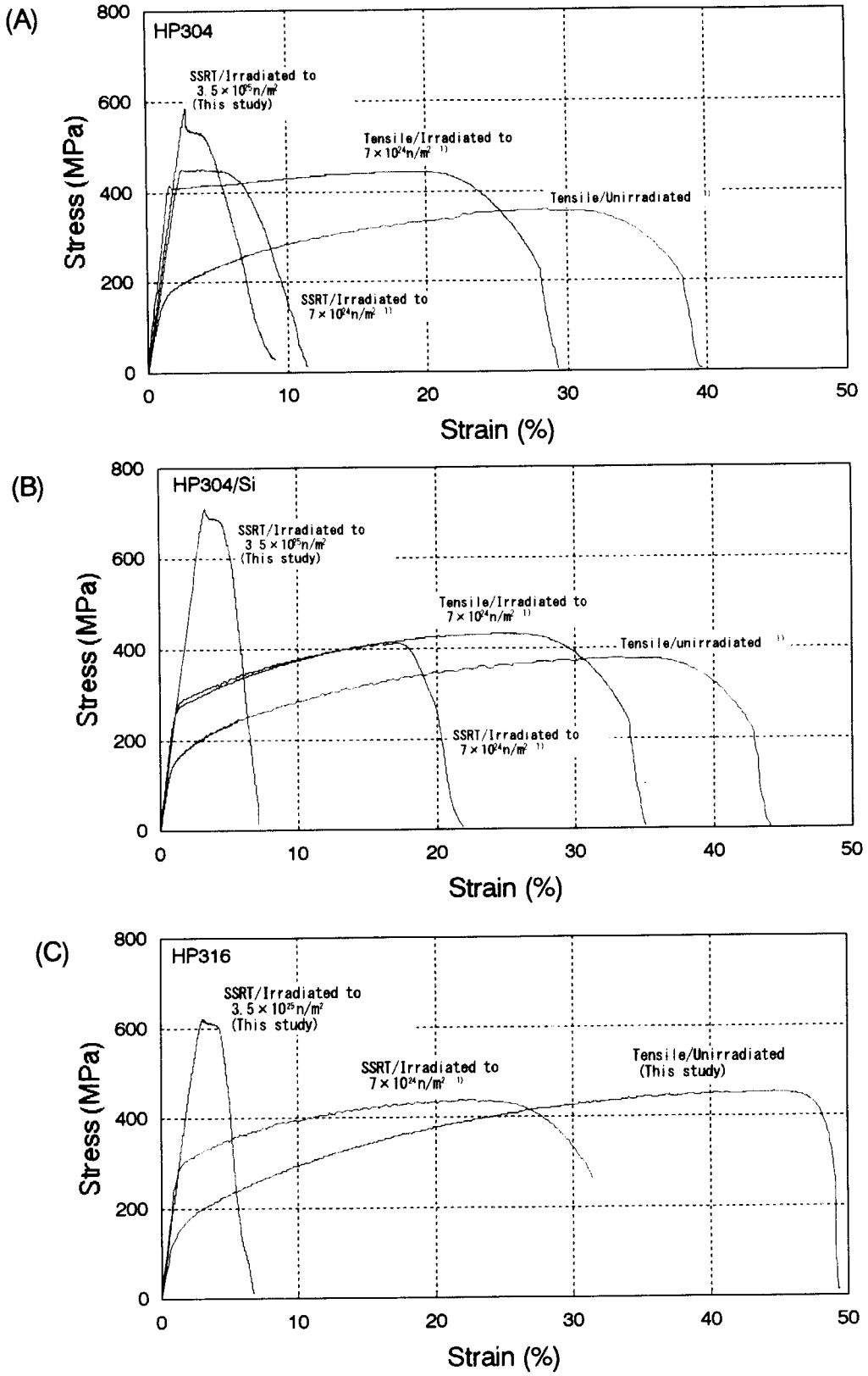

Fig. 6.2.1 Stress-strain curves obtained from this study and reference[1]: (A) HP304, (B) HP304/Si and (C) HP316.

6.3 Effect of Test Temperature and Strain Rate on IASCC Susceptibility of Type 316 Stainless Steels

Y. Miwa, T. Tsukada and H. Tsuji
(*miway@popsvr.tokai.jaeri.go.jp*)

Effect of test temperature and strain rate on irradiation assisted stress corrosion cracking (IASCC) was studied. IASCC is caused by the material's degradation, aggressive environment and stress. Many investigators studied the materials degradation such as radiation-induced segregation and effects of water environment such as hydrogen water chemistry relating to IASCC. However, study about effects of water temperature and stress condition such as strain rates is scarce. In this study, to understand IASCC mechanism based on conventional SCC mechanism, those effects were studied in type 316 and 316LN stainless steels (SSs) irradiated up to 17 dpa.

The used materials are solution-annealed type 316 and 316LN stainless steels. Some of 316LN specimens were prepared from plates jointed by hot isostatic pressing (HIPing) at 1323 K for 2h. Then the plates were furnace-cooled. Previous reports showed that there was no effects of fabrication process on tensile and (IA)SCC properties[1,2]. Sheet type specimens were irradiated at nominal temperature of 473K in High Flux Isotope Reactor (HFIR) at Oak Ridge National Laboratory. The calculated doses are 1 dpa for 316LN SS and 17 dpa for 316 SS. After irradiation, slow strain rate testing (SSRT) was performed at temperatures of 423, 513, 573 and 603K in oxygenated (DO=7-32 ppm) water. Strain rate ranged over from 2×10^{-8} to 2×10^{-5}/s. To identify fracture mode, scanning electron microscopy was also conducted.

On 316LN SS irradiated to 1 dpa, IASCC occurred in high temperature water above 573K, but not below 513K. On 316 SS irradiated to 17dpa, only ductile fracture was observed after SSRT at 513K. All tests were conducted at strain rate of $2\text{-}10\times10^{-7}$/s commonly used for laboratory tests at JAERI. Fig.6.3.1 summarized dependence of test temperature and dose on IASCC. Reference data[3-6] are also indicated in the figure. As seen in the figure, IASCC never occurred below 513K. It is well known, however, ordinary SCC on un-irradiated alloys occurs even at 323K[7] and its susceptibility based on crack growth rate measurements[8] reaches the maximum around 523K. Therefore the test temperature dependence of IASCC may be different from that of ordinary SCC. It is considered that corrosion behavior of irradiated materials in this study is not different from that on thermally-sensitized materials, because 316LN irradiated to 1 dpa showed IGSCC susceptibility in 573K water. Irradiation to 17dpa is enough to cause Cr depletion at grain boundaries (GBs) but it is not sufficient condition for IASCC at 513K. We think other mechanism except Cr depletion at GBs may act on IASCC.

As mentioned above, IASCC did not occur below 513K at practical strain rate in the laboratory. SCC is considered to be controlled by thermal activation process and therefore SCC susceptibility may show the Arrhenius type temperature dependence. At lower test temperature, longer test period is needed to evaluate the susceptibility. So to make the test temperature dependence clear, effect of process time on IASCC susceptibility was studied by changing the stress condition by means of strain rate control. 316LN specimens were SSR tested at various strain rate and temperature. Fig. 6.3.2 shows the results of SSRT. The upper limit strain rate for IASCC occurrence is indicated by line in figure. We estimated from the area ratio of fracture surface and fracture strain that strain rates of $1x10^{-6}$/s and $3x10^{-6}$/s were upper limit at 573K and 603K, respectively. It is expected form these results that in 513K water, IASCC may occur by SSRT with strain rate of $2x10^{-8}$/s, so that now we are performing SSRT at $2x10^{-8}$/s.

References

1) J. Nakano et al., J. Nucl. Mater. 307-311 (2002) 1568-1572.
2) Y. Miwa et al., J. Nucl. Mater 307-311 (2002) 347-351.
3) T. Tsukada et al., Proceedings of 8th int. Symp. on Environmental Degradation of Materials in Nuclear Power Systems – Water Reactors, ANS, (1997) p.795.
4) T. Tsukada et al., Corrosion 92, (1992) paper No.104.
5) P. Lorenzotto et al., J. Nucl. Mater. 233-237 (1996) p.1387.
6) G. R. Caskey and R. S. Ondrejcin, "Effect of Irradiation on Intergranular Stress Corrosion Cracking of Type 304 Stainless Steel", WSRC-RP-89-965 (1989).
7) F. P. Ford et al., Corrosion Vol.35, (1979) p.569.
8) P. L. Andresen, Corrosion Vol.49, No.9 (1993) p.714.

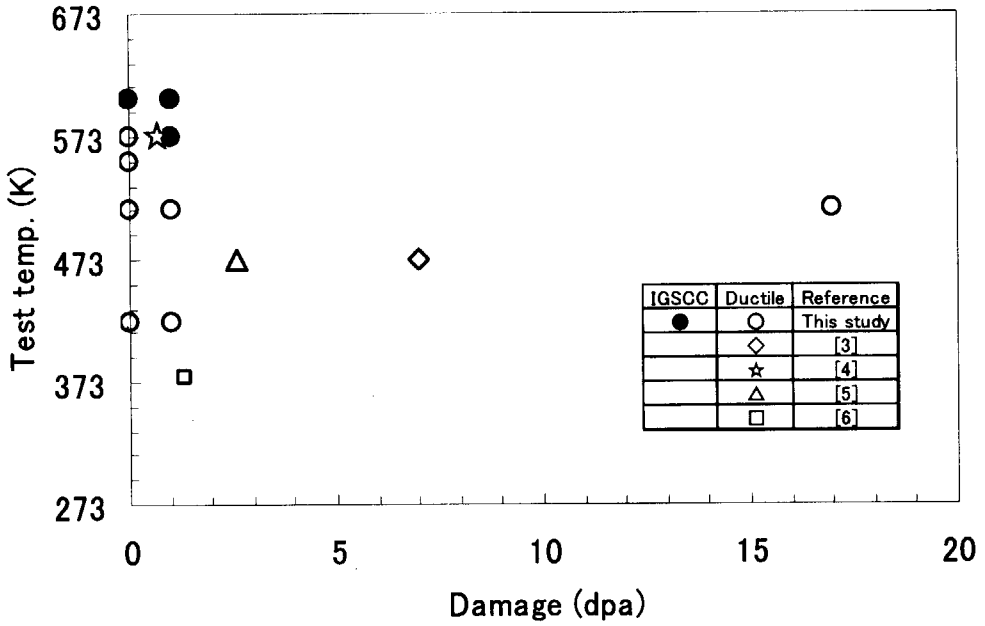

Fig. 6.3.1 Test temperature and dose dependence of IASCC

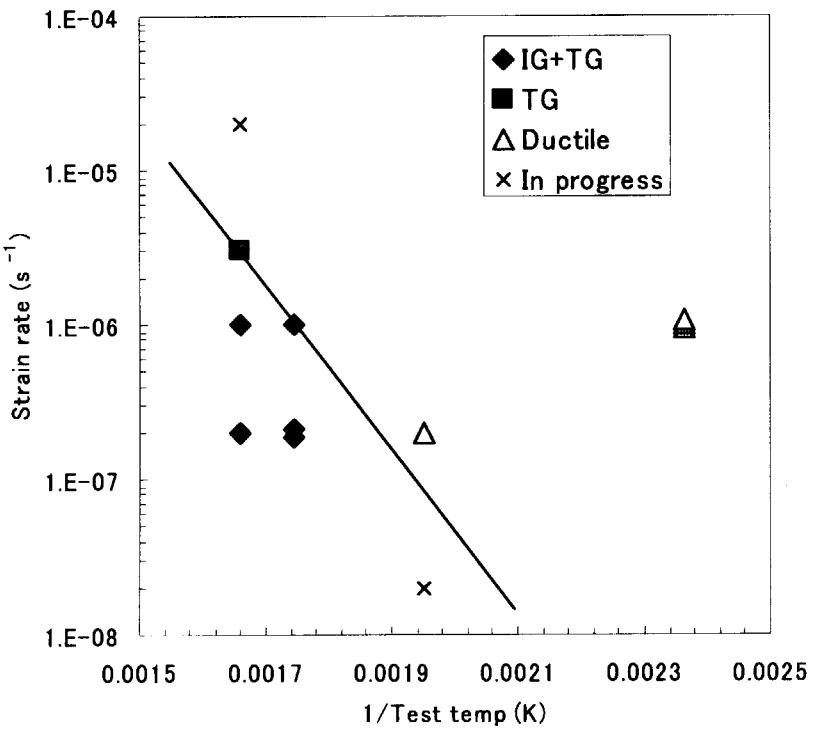

Fig. 6.3.2 Test temperature and Strain rate dependence of IASCC

6.4 Development of Damage Evaluation Techniques for LWR and FBR Structural Materials Based on Corrosion and Magnetic Properties along Grain Boundaries

F. Ueno, Y. Nemoto, Y. Miwa, T. Tsukada, H. Tsuji, T. Hoshiya*, Y. Nagae*, K. Aoto*, Y. Abe*, Y. Nakamura*, M. Ohmi and J. Saito
(E-mail: ueno_f@popsvr.tokai.jaeri.go.jp)

A new collaboration research has been started between JAERI and Japan Nuclear Cycle Development Institute (JNC) in the middle of fiscal year 2002 (FY2002). This collaboration research is one of the activities of the unification project between JAERI and JNC which is planned up to FY2005. It is aimed that the collaboration between two institutes can contribute to remarkable progress and result of the research rather than individual.

The objective of this research is a development of damage evaluation techniques for the irradiated and damaged structural materials of Light Water Reactor (LWR) and Fast Breeder Reactor (FBR). These techniques are based on the quantitative evaluation of corrosion and magnetic properties along grain boundaries (GBs) in the materials, which are studied individually at JAERI and JNC, respectively, Because it is commonly considered that GB properties of structural materials under LWR and FBR environments are closely related to the material degradation dominating safety and lives of the plants.

At JAERI, radiation damage mechanism has been researched as one of the items of a study on irradiation assisted stress corrosion cracking (IASCC) in LWR. A new evaluation procedure based on corrosion property of irradiated stainless steel has been developed by Nemoto, et al.[1-2] In this method, electrochemically etched specimens are examined on its corrosion property by Atomic Force Microscope (AFM). This is applicable to the present research as the evaluation method to be focused on the analysis of GB damage caused by neutron irradiation.

On the other hand, at JNC, creep damage mechanism has been studied with the aim of FBR plant life evaluation and safety maintenance. A new detection technique of creep damage in stainless steel was developed based on magnetic property by Nagae, et al.[3-4] Creep tested specimens were evaluated by the technique through the natural magnetization obtained by very sensitive Flux-gate (FG) sensor.

The integration of these techniques to study irradiation damage mechanism along GB will make it possible to understand the correlation between microstructural change by irradiation and degradation of corrosion and mechanical properties in detail.

*Japan Nuclear Cycle Development Institute

The concept of the collaboration research is shown in Fig.6.4.1. Special analytical instruments, *e.g.* remote-controlled type AFM and FG sensor, will be newly developed and installed at the Hot Laboratories; JMTR Hot Laboratory (JAERI) and Materials Monitoring Facility (JNC), in FY2003. Tests on neutron irradiated materials will be started at both facilities in FY2004. Specimens after neutron and/or ion irradiation will be commonly used for damage analysis in both institutes, by using Japan Materials Testing Reactor (JMTR), JOYO and Takasaki Ion Accelerators for Advanced Radiation Application (TIARA). In addition, microstructures of materials tested in high temperature and specimens tested in high temperature pressurized water will be examined by other analytical equipments, e.g. SEM, TEM, Kerr Effect Microscope (KEM) and etc., for analyses of damage phenomena.

References

1) Y. Nemoto, Y. Miwa, T. Tsukada and H. Tsuji: "AFM Evaluation of Grain Boundary Corrosion Behavior on Ion Irradiated Stainless Steel", JAERI-Conf 2003-001, pp. 397-404 (2003).
2) Y. Nemoto, Y. Miwa, H. Tsuji and T. Tsukada: "AFM Evaluation for Corrosion Behavior of Ion Irradiated Stainless Steel", Proc. 11th Int. Conf. on Nucl. Eng. (ICONE11), ICONE11-36093 (2003) [CD-ROM].
3) Y. Nagae and K. Aoto: "A Study on the Detection of Creep Damage in Type 304 Stainless Steel Base on Natural Magnetization", Int. J. of Appl. Electromagn. and Mech., 15, pp.295-300 (2001/2002).
4) Y. Nagae and K. Aoto: "The Effect of Microstructural Change on Magnetic Property in Type 304 Stainless Steel Subjected to Creep Damage", J. of The Japan Soc. of Appl. Electromagn. and Mech., 10-4, pp.360-365 (2002) [in Japanese].

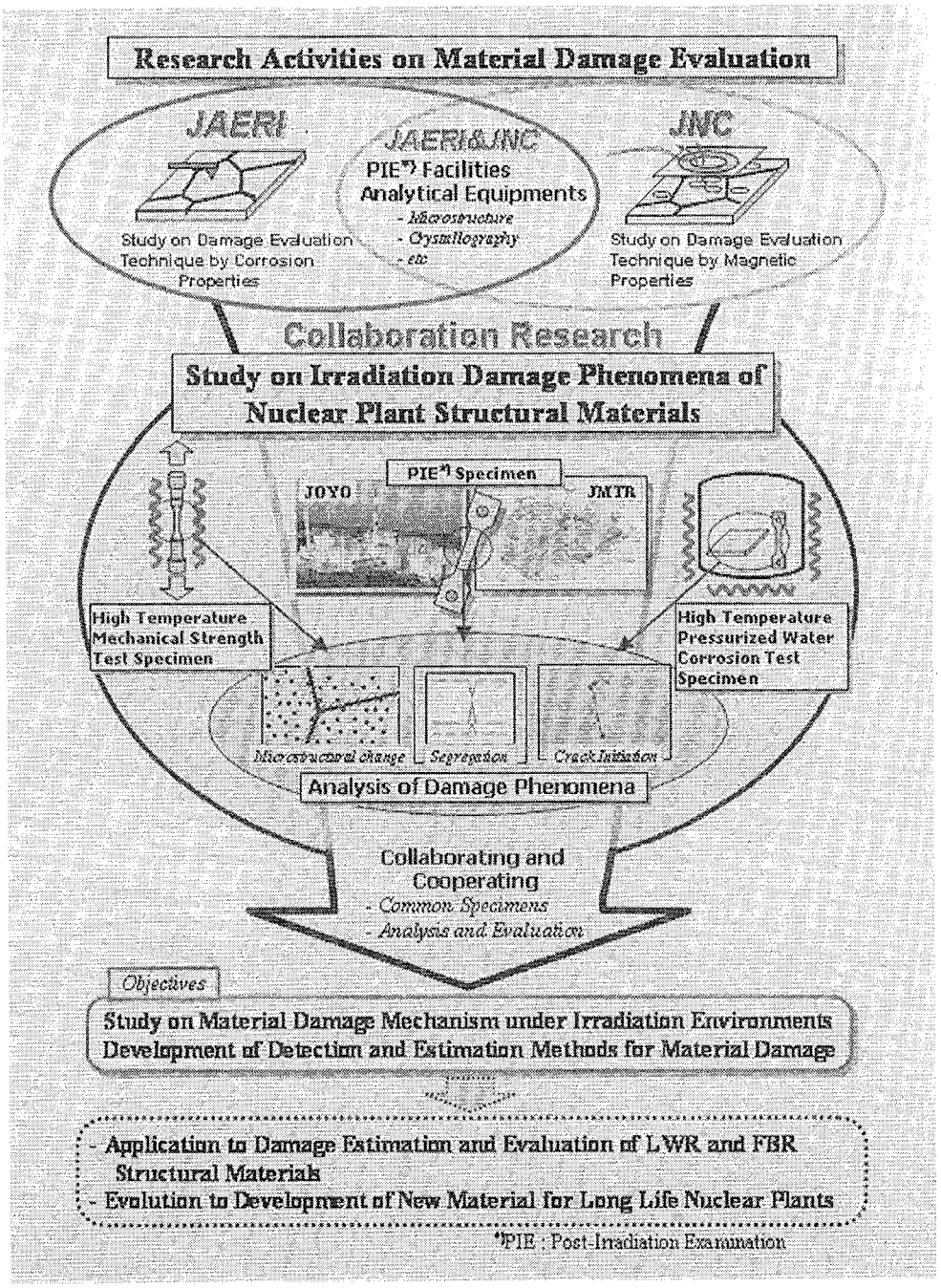

Fig. 6.4.1 A concept of new collaboration research between JAERI and JNC titled as "Study on Irradiation Damage Phenomena of Nuclear Plant Structural Materials".

6.5 Development of Technique for In-pile IASCC Growth Test in JMTR

Y. Kaji, M. Ohmi, Y. Matsui, H. Ugachi, T. Tsukada and H. Tsuji

(*E-mail:* kaji@popsvr.tokai.jaeri.go.jp)

The irradiation assisted stress corrosion cracking (IASCC) is one of the major concerns on the integrity of in-core materials not only for the light water reactors (LWRs) but also for the materials to be cooled by water in fusion reactor. Since the synergies of neutron/gamma radiation, stress and high temperature water can not be reproduced outside reactor core, the in-pile IASCC testing is one of the key experiments to understand IASCC behavior in the core. A high temperature water loop facility was, therefore, installed at the Japan Materials Testing Reactor (JMTR) to carry out the in-core testing. And research and development of several techniques for performing the in-pile IASCC testing have been conducted.

As for the method of loading in a specimen, the general mechanical loading method can not be applicable in in-core of JMTR. Therefore, stress is applied to a 0.4TCT specimen in term of metal bellows pressured by helium gas. Pressure of helium gas in the bellows is controlled by the load-control system using electro-magnetic valves and several types of capillary tubes according to the water pressure outside of bellows. An example of performance test result is shown in Fig. 6.5.1. Pressure of helium gas was able to be precisely controlled according to change of water pressure under increasing, steady and decreasing water pressure condition. High reliability of the load-control system was confirmed in the performance test by using the out-of-pile loop facility.

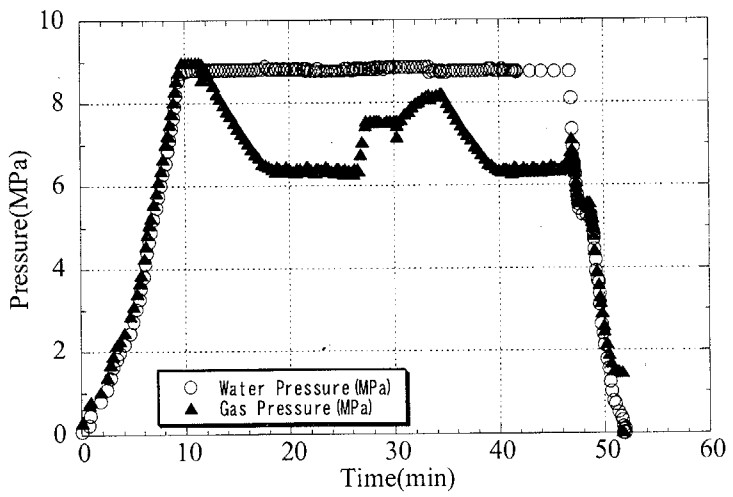

Fig. 6.5.1 Example of performance test result

In order to evaluate the characteristics of direct current potential drop (DCPD) and alternative current potential drop (ACPD) methods, the crack growth tests were performed at room temperature in air for monitoring crack length of austenitic stainless steels by both DCPD and ACPD methods [1]. The difference between ACPD and DCPD methods was not observed in this fatigue crack growth tests for type 304 stainless steels in air. It is possible to measure the crack length of the 0.5TCT specimens for type 304 stainless steels by both ACPD and DCPD methods. As comparison between DCPD and ACPD methods, the DCPD method is determined to adopt in the in-pile crack growth test, because the DCPD method is unaffected by the position of measurement cables and large current can be applied in the DCPD method.

In order to evaluate the influence of the several noises on the monitoring of the crack and long time stable measurement by the DCPD method, a crack growth test was performed in the autoclave for the trial crack-monitoring test [2]. Although the crack growth test was conducted for about 700 hours, it is found that the level of the noise is not large and long time stable measurement is possible for the monitoring of the crack by the DCPD method. Potential drop stably increased with increasing of the crack length in this test.

Since the length of MI cables used in the DCPD method for in-pile measurement is about 20m and the temperature distribution is found in the CT specimen in the in-pile crack growth test, the applied current should be very small in the DCPD method and the temperature compensation is necessary for the CT specimen. Therefore we adopt the six terminals DCPD method [3], because it is easy to compensate the temperature fluctuation of the specimen and two terminals can be used for the spare of the DCPD measurement. The DC potential drop method is applied to monitor crack extension in the 0.4TCT specimens of in-pile IASCC growth test. The technique consists of introducing a current of 1A across the CT specimen and measuring the drop in voltage between 2 pairs of potential wires in order to compensate the electromotive force due to the temperature difference in the specimen. The averages of the potential drop readings obtained at each probe pair are then converted to changes in crack length. Six terminals DCPD method was confirmed to be able to monitor the crack length in in-core of JMTR.

Since specimens pre-irradiated over a certain threshold fluence level of fast neutron for IASCC will be used in the in-pile IASCC testing, the testing unit including bellows and test rig for DC potential drop method was newly designed and the verification mock-up tests were conducted in the hot-cell. Moreover, verification test of water flow near crack tip of the CT specimen was performed, because many measuring cables installed in the narrow capsule. The normal water flow near the crack tip was confirmed by optimizing the location of flow path in the testing unit. Optimized testing unit [4] for in-pile IASCC growth test is shown in Fig.

6.5.2. Now out-of-pile SCC growth test using this type of testing unit has been conducted for comparison between out-of-pile and in-pile IASCC growth test results.

Reference

1) Y. Kaji and H. Tsuji: "Evaluation of DCPD and ACPD Methods for Monitoring of Crack Length", JAERI-Review 2001-010 (2001).

2) Y. Kaji, M. Ohmi, Y. Matsui and H Tsuji: "Development of Crack Monitoring Technique in High Temperature Water", JAERI-Review 2002-005 (2002).

3) T. M. Karlsen and E. Hauso: "Qualification and Application of Instrumented Specimens for In-Core Studies on Cracking Behavior of Austenitic Stainless Steels", Proc. of 9th Int. Symp. on Environmental Degradation of Materials in Nuclear Power Systems –Water Reactors, Newport Beach, CA, pp 951-959 (1999).

4) Y. Kaji, M. Ohmi, Y. Matsui, S. Kita, T. Tsukada, H. Tsuji, N. Nagata, K. Dozaki and H. Takiguchi: "PROGRAM OF IN-PILE IASCC TESTING UNDER THE SIMULATED ACTUAL PLANT CONDITION –Development of technique for in-pile IASCC growth test in JMTR", Proc. of 11th Int. Conf. on Nuclear Engineering (ICONE-11), ICONE11-36119, Tokyo, Japan, (2003).

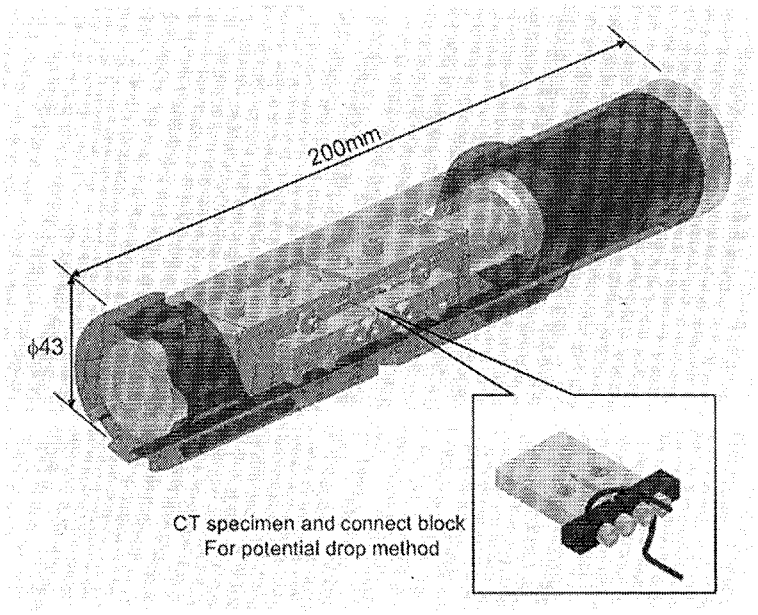

Fig. 6.5.2 General view of newly developed testing unit for IASCC growth test

6.6 Development of Technique for In-pile IASCC Initiation Test in JMTR

H. Ugachi, T. Tsukada, Y. Matsui, Y. Kaji and H. Tsuji
(E-mail: ugachi@cat.tokai.jaeri.go.jp)

IASCC phenomenon is caused by the synergistic effects of the stress in structural materials, water environment and radiation in core. The behavior of materials under such a complicated condition cannot be evaluated fully by only post-irradiation examination (PIE), therefore the in-pile SCC is desired for IASCC study. In-pile SCC test, however, has many technical hurdles on the experimental techniques, e.g., loading specimen, monitoring of crack length and water environment under irradiation. It is difficult to detect the crack initiation during in-pile SCC tests, but the crack initiation can be evaluated by the detection of specimen rupture if the cross section area of the specimen is small enough. Therefore, we adopted the uniaxial constant loading (UCL) test [1,2,3] with small tensile specimens.

Configuration of the test specimen and the conceptual figure of UCL test unit are shown in Fig 6.6.1. The size of the UCL specimen is 30 mm in length, 12 mm in gage length and 1.5mm in diameter. In irradiation capsule, pressurized high temperature water flows through this unit. Loading level is controlled by the pressure difference between the internal helium gas of the bellows and the external water. When the internal gas pressure of the bellows is less than the external water pressure, the specimen pulled with bellows contracting in axial direction. In the case of specimen failure, the bellows is contracted in axial direction rapidly, the contact point connected with the core cable or the sheath tube of MI cable attach in the bellows, the electrical resistance between the contact points is reduced. During UCL tensile test, the electrical resistance is monitored at a remote monitoring area.

A schematic figure of monitoring system for crack initiation or failure is shown in Fig.6.6.2. There is long distance (about 30 meters) from irradiation capsule to monitoring area, it is difficult to measure the electrical resistance between the contact point directly for reduction of electric current, so the electrical resistance is converted to electric voltage. In order to calibrate the relationship between tensile load and pressure difference outside and inside of bellows, a measuring system with a pressure vessel, load cell and stroke sensor was designed. UCL test unit is inserted into the vessel, and outside of the unit is pressurized by helium gas, and then the pressure inside of the bellows keeps to atmosphere at room temperature. With increasing the outer pressure, the load and stroke of specimen were measured.

As a test for evaluation of fundamental properties of the test units, three types of

bellows (DASH12, DASH10 and DASH08) with different diameter were examined. Fig.6.6.3 shows the relationship between pressure difference (outer and inner of bellows) and tensile stress at RT. All types of bellows showed good linear relationship between pressure difference and tensile stress.

Fig.6.6.4 shows changes in tensile stress and the resistance between core cable and sheath tube during tensile test at room temperature and 288℃. When the specimen is ruptured, the resistances between core cable and sheath tube decreased rapidly. From these results, it is confirmed that the rupture detecting system using changes electrical resistance between contact points in bellows is effective on UCL tensile test.

References

1) E8 Test Methods for tension Testing of Metallic Materials, Annual Book of ASTM Standards, Vol. 03.01.

2) G49 Standard Practice for Preparation and Use of Direct Tension Stress-Corrosion Test Specimen, Annual Book of ASTM Standards, Vol. 03.02.

3) R. Katsura et al, Proc. 6th International Symposium on Environmental Degradation of Materials in Nuclear Power Systems – Water Reactors, pp. 625 (1993)

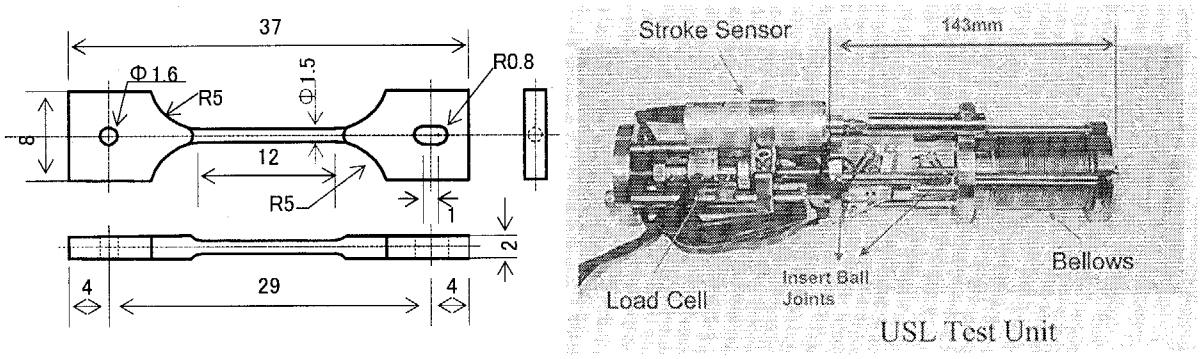

Fig.6.6.1 Specimen and loading unit for UCL test.

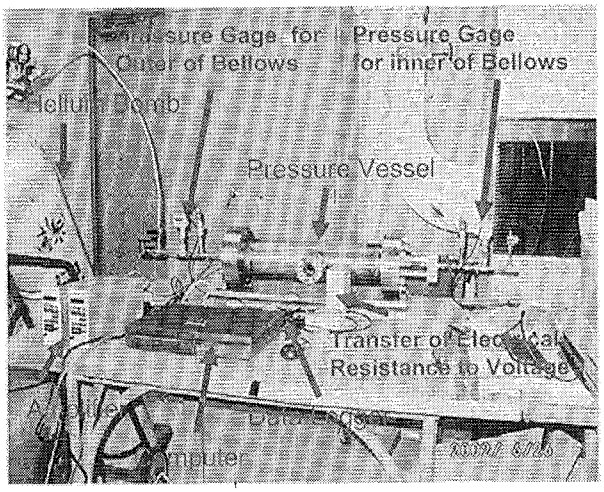

Fig.6.6.2 Monitoring system for specimen rupture.

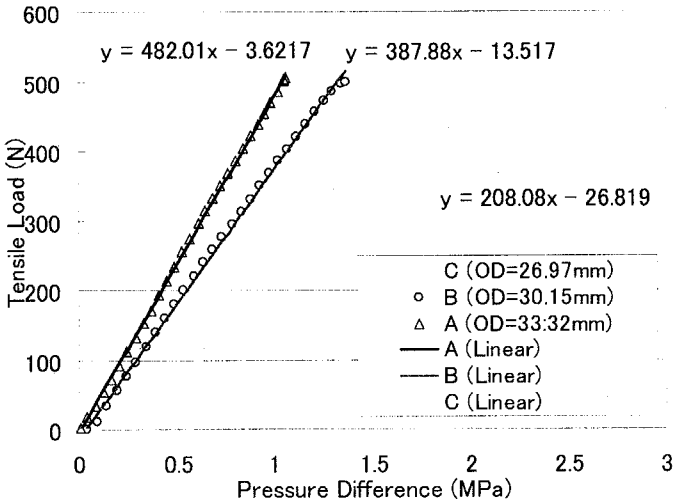

Fig.6.6.3 Relationship between pressure difference and tensile load

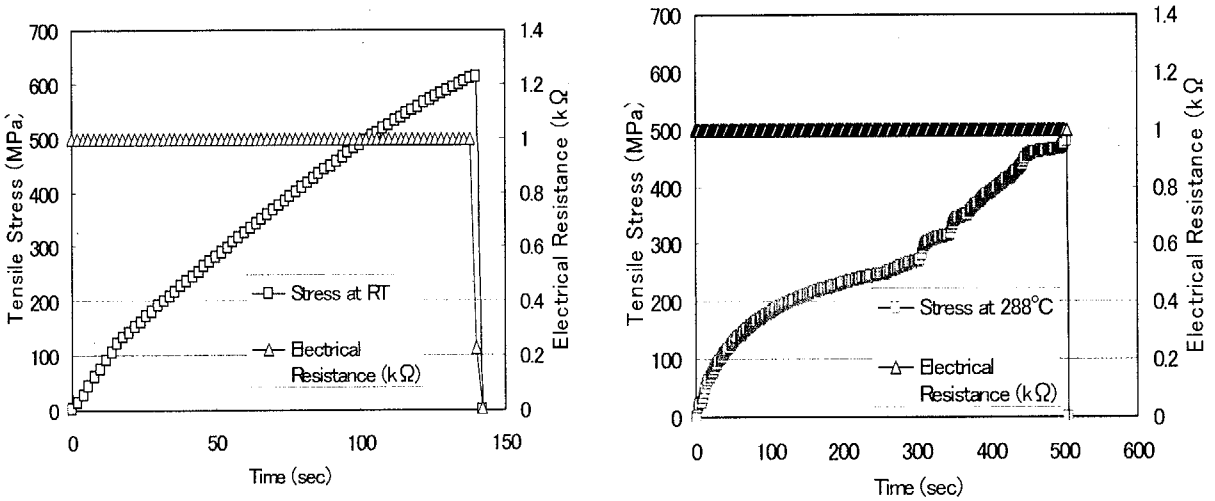

Fig. 6.6.4 Changes in electrical resistance on tensile test

6.7 Neutron Irradiation of Specimens for IASCC Studies in BWR Simulated High Temperature Water at JMTR

T. Tsukada, Y. Kaji, H. Ugachi, J. Nakano, Y. Itabashi, E. Nabeya, Y. Matsui, Y. Komori, T. Ishii, M. Niimi, H. Tsuji and H. Nakajima
(*E-mail:* ttsukada@popsvr.tokai.jaeri.go.jp)

It is well known that irradiation assisted stress corrosion cracking (IASCC) can be reproduced on the austenitic stainless steels irradiated over a certain threshold fluence of fast neutron by means of post irradiation examinations (PIEs). However, the reproduced IASCC by PIEs must be carefully distinguished from the actual IASCC that occurs in the core under simultaneous effects of radiation, stress and high temperature water environment. Since these synergies are significant to understand IASCC behavior in the reactor core but not reproducible by PIEs, the in-pile IASCC testing has been recognized as a critical experiment and, therefore, the new high temperature water loop facility has been installed at the Japan Materials Testing Reactor (JMTR). Two loop facilities were commissioned at the end of FY2001 for the in-core IASCC testing program in the framework of cooperative research program between JAERI and the Japan Atomic Power Company, and also for the IASCC national project conducted by the Japan Power Engineering and Inspection Corporation (JAPEIC) in which JAERI is participating.

The water loop facilities were designed to simulate BWR environment and supply high temperature pure water into five irradiation capsules at a time by each facility[1]. Using the loop facility at JMTR, in-pile IASCC tests will be carried out which are including the IASCC initiation tests by applying uni-axial constant loading (UCL) test technique and the IASCC propagation or crack growth tests with compact tension (CT) type specimens as described in sections 6.5 and 6.6. In FY2002, pre-irradiation of the specimens for in-pile IASCC tests has been carried out under simulated BWR condition in the irradiation capsules connected to the loop facility, and the in-core tests will be started in FY2003.

In the year 2000, the Ministry of International Trade and Industry (MITI) which is the present Ministry of Economy, Trade and Industry (METI) has begun the project for IASCC technological development as a part of the more comprehensive program for technological development of countermeasures for aged of LWRs[2]. In the project for IASCC technological

development, the basic essential data were planned to be prepared for the maintenance standard and safety evaluation of core internals under a promotion of JAPEIC. The project for IASCC technological development consists of BWR and PWR relevant works. JAERI is engaged in the BWR related testing and research program, which includes the neutron irradiation at JMTR and PIEs shared by the participants. In a part of the METI project aiming at IASCC of BWR, the objective is to evaluate IASCC initiation and propagation data necessary for making IASCC database satisfactory to contribute for preparing the maintenance standard against IASCC, which will be used for the assessment of timing and intervals of the inspections of core internals.

In the IASCC national project for BWR, core internal materials used for BWR, i.e. types 304, 304L and 316 stainless steels will be examined at hot laboratories after irradiation at JMTR up to four target levels of neutron fluence of $5x10^{24}$, $1x10^{25}$, $3x10^{25}$ and $1x10^{26}$ n/m^2 (E>1 MeV) to assess dependency of IASCC behavior on the neutron fluence. Experimental data to be obtained through the PIEs are the crack propagation rate data, IASCC susceptibility data form slow strain rate testing (SSRT) and UCL tests in high temperature water, irradiation-induced stress relaxation data. For the national project, irradiation of the various types of specimens were started in the irradiation capsules at the end of FY2001 and continued in FY2002.

References

1) T. Tsukada et al.: "New In-Pile Water Loop Facility for IASCC Studies at JMTR," Proc. Int. Conf. Water Chemistry in Nuclear Reactor Systems – Operational Optimization and New Developments, Avignon, April, 2002, Paper No.91, (2002).

2) H. Nakajima et al.: "Recent Japanese experiences on SCC of structural materials in LWRs and future direction of relevant R&D," Proc. Quadripartite meeting of the national advisory committees of France, German, Japan and USA, Berlin, October, 2002.

6.8 Present Status and Improvement of Function of JAERI Material Performance Database (JMPD) for IASCC Study

Y. Kaji, T. Tsukada and H. Tsuji
(*E-mail:* kaji@popsvr.tokai.jaeri.go.jp)

Fundamental studies of structural materials have been performed at Japan Atomic Energy Research Institute (JAERI) regarding practical applications for nuclear plants. For the evaluation of reliability of structural materials, various kinds of material data, which are fatigue crack growth, creep, tensile, low-cycle fatigue, slow strain rate testing (SSRT) etc., have been accumulated through the above-mentioned research activities. The JAERI Material Performance Database (JMPD) was developed with a view to utilizing such material performance data efficiently[1)-3)]. This paper will describe the interface which has been improved and the future direction of the JMPD.

The JMPD was designed for effective utilization of material data especially for the environmentally assisted degradation, e.g., fatigue or SCC/IASCC behavior in aqueous or gaseous environments. As for a part of IASCC database, about 300 data of post irradiation SSRT from our experimental works and 20 open published papers were input. The IASCC data consist of those of type 304 and 316 materials at irradiation temperatures between 333 and 573 K. The fast neutron fluences to the materials are in the range of from $1x10^{22}$ n/m^2 to $8x10^{26}$ n/m^2 (E>1MeV). The IASCC susceptibility of the materials has been examined by SSRT at around 573 K in high-temperature water containing dissolved oxygen concentration between 1ppb and 32ppm. Data analyses were performed with the knowledge on the factors controlling IASCC obtained by our results of the post irradiation SSRT [4)-6)].

At JMTR, in FY 1999 a design activity for the new water loop system was started focusing on the irradiation and in-pile testing for IASCC studies, and the loop was commissioned at the end of FY 2001. The loop facility is designed for material irradiation under BWR conditions, the maximum operational parameters are as follows; temperature: 593 K, pressure: 10 MPa and flow rate: 1 m^3/h. To simulate the normal water chemistry (NWC) and hydrogen water chemistry (HWC) conditions of BWR, the dissolved oxygen and dissolved hydrogen concentrations can be controlled at levels up to 200 ppb and 1 ppm respectively. Therefore, to store the irradiation condition at JMTR and experimental IASCC

data, some data items and functions are added in the JMPD. Figure 6.8.1 shows example of the data for water chemistry in the JMTR stored in the JMPD. The data for irradiation capsule including irradiation condition of specimens are also stored in the JMPD.

References

1) N. Yokoyama, T. Tsukada and H. Nakajima, JAERI-M90-237 (in Japanese) (1987).

2) H. Tsuji, N. Yokoyama, T. Tsukada and H. Nakajima, J. Nucl. Sci. Technol., Vol. 30, No. 12, pp.1234-1242 (1993).

3) N. Yokoyama, H. Tsuji, T. Tsukada and M. Shindo, ASTM STP 1311, pp.261-272 (1997).

4) T, Tsukada, Y. Miwa, H. Tsuji, H. Mimura, I. Goto, T. Hoshiya and H. Nakajima, Proc. 7th Int. Conf. on Nucl. Engng. (ICONE-7), L4-3 (1999).

5) T. Tsukada, Y. Miwa and H. Nakajima, Proc. 7th Int. Symp. On Environmental Degradation of Materials in Nuclear Power Systems –Water Reactors, Vol.B, p.1009 (1995).

6) T. Tsukada, Y. Miwa, H. Nakajima and T. Kondo, Proc. 8th Int. Symp. On Environmental Degradation of Materials in Nuclear Power Systems –Water Reactors, Vol.B, p.795 (1997).

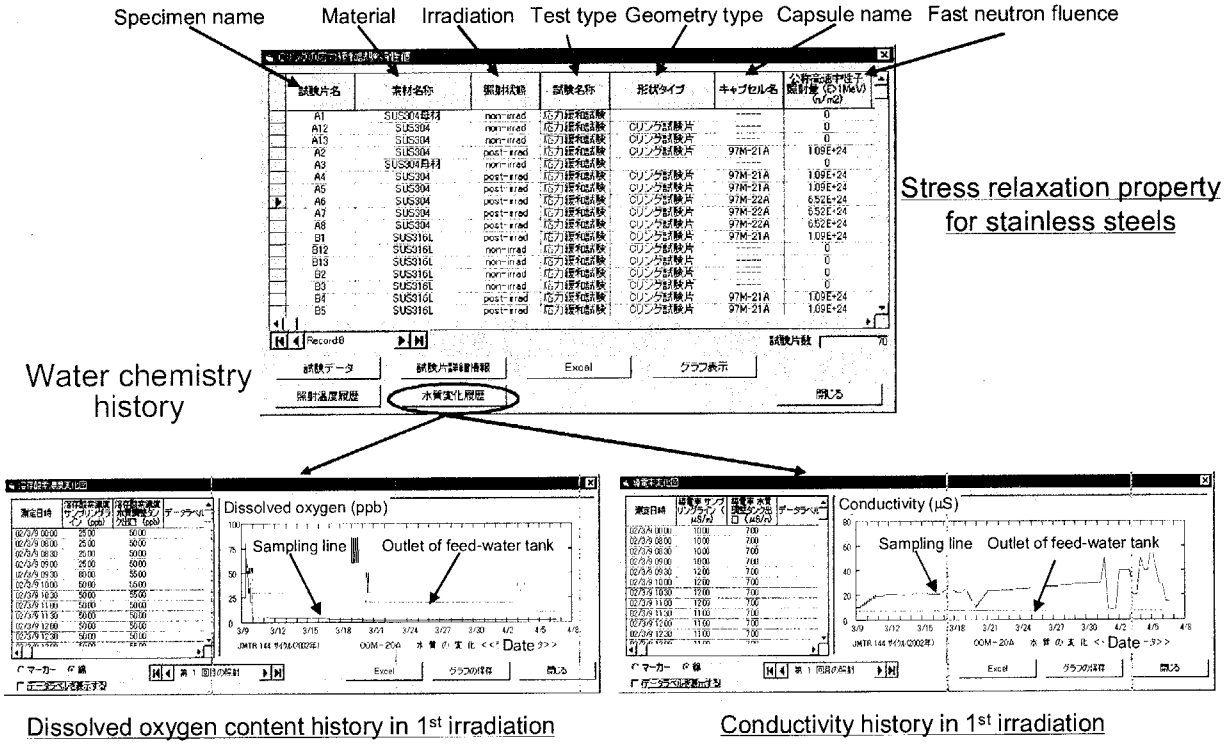

Fig. 6.8.1 Example of additional function for IASCC data in JMPD

7. Development of New Cladding Materials Applied to the Advanced Nuclear Reactors

The development of new cladding alloys applied to the high Pu enriched MOX fuels has been proceeded to obtain the sufficient reliability of fuel elements used in the advanced nuclear reactors. These are designed for achieving the ultra-high burnup (UHB-BWR), controlling fast neutron spectra with high breeding ratio (RMWR) and using super-critical water with high thermal efficiency (SCWR) respectively. The materials research for RMWR and SCWR has been started from this fiscal year. The modified austenitic stainless steel (SS) was selected for the candidate cladding alloy applied to UHB-BWR and RMWR, because the irradiation properties, mechanical strength and corrosion resistance are superior to these of Zircaloys. The nuclear economy of SS is possible to achieve as same as that of Zircaloy. The important issues on this development are to improve the ductility loss, the resistance against IASCC and PCI respectively. The industrial manufacturing process for cladding tubes was optimized for the stable austenite 25Cr-35Ni-0.2Ti steel with Nb-5W alloy lining selected as candidates by JAERI. The corrosion resistance and mechanical properties of cladding tubes made of candidate alloy were markedly improved the optimization of purification process by electron beam melting (UHP grade) and thermo-mechanical treatment so-called SAR. The ductility of Nb-5W alloy is also improved by optimizing electron beam melting. Irradiation properties were examined by triple ion been irradiation tests at operation temperature. The growth of secondary irradiation defects such as Frank loop was markedly inhibited in modified SS compared with that of Type 304 used in nuclear ship `Mutsu`. From microanalysis by STEM, the depletion of Cr at grainboundaries accompanied with the irradiation assisted segregation (RIS) was saturated in values less than 10wt% within 50dpa. It was verified that modified SS with 25Cr is possible to maintain the sufficient Cr content at grainboundaries required to the resistance against IASCC. The Major parameters in relation to IASCC such as material properties, environmental effects and stress were evaluated with empirical and numerical means. The high temperature water loop with several testing sections for evaluating these properties was arranged in WASTEF. The irradiation enhanced corrosion and the susceptibility against IASCC are possible to evaluate by simulating the heat flux and irradiation conditions to both post-irradiation and under γ-ray irradiation tests. From reference tests using non-irradiated specimens, the difference in corrosion behavior between heat transfer and immersion surfaces was clarified.

The materials requirement and selection of candidate alloys for core materials used in RMWR was basically examined. The corrosion resistance at high temperature in super-critical water was controlled with the function as a diffusion barrier of oxide film, because the excited oxygen and hydrogen on surfaces are easily formed by the low energy electrons excitation under heavy irradiation. It was clarified that the sufficient corrosion resistance is only obtained in heat resistance alloys with high Cr contents. The high Cr-W-Si Ni base alloy developed by JAERI was selected for the candidate alloys. Mechanical properties of dissimilar metal joints of Cu alloy and stainless steel used in the advanced reactor components were examined with FEM analysis. The elastic-plastic analysis was performed with ABAQUS code for evaluating fracture position and fatigue life of dissimilar metal joints.

7.1 Development of Testing Apparatus for Evaluating Environmental Cracking and Corrosion of Irradiated New Fuel Cladding Materials under High Temperature Water

I. Ioka, K.Tachibana, K.Suzuki, K.Kiuchi, T.Kohya, S.Endoh, K. Yamamoto*[1] and H.Kitamura*[2]
(*E-mail:* ioka@popsvr.tokai.jaeri.go.jp)

As for development of new fuel cladding materials applied for ultra high burnup and/or advanced water-cooled reactors, it is important to evaluate changes in mechanical properties and corrosion resistance of irradiated ones. So, the testing apparatus was set up for evaluating environmental cracking and corrosion resistance at high temperature and high pressure water.

The testing apparatus for irradiated specimens was installed in a hot cell of Waste Safety Testing Facility (WATEF) at JAERI. A schematic diagram of the apparatus is shown in Fig. 7.1.1. The upper limit to the temperature is 370°C and the upper limit to the pressure is 25MPa. The testing apparatus consists of two testing units (Environmental cracking unit, Corrosion under heat transfer unit), a water make up section, a pressurized high temperature water circulation system, a monitoring/purification system and the control and recording systems. Dissolved oxygen and hydrogen in the circulation water are controlled in the water make up section. In addition, it is possible to inject hydrogen peroxide into the circulation water during test. The main specification of the testing apparatus is shown in Table 7.1.1. Performance about each parameter of this apparatus at high temperature and high pressure was tested. Temperature and pressure could be controlled within ±0.3% and ±0.2% at all range, respectively. The minimum dissolved oxygen (DO) was 0.4-0.6ppb and DO was controlled within ±0.3% for set values. The flow rate was controlled on ±2% at 400L/h.

Slow strain rate tensile tests were conducted at a temperature of 288°C, a pressure of 9MPa, DO of 8ppm, an electric conductivity of 0.16 μS/cm, a flow rate of 400L/h and a strain rate of $1.1\times10^{-6}s^{-1}$ for unirradiated candidate material (Fe-25Cr-35Ni). Two type specimens were used in the trail run. One is a tube type specimen with 42mm in length,

---

*[1] The Japan Atomic Power Company
*[2] Tokyo Electric Power Company

11.3mm in diameter and 0.4mm in thickness. The other is a plate type specimen. The gauge section is 16mm in length, 2mm in width and 2mm in thickness. The results are summarized in Table 7.1.2. Both specimens were fractured at the gauge section. The 0.2% proof strength and ultimate tensile strength of tube type specimen was larger than those of plate type one. The fracture elongation of tube type specimen was lower than that of plate type one. It is considered that the difference was attributed to the degree of cold-worked and the stress condition depending on the configuration of specimen.

Table 7.1.1 Main specification of the testing apparatus installed in WASTEF

Autoclave capacity	0.8L	
Autoclave material	Inconel 625	
Autoclave seal	Edge type (Ni seal ring)	
Control range	Load	Max. 20kN
	Temperature	R.T.-370℃
	Pressure	Max. 25.0MPa
	DO (Dissolved oxygen)	0.5ppb-saturated
	DH (Dissolved hydrogen)	Max. 2.8ppm
	Flow rate	Max. 500L/h

Table 7.1.2 Tensile test results of tube and plate type specimens

Type	Material	Atmosphere	0.2% proof strength, MPa	Ultimate tensile strength, MPa	Fracture elongation, %
Tube	Fe-25Cr-35Ni UHP SAR*	High temperature water	525	589	12.6
Plate	Fe-25Cr-35Ni UHP SAR*	High temperature water	439	534	20.7

*UHP : Ultra High Purity

*SAR : Strained, Aged and recrystallized treatment

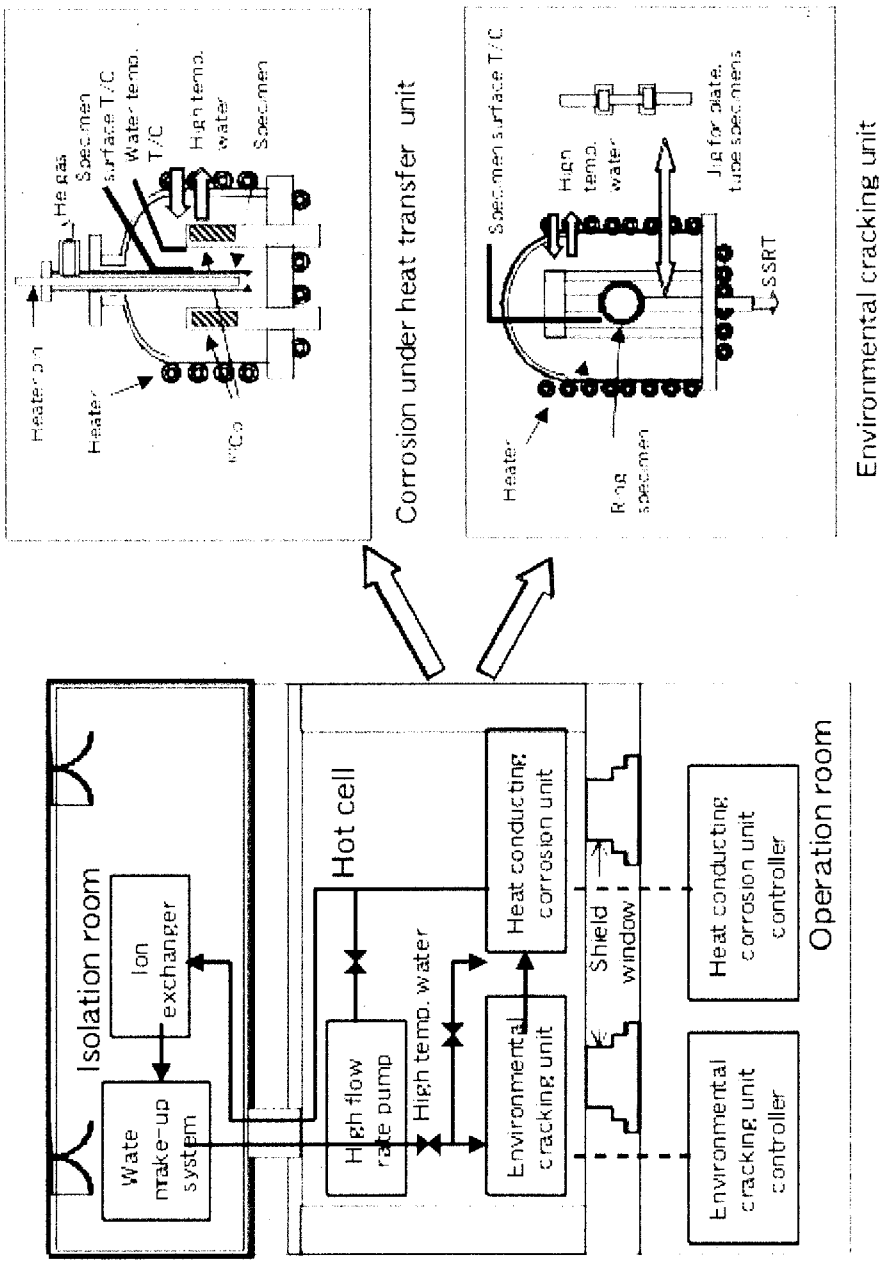

Fig. 7.1.1 Schematic diagram of the testing apparatus

7.2 Preliminary Study of Corrosion Behavior for New Fuel Cladding Materials under Heat Transfer Condition

I.Ioka, K.Tachibana, K.Suzuki, K.Kiuchi, K. Yamamoto*[1] and H.Kitamura*[2]
(*E-mail*: ioka@popsvr.tokai.jaeri.go.jp)

Advanced light water reactors with ultra high burnup and/or fast neutron spectrum tailoring are considered to be effective in view of economical and ecological points. Cladding materials with the excellent performance under irradiation are required to these developments. Corrosion resistance of candidate materials (Fe-25Cr-35Ni) used in new fuel cladding is one of important issues, since the corrosion would be accelerated by heat transfer and neutron irradiation. As a preliminary study, corrosion behavior of the candidate material was investigated under heat transfer condition at high temperature and high pressure water.

The materials used were Fe-25Cr-35Ni and Fe-18Cr-8Ni. Fe-25Cr-35Ni is subjected to thermo-mechanical treatment (SAR:Strain-Aging Recrystallization) and purification. The chemical compositions of the materials are shown in Table 7.2.1. A tube type specimen with 150mm in length, 11.3mm in diameter and 0.4mm in thickness was used in the preliminary test. A pipe heater was inserted in the specimen for making heat transfer condition. Corrosion tests were conducted at a temperature of 278°C, a pressure of 7.2MPa, DO of 8ppm, an electric conductivity of 0.2 μ S/cm, a flow rate of 1L/h and a corrosion time of 300h. A heat flux was about 130kW/m^2. In this condition, boiling on the surface of specimen was confirmed by the previous test.

Figure 7.2.1 shows surfaces of heat transfer and non-heat transfer specimens (Fe-25Cr-35Ni) by SEM observation. Needlelike fine deposits were observed on surface of heat transfer specimen. In non-heat transfer, on the other hand, fine granular deposition were existed on the surface. The surface condition of Fe-18Cr-8Ni was the same as Fe-25Cr-35Ni. The area analysis for heat transfer surface of Fe-25Cr-35Ni using EDX(Energy Dispersive X-ray Spectroscopy) is also shown in Fig.7.2.2. The chemical composition of the surface deposition is almost uniform in both heat transfer and non-heat transfer conditions. Figure 7.2.3 shows the results of the point analysis of heat transfer and non-heat transfer specimens (Fe-25Cr-35Ni) by EDX. The relative increase in Fe was observed in non-heat transfer surface. On the other hand, the relative increase in Ni was obtained in heat transfer surface. As this reason, it seems that the Ni was deposited preferentially in a boiling state, because the Ni is the easiest to dissolve in high temperature water among main compositions.

---

*1 The Japan Atomic Power Company
*2 Tokyo Electric Power Company

Table 7.2.1 Chemical compositions of the materials used (wt%)

Material	Fe	Cr	Ni	Ti	C	O	N	Si	Mn	P	S
Fe-18Cr-8Ni	bal.	18.52	9.08	-	0.047	-	0.034	0.54	0.78	0.024	0.003
Fe-25Cr-35Ni	bal.	24.55	34.99	0.18	0.0013	0.0011	0.0014	<0.005	0.001	0.001	0.0009

(a) Heat transfer specimen (b) Non-heat transfer specimen

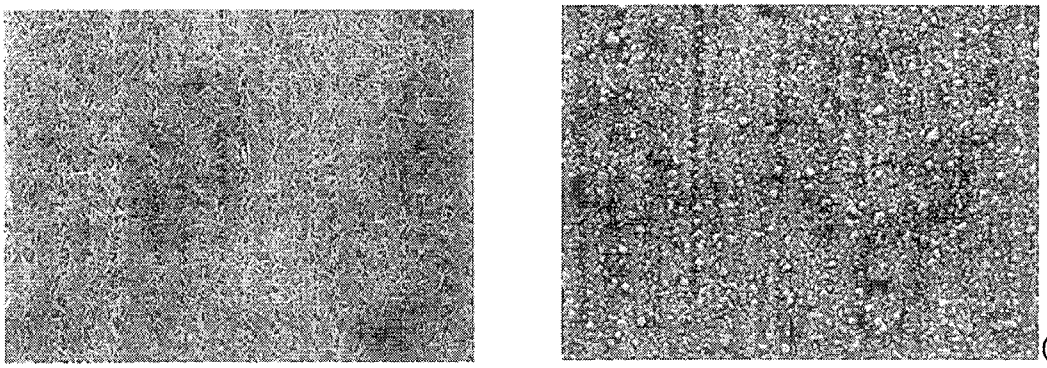

(x5000)

Fig.7.2.1 Surface of heat transfer and non-heat transfer specimens (Fe-25Cr-35Ni)

(a)SEM (b) Fe

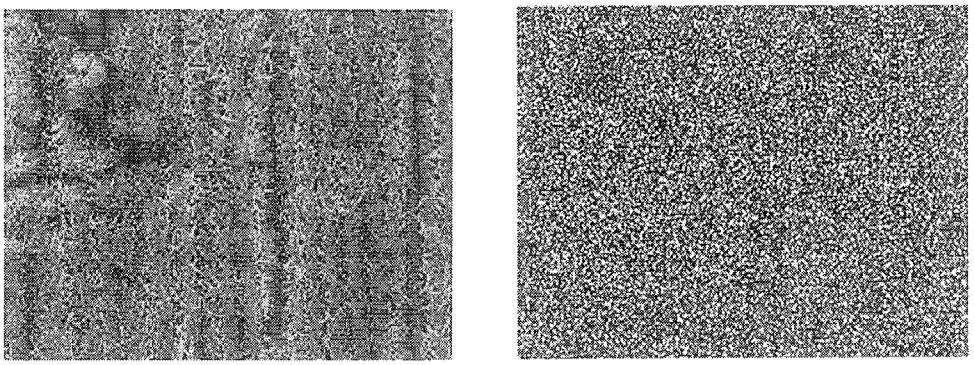

(c) Cr (d) Ni

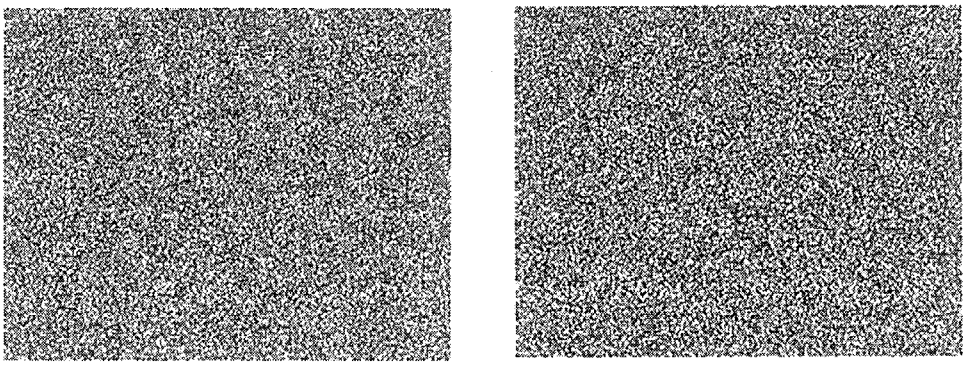

(x5000)

Fig.7.2.2 Area analysis of Fe-25Cr-35Ni using EDX

(a) Heat transfer specimen

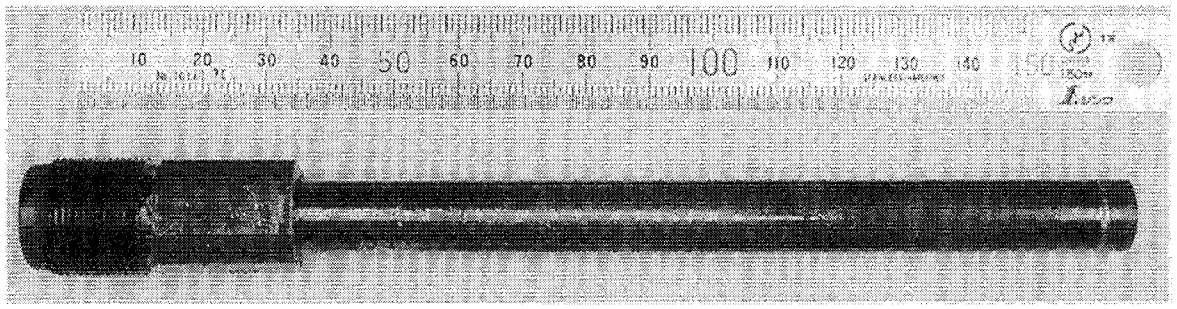

(b) Non-heat transfer specimen

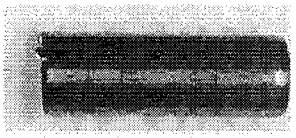

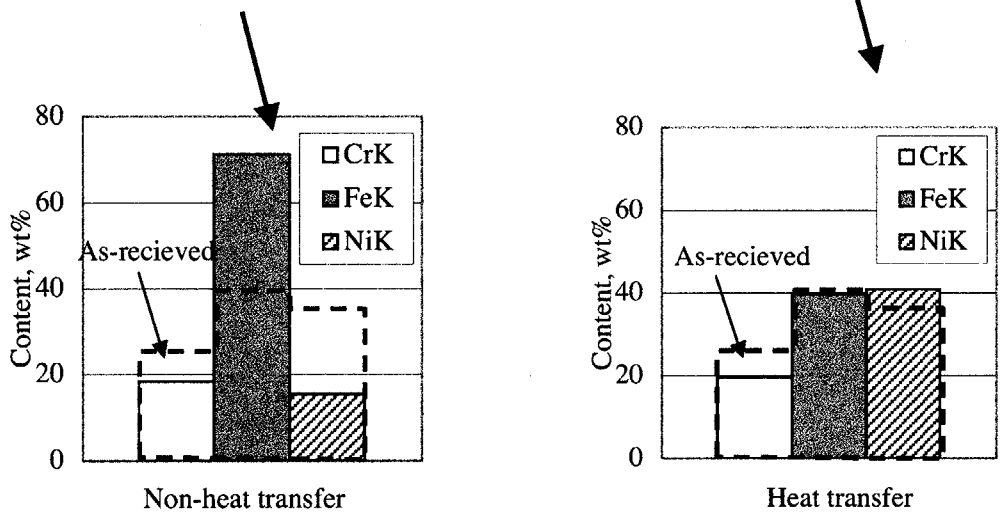

Fig.7.2.3 Point analysis of heat transfer and non-heat transfer specimens (Fe-25Cr-35Ni) by EDX

7.3 High-Quality Nb-Mo Alloy Applicable to Lining for Stainless Fuel Cladding Tube

N.Maruyama, M.Tanabe, I.Ioka and K.Kiuchi
(*E-mail* : maruyama@galileo.tokai.jaeri.go.jp)

Fully austenitic stainless steels with high chromium and nickel content were selected for candidate materials for fuel cladding tubes to be used under ultra-high burnup condition. Stainless steels, however, show higher permeability of tritium than zircaloys. Therefore, the tritium formed at the inside of stainless cladding tube is easily discharged to the outside in comparison with the case of zircaloy tube. From the fact that niobium has inherently high solubility of hydrogen, the niobium lining seems very effective to solve the problem of tritium permeation. In addition, the niobium lining seems to have advantages in suppressing the pellet cladding interaction. In this work, Nb-5mass%Mo alloy was selected for lining material in the light of the improvement of corrosion resistance to high temperature water without reducing workability of niobium.

In order to produce high-quality Nb-5Mo alloy ingot, an electron beam double melting method was adopted. Figure7.3.1 shows a schematic view of the electron beam double melting. The melting modes for first and second melting were horizontal drip melting and vertical drip melting, respectively. In general, a structure of feed stock for first melting is very important because compositional homogeneity of a second melted ingot is strongly influenced by the structure. Schematic view of the feed stock for first melting used in this work is illustrated in Fig.7.3.2. The feed stock was specially designed to have a constant cross sectional ratio of molybdenum to niobium over the total length. The ingot of 85mm in diameter and 550mm in length was obtained by the double melting. Chemical composition of the ingot is shown in Table7.3.1. The ingot showed homogeneous molybdenum content in longitudinal direction and extremely low content of interstitial impurities. Figure7.3.3 shows Vickers hardness of the ingot together with those of Nb-20Mo and Nb-30Mo ingots obtained in a previous work by the same method as this work. From the previous work, it was clarified that the niobium alloys of high molybdenum content showed poor workability because of high hardness. On the other hand, the Nb-5Mo ingot showed sufficiently low Vickers hardness of about 120, so it seemed to have good workability. Plates of 5mm in thickness were manufactured with tentative process as shown in Fig.7.3.4. A plate of 24mm in thickness and 100mm in width was obtained by the forging from the ingot, which was heated at 1023K for 120min at the beginning. Cold rolling was carried out with 76% reduction of the plate (21mm→5mm in thickness). No cracks were observed in both of the forging and cold rolling. It was confirmed that the electron beam double melted ingot has excellent workability.

Figure7.3.5 shows annealed structure after cold rolling of 76% reduction in thickness. The annealing was carried out in argon atmosphere at 1473K for 60 min. Although grain size was scattered to some extent, recrystallized structure was obtained over the whole matrix. Tensile properties of the manufactured plates are shown in Fig.7.3.6. The material showed sufficient elongation near the room temperature. From the viewpoint of workability, the material seemed to have high applicability to lining.

A preliminary bonding test was performed, in which an austenitic stainless plate and a pure niobium plate were piled in a vacuum capsule of carbon steel and then hot rolled with 90% reduction in thickness at temperature of 1423K in the beginning. Figure7.3.7 shows a representative micro-structure of the bonded interface after the hot rolling. At the interface there were no defects such as intermetallic compounds and voids. In addition, each of the plate showed approximately constant reduction in thickness. No break away was maintained throughout the subsequent cold rolling with 60% reduction in thickness. Furthermore, it was confirmed from EPMA analyses that compositional properties near the interface were substantially not affected throughout additional heat treatments at 823K for 60min and subsequently at 1123K for 60min. The fuel cladding tubes of austenitic stainless steel lined with Nb-5Mo alloy seemed to be producible because metallurgically sufficient bond interface was attained with regard to pure niobium.

Further evaluations, containing bonding test on Nb-5Mo alloy, have been conducted with the intention of manufacturing the fuel cladding tubes lined with the niobium alloy.

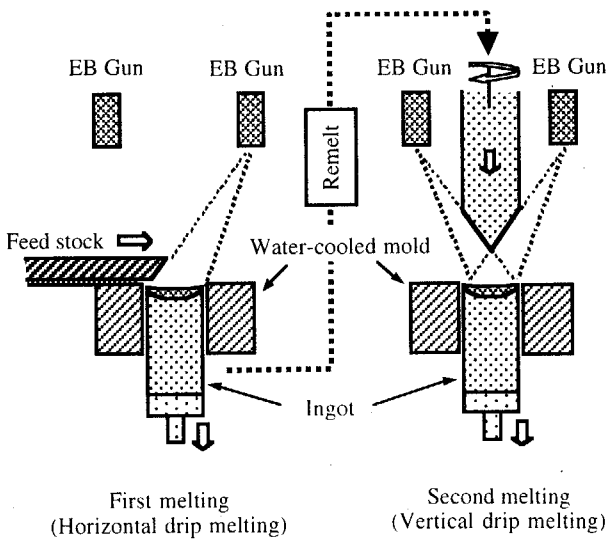

Fig.7.3.1 Schematic view of the electron beam double melting

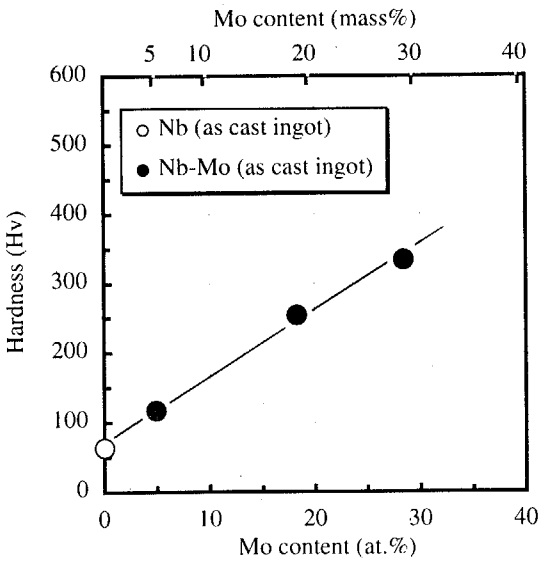

Fig.7.3.3 Vickers hardness of high purity Nb-Mo alloy

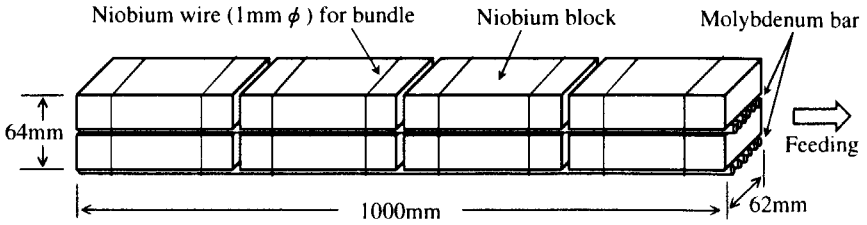

Fig.7.3.2 Schematic view of the feed stock for electron beam first melting

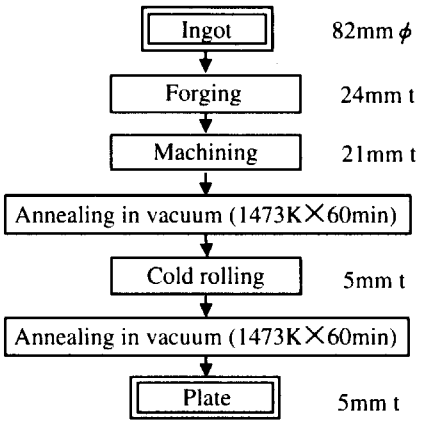

Fig.7.3.4 Process for trial manufacture of Nb-5Mo alloy plate

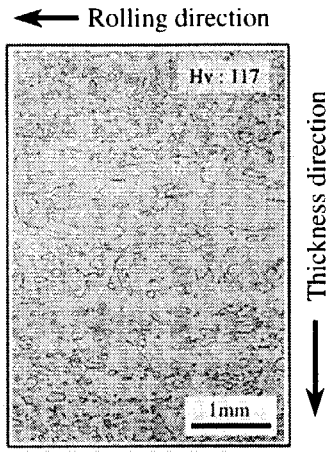

Fig.7.3.5 Recrystallized structure of Nb-5Mo alloy annealed at 1473K for 60min after cold rolling with 76% reduction in thickness

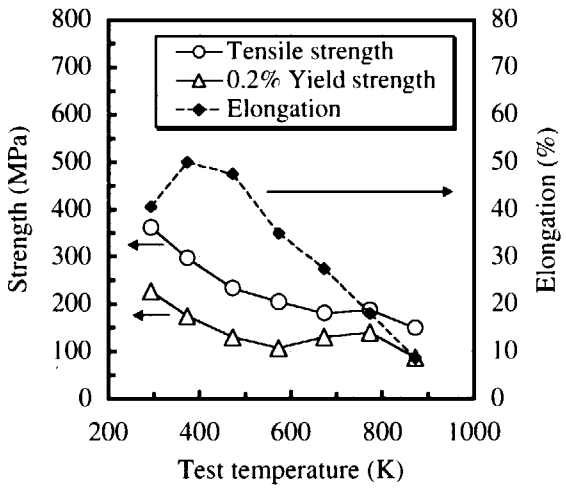

Fig.7.3.6 Effect of temperature on the tensile properties of Nb-5Mo alloy

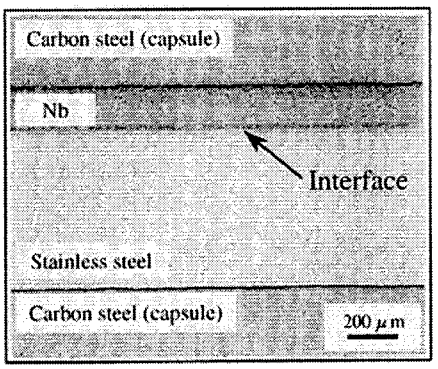

Fig.7.3.7 Micro-structure of niobium / stainless-steel bond interface after hot rolling with 90% reduction in thickness

Table 7.3.1 Chemical composition of electron beam double melted Nb-5Mo alloy ingot

mass%

Material	Analyzed position	Mo	Fe	C	O	N	H
Nb-5Mo	Ingot top	5.04	<0.01	0.001	0.0018	0.0025	<0.0005
	Ingot bottom	5.10	<0.01	0.001	0.0014	0.0022	<0.0005
	Average	5.07	<0.01	0.001	0.0016	0.0024	<0.0005

7.4 Irradiation Effects on Interactions between Supercritical Water and Core Materials for SCWR

Y. Nakahara, K. Kiuchi, I. Ioka, H. Ogawa, M. Tanabe and M. Takizawa*
(*E-mail*: nakahara@popsvr.tokai.jaeri.go.jp)

The concept of Supercritical-Water-Cooled Reactors (SCWR) was proposed ten years ago by Oka research group[1]. The system of SCWR can be compact by use of supercritical water as the primary reactor coolant. The thermal efficiency of SCWR is expected to be raised up to 40 % using supercritical water with the high thermal conductivity and the high temperature of around 600℃. It is one of the most promising reactors chosen in Generation IV by DOE[2]. The advantage of SCWR is that the technology of LWRs and fossil-fired power plants seems to be applicable to the development. One of the most important issues for the development of SCWR is to evaluate irradiation effects on the reliability of the core materials used in supercritical water. The temperature and pressure of the primary coolant in SCWR are higher than those of LWRs as shown in Fig. 7.4.1. The radiation effects would be affected through the water chemistry of the primary coolant. Interactions between the materials and the coolant should be strongly dependent on the temperature, because the state of water changes from sub-critical to supercritical at the critical temperature of 374 °C.

Basic researches on interactions between the core material candidates and supercritical water have been pursued in respect of the degradation mechanism and the improvement of the materials in order to develop SCWR core system. At the beginning of this project, a corrosion testing apparatus with the high temperature water loop and water control system was refined for simulating the core environment in SCWR. The cylindrical test cell (8 cm in diameter and 15 cm in height) was made to attain high temperature (~600 °C) and high pressure (~30 MPa) water. In order to simulate the effect of radiolysis on the water chemistry in the reactor core, a direct injection system of hydrogen peroxide with the maximum injection rate of 20 ml/min and a monitoring system (DO, electrical conductivity and pH) on the downstream of the test cell were prepared in the circulation loop of the apparatus. A test device for analyzing the mechanism of reactions with reactants like chemically active oxygen excited by low energy electron on material surfaces under heavy neutron irradiation was also improved through

*Safety Eng. and Tech. Dep., Mitsubishi Research Institute, Inc.

expanding the test temperature range up to 600 °C. A Fourier transform infrared spectrometer was arranged for characterizing oxide films formed by corrosion on the surfaces.

A document survey has been carried out to elucidate the questions about the candidate materials for SCWR and the interactions with high-temperature water. The major requirements of core materials for SCWR are the mechanical strength at high temperature and the corrosion resistance at high oxidation potential caused by radiolysis. Refractory materials with high mechanical strength such as titanium alloys are not attractive, because of the high solubility of hydrogen. The high corrosion resistance is required to reduce radioactive crud which is difficult to remove from the primary coolant system operated at high pressure of supercritical water. Superalloys with high chromium contents of over 25 % seem to have a sufficient corrosion resistance as shown in Fig. 7.4.2. Therefore, we selected the superalloys for candidate materials as shown in Table7.4.1 in this study. The preparation of the materials has just started.

The establishment and modification of numerical simulation codes to analyze the radiation effects on the interactions theoretically have been also carried out. The thermodynamic properties of supercritical water and the formation of excited species in supercritical water under irradiation condition were acquired. The applicability and merits of existing numerical analysis codes for understanding the interaction mechanism in the supercritical water environments were elucidated.

References

1) Y. Oka and S. Koshizuka: J. Nucl. Sci. Tech. 38 1081 (2001).
2) "A Technology Roadmap for Generation IV Nuclear Energy Systems" (2002), (http://www.nuclear.gov/nerac/FinalRoadmapforNERACReview.pdf)

Table 7.4.1 Chemical composition of candidate materials (mass%).

		C	Si	Mn	P	S	Ni	Cr	Fe	Ti	Co	Mo	Nb	Al	O	N
Stainless Steel	25Cr−20Ni−Ti	<0.001	<0.01	<0.01	<0.003	<0.003	20	25	Bal.	0.2	<0.003				<0.005	<0.005
	25Cr−35Ni−Ti	<0.001	<0.01	<0.01	<0.003	<0.003	35	25	Bal.	0.2	<0.003				<0.005	<0.005
Ni−Cr−Fe	Alloy 690	0.03					60	30	9.5							
Ni−Cr−Fe−Mo	Alloy 718	0.05					52	19	19			3	5	0.5		
Ni−Cr−W−Si	RW Alloy	0.007	2.7	<0.01	<0.005	<0.001	58	30							0.01	0.01

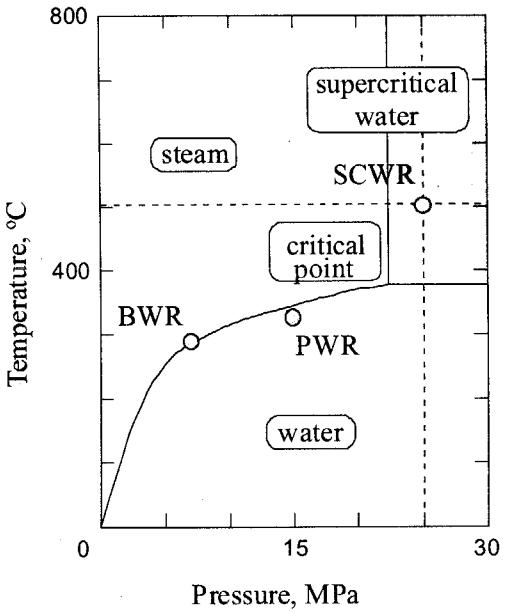

Fig. 7.4.1 Condition of primary reactor coolants in SCWR and LWRs.

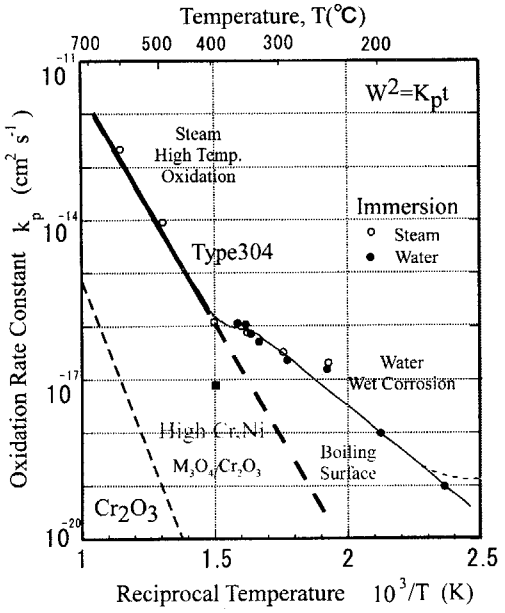

Fig. 7.4.2 Temperature dependence of the growth of oxide films.

7.5 Elastic-plastic FEM Analysis on Low Cycle Fatigue Behavior of Dissimilar Metal Joint

H. Nishi
(*E-mail*: nishi@popsvr.tokai.jaeri.go.jp)

Various aspects concerning with interfacial crack and fracture of dissimilar joints have been investigated in recent years. Fracture problem of the interface between dissimilar metals is often encountered in engineering components. We have carried out research on the bonding method and strength for the joint between Alumina dispersion-strengthened copper (DS Cu) and 316 stainless steel. In the previous study, the low cycle fatigue strength of joint between the DS Cu and 316 stainless steel was smaller than that of the DS Cu, as shown in Fig.7.5.1. The joint fractured at the DS Cu near the interface in the case of small strain range of the fatigue test. For large strain range, however, the fracture point was in the DS Cu about 6 mm from the interface. In this study, elastic-plastic finite element analysis was performed for the low cycle fatigue behavior of the joint in order to investigate the fatigue life and the fracture behavior of joint.

The FEM model was a parallel part of the round bar specimen, in which the DS Cu and stainless steel were bonded in the middle of parallel part, as indicated in Fig.7.5.2. The mesh was divided among only a half of the specimen because of an axial symmetry of its deformation and was constructed with isoparametric 8-node biquadratic axisymmetric element. Taking account for the stress singularity at the bonded edge, a size of element was diminished as the element was close to the interface or the edge. Used Young's moduli, Poisson's ratios and cyclic stress-strain curves of the stainless steel and DS Cu were obtained by tensile and low cycle fatigue test. The stress-strain curve of stainless steel intersected that of DS Cu at strain amplitude of approximately 0.55%. In plastic range, the deformation stress of the stainless steel was smaller than that of DS Cu at less than the intersecting strain amplitude.

The elastic-plastic analysis was performed with a computer program ABAQUS on tensile and fatigue analysis. As for the boundary conditions, a uniform displacement was applied to the top nodes of model (DS Cu). The displacements of nodes on z axis and lower end (stainless steel) were fixed in the radial and z direction, respectively. Concerning with the fatigue analysis, cyclic displacement was applied up to four cycles as a kinematic hardening

material for DS Cu and stainless steel.

Figure 7.5.3 shows distributions of axial stress, σ_z, on the interface near the edge obtained by the tensile analysis. In this figure, the stress was compared with a ratio of distance from the edge, r, to a radius of the specimen, w. Moreover an index of the stress singularity, λ, which was a slope of the stress distribution around the edge, was also described. Stress singularity existed slightly in the edge for the combination between stainless steel and DS Cu. The index λ was 0.0203 for the elastic analysis, which was well in accordance with Bogy's result λ=0.0204 in this joint. As the strain was advanced to the plastic range ε=0.2-0.5 %, the stress singularity decreased, while the stress concentration occurred again near the edge at more than 0.75% nominal strain.

As for the fatigue analysis, the results were discussed on the forth cycle, because the stress-strain hysterysis loop was closed before the forth cycle. Distributions of axial strain, ε_z, on specimen surface along the loading direction were designated in Fig.7.5.4 as an example. In this figure, the strain distributions of the maximum tension and compression sides were exhibited for the strain range $\Delta\varepsilon_t$=0.75 and 1.5%, for which the joint specimen fractured at the DS Cu near the interface and in the DS Cu from the interface in the fatigue test respectively. As for the strain range $\Delta\varepsilon_t$= 0.75%, the computed strain range on the part of DS Cu, which was bounded on the axial strain between the maximum tension and compression sides, was smaller than that on the stainless steel, since the deformation stress of the DS Cu was large rather than that of the stainless steel. In the case of $\Delta\varepsilon_t$= 1.5%, however, the computed strain range on the part of DS Cu was larger than that on the interface and stainless steel. These results were in accordance with the fracture point of specimens in the fatigue test.

In order to discuss the fracture point and fatigue life of the low cycle fatigue test, the computed strain range on the end of DS Cu, the interface (DS Cu 0.01 mm from interface) and the end of stainless steel were compared for the various strain range, as shown in Table7.5.1. The table also designated the observed number of cycles to failure, the fracture point and the predicted number of cycles to failure, which were obtained from substituting the computed strain range, $\Delta\varepsilon$, for each low cycle fatigue life obtained by the fatigue test in respect of DS Cu and stainless steel base metals. The minimum predicted number of cycles to failure among the parts of the DS Cu, interface and stainless steel was marked with a circle. The predicted fatigue life and the fracture point were consistent with the low cycle fatigue test. The fracture point of specimen depending on its strain range was attributed to the strain concentration.

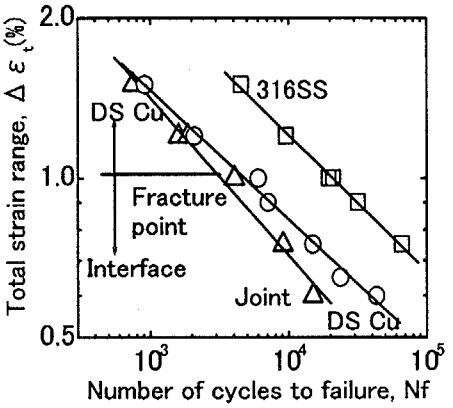

Fig.7.5.1 Comparison of low cycle fatigue lives.

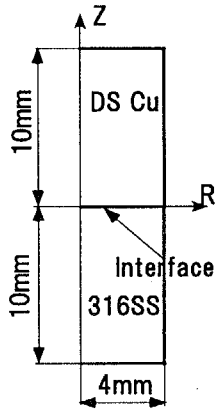

Fig.7.5.2 FEM analysis model.

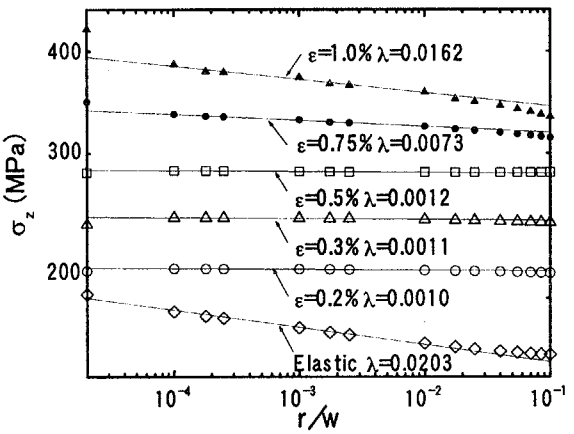

Fig.7.5.3 Axial stress distribution on interface near edge.

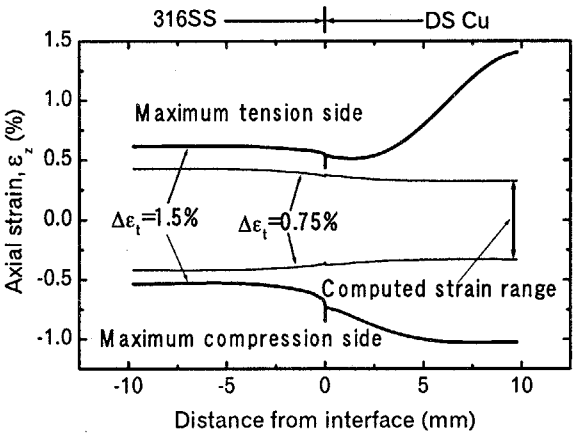

Fig.7.5.4 Axial strain distribution of specimen surface along loading direction.

Table7.5.1 Results of computed strain range and comparison between predicted and observed N_f.

Δ ε t(%)	Position	Computed Δ ε (%)	Predicted N_f	Observed N_f Fracture point
0.6	DS Cu	0.554	54600	15100
	Interface(DS Cu)	0.602	○ 38000	Interface
	Stainless steel	0.65	112000	
0.75	DS Cu	0.657	27100	9080
	Interface(DS Cu)	0.753	○ 15400	Interface
	Stainless steel	0.846	40000	
1	DS Cu	0.896	7560	4056
	Interface(DS Cu)	1.03	○ 4250	Interface
	Stainless steel	1.09	14900	
1.2	DS Cu	1.33	○ 1490	1590
	Interface(DS Cu)	1.22	2120	DS Cu
	Stainless steel	1.14	12500	
1.5	DS Cu	2.43	○ 140	750
	Interface(DS Cu)	1.28	1750	DS Cu
	Stainless steel	1.15	12000	

8. Research on Advanced Transuranium Bearing Fuels

Research Group for Advanced Fuel is carrying out the experimental study using transuranium (TRU) elements for demonstrating innovative fuel cycle technologies, which include nitride fuel, rock-like oxide (ROX) fuel and pyrochemical process based on molten salt electrorefining. In addition, some basic properties of TRU compounds are investigated for contributing to preparation of thermodynamic database.

Destructive post irradiation examinations (PIEs) of (U,Pu)N and (U,Pu)C fuel pins irradiated at JOYO were completed under a joint research with JNC. From the results of nondestructive and destructive PIEs a good performance of the fuels was demonstrated under the irradiation condition. On the other hand, the irradiation test of (Pu,Zr)N and PuN+TiN pellets simulating dedicated fuel for minor actinide (MA) transmutation was started at JMTR. Typical characteristics of the pellets subjected to irradiation were clarified. With regard to pyrochemical process, electrotransport of U and Pu into liquid cadmium cathode (LCC) was investigated at much higher cathodic current density than previous study. The U/Pu ratio recovered in LCC was not only analyzed experimentally but also estimated from the separation factor, (U/Pu ratio in Cd)/(U/Pu ratio in salt), previously reported. Further, irradiation performance of MA-bearing ceramic fuels will be evaluated under an integration research with JNC, preceding the integration of JAERI and JNC forecasted in FY2005. As a cold run without using MA, mechanical properties of candidate ceramics for inert matrix was measured.

The joint irradiation test on Pu-ROX fuels was finished at HFR, NRG-Petten, the Netherlands, after attaining transmutation of about 60% of initial-loaded Pu. The PIEs are started in FY2003. On the other hand, geological stability of ROX fuel was investigated by use of five kind of U-ROX fuels irradiated at JRR-3. Leaching tests were performed in deionized water at 363K for up to 173day and leaching rates of main constituting elements in U-ROX fuel such as U, Zr Al and Y were determined. Solid solutions of NpO_2 and yttria-stabilized zirconia (YSZ) were prepared and the lattice parameter of fluorite phase was measured. Valence state of Np ion in the solid solution, which is important for evaluating leaching behavior of Np, was speculated from the results of Mössbauer spectroscopy besides the change in lattice parameter. Further, by calculation using SRAC95 system with JENDL-3.2 based data library, power distribution flattening of PWR core fully loaded with ThO_2-added ROX fuel, which has an advantage of high Pu transmutation capability, was carried out. The power peaking factor can be improved to the comparable value to UO_2-added ROX fueled core.

8.1 Preparation of (Zr,Pu)N and TiN+PuN Pellets for Irradiation Tests

K. Nakajima, T. Iwai, H. Kikuchi, H. Serizawa and Y. Arai
(E-mail: kuni@popsvr.tokai.jaeri.go.jp)

Japan Atomic Energy Research Institute (JAERI) has proposed accelerator driven system (ADS) that transmutes minor actinides (MAs). A nitride is one of the candidates for the target fuel of the system[1]. The nitride fuel has various advantages compared to other one; high melting point, high thermal conductivity and high heavy metal density. Further, actinide nitrides have the probable mutual solubility because they have the same fcc cubic structure (NaCl-type) and the similar lattice parameters. The superior thermal properties can enhance the safety margin of the ADS and the segregation and migration problems of the fuel element during the operation are mitigated. High transmutation rate of MAs can be also realized by making full use of these characteristics. However, it is necessary to control a large reactivity change and adjust an adequate linear rate of the ADS core during the operation. So the fuel needs to be diluted with neutronically inert materials. In JAERI, ZrN and TiN, which have high thermal conductivity and high melting point, have been selected as the diluents of the fuel. Their preparation tests containing PuN as a surrogate for MAs have been conducted[2]. This report concerns the preparation of (Zr,Pu)N and PuN+TiN fuel pellets for the tests in JMTR, which started in May 2002 for the target burnup close to 20 GWd/t.

Photo. 8.1.1 shows the appearance of the (Zr,Pu)N and PuN+TiN fuel pellets for the tests. Fuel pellets for the irradiation test were prepared from PuN synthesized by the carbothermic reduction method and ZrN with the purity of 99.5% and the particle size of 3-6 μm (Rare Metallic Co. Ltd.) or TiN with the purity of 99.5% and the particle size of 1-2μm (Rare Metallic Co. Ltd.) by a mechanical blending method. ZrN+PuN of 32.6g and TiN+PuN of 22.8g, each of which included 20wt% Pu, were blended using the tumbler ball mill pot (400cc inside volume) and 100 balls of 10ϕ in diameter (~320g) made of zirconia. In the case of the preparation of (Zr,Pu)N, the mixture of PuN and ZrN ball-milled for 10hr was pressed into disks and heated at 1673K in N_2-8%H_2 mixed gas stream for 9hrs. These procedures were repeated 3 times to confirm the formation of the solid solution. The heattreated samples were ball-milled again for 190hrs, then compacted into green pellets of 9.5ϕ in diameter under 190MPa for 10sec with 0.5wt% of wax-type pore former particles purchased from Kawaken Fine Chemical Co. Ltd. These green pellets were sintered at 1973K for 5hr in flowing Ar-8%H_2, followed by heating at 1673K for 9hr in N_2-8%H_2 stream for homogenization. In the case of the preparation of TiN+PuN, which had negligible mutual solubility, the fine mixed powder for sintering was ball-milled for 49hr and compacted into green pellets of 9.3ϕ in diameter under 200MPa for 10sec with 1.0wt% of wax-type pore former particles. Sintering condition was the same as that of the preparation of (Zr,Pu)N

pellet. All the processes mentioned above were conducted in Ar gas atmosphere glove boxes where oxygen and water contents were kept less than 3ppm. The sintered pellets were shaved in flowing spindle oil to adjust their diameters to 8.22±0.02mmϕ and then rinsed out in a ultrasonic washer filled with acetone to remove the oil. At last the pellets were degassed at 1473K for 1hr in vacuum.

The characteristics of (Zr,Pu)N and TiN+PuN pellets are given in Table 8.1.1. The table also includes the previous results for comparison[2,3]. As shown in the table, the stoichiometry of TiN+PuN pellets significantly shifted to the hypo-stoichiometric composition range like the previous result. It was found that the amount of the occluded gas was higher than those of (U,Pu)N and (Zr,Pu)N pellets. This might be relative to the existence of large monophasic area in the hypo-stoichiometric composition range of TiN. According to the previous result, the density of TiN+PuN pellet reached just only 76%TD (TD: theoretical density), indicating that a sintering aid is required to increase its density. However, the present TiN+PuN pellet density increased up to >90%TD and needed to be lowered by adding the pore former to meet the specification of the fuel pellets for irradiation tests. On the other hand, both the oxygen impurity contents of (Zr,Pu)N and TiN+PuN pellets were found to become lower than that of the previous ones. These superior characteristics of the pellets obtained in this study might be due to the difference of the characteristics of the starting materials of ZrN and TiN powders. The microstructures of the as-etched pellets of (Zr,Pu)N and TiN+PuN are shown in Photo. 8.1.2(a) and (b), respectively. Although the distribution of pores did not seem perfectly uniform, all the pellets kept structural integrity. The grain sizes of (Zr,Pu)N and TiN+PuN pellets were found to be much smaller than those of typical (U,Pu)N pellets (15~20μn)[3]. TiN and PuN phases in diphasic TiN+PuN pellets could not be distinguished each other from this photo.

References

1) Takizuka, T. et al.: in Proceedings of the Fifth OECD/NEA Information Exchange Mtg. on P & T. Mol, 25-27 November 1998, p. 95.

2) Arai, Y. and Nakajima: K., J. Nucl. Mater. 281 (2000) 244.

3) Arai, Y. et al.: J. Nucl. Sci.Technol. 30 (1993) 824

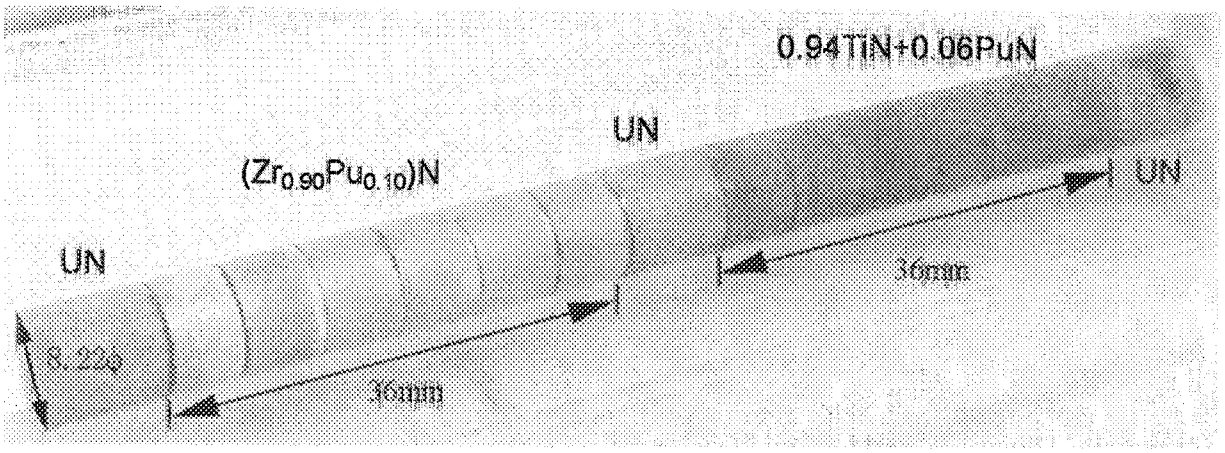

Photo. 8.1.1 Appearance of the (Zr,Pu)N and PuN+TiN fuel pellets

Table 8.1.1 Typical characterisitics of the (Zr,Pu)N and PuN+TiN fuel pellets together with the previous results

Fuel pellets	Pu content (wt%)	Nitrogen content (wt%) (N/M)	Oxygen content (wt%) (O/M)	Carbon content (wt%) (C/M)	Density (%TD)	Occluded gases (μl·atm/g) (at 1673K)
(Zr,Pu)N (This work)	20*	11.32 (0.96)	0.28 (0.02)	0.35 (0.03)	90#	74
TiN+PuN (This work)	20*	14.42 (0.70)	0.79 (0.03)	0.50 (0.03)	85#	220
(Zr,Pu)N (Previous work)[2]	40*	9.15 (0.88)	0.94 (0.08)	0.25 (0.03)	95	n.d.**
(Zr,Pu)N (Previous work)[2]	60*	7.95 (0.90)	0.44 (0.04)	0.25 (0.03)	90	n.d.**
TiN+PuN (Previous work)[2]	50*	12.21 (0.80)	0.76 (0.04)	0.25 (0.02)	76	n.d.**
(U,Pu)N (Previous work)[3]	18	5.56 (1.01)	0.12 (0.02)	0.20 (0.04)	83#	82
(U,Pu)N (Previous work)[3]	20	5.42 (0.98)	0.14 (0.02)	0.20 (0.04)	86#	52

*Nominal amount #addition of pore former **not determined

Photo. 8. 1. 2 Microstructure of (a) (Zr,Pu)N and (b) PuN+TiN fuel pellets (as-etched)

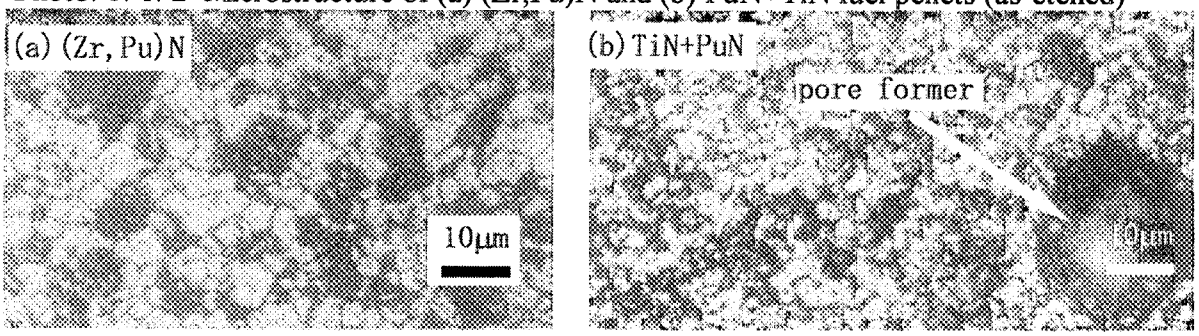

8.2 Pre-examination on the Mechanical Property for Some Ceramics by Ultrasonic Measurement

H. Serizawa, T. Iwai and Y. Arai
(*E-mail:* serizawa@popsvr.tokai.jaeri.go.jp)

Our research group is working on a new type of inert matrix fuel containing Minor Actinides (MA) that can be introduced into the fuel reprocessing cycle, thereby reducing the impact on the environment. As part of this study, it is important to clarify the mechanical properties of this fuel, as the elastic moduli of the pellet closely relates to the Pellet Cladding Mechanical Interaction (PCMI). We have set up a pulse method-type High-Temperature Ultra Sonic Measuring system (Toshiba Tungaloy Co.,LTD.) that can measure a series of elastic properties of ceramics and their temperature dependencies. Before the system is set up in the glove box, a cold run was carried out using one of the candidates for the matrix of the new-type fuel, MgO.

Figure 8.2.1 shows a schematic of part of the measuring system. The important point to note is the 30μm thick aluminum foil inserted between the sample and the wave-guide. The role of the foil is to adhere the sample to the head of the wave-guide. An acoustic wave is then effectively transferred from the wave-guide to the sample through the foil. The sample was firmly fixed on the wave-guide with a molybdenum box nut. Before the measurement, the sample was heated at 1123 K for 1 min. to confirm the adhesion of the sample. The sample was then heated at a rate of 50 K/min. up to 1273 K and 20 K/min. from 1273 K to 1770 K. Measurement in the cooling run could not be made due to the occurrence of cracks. Both the longitudinal and shear velocities (Vl and Vs) were measured in the same run.

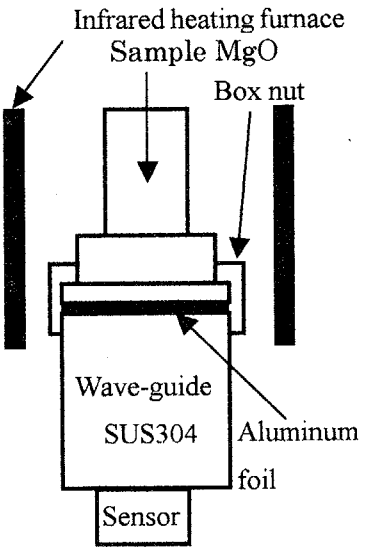

Fig. 8.2.1 the arrangement of a sample and a wave guide.

The acoustic wave velocities and the acoustic wave anisotropy measured for MgO are given in Figs. 8.2.2 and 8.2.3. The acoustic wave velocity decreases continuously with increasing temperature. The temperature dependence of the acoustic wave velocity anisotropy of MgO shows that the longitudinal wave velocity exceeds that of the shear wave over the whole temperature range. The difference between these two wave velocities decrease with increasing temperature. The reduction suggests activation of the shear mode. The tendency of the change in the anisotropy

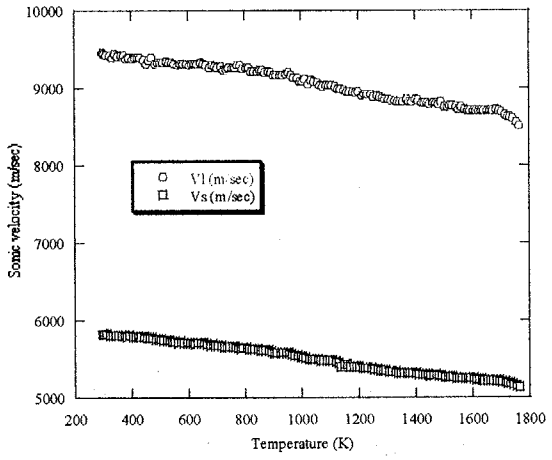

Fig. 8.2.2 the acoustic wave velocities of MgO

indicates that the effect of the residual stress and deformation mode decrease respectively, as the temperature increases[1].

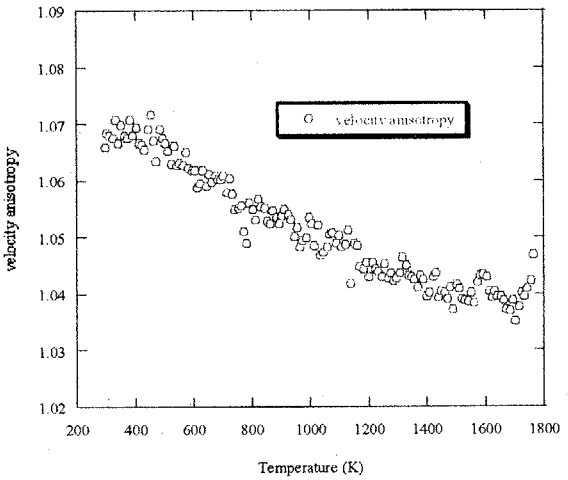

Fig.8.2.3 The temperature dependence of the acoustic wave velocity anisotropy of MgO

Three elastic moduli and the Young's modulus/Bulk modulus ratio (E/K) of MgO are shown in Figs. 8.2.4 and 8.2.5. There are some reports for the mechanical properties of MgO in the literature, however, the data are rather old. Young's modulus for MgO was reported by Wachtman[2] and according to him, the Young's modulus of MgO, measured by a resonance method, decreases rapidly and nonlinearly at temperatures greater than 1473 K. The data shown in Fig 8.2.4, however, does not show such a reduction in the modulus. The nonlinear variation was considered attributable to the measuring method. It is known that the resonance method sometimes damages the sample: the data obtained by this method deviates from the true value especially in the high temperature range. The bulk modulus of MgO was

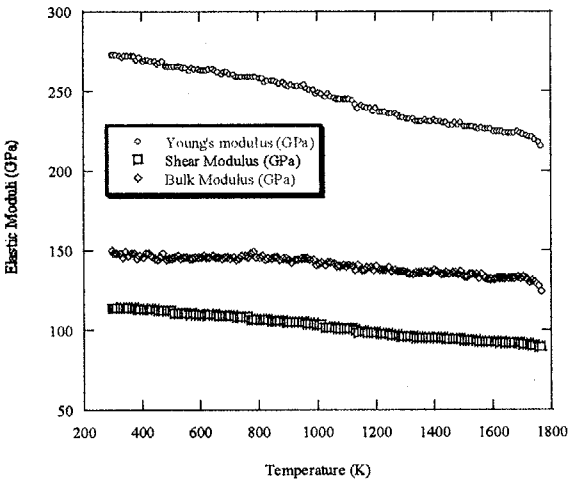

Fig.8.2.4 Temperature dependences of three elastic moduli for MgO

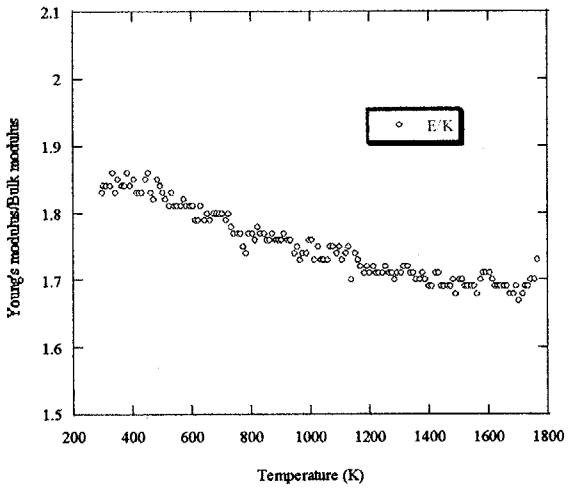

Fig. 8.2.5 Temperature dependence of Young's modulus/Bulk modulus ratio

reported by Anderson[3], however the present data is somewhat lower than this value. It is thought that the deviation may be attributable to the difference in the method. However, the E/K (another elastic parameter) plotted in Fig. 8.2.5 does not show this anomalous temperature dependence; the tendency resembles that of the velocity anisotropy given in Fig. 8.2.3. Therefore, we have confidence in the elastic moduli obtained in this study.

References

1) M. FUKUHARA and I. YAMAUCHI: J. Mater. Sci., 28, 4681(1993).

2) J. B. WACHTMAN, J. and J. D. G. LAM: J. Am. Cera, Soc., 42(5), 254(1959).

3) O. L. ANDERSON: Phys. Rev., 144(2), 553(1966).

8.3 Simultaneous Recoveries of U and Pu into Liquid Cd Cathodes at High Current Densities

T. Kato*, K. Uozumi**, O. Shirai, and T. Iwai
(E-mail:tkato@criepi.denken.or.jp)

The molten salt electrolysis with eutectic LiCl-KCl is applied for recovering the heavy metals (HM), i.e. U, Pu and minor actinides (MA) from spent metallic and nitride fuels. Plutonium is recovered into a liquid cadmium cathode (LCC) with U and MA. In our previous experiments to recover Pu and U into LCCs at various U/Pu ratios in the salt composition, the relationship between the U/Pu ratios in the salts and in LCC has been already studied[1]. An appropriate current densities for the successful U and Pu recovery must also be found for the process designs, because too high current densities lead to the growth of the deposit on LCC, which might not collect Pu but recover only U as a solid cathode[2].

In this work, the electrolysis experiments were carried out at relatively high cathode current densities, 101 mA/cm^2 in RUN 1 and 156 mA/cm^2 in RUN 2, compared with 23 mA/cm^2 in the previous study[1]. Then, the morphology of LCCs, the current efficiencies, and the U/Pu ratios in LCCs were investigated.

The same electrolysis apparatus as in the previous work was used[1]. The electrolyses were conducted at 773 K in an argon atmosphere. The molten salt of 1.2 kg and the liquid Cd pool of 1.5 kg were put in the iron vessel of 14 cm diameter. The HM composition and U/Pu ratio in the salt were approximately 7.5 wt. % and 1/2. The Cd pool was used as the counter electrode. Uranium and plutonium dissolving in the Cd pool were transported anodically to the salt. The liquid Cd cathodes of 120 g were contained in aluminum nitride crucibles of 42 mm diameter. A paddle stirrer was used for the agitations around the surface of LCC and the stirring rate was 40 rpm. The passed charges were corresponding to 10 wt. % HM recovered in LCC, which is the tentative target in our process design.

The cathode potentials during the electrolyses are shown in Fig. 8.3.1. The silver/silver chloride electrode was used as the reference electrode to measure the cathode potentials. The horizontal axis in the figure indicates the passed charge, which

---

*A guest researcher from the Central Research Institute of Electric Power Industry, from April 2002

**A guest researcher from the Central Research Institute of Electric Power Industry, from October 1999 to December 2001

was converted to the HM weight ratio in LCC on the assumption that HM would be recovered by 100 % of the current efficiency. The cathode potentials gradually descended until about 4 wt. % HM was recovered in LCC. Then, the potential in RUN 1 remained stable around −1.56 V. The descent is corresponding to the increasing HM concentration in the liquid Cd and the stability means the constant chemical activity of HM due to the saturations. In RUN 2, the potential ascended after around 8 wt. % HM was recovered. It is similar to typical potential changes observed when dendritic deposit grew on LCC in the electrolyses with only U[2].

After the electrolysis was completed, the apparatus was cooled in the furnace to the ambient temperature. The solidified cathode of RUN 1 was a bulk ingot as shown in Photo 8.3.1. The ingot was cut and an 18 g piece against 130 g of the whole was used for the composition determination. The weight ratios of Pu and U in the ingot were 5.7 wt. % and 4.7 wt. %, respectively. The total HM of 10.4 wt. % was in good agreement with 10.5 wt. % calculated from the passed charge, thus the current efficiency was almost 100 %.

The ratio between U and Pu in LCC was estimated applying the separation factor (SF). The separation factor is defined as the following ratio.

$$SF=(U/Pu \text{ ratio in Cd})/(U/Pu \text{ ratio in salt}) \quad (1)$$

The value of SF at 773 K was reported to be 1.88, which was obtained in the equilibrium system of unsaturated liquid Cd/LiCl-KCl eutectic salt[3]. The calculated ratio was 52.8 wt. % for Pu in U+Pu, which was close to 55.1 wt. % of the experimental value.

After RUN 2, some deposit was observed outside of the cathode crucible as expected from the potential change during the electrolysis. Samples were taken from the deposit outside of the crucible and the composition analysis was carried out. It showed more than 60 wt. % of the deposit was Cd and the ratio of Pu in U+Pu was 57.8 wt. %, compared with 52.3 wt. % for the calculated value. X-ray diffraction analysis of the deposit was also carried out. The diffraction pattern was corresponding to that of $PuCd_{11}$ as shown in Fig. 8.3.2 except for the peaks contributed by KCl and Cd metal. These analyses indicate that even though the deposit grew on LCC, the cathode in RUN 2 still worked to collect Pu and U, which formed the compound involving Cd.

References

1) K. UOZUMI, et al.: "Behaviors of Uranium and Plutonium at Simultaneous Recoveries into Liquid Cadmium Cathodes", JAERI-Review 2003-004, pp.183-185 (2003).

2) T. KOYAMA, et al.: J. Nucl. Mater., **247**, 227, (1997).
3) T. KOYAMA, et al.: J. Alloys Compd., **189**, 37, (1992).

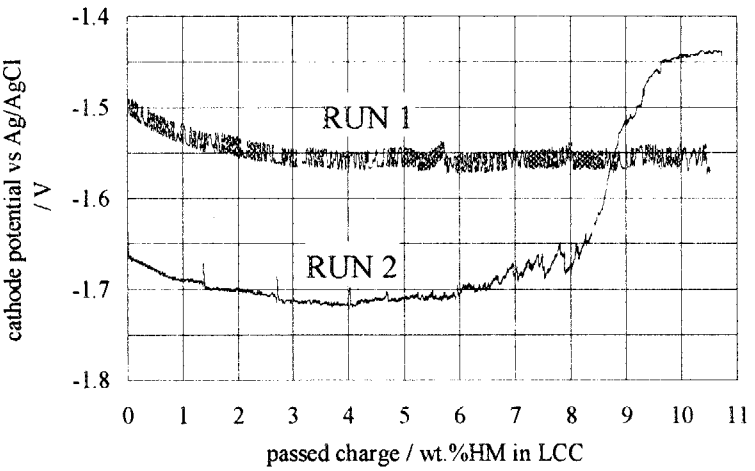

Fig. 8.3.1 Change of the cathode potentials.

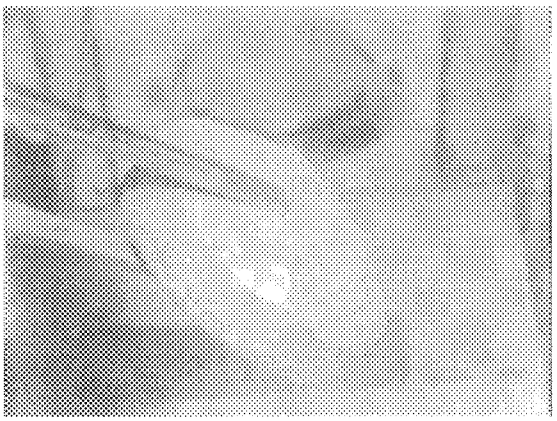

Photo 8.3.1 Solidified LCC ingot of RUN 1.

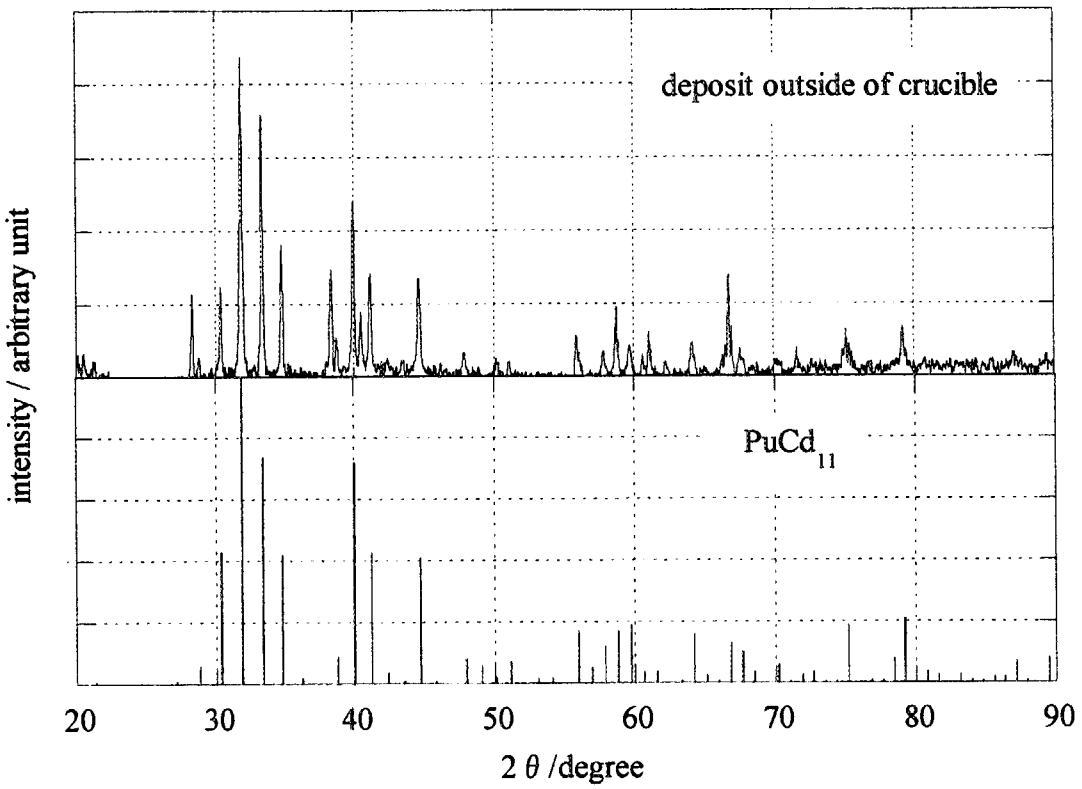

Fig. 8.3.2 X-ray diffraction pattern of the deposit outside of the cathode crucible in RUN 2.

8.4 Power Distribution Flattening of PWR Core Fully Loaded with Thoria Added Zirconia Based Plutonium Rock-like Oxide Fuel

H. Akie

(*E-mail*: akie@mike.tokai.jaeri.go.jp)

In plutonium rock-like oxide (ROX) fuel (PuO_2-$(Zr,Y,Gd)O_2$-$MgAl_2O_4$) during burnup in a LWR, the neutron absorption varies much more than that in conventional UO_2 and MOX fueled cores due to the reduction of plutonium density. This causes a larger burnup reactivity swing and therefore larger power peaking than in UO_2 and MOX LWRs, which arises one of the most important reactor physics problems of ROX fueled cores together with the smaller negative reactivity coefficients [1]. There have been proposed several different ROX fueled PWR cores to improve the reactivity coefficients, by adding depleted UO_2, Er_2O_3 or ThO_2 in ROX fuel, or by considering 1/3 ROX and 2/3 UO_2 assemblies partial loading core. All the proposed cores successfully realized an improved reactivity coefficient as well as a power peaking factor, while the power peaking was not well reduced in the core fully loaded with thoria (ThO_2) added ROX as shown in Table 8.4.1 [2].

Table 8.4.1 Calculated fuel temperature coefficient (FTC) for a fuel temperature change from 900 to 1200 K and power peaking factor of weapons-grade Pu ROX fueled PWR cores at BOC

	FTC (pcm/K)	peaking factor
Weapons-Pu		
Original ROX	-0.33	2.7
24 at.% Th added	-1.9	2.4
15 at.% U and Er added	-2.0	2.1
1/3ROX + 2/3UO_2	-1.8	1.7
UO_2	-2.5	2.0

For the power distribution flattening of ThO_2 added ROX fueled core, in the same manner as in the UO_2 added ROX core, the Er_2O_3 additive is also considered, and the Gd_2O_3 additive content is adjusted to have the reactivity effect only at BOL. In the original ROX fuel in order to suppress the large excess reactivity, Gd_2O_3 burnable poison was used, and caused a large burnup reactivity swing and a large power peaking [1].

Two-dimensional X-Y core burnup calculations are carried out for weapons- and reactor-grade Pu ThO_2 added ROX fueled PWR cores. The core specification is based on the conventional 1100 MW_e class 17×17 type PWR. In the core burnup calculations, a three batch refueling and shuffling scheme of assemblies is taken into consideration for the power distribution flattening. The plutonium enrichment is adjusted to achieve the discharge burnup of about 1200 EFPD (Effective Full Power Days, 400 EFPD × 3 batches), which corresponds to about 45 GWd/t in UO_2 and MOX fueled cores. In order to estimate the core axial power profile and the local power peaking within an assembly, one-dimensional core calculations and fuel assembly calculations are also performed. These calculations are made by using the SRAC95 system [3] with the JENDL-3.2 based data library, the same data and method as the case in Table 8.4.1.

The estimated core characteristics of the improved ThO_2 added ROX fueled core are summarized in Table 8.4.2 for W-Pu and R-Pu ROX cores at BOC, in comparison with the other ROX and UO_2 fueled cores. As shown in this table, the power peaking factor can be improved to the comparable value to UO_2 added ROX fueled cores. It can be also seen a slight effect of Er additive on fuel temperature coefficient.

Table 8.4.2 Improved core characteristics of ThO_2 added weapons- and reactor-grade Pu ROX fueled PWR cores at BOC.

	FTC (pcm/K)	peaking factor
Weapons-Pu		
Original ROX	-0.33	2.7
24 at.% Th and Er added	-2.0	2.2
15 at.% U and Er added	-2.0	2.1
1/3ROX + 2/3UO_2	-1.8	1.7
Reactor-Pu		
18 at.% Th and Er added	-2.1	2.2
8 at.% U and Er added	-2.0	2.2
1/3ROX + 2/3UO_2	-1.6	1.8
UO_2	-2.5	2.0

An advantage of the ThO_2 added ROX fuel over the UO_2 added one is the plutonium transmutation capability. The plutonium transmutation rate in ROX fueled cores is compared with that in the MOX fueled core in Table 8.4.3. In this table, there are shown the input and

transmuted amount of plutonium per 300 EFPD operation per 1 GW_e reactor power, and the transmuted percentage as a ratio of transmuted/input amount. Although the fertile isotope ^{232}Th produces new fissile isotope ^{233}U, the transmutation amount and percentage of plutonium is still higher than that in the UO_2 added ROX fueled core.

Table 8.4.3 Input and transmuted amount (t/GW_e/300EFPD) of plutonium in ROX and MOX fueled cores (1200 EFPD discharge burnup, corresponding to 45GWd/t in MOX core)

		Weapons-Pu			Reactor-Pu		
		Input	Transmuted		Input	Transmuted	
		(t)	(t)	(%)	(t)	(t)	(%)
Th and Er added	Pu-239	0.97	0.94	97	0.80	0.75	93
	total Pu	1.03	0.82	79	1.37	0.90	66
U and Er added	Pu-239	0.93	0.85	92	0.80	0.70	88
	total Pu	0.99	0.69	69	1.36	0.81	60
MOX (once-through)	Pu-239	0.88	0.56	63	0.99	0.44	45
	total Pu	0.94	0.30	32	1.69	0.41	25
(recycle once)	Pu-239	0.76	0.54	71	0.76	0.44	58
	total Pu	0.81	0.35	43	1.30	0.48	37

ROX results with 2-dimensional core calculations, and MOX results (shaded) with cell calculations.

References

1) H. Akie, H. Takano, and Y.Anoda : J. Nucl. Mater. 274, 139-145 (1999).

2) H. Akie, Y. Sugo and R. Okawa : to be published in J. Nucl. Mater. 319 (2003).

3) K. Okumura, K. Kaneko and K. Tsuchihashi : JAERI-Data/Code 96-015 "SRAC95; General Purpose Neutronics Code System" (1996) (in Japanese).

8.5 Results of Leaching Test for Irradiated Rock-Like Oxide (ROX) Fuels (1) - Leaching Behavior of Fuel Matrix Elements -

K. Kuramoto, N. Nitani and T. Yamashita
(E-mail: kura1@nucef.tokai.jaeri.go.jp*)*

The concept for rock-like oxide (ROX) fuel consists of almost complete Pu burning in LWR, and disposal of chemically stable spent fuels. In order to evaluate the geological stability of spent ROX fuels, leach tests were performed in a deionized water at 363 K for up to 173 d with reference to the MCC-1 method. Five irradiated fuel pellets, a single phase fuel of a yttria-stabilized zirconia containing UO_2 (Z fuel), two fuels of U-YSZ particle dispersed in $MgAl_2O_4$ (SPI) or Al_2O_3 (COR) matrix (SD or CD fuel), two homogeneous-blended fuels of U-YSZ and SPI or COR powders (SH or CH fuel), were submitted to the tests. Nuclides leached from the irradiated ROX fuel may exist as ions and/or colloidal species in the leachate and as precipitates on a vessel and a sample holder. The leach rate of the important nuclides and elements must be estimated by the total amount existing in leachate and precipitates. In addition, because the colloidal species will influence the solution equilibrium and migration of the nuclides and the elements, the amount of colloids is estimated quantitatively. The first leaching data mainly dealing with matrix elements of irradiated ROX fuels were shown in the report.

As a result of pH measurement, the leachate pH decreased rapidly from 5.9 to 4.0 - 4.3 in the early leaching period, and then pH of the leachates were increasing gradually with increasing leaching period. It was reported that leachate pH decreased suddenly by the water radiolysis in the high γ-irradiation field and as a result alkaline element leaching was also accelerated. The pH increasing tendency is also well known in glass waste form leaching behavior because of dissolution of alkaline elements such as Na and Cs to leachate. A similar phenomena occurred in this test, that is, rapid pH decrease by the water radiolysis and slow pH increase by harmonic Cs leaching.

Figures 8.5.1 (a), (b) and (c) show the normalized leach rate of Zr, Y and U (NL_{Zr}, NL_Y and NL_U) for 5 irradiated ROX fuels, and Fig. 8.5.1 (d), (e) and (f) indicate the normalized leach amount of Zr, Y and U (NLA_{Zr}, NLA_Y and NLA_U) of the Z fuel. The NL_{Zr} decreased with increasing leaching time. The NL_{Zr} of the Z fuel was ~ 3 x 10^{-8} g cm^{-2} d^{-1} after 173 d, and those of the other fuels were 5 to 25 times higher. The NL_U of the Z fuel was also the

lowest among the 5 fuels, however, NL_Y of the Z fuel was two or three orders of magnitude higher than those of the other fuels. This means that a part of Y did not dissolve with Zr and U congruently suggesting formation of Y_2O_3 with low durability in water. In addition, NL_U of homogeneously-blended fuels were about triple of those of particle-dispersed fuels.

The NL_Y and NL_U were also decreased with increasing leaching time as in the case of NL_{Zr}. These decreasing leach rates mean that rapid and large amount dissolution of these elements occurred in the early leaching period within the first 8 d, and then only a limiting amount of these elements had been leached. Therefore the measured NL_k was not the true normalized leaching rate in this case. The NLA_{Zr} of the Z fuel was increasing with increasing leaching time as shown in Fig. 8.5.1 (d), and NLA_U and NLA_Y were also increasing slightly after 173 d. A similar tendency was observed for the other fuels. The required leach rate of element k can be obtained from the slope of NLA_k against leaching periods. The normalized leach rates of Zr, Y and U evaluated by the slope method were ~2 x 10^{-9}, ~5 x 10^{-6} and ~1 x 10^{-9} g cm^{-2} d^{-1} (for the period from 8 to 173 d), respectively. Thus, it could be summarized that the leach rate order of matrix elements was as follows: Zr and U < Y.

As for the behavior of dissolved Zr, the precipitation fraction of Zr, $NLA_{Zr\text{-}LC}$ (Zr-LC marked by ○ in Fig. 8.5.1(d)), was very small, and the ratio of the ionic and colloidal fraction of Zr, $NLA_{Zr\text{-}LA}$ (Zr-LA by △ in Fig. 8.5.1(d)), and the ionic fraction of Zr, $NLA_{Zr\text{-}LB}$ (Zr-LB by + in Fig. 8.5.1(d)), were roughly 5 : 4. From these facts it can be concluded that 80 % of leached Zr existed as ion species and the rest Zr formed colloidal species in the leachate. On the other hand, the dissolved U showed a quite different behavior from that of Zr. The ionic and colloidal fraction, $NLA_{U\text{-}LA}$ (U-LA by △ in Fig. 8.5.1(f)), and the ionic fraction, $NLA_{U\text{-}LB}$ (U-LB by + in Fig. 8.5.1(f)), were negligible, and the precipitation fraction, $NLA_{U\text{-}LC}$ (U-LC by ○ in Fig. 8.5.1(f)), was almost the same as the normalized total leaching amount of U, NLA_U (U-LA+LC by □ in Fig. 8.5.1(f)), and this phenomenon became distinct with increasing leaching time. This means that dissolved U gradually formed precipitates on the vessel and the sample holder as leaching periods increased.

Figures 8.5.1 (g) and (h) show the normalized leach rate of Al (NL_{Al}) of 4 irradiated ROX fuels and leach amounts of Al for the CH fuel. The NL_{Al} gradually decreased with increasing leaching time, similar to the other matrix elements. The normalized leach amount of Al, NLA_{Al}, was almost constant, independent of leaching periods as well as fuel types.

These findings clearly showed the evidence that leaching behavior of SPI and COR resembled each other in irradiated ROX fuels.

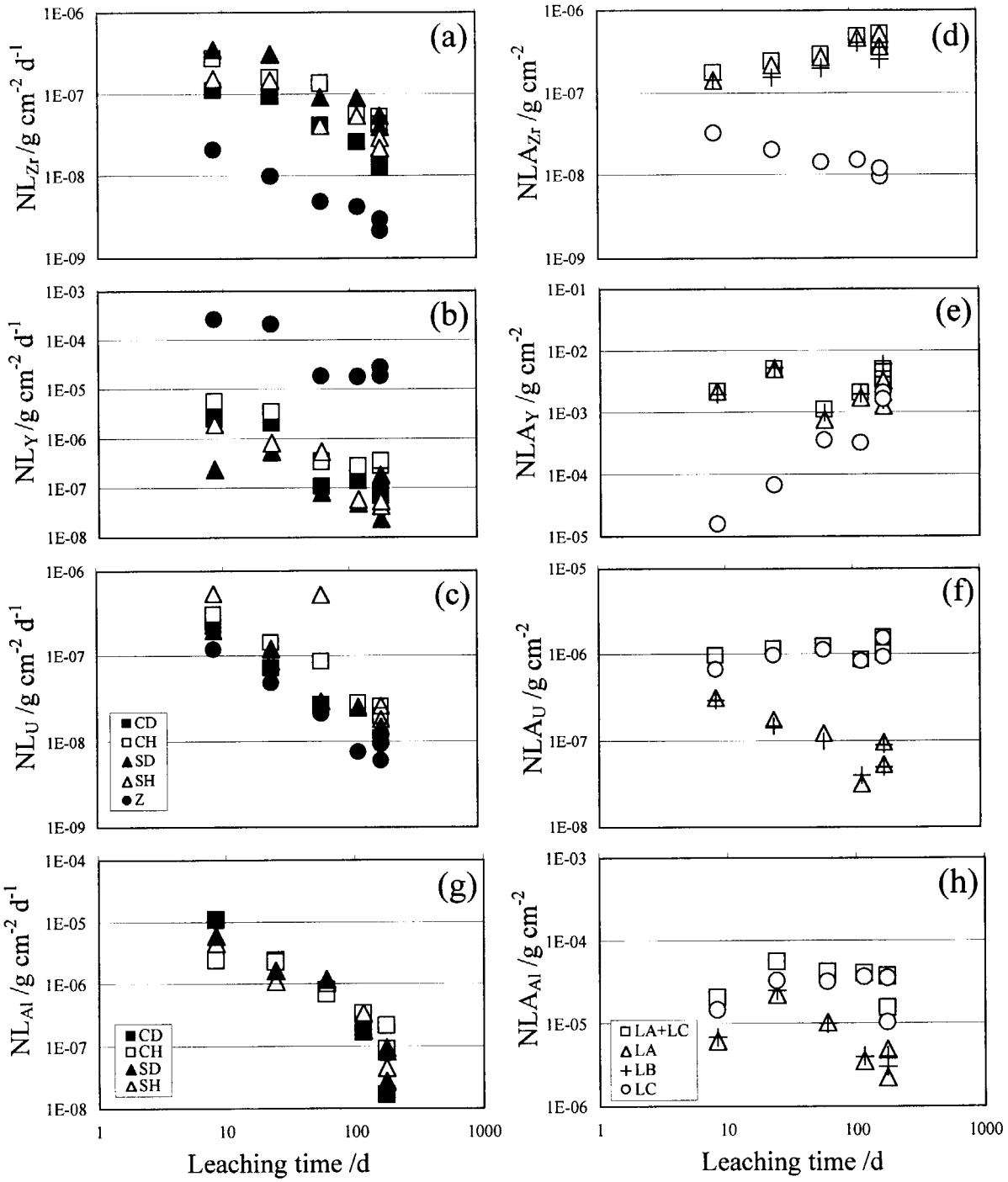

Fig.8.5.1 Normalized leach rates (*NL*, in g cm^{-2} d^{-1}) and normalized leach amounts (*NLA*, in g cm^{-2}) of Zr, Y and U for the Z fuel and normalized leach rates and normalized leach amounts of Al for the CH fuel.
(a): NL_{Zr} (b): NL_Y (c): NL_U (d): NLA_{Zr} (e): NLA_Y (f): NLA_U (g): NL_{Al} (h): NLA_{Al}

8.6 Neptunium Solubility and Oxidation State in Yttria Stabilized Zirconia

N. Nitani, K. Kuramoto, M. Nakada and T. Yamashita
(*E-mail:* yamasita@popsvr.tokai.jaeri.go.jp)

Actinides solubility in yttria stabilized zirconia (YSZ) and their oxidation states in the solid solution are of importance to access the stability of YSZ matrix during irradiation and after disposal in a deep geological formation. Neptunium is expected to be tetra-valent in the YSZ solid solution. However, if a part of Np exists as penta-valent state, leaching behavior of Np may be extremely complicated. In the present study, Np solubility in YSZ was investigated by X-ray diffraction technique and Np oxidation state was clarified by Mössbauer spectroscopy. Solid solution of YSZ and CeO_{2-x} was also investigated to develop a model which enables one to predict lattice parameter variation of YSZ solid solutions based on ionic radii of cations.

Solid solutions of YSZ-NpO_2 and YSZ-CeO_{2-x} were prepared by heating appropriate mixtures of NpO_2 and YSZ or CeO_2 and YSZ powders at 1773 K for 80 hrs under a stream of either air or 3%H_2/Ar. YSZ composition was $YO_{1.5}$:ZrO_2=14.3:85.7. Products, YSZ solid solutions, were pulverized in an agate mortar and subjected to X-ray diffraction analyses at room temperature. For Mössbauer measurements, the powder samples were triply sealed in graphite, inner aluminum and outer aluminum sample holders. Mössbauer spectrum was taken at 10 and 50 K.

Lattice parameters of the NpO_2-YSZ and CeO_{2-x}-YSZ solid solutions are plotted in Fig. 8.6.1 against the Np or Ce contents. Triangles show the lattice parameter of NpO_2-YSZ samples prepared in air and 3%H_2/Ar. The difference in the lattice parameters between samples heated in air and H_2/Ar was very slight: almost within the experimental error of $\pm$ 0.00005 nm. Lattice parameters of the solid solutions increase in proportion to the Np content. The observed phase had a fluorite structure without any indication of a pyrochlore structure or a second phase. Circles show the lattice parameters of the CeO_2-YSZ samples prepared in air, and squares represent Ce_2O_3-YSZ samples prepared in H_2/Ar. Above 12mol% Ce, the samples heated in H_2/Ar are two-phase mixtures of the fluorite and pyrochlore phases, and the lattice parameter of the fluorite phase did not change. The thin solid and dotted lines indicate the expected lattice parameters based on the mean cation ionic radii (MCIR) model for a

CeO_2-YSZ solid solution and a Ce_2O_3-YSZ solid solution, respectively. The lines predict well the observed lattice parameter of the Ce-doped YSZ solid solutions. The lattice parameter of the Np-doped YSZ solid solutions increases with the Np content, and its variation seems to be close to the MCIR model's calculated line for the tetravalent dopant.

Wide range Mössbauer absorption spectra, which covered the Doppler velocity from 150 to -170 mm/s, were taken in order to investigate the oxidation state of Np in the NpO_2-YSZ solid solutions. Figure 8.6.2 shows the Mössbauer absorption spectrum measured at 10 K for the $(Zr,Y)_{0.8}Np_{0.2}O_{2-x}$ solid solution prepared in a reducing atmosphere. A large absorption at isomer shift (IS) of -7.9 mm/s and a small absorption at IS = -36.9 mm/s are assigned to Np^{4+} and Np^{5+}, respectively, based on the well-known correlation between the isomer shift of ^{237}Np and the oxidation state of Np[1]. Appearance of penta-valent Np in YSZ solid solution was first observed in the present investigation by means of Mössbauer spectroscopy. An absorption peak due to Np^{3+} should appear around IS=35 mm/s from the correlation but was not observed, indicating the absence of Np^{3+} in the solid solution.

The fraction of Np^{4+} and Np^{5+} can be determined from their intensities. The fraction of Np^{5+} in $(Zr,Y)_{0.8}Np_{0.2}O_{2-x}$ and $(Zr,Y)_{0.6}Np_{0.4}O_{2-x}$ samples are 13 and 10% of total Np, which corresponds to 2.3 and 4.0% of total cations, respectively. There are two possible ways of distribution of Np^{5+} over cation sites of the fluorite lattice; one is a statistical distribution and the other is the preferential pairing of Np^{5+}-Y^{3+} as suggested by Li et al.[2] and Conradson et al.[3]. In the case where the Np^{5+} distribution is statistical, the Np^{5+} amount is proportional to the product of total Np fraction and Y^{3+} fraction. On the other hand, the Np^{5+}-Y^{3+} pairing is favorable, the Np^{5+} amount is proportional to the Y^{3+} fraction alone. The amount of Np^{5+} will decrease with increasing Np content because Y^{3+} content decrease with increasing Np content. In the present $(Zr,Y,Np)O_{2-x}$ solid solutions, the amounts of Np^{5+} are found to be nearly equal to the product of Np fraction and Y fraction. This fact supports that Np^{5+} as well as Np^{4+} and Y^{3+} distribute statistically on the available cation sites.

Taking these findings into account, evaluation of lattice parameter change of the $(Zr,Y,Np)O_{2-x}$ solid solutions was carried out based on the MCIR model. Because Np^{5+} makes always a pair with Y^{3+}, the effective oxidation state of the Np^{5+}-Y^{3+} pair is four, and the pair has practically no effect on the oxygen non-stoichiometry. Oxygen vacancies will be introduced to the solid solution in the quantity of a half of difference between Y^{3+} and Np^{5+} fractions. The expected lattice parameters are shown as a thick solid line in Fig. 8.6.1. The

calculated values represent the observed values fairly well although the observed value deviates slightly from the line at low Np content region.

References

1) M. Saeki, M. Nakada, T. Nakamoto, T. Yamashita, N.M. Masaki and N.N. Krot: J. Radioanal. Nucl. Chem., 239, 221 (1999).

2) P. Li, I.W. Chen and J.E. Penner-Hahn: J. Am. Ceram. Soc., 77, 1289 (1994).

3) S.D. Conradson, C.A. Degueldre, F.J. Espinosa-Faller, S.R. Foltyn, K.E. Sickafus, J.A. Valdez and P.M. Villella: Prog. Nucl. Energy, 38, 221 (2001).

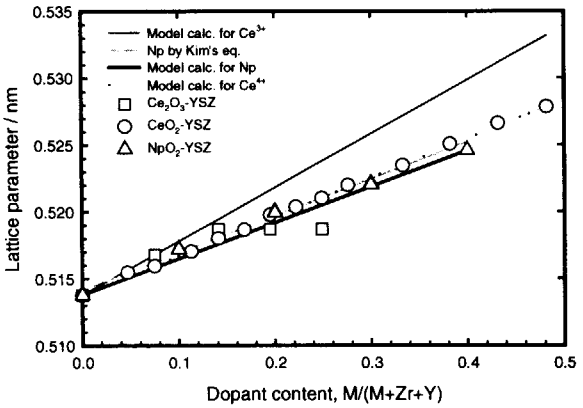

Fig. 8.6.1 Lattice parameters of Np and Ce-YSZ solid solutions as a function of Np or Ce contents. △: Np; ○: Ce in air; □: Ce in 3%H_2/Ar. Expected lattice parameters based on the MCIR model are shown as lines.

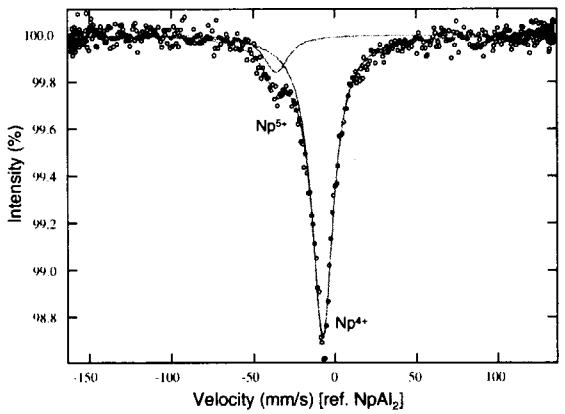

Fig. 8.6.2 ^{237}Np Mössbauer absorption spectrum at 10 K for $(Zr,Y)_{0.8}Np_{0.2}O_{2-x}$ solid solution.

9. Nuclear Data

Both projects for JENDL-3.3 General Purpose File and JENDL Special Purpose Files have progressed significantly with the cooperation of the Japanese Nuclear Data Committee during this period.

The latest version of JENDL-3.3 (9.1) was released to the public on the 10th of May 2002 through JAERI Nuclear Data Center home page (URL http: //wwwndc.tokai.jaeri.go.jp/jendl/jendl.html). After 8 years' endurable evaluation and validation works, a total of 337 nuclides in energy range from 10^{-5} eV to 20 MeV are available in the library. A CD-ROM and brochures (plot graphs and comments of all nuclides) were also published and made available upon request.

As to the Special Purpose File, JENDL (α,n) Reaction Data File (9.2) was newly released. This file was requested from criticality safety group and/or shielding group for spent fuel storage or transport applications. Neutron production by alpha particles coming from alpha-decay of minor actinides is the main issues. The data are also available in our home page.

For the Intermediate Energy File (9.3), which is important for the accelerator-driven system in the neutron science research, many efforts have been made to develop JENDL High Energy File, JENDL PKA/KERMA File and JENDL Photonuclear Data File.

Mass chain evaluation has been continued within the framework of the international cooperation for the ENSDF File. The evaluation of mass chain A=120 and 126 (9.4) was made in the FY2002 out of 12 Japanese responsible mass chains.

FP Decay Data File project was completed by releasing JENDL FP Decay Data File 2000 in FY2000. Photon and Decay Data Libraries for ORIGEN2 (9.5) have been compiled from this library. Significant improvements were attained for FP gamma-ray spectrum for typical major actinides.

Re-evaluation of ^{129}I and ^{143}Nd (9.6), which are very important nuclides for FP, has been made in connection with JENDL-3.3 evaluations due to the availability of recent measured data in Japan.

Evaluation of ^{210m}Bi/^{210g}Bi branching ratio (9.7) has been performed in the fast reactor energy range. Recently many attentions are given to the Pb-Bi coolant FBRs. In the design of such reactors, the branching ratio can affect reactor performances and reactor safety significantly. Evaluation was made based on new measurements and calculations.

A new code of Coupled-channel Optical Model calculation (9.8) necessary for actinide nuclides having deformed shape has been being developed.

A systematics of fission product mass yields (9.9) has been developed.

9.1 Release of Japanese Evaluated Nuclear Data Library Version 3 Revision-3: JENDL-3.3

K. Shibata and Japanese Nuclear Data Committee
(*E-mail:* shibata@ndc.tokai.jaeri.go.jp)

The latest version of Japanese Evaluated Nuclear Data Library, JENDL-3.3[1], was officially released in May 2002. The library provides the neutron-induced reaction data for 337 nuclides in the energy region from 10^{-5} eV to 20 MeV.

We kept a policy of isotopic evaluations without producing elemental data files. This was done to avoid the inconsistency between the elemental and isotopic evaluations that was seen in JENDL-3.2[2]. There are only two elemental data files in JENDL-3.3: carbon and vanadium. Experimental data on natural elements were however considered to evaluate isotopic data.

Cross sections for threshold reactions on many nuclei were modified by using statistical-model calculations. The cross sections for the ^{60}Ni(n,p) reaction are illustrated in Fig. 9.1.1. In this reaction, the JENDL-3.2 evaluation is obviously based on the old measurements, whereas the present evaluation reproduces recent measurements.

The overestimation of k_{eff} is the biggest problem with JENDL-3.2 when the library is applied to thermal fission reactors. In order to solve the problem, we re-evaluated the resonance parameters of ^{235}U and the prompt fission neutron spectra from ^{235}U. The resonance parameters were replaced with those obtained by Leal et al.[3] The fission neutron spectra were re-calculated by Ohsawa[4] with a multi-modal fission analysis.

Fission cross sections above the resonance region are also important for reactor calculations. We adopted a simultaneous evaluation method[5] to obtain the fission cross sections of major actinides above 30 keV. The experimental data on ^{233}U were included in the present evaluation, while the ^{233}U data were evaluated separately from the simultaneous evaluation for JENDL-3.2. The fission cross sections of ^{233}U obtained for JENDL-3.3 are systematically lower than those for JENDL-3.2 in the energy range above several hundred keV. This fact led to an improvement of criticalities for fast neutron cores containing ^{233}U fuels.

In the JENDL-3.2 evaluation, the capture cross sections in the MeV region were often ignored, since the cross sections became extremely small when the Hauser-Feshbach statistical model was used to calculate them. It is known that the direct/semi-direct (DSD) capture model should be applied to calculate capture cross sections in this energy region. In the present work, we took account of the DSD contributions.

Angle-dependent neutron emission spectra were mainly taken from JENDL Fusion File 99[6]. The number of nuclides which contain gamma-ray production data was increased from 66 to 114.

The numerical data of JENDL-3.3 are available on the homepage of the Nuclear Data Center (URL http://wwwndc.tokai.jaeri.go.jp/jendl/jendl.html). The books[7,8] of figures and comments and CD-ROMs are also available on request.

References

1) K. Shibata et al.: "Japanese Evaluated Nuclear Data Library Version 3 Revision-3: JENDL-3.3," J. Nucl. Sci. Technol., **39**, 1125 (2002).
2) T. Nakagawa et al.: J. Nucl. Sci. Technol., **32**, 1259 (1995).
3) L.C. Leal et al.: Nucl. Sci. Eng., **131**, 230 (1999).
4) T. Ohsawa, JAERI-Conf 2001-006, p.157 (2001).
5) T. Kawano et al.: J. Nucl. Sci. Technol., **37**, 327 (2000).
6) S. Chiba et al.: J. Nucl. Sci. Technol., **39**, 187 (2002).
7) T. Nakagawa et al. (Eds.): "Curves and Tables of Neutron Cross Sections in JENDL-3.3," JAERI-Data/Code 2002-020 (2002).
8) K. Shibata (Ed.): "Descriptive Data of JENDL-3.3," JAERI-Data/Code 2002-026 (2002).

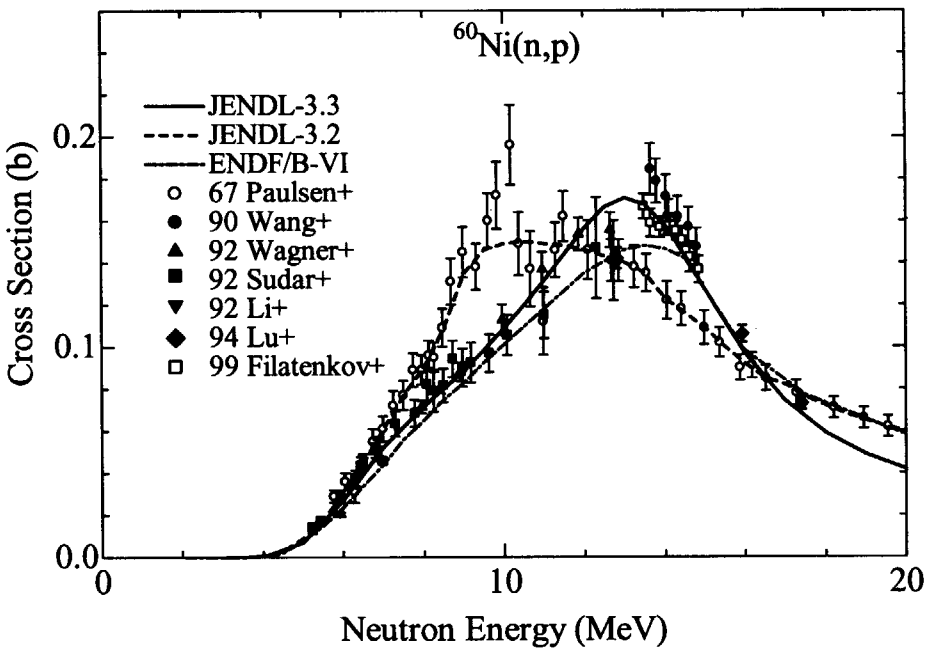

Fig. 9.1.1 ^{60}Ni(n,p) reaction cross section

9.2 JENDL (α,n) Reaction Data File

H. Matsunobu[*1], T. Murata[*2] and K. Shibata
(*E-mail:* shibata@ndc.tokai.jaeri.go.jp)

(α,n) reactions play an important role in the fields of radiation shielding and criticality safety related to storage, transport, and handling of spent nuclear fuels. An evaluated (α,n) reaction data file was required to estimate neutron production. The present work was undertaken by the Charged-particle Nuclear Data Working Group of the Japanese Nuclear Data Committee. Neutron production cross sections and emitted neutron spectra were evaluated for the α-particle induced reactions on 13 nuclei: ^{6}Li, ^{7}Li, ^{9}Be, ^{10}B, ^{11}B, ^{12}C, ^{13}C, ^{14}N, ^{15}N, ^{17}O, ^{18}O, ^{19}F, and ^{23}Na, below 15 MeV.

Resonance analyses were performed for light nuclei, since cross sections exhibit resonance structure. For some light nuclei, the (α,n_0) cross section was obtained from experimental data on (n,α_0) reactions by using the detailed balance. In the high energy region for light nuclei where no measurements are available, the statistical-model code mEXIFON[1] was used to evaluate cross sections and spectra. Figure 9.2.1 shows total neutron production cross sections of ^{18}O together with the measurements of Bair-Willard[2] and Hansen et al.[3] In this figure, the results of Bair-Willard were multiplied by a factor 1.35, which was suggested by Bair et al.[4]

As for ^{19}F and ^{23}Na, the statistical-model code EGNASH[5] was used to evaluate all cross sections and spectra. Concerning input to EGNASH, the default values were employed except level scheme data. The evaluated neutron production cross section of ^{23}Na is illustrated in Fig. 9.2.2 together with the experimental data of Norman et al.[6] It is found from the figure that the evaluation reproduces the measurements.

The evaluated data were compiled in the ENDF-6 format[7], and they are available on the homepage of the JAERI Nuclear Data Center with the following URL: http://wwwndc.tokai.jaeri.go.jp/jendl/jendl.html.

References

1) T. Murata: JAERI-Conf 97-005, p.286 (1997).
2) J.K. Bair and H.B. Willard: Phys. Rev., **128**, 299 (1962).
3) L.F. Hansen et al.: Nucl. Phys., **A198**, 25 (1967).

[*1] Data Engineering, Inc.
[*2] AITEL Corp.

4) J.K. Bair et al.: Nucl. Sci. Eng., **71**, 18 (1979).
5) N. Yamamuro: JAERI-M 90-006 (1990).
6) E.B. Norman et al.: Nucl. Phys., **A390**, 561 (1982).
7) Cross Section Evaluation Working Group: BNL-NCS-4495-01/04-Rev. (2001).

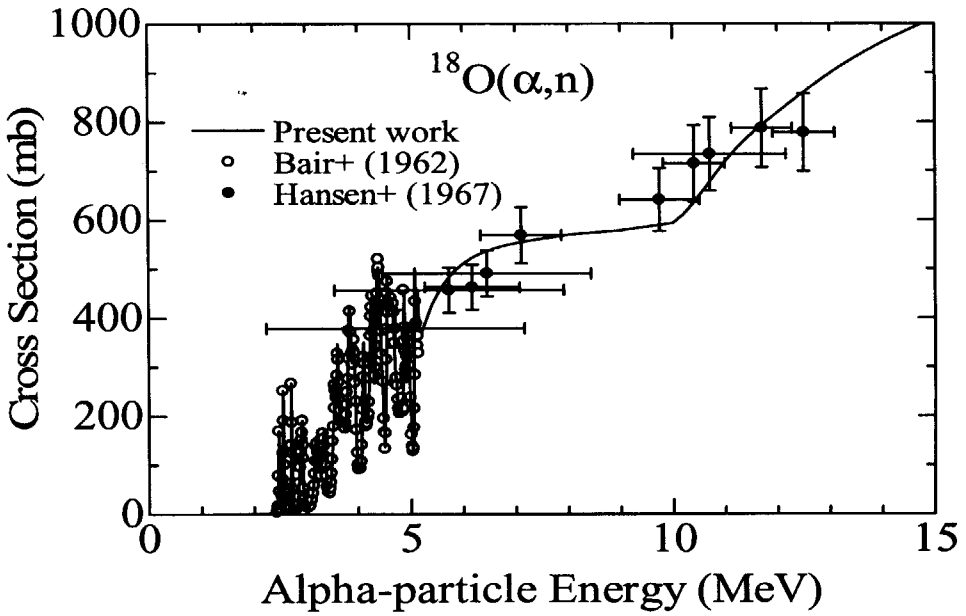

Fig. 9.2.1 (α,n) cross section of ^{18}O

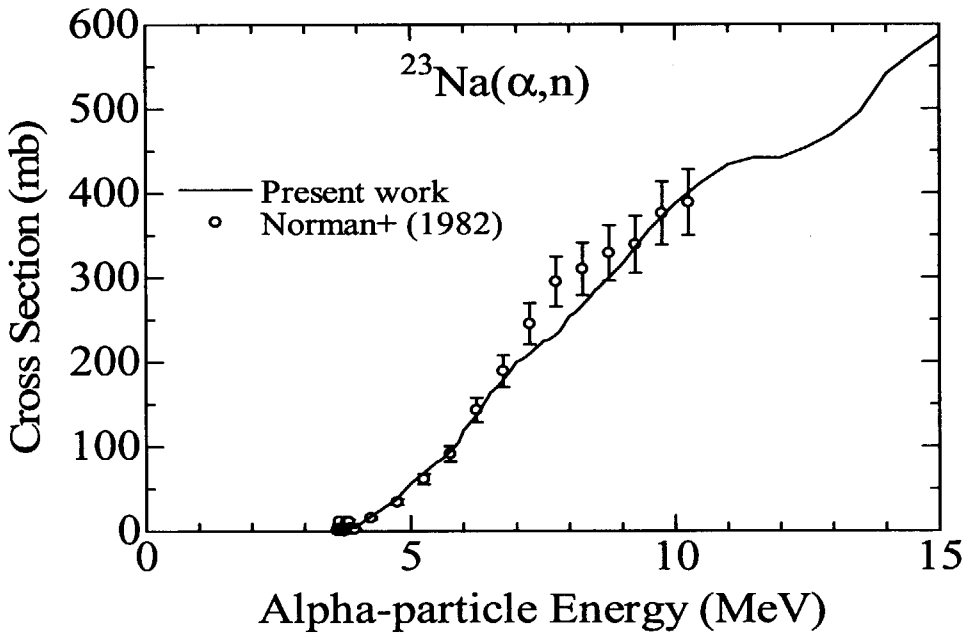

Fig. 9.2.2 (α,n) cross section of ^{23}Na

9.3 Nuclear Data Evaluation and Compilation for JENDL Intermediate Energy Files in 2002

T. Fukahori and Japanese Nuclear Data Committee (High Energy Nuclear Data Evaluation WG)
(*E-mail*: fukahori@ndc.tokai.jaeri.go.jp)

The JAERI Nuclear Data Center has been continuing evaluation work in cooperation with Japanese Nuclear Data Committee (JNDC) to produce intermediate energy files, which are JENDL High Energy File, JENDL PKA/KERMA File and JENDL Photonuclear Data File.

The JENDL High Energy File includes nuclear data for proton- and neutron-induced reactions. Below 20 MeV, the data of JENDL-3.3 are adopted. The neutron file for IFMIF[1] in the energy range up to 50 MeV has been merged with files below 20 MeV. The evaluation work for the neutron and proton files with energy range up to 3 GeV is performed for the second-priority 42 nuclei by mainly using the "quick-GNASH system"[2], JQMD code[3] and NMTC/JAM code[4]. The target isotopes included in the JENDL High Energy File are summarized in Table 9.3.1 as well as priorities and status. Until year 2002, evaluation of 73 nuclides for proton- and neutron-induced reactions has been done, including important actinide nuclides of ^{235}U and ^{238}U. The evaluated data were compiled in ENDF-6 format. Those data were checked by "differential review", whose procedure has been decided by High Energy Nuclear Data Evaluation WG. The differential review was performed by a review kit, consisting of format check by DOUBLEP code prepared by JAERI Nuclear Data Center and CHECKR, FIZCON and PSYCHE codes distributed by National Nuclear Data Center at Brookhaven National Laboratory, and plots of cross sections and double differential cross sections comparing with experimental data in EXFOR if available. For this purpose, a code system "jpts" has been developed to create a review kit automatically. Compiled data after passing the review process will be checked by some benchmark calculations. After these procedures, the JENDL High Energy File is planned to be partly released in 2003 year.

The JENDL Photonuclear Data File is being developed for gamma-ray induced reaction data up to 140 MeV. The photon absorption cross section is evaluated with the

giant dipole resonance model and quasi-deuteron model, and the decaying processes are estimated with the statistical model with preequilibrium correction by using MCPHOTO[5] and ALICE-F[6] codes. Evaluated results for 26 target nuclides were compared with the other photonuclear data files evaluated at Los Alamos, Beijing, Moscow and Obninsk as well as experimental data. The evaluation work has been finished for all the 69 target nuclides listed in Table 9.3.2. The evaluated results were compiled in ENDF-6 format and that preliminary review was performed. After same procedure as the case of JENDL High Energy File, the JENDL Photonuclear Data File will be released as soon as possible.

The JENDL PKA/KERMA File is generated to supply primary knock-on atom (PKA) spectra, damage energy spectra, DPA (displacement per atom) cross sections and kerma factors by neutron-induced reactions in the energy region up to 50 MeV. A processing code system, ESPERANT[7] was developed to calculate above quantities from evaluated nuclear data file by using effective single particle emission approximation (ESPEA). For light mass nuclei, SCINFUL/DDX code, which considers break-up reactions with PKA spectra, is used as well as EXIFON code which can calculate with correction of preequilibrium process.

References

1) K. Noda: Proc. of 1994 Symposium on Nuclear Data, Tokai, Japan, Nov. 17-18, 1994, JAERI-Conf 95-008, p.112 (1995).
2) M.B. Chadwick and P.G. Young: Phys. Rev., **C47**, 2255 (1993).
3) K. Niita and S. Chiba: "JQMD: Quantum Molecular Dynamics and Statistical Decay Model Code", private communication.
4) K. Niita: "NMTC/JAM Code", private communication.
5) N. Kishida and H. Kadotani: private communication.
6) T. Fukahori: Proc. Specialists' Meeting on High Energy Nuclear Data, Tokai, Ibaraki, Oct. 3-4, 1991, JAERI-M 92-039, p.114 (1992).
7) T. Fukahori, et al.: Proc. of the Third Specialists' Meeting on Nuclear Data for Fission Reactors, Tokai, Japan, Nov. 29-30, 1995, JAERI-Conf 96-005, p.130 (1996).

Table 9.3.1 Isotopes included in neutron and proton file up to 3 GeV with their priorities and status

Priorities	Under Compilation or Review	Under Evaluation	Planning
1st priority (40 nuclides)	H-1, C-12, Al-27, Cr-50,52-54, Fe-54,56-58, Ni-58,60-62,64, W-180,182-184,186, Hg-196,198-202,204, U-235,238	N-14, O-16, Cu-63,65, Pb-204,206-208, Bi-209	Au-197
2nd priority (45 nuclides)	Mg-24-26, Si-28-30, K-39,41, Ca-40,42-44,46,48, Ti-46-50, V-51, Mn-55, Co-59, Zr-90-92,94,96, Nb-93, Pu-238-242	H-2	Be-9, B-10,11, Mo-92,94-98,100, Ta-181
3rd priority (37 nuclides)	C-13, Zn-64,66-68,70, Np-237, Am-241,242,242m	F-19, Na-23, Cl-35,37, Ar-35,38,40, Ga-69,71, Ge-70,72-74,76, As-75, Th-232, U-233,234,236, Am-243,	Li-6,7, Y-89, Cm-243-246
4th priority (2 nuclides)			N-15, O-18
total	73	30	21

Table 9.3.2 Isotopes included in JENDL Photonuclear Data File

Under Review	Under Compilation
H-2, Li-6,7, Be-9, B-10,11, C-12, N-14, O-16, F-19, Na-23, Mg-24-26, Al-27, Si-28-30, P-31, Ca-48, Ti-46, V-51, Cr-52, Mn-55, Fe-54,56, Co-59, Cu-63,65, Nb-93, Mo-92,94,96,98,100, Cs-133, Ta-181, W-180,182,184,186, Au-197, Pb-206-208, U-235,238, Np-237 (48 nuclides)	He-3, Ca-40, Ni-58,60, Zn-64, Zr-90, Gd-152,154-158,160, Hg-196,198-202,204, Bi-209 (21 nuclides)

9.4 Evaluation and Compilation of Nuclear Structure and Decay Data in 2002

J. Katakura and ENSDF Group*
(*E-mail*: katakura@ndc.tokai.jaeri.go.jp)

The international network on nuclear structure and decay data evaluation aims at complete and continuous nuclear structure and decay data evaluation of all mass chains. The evaluated data are compiled as ENSDF (Evaluated Nuclear Structure Data File) file. The data file is maintained and distributed by National Nuclear Data Center, Brookhaven National Laboratory (BNL), U.S.A. As a member of the network, Japanese group, whose data evaluation center is Nuclear Data Center, Japan Atomic Energy Research Institute, has responsibility for evaluating 12 mass chains with A=118-129.

In the fiscal year of 2002 (from April 2002 to March 2003), the evaluations of A=120 and A=126 mass chains were published in Nuclear Data Sheets [1, 2]. The evaluation includes all experimental data available after the last evaluations performed in 1987 for A=120 and 1993 for A=126. The published data sets of A=120 and A=126 are listed in tables 9.4.1 and 9.4.2. These data sets have been evaluated based on the all available measured data relating to A=120 and A=126 masses. Each data set excepting "Adopted Levels, Gammas" or "Adopted Levels" data sets is the evaluated data set from the same kind of measurements categorized in the name of the data set. The "Adopted Levels, Gammas" or "Adopted Levels" data sets are compiled from the each data set in the same nuclide.

The new data from the last evaluation of other mass chains to which Japanese group has the responsibility are reviewed and being prepared for update of the last mass chain evaluation.

References

1) K. Kitao, Y. Tendow and A. Hashizume: Nucl. Data Sheets, **96**, 241 (2002)

2) J. Katakura and K. Kitao: Nucl. Data Sheets, **97**, 765 (2002)

*Members are H. Iimura, M. Oshima, S. Ohya, J. Katakura, M. Kanbe, K. Kitao and Y. Tendow

Table 9.4.1 Evaluated data sets of A=120

Nuclide	Data Type
^{120}Ru	Adopted Levels
^{120}Pd	Adopted Levels
	^{128}Ag β^- Decay
^{120}Ag	Adopted Levels, Gammas
	^{120}Pd β^- Decay
	^{120}Ag IT Decay (0.32 s)
^{120}Cd	Adopted Levels, Gammas
	^{120}Ag β^- Decay (0.32 s)
	^{120}Ag β^- Decay (1.23 s)
	^{124}Sn(d,^{6}Li)
	^{124}Sn(^{3}He,^{7}Be)
	^{173}Yb(^{24}Mg,F),^{208}Pb(^{18}O,F)
^{120}In	Adopted Levels, Gammas
	^{120}Cd β^- Decay (50.80 s)
^{120}Sn	Adopted Levels, Gammas
	^{120}In β^- Decay (3.08 s)
	^{120}In β^- Decay (46.2 s)
	^{120}In β^- Decay (47.3 s)
	^{120}Sb β^+ Decay (15.89 min)
	^{120}Sb ε Decay (5.76 d)
	^{118}Sn(t,p)
	^{119}Sn(d,p),(t,d),(pol d,p))
	^{120}Sn(γ,γ')
	^{120}Sn(e,e')
	^{120}Sn(e,e'p) IAR
	^{120}Sn(π^+,π^0),(π^-,π^0)
	^{120}Sn(n,n'γ)
	^{120}Sn(p,p'),(^{3}He,^{3}He'),(α,α')...
	^{120}Sn(p,p'γ)
	^{120}Sn(d,d')
	Coulomb Excitation
	^{121}Sb(μ^-,nγ)
	^{121}Sb(d,^{3}He),(t,α)
	^{122}Sn(p,t)
	^{122}Sn(^{16}O,^{18}O)
	^{123}Sb(p,α)

Nuclide	Data Type
^{120}Sn	^{124}Te(d,^{6}Li)
	(HI,xnγ)
	^{128}Te(^{3}He,t) IAS
^{120}Sb	Adopted Levels, Gammas
	^{116}Cd(^{7}Li,3nγ)
	^{119}Sn(p,n) IAR
	^{120}Sn(p,n): Bound States
	^{120}Sn(p,np) IAR
	^{120}Sn(p,nγ)
	^{120}Sn(^{3}He,t) IAR
	^{121}Sb(p,d),(d,t)
^{120}Te	Adopted Levels, Gammas
	^{120}I ε Decay (53 min)
	^{120}I ε Decay (81.6 min)
	^{117}Sn(α,nγ),^{110}Pd(^{13}C,3nγ)
	^{118}Sn(^{3}He,n)
	^{118}Sn(α,2nγ)
	^{119}Sn(α,3nγ)
	^{120}Sn(^{3}He,3nγ)
	Coulomb Excitation
	^{121}Sb(p,2nγ)
	^{122}Te(p,t)
^{120}I	Adopted Levels, Gammas
	^{120}Xe ε Decay
	(HI,xnγ)
^{120}Xe	Adopted Levels, Gammas
	^{120}Cs ε Decay (64 s+57 s)
	(HI,xnγ)
^{120}Cs	Adopted Levels, Gammas
	^{120}Ba ε Decay
	(HI,xnγ)
^{120}Ba	Adopted Levels, Gammas
	^{120}Ba εp Decay
	(HI,xnγ)
^{120}La	Adopted Levels

Table 9.4.2 Evaluated data sets of A=126

Nuclide	Data Type
^{126}Ag	Adopted Levels
^{126}Cd	Adopted Levels, Gammas ^{126}Ag β^- Decay
^{126}In	Adopted Levels, Gammas ^{126}Cd β^- Decay
^{126}Sn	Adopted Levels, Gammas ^{126}In β^- Decay (1.64 s) ^{126}In β^- Decay (1.53 s) ^{127}In β^-n Decay (1.09 s) ^{127}In β^-n Decay (3.67 s) ^{124}Sn(t,p) ^{124}Sn(^{14}C,^{12}C) ^{130}Te(d,^{6}Li) ^{124}Sn(^{136}Xe,Xγ),(^{238}U,Xγ) ^{124}Sn(^{18}O,^{16}O)
^{126}Sb	Adopted Levels, Gammas ^{126}Sn β^- Decay ^{126}Sb IT Decay (19.15 min)
^{126}Te	Adopted Levels, Gammas ^{126}Sb β^- Decay (12.35 d) ^{126}Sb β^- Decay (19.15 min) ^{126}I ε Decay ^{124}Sn(^{3}He,n) ^{124}Sn(α,2nγ) ^{125}Te(n,γ) ^{125}Te(d,p) ^{126}Te(γ,γ') ^{126}Te(n,n'γ) ^{126}Te(p,p') ^{126}Te(d,d') Coulomb Excitation ^{127}I(μ^-,nγ) ^{127}I(d,^{3}He)
^{126}Te	^{128}Te(p,t) ^{130}Te(^{64}Ni,Xγ) ^{232}Th(^{37}Cl,X)
^{126}I	Adopted Levels, Gammas ^{126}Te(p,nγ) ^{127}I(γ,n) ^{127}I(n,2nγ)
^{126}Xe	Adopted Levels, Gammas ^{126}I β^- Decay ^{126}Cs ε Decay ^{116}Cd(^{13}C,3nγ) ^{123}Te(α,nγ) ^{124}Te(^{3}He,n) ^{124}Te(α,2nγ) ^{126}Te(^{3}He,3nγ),^{126}Te(α,4nγ) Coulomb Excitation ^{127}I(p,2nγ)
^{126}Cs	Adopted Levels, Gammas ^{126}Ba ε Decay (HI,xnγ)
^{126}Ba	Adopted Levels, Gammas ^{126}La ε Decay (54 s+50 s) (HI,xnγ)
^{126}La	Adopted Levels, Gammas ^{126}Ce ε Decay (HI,xnγ)
^{126}Ce	Adopted Levels, Gammas ^{126}Pr ε Decay (HI,xnγ)
^{126}Pr	Adopted Levels, Gammas ^{92}Mo(^{40}Ca,αpnγ)
^{126}Nd	Adopted Levels

9.5 Compilation of Photon and Decay Data Libraries for ORIGEN2 Code

J. Katakura and H. Yanagisawa
(*E-mail*: katakura@ndc.tokai.jaeri.go.jp)

Photon and decay data libraries for ORIGEN2 code [1] have been developed in the basis of JENDL FP Decay Data File 2000 (JENDL/FPD-00) [2]. There are decay data of 1087 unstable nuclides in the JENDL/FPD-00 file as shown in Table 9.5.1. The original libraries of the ORIGEN2 code contains the decay data of 858 FP nuclides. In the development of the libraries, the number of FP nuclides is not changed and the decay data of them are just replaced by those of the JENDL/FPD-00 file.

Table 9.5.1 Contents of JENDL FP Decay Data File 2000

No. of Nuclides		Data Type, Comments
1087		Unstable nuclides or states
	197	First isomeric states
	8	Second isomeric states
1087		Average gamma decay energy values
	506	Measured (From ENSDF)
	581	Theoretically estimated
1087		Average beta decay energy values
	544	Measured
	543	Theoretically estimated
1053		Gamma ray spectra
	496	Measured spectrum only
	431	Theoretically estimated spectrum only
	126	Measured + Estimated
899		Beta ray spectra
	374	Measured spectrum only
	432	Theoretically estimated spectrum only
	93	Measured + Estimated

One of the main feature of the JENDL/FPD-00 file is to provide gamma- or beta-ray spectra for all unstable nuclides. The original photon library of ORIGEN2 code contains the spectrum data for only 240 nuclides out of 857 FP nuclides. Using the

JENDL/FPD-00 file is not only to replace the original data by those of the JENDL/FPD-00 file but also to compensate the deficiency of the original file. The new photon library includes spectrum data of 695 FP nuclides. The increase of the number of FP nuclides with photon spectrum data improves the predictability of the spectrum calculation by ORIGEN2 code.

Figure 9.5.1 shows the comparison of photon spectrum between the calculation using the new library and the measured data [3].

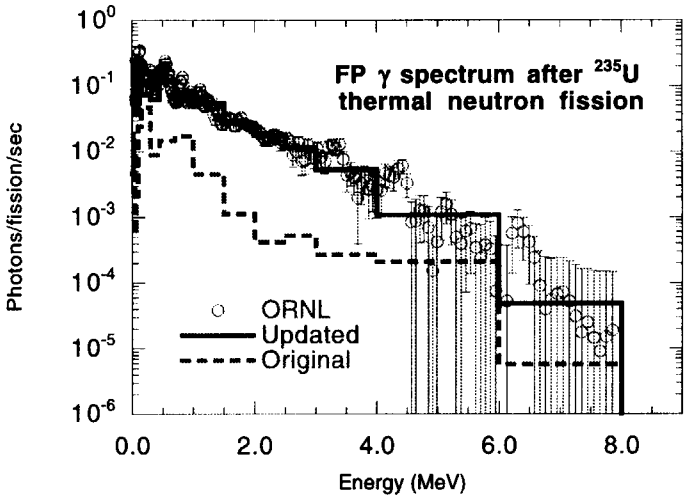

Fig. 9.5.1 Aggregate FP photon spectrum
(Measurement was performed for 1 s at 1.7 s after 1 s Irradiation)

As seen in this figure, the new library can produce the measured data rather well, although the original library shows the deficiency for whole energy range. In this way it has become possible to calculate photon spectrum at very short cooling time after fission event.

References

1) A. G. Croff: "ORIGEN2 - A Revised and Updated Version of the Oak Ridge Isotope Generation and Depletion Code," ORNL-5621 (1980).

2) J. Katakura and H. Yanagisawa: "Photon and Decay Data Libraries for ORIGEN2 Code Based on JENDL FP Decay Data File 2000," JAERI-Data/Code 2002-021 (2002).

3) J. K. Dickens et al.: "Delayed Beta- and Gamma-Ray Production Due to Thermal-Neutron Fission of ^{235}U: Spectral Distributions for Times After Fission Between 2 and 14000 sec: Tabular and Graphical Data," NUREG/CR-0162, ORNL/NUREG-39 (1978).

9.6 Evaluation of Nuclear Data for ^{129}I and ^{143}Nd

T. Nakagawa and A. Hasegawa
(*E-mail*: nakagawa@ndc.tokai.jaeri.go.jp)

I-129

The resonance parameters were revised on the basis of new analysis of Noguere et al.[1], and thermal capture cross section of 30.3±1.2 barns and resonance integral of 33.8±1.4 barns measured by Nakamura et al.[2] The cross sections in the low energy region were changed from JENDL-3.3 by this modification. The present data give the thermal capture cross section of 30.0 barns and the resonance integral of 33.9 barns. Figure 9.6.1 compares the present result with preliminary capture cross sections measured by Kobayashi et al.[3] The data of Kobayashi et al. were normalized to 27.04 b at 0.0253 eV which is smaller than the data of Nakamura et al. Therefore the present results are slightly larger than Kobayashi et al.

Above the resonance region, theoretical calculation was performed. The optical model parameters were determined so as to reproduce well the total cross section measured by Foster and Glasgow[4] for ^{127}I. Statistical model calculation was done with the statistical model code CASTHY[5] using level density parameters newly determined. The γ-ray strength function was normalized to the recent experimental data of Kobayashi et al. and Matsumoto et al.[6] which are smaller than previous experimental data. The capture cross section is shown in Fig. 9.6.2. All the other cross-section data, angular distributions and energy distributions were also revised with the present calculations by CASTHY, EGNASH and DWUCK codes.

Nd-143

Concerning the resonance parameters, only the parameters of a negative resonance were revised to improve energy dependence of cross sections in the low energy region.

Above the resonance region, the cross sections were calculated with the optical and statistical model. The optical model parameters were improved to reproduce the total cross section. As shown in Fig. 9.6.3, the capture cross section calculated with the CASTHY code reproduces well the recent experimental data of Wisshak et al.[7, 8] and Veerapaspong et al.[9] Other data were also revised with the present calculations.

References

1) G. Noguere, et al.: Proc. Int. Conference on Nucl. Sci. and Thechnol., Tsukuba, Oct. 7 – 12, 2001, Vol., 2, p.184 (2001).
2) S. Nakamura, et al.: J. Nucl. Sci. Technol., 33, 283 (1996).
3) K. Kobayashi, et al.: Proc. 11th Symposium on Reactor Dosimetry, Brussels, 19 – 23 Aug., 2002.
4) D.G. Foster Jr. and D.W. Glasgow: Phys. Rev., C3, 576 (1971).
5) S. Igarasi and T. Fukahori: JAERI 1321, "Program CASTHY –Statistical Model Calculation for Neutron Cross Sections and Gamma Ray Spectrum," (1991).
6) T. Matsumoto, et al.: private communication (2002).
7) K. Wisshak, et al.: KfK5967 (1997).
8) K. Wisshak, et al.: Phys. Rev., C57, 391 (1998).
9) Veerapaspong et al.: J. Nucl. Sci. Technol., 36, 855 (1999).

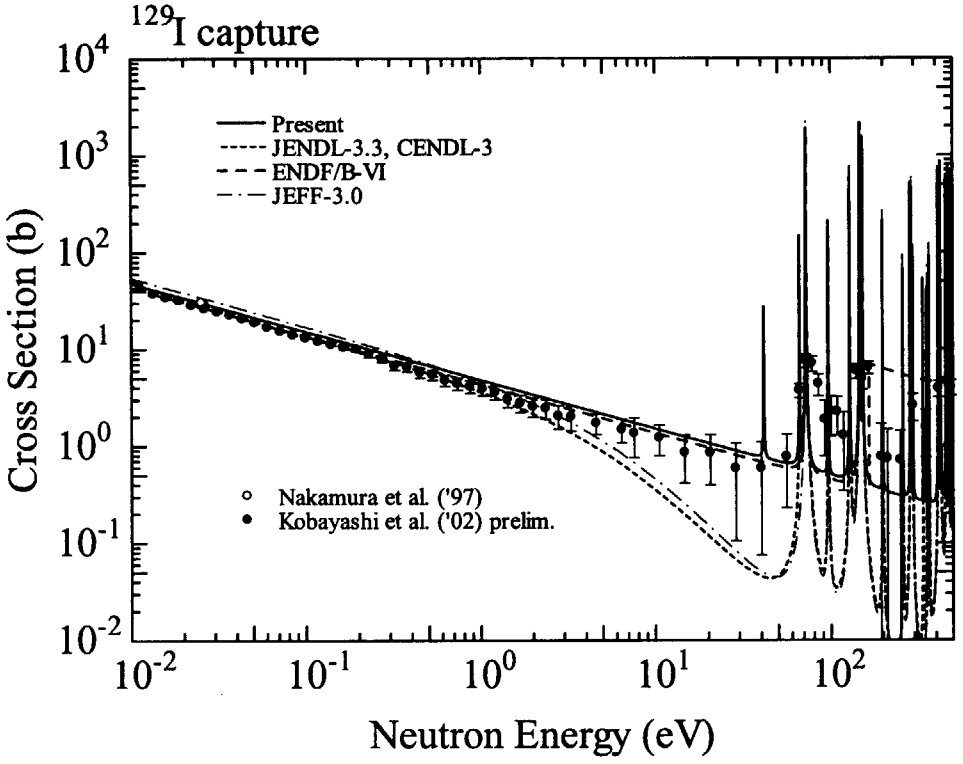

Fig. 9.6.1 ^{129}I capture cross section in the low energy region

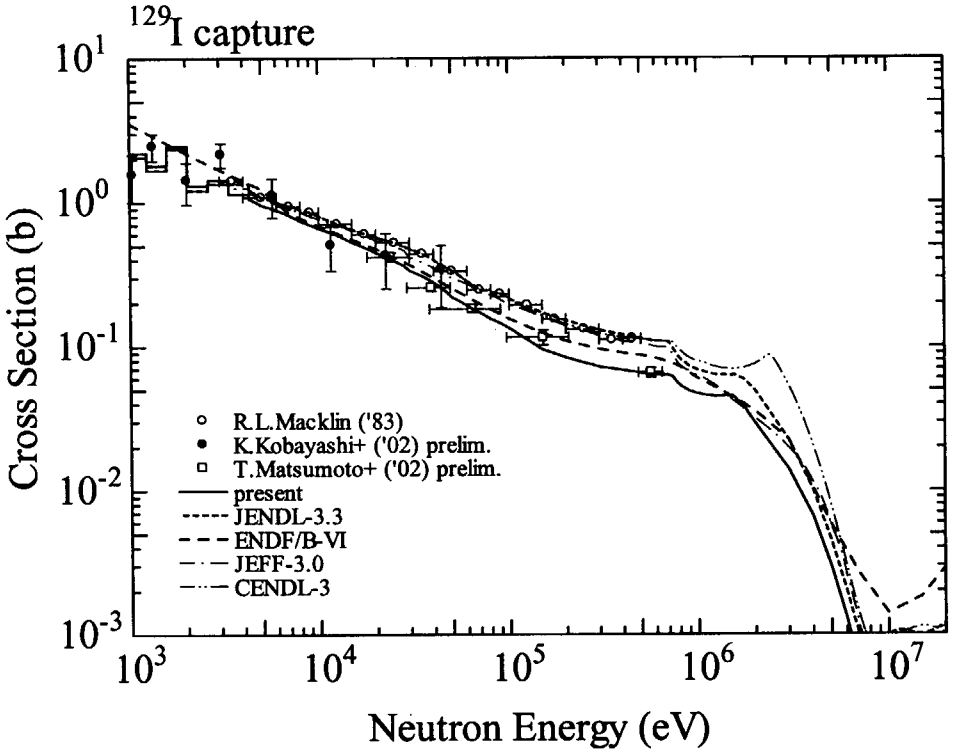

Fig. 9.6.2 ^{129}I capture cross section above 1 keV

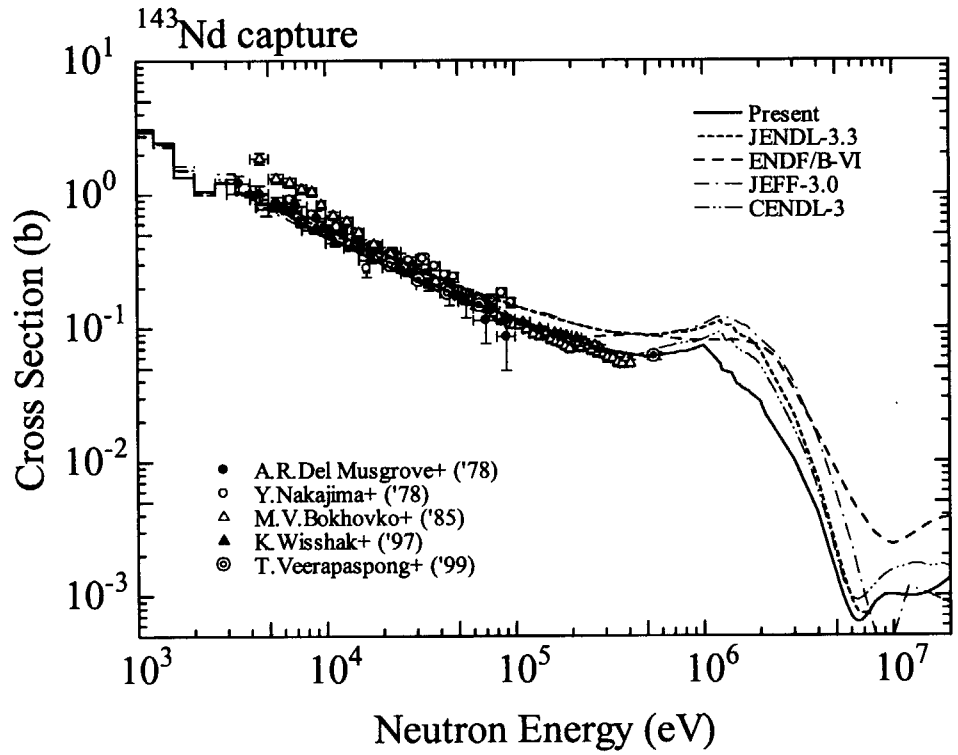

Fig. 9.6.3 ^{143}Nd capture cross section above 1 keV

9.7 Evaluation of the ^{210m}Bi/^{210g}Bi Branching Ratio of the ^{209}Bi(n, γ)^{210}Bi Cross Section in the Neutron Energy Range of 200 keV to 3 MeV

A.Ichihara and K.Shibata

(*E-mail:* ichihara@ndc.tokai.jaeri.go.jp)

The Pb-Bi alloy has been studied as a candidate of the coolant material of fast reactor. In the reactor, ^{210}Bi is produced by neutron capture. ^{210}Bi in the ground (1^-) state (^{210g}Bi) decays to ^{210}Tl by the β-ray emission with half life of $T_{1/2}$=5.013 days, where ^{210}Tl is the α decay nucleus with $T_{1/2}$=138.4days. On the other hand, ^{210}Bi in the second (9^-) excited state (^{210m}Bi) is the α decay nucleus with $T_{1/2}=3.04\times10^6$ years. Thus the difference of life times for ^{210g}Bi and ^{210m}Bi is quite large. The production of ^{210g}Bi affects the control of reactor, while the production of ^{210m}Bi affects the processing of nuclear wastes. Therefore, accurate knowledge of the ^{209}Bi(n, γ)^{210}Bi cross section and its ^{210m}Bi/^{210g}Bi production ratio is required for reactor design. Recently, these cross sections have been measured at Tokyo Institute of Technology in the keV neutron energy region. In JENDL-3.3, which was published in 2002, the ^{209}Bi(n, γ)^{210}Bi cross section was revised on the basis of the experimental data in the neutron energy (E_n) range from 200 keV to 3.0 MeV. In the present work, we have reevaluated the ^{209}Bi(n, γ)^{210}Bi cross section and the ^{210m}Bi/^{210g}Bi production ratio for 200 keV $\leq E_n \leq$ 3.0 MeV with the latest experimental data.

The ^{209}Bi(n, γ)^{210}Bi cross section has been evaluated by the Hauser-Feshbach (HF) statistical model calculation. The partial ^{210g}Bi and ^{210m}Bi production cross sections were obtained by the γ-ray cascade calculation. Numerical calculation was carried out with the program code SINCROS-II[1], which has been changed partly to evaluate cross sections. In the present work, the ^{209}Bi optical model potential (OMP) developed by Koning and Delaroche[2] has been used to obtain reaction cross section. The level densities developed by Mengoni and Nakajima[3] have been used for the continuum states of ^{209}Bi and ^{210}Bi. Their level density parameters are given by the energy dependent formula to include nuclear shell effects. Also, 11 discrete levels were considered for both ^{209}Bi and ^{210}Bi. The position and width of the giant dipole resonance for the ^{209}Bi(n, γ)^{210}Bi reaction were taken to be 13.5 MeV and 4.0 MeV, respectively. The γ-ray strength function was set to be 0.14×10^{-4}.

Figure 9.7.1 shows the ^{209}Bi(n, γ)^{210}Bi cross section and partial cross sections for the ^{210m}Bi and ^{210g}Bi production as a function of E_n. In the present calculation, the ^{209}Bi(n, γ)^{210}Bi cross section has the minimum at about 600 keV and has the maximum at about 2.7 MeV. For E_n ~ 300 keV, the magnitude of the ^{210g}Bi and ^{210m}Bi production cross sections is almost same. The ^{210g}Bi production cross section is larger than the ^{210m}Bi production cross section for E_n < 300 keV, while the ^{210m}Bi production are larger than the ^{210g}Bi production for E_n > 300 keV. It can be seen from Fig.9.7.1 that the cross sections obtained in the present work at 534 keV (the ^{209}Bi(n, γ)^{210}Bi cross section = 1.41 mb, the ^{209}Bi(n, γ)^{210g}Bi cross section = 0.64 mb, and the ^{209}Bi(n, γ)^{210m}Bi cross section = 0.77 mb) agree with the measured data[4] within experimental uncertainties.

References

1)N.Yamamuro : JAERI-M 90-006 (1990).

2)A.J.Koning and J.P.Delaroche : Nucl. Phys. **A713**, 231 (2003).

3)A.Mengoni and Y.Nakajima : J. Nucl. Sci. Thechnol. **31**, 151 (1994).

4)K.Saito, et.al. : Proc. 2002 Symp. Nucl. Data, Tokai, Japan, Nov.21-22, in press.

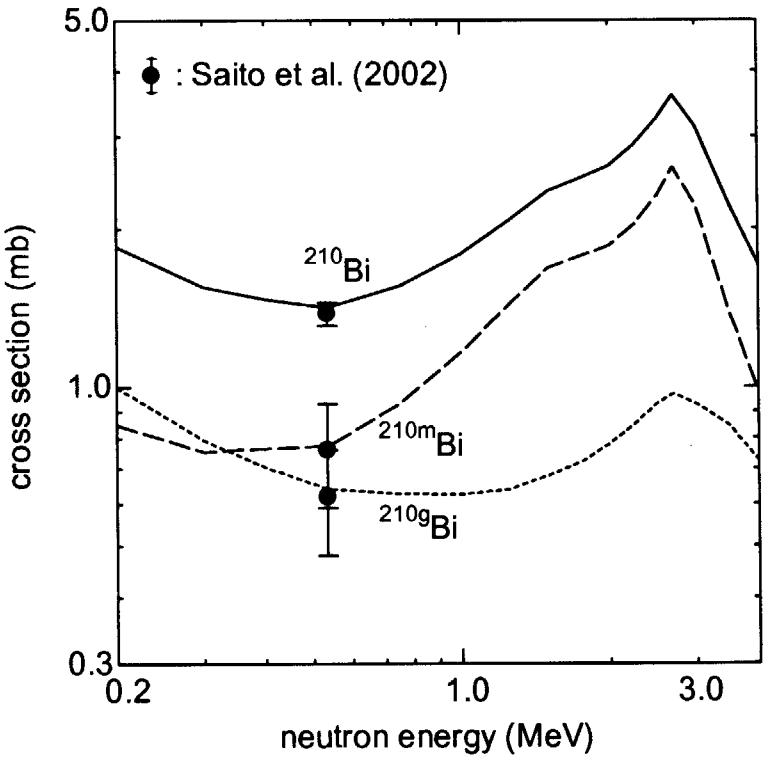

Fig.9.7.1 The ^{209}Bi(n, γ)$^{210g, 210m, 210}$Bi cross sections as a function of neutron energy

9.8 Development of a New Code of Coupled-channels Optical Model Calculation

O. Iwamoto

(*E-mail:* iwamoto@ndc.tokai.jaeri.go.jp)

Optical model is one of important methods for the evaluation of nuclear reaction data, since it is used for the estimation of total and scattering cross sections, and of transmission coefficients for statistical model calculation. In order to make the Japanese Evaluated Nuclear Data Library(JENDL), spherical optical model codes with statistical model calculation such as ELIESE[1] and CASTHY[2] were developed at the Nuclear Data Center in JAERI. For the actinide nuclei, however, coupled-channels(CC) optical model[3),4)] can describe scattering process better, because such nuclei having large deformation cause strong coupling between levels in the rotational band. In the present work, a new code of coupled-channels optical model calculation has been developed for the evaluation of actinide nuclei. Models used in the code and examples of calculations will be described briefly as follows.

A model Hamiltonian of the system is written as

$$H = H_A + H_a + T + V, \tag{1}$$

where H_A and H_a are Hamiltonians of the target and projectile, respectively. T and V are kinetic energy operator and optical potential of relative motion of target and projectile, respectively. The wave function of target Φ_n in the state n is eigen function of H_A: $H_A\Phi_n = \epsilon_n\Phi_n$. Expanding by angular momentum, total wave function is written as

$$\Psi = \sum_{c,J,M} \psi_c^{JM} r^{-1} f_c^{JM}(r), \tag{2}$$

$$\psi_c^{JM} = \left[\left[i^l Y_l \otimes \chi_s\right]_j \otimes \Phi_{n(I)}\right]_{JM}, \tag{3}$$

where c is channel of reaction representing $\{l, j, n\}$, I is spin of target in the state n, Y_l is spherical harmonics, χ_s is the wave function of projectile having spin s and

$[\phi_{j_1} \otimes \phi_{j_2}]_{JM} = \sum_{m_1,m_2} \langle j_1 j_2 m_1 m_2 | JM \rangle \phi_{j_1} \phi_{j_2}$. The radial wave function $f_c^{JM}(r)$ obeys following Shrödinger equation,

$$\left(\frac{d^2}{dr^2} - \frac{l_c(l_c+1)}{r^2} + k_c^2 \right) f_c^{JM}(r) = \sum_{c'} \langle \psi_c | V | \psi_{c'} \rangle \, f_{c'}^{JM}(r), \tag{4}$$

where k_c indicates wave number in the channel c. The optical potential is assumed to have Woods-Saxon or its derivative shape with changing radial parameter with respect to the angle (θ' and ϕ') in the body-fixed frame, and the radial parameters are expanded by spherical harmonics.

$$R(\theta', \phi') = R_o \left\{ 1 + \sum_{\lambda} \beta_{\lambda 0} Y_{\lambda 0}^*(\theta', \phi') \right\}, \quad \lambda = 2, 4, 6, ... \tag{5}$$

Here potential is assumed as axial symmetric and not changed by the rotational excitation.

By solving eq. 4 numerically, scattering matrix is obtained. Cross sections such as total, reaction, elastic and inelastic scattering and their angular distributions are deduced from the scattering matrix. The code is written by C++ language. Figures 9.8.1 and 9.8.2 show examples of neutron cross sections calculated by the new code for ^{238}U using optical potential in the reference[5] including 5 levels.

References

1) S. Igarasi: "*Program ELIESE-3; Program for Calculation of the Nuclear Cross Sections by Using Local and Non-local Optical Models and Statistical Model*", JAERI 1224 (1972)

2) S. Igarasi, T. Fukahori: "*Program CASTHY — Statistical Model Calculation for Neutron Cross Sections and Gamma Ray Spectrum —*", JAERI 1321 (1990)

3) T. Tamura: Rev. Mod. Phys. **37**, 679 (1965)

4) G. R. Satchler: *"Direct Nuclear Reactions"*, Oxford University Press, Oxford (1983)

5) E. Sh. Sukhovitskiĭ, O. Iwamoto, S. Chiba, T. Fukahori: J. Nucl. Sci. Technol., **37**, 120 (2000)

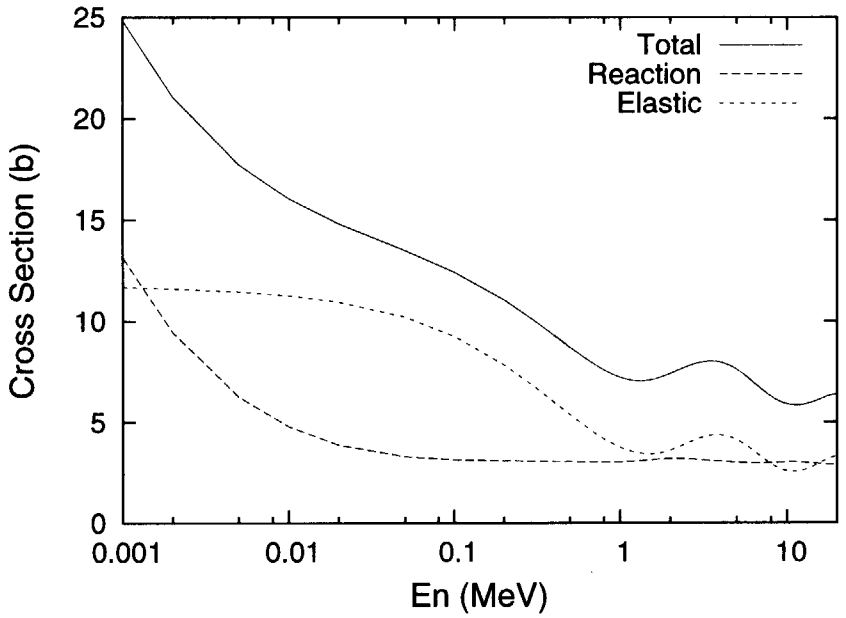

Fig. 9.8.1 Energy dependence of total, reaction and elastic scattering cross sections of ^{238}U calculated by the new code with coupling 5 levels

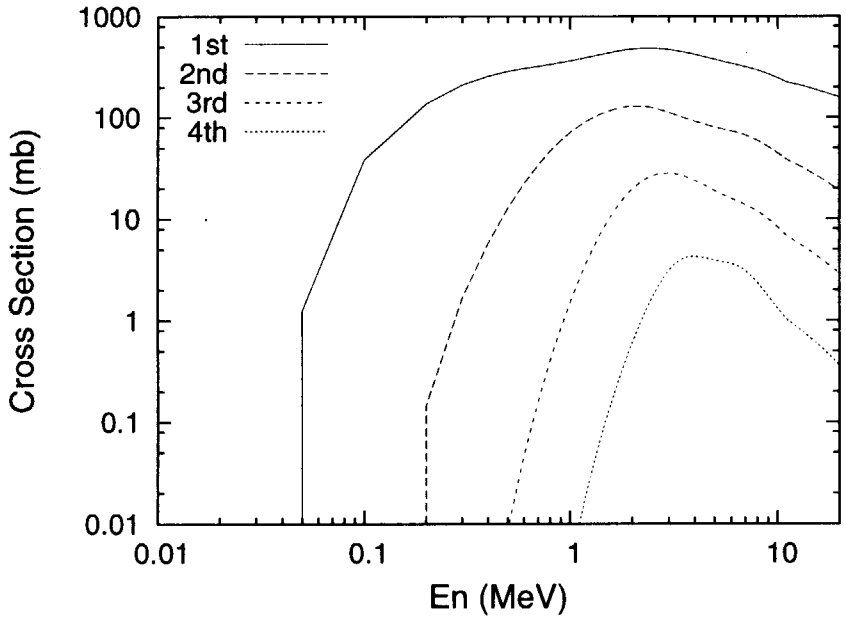

Fig. 9.8.2 Energy dependence of inelastic scattering cross sections to 1st, 2nd, 3rd and 4th excited levels for ^{238}U calculated by the new code with coupling 5 levels

9.9 Development of Fission Yields Systematics with 5 Gaussian Functions

J. Katakura
(*E-mail*: katakura@ndc.tokai.jaeri.go.jp)

A systematics of fission product mass yields has been developed using 5 Gaussian functions. [1] The mass yields $\psi(A,E)$ is a function of fission product mass A and energy E of incident particle. In this systematics, the mass distribution is expressed as follows:

$$\begin{aligned}\psi(A,E) &= N_s\psi_s(A,E) + N_a\psi_a(A,E) \\ &= N_s\psi_s(A,E) + N_a\left[\psi_{h1}(A,E) + \psi_{l1}(A,E) + F\left\{\psi_{h2}(A,E) + \psi_{l2}(A,E)\right\}\right],\end{aligned}$$

where N_s, N_a and F are normalization factors. Now when R values is defined as the ratio of asymmetric component to symmetric component, the N_s and N_a values are related to F and R as follow:

$$\begin{aligned}N_s &= 200/(1+2R), \\ N_a &= 200R/\left\{(1+F)(1+2R)\right\}.\end{aligned}$$

The five components are assumed to be Gaussian distribution:

$$\begin{aligned}\psi_s(A,E) &= \frac{1}{\sqrt{2\pi}\sigma_s}\exp\left\{-(A-A_s)^2/2\sigma_s^2\right\}, \\ \psi_{h1}(A,E) &= \frac{1}{\sqrt{2\pi}\sigma_{h1}}\exp\left\{-(A-A_{h1})^2/2\sigma_{h1}^2\right\}, \\ \psi_{h2}(A,E) &= \frac{1}{\sqrt{2\pi}\sigma_{h2}}\exp\left\{-(A-A_{h2})^2/2\sigma_{h2}^2\right\},\end{aligned}$$

and the other two functions $\psi_{l1}(A,E)$ and $\psi_{l2}(A,E)$ for the light fragment are given by reflecting $\psi_{h1}(A,E)$ and $\psi_{h2}(A,E)$ about the symmetric axis $A_s = (A_f - \bar{\nu})/2$. Here A_s, A_{h1} and A_{h2} are the mass numbers corresponding to the peak positions of the Gaussian distribution curves, and σ_s^2, σ_{h1}^2 and σ_{h2}^2 are the dispersions of these distributions. A_f denotes the mass number of the fissioning nuclide. The quantity $\bar{\nu}$ is the average number of prompt neutrons emitted per fission.

There exist 8 parameters in this systematics to be determined. These parameters were determined by examining various kind of measured mass distributions.The

determined parameters are expressed as follows:

$$
\begin{aligned}
\bar{\nu} &= 1.404 + 0.1067(A_F - 236) + [14.986 - 0.1067(A_F - 236)] \cdot [1.0 - \exp(-0.00858E^*)], \\
R &= [112.0 + 41.24\sin(3.675S)] \cdot \frac{1.0}{BN^{0.331} + 0.2067} \cdot \frac{1.0}{E^{0.993} + 0.0951}, \\
F &= 10.4 - 1.44S, \\
\sigma_s &= 12.6, \\
\sigma_{h1} &= (-25.27 + 0.0345A_f + 0.216Z_f)(0.438 + E + 0.333BN^{0.333})^{0.0864}, \\
\sigma_{h2} &= (-30.73 + 0.0394A_f + 0.285Z_f)(0.438 + E + 0.333BN^{0.333})^{0.0864}, \\
A_{h1} &= 0.5393(A_f - \bar{\nu}) + 0.01542A_f(40.2 - Z_f^2/A_f)^{1/2}, \\
A_{h2} &= 0.5612(A_f - \bar{\nu}) + 0.01910A_f(40.2 - Z_f^2/A_f)^{1/2},
\end{aligned}
$$

where E^* is the excitation energy of fissioning nuclide, BN the binding energy of the incident particle and S the shell energy given by Meyers and Swiatecki [2]. The excitation energy is the sum of the incident energy E and the binding energy BN.

The mass distributions calculated by the present systematics were compared with measured data. Figure 9.9.1 shows examples of the comparisons. In this figure mass

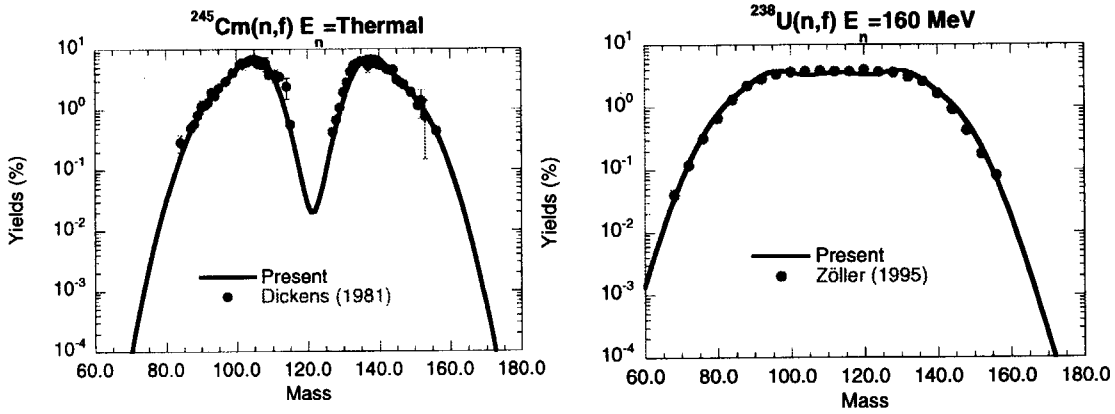

Fig. 9.9.1 Comparisons bwtween measured data and the present systematics

distributions by thermal and high energy neutrons are compared. The measured data are by Dickens [3] and Zöller [4]. The present systematics shows rather good agreement with measured data by both thermal and high energy neutrons.

References

1) J. Katakura: "A Systematics of Fission Product Mass Yields with 5 Gaussian Functions," JAERI-Research 2003-004 (2003).

2) W. D. Meyers and W. J. Swiatecki: *Nucl. Phys.* **81**, 1 (1966).

3) J. K. Dickens and J. W. McConnel: *Phys. Rev.* **C23**, 331 (1981).

4) C. M. Zöller et al.: Proc. VII School on Neutron Physics, Ratmino, E. Kornilov (Ed.) JINR, Dubna, 1995 Vol. I p130 (1995).

10. Facility Operation and Techniques Development

There are four reactor-engineering facilities such as Heat Transfer Fluid Flow Test Facility, Fast Critical Assembly (FCA), Tank-type Critical Assembly (TCA) and Very High Temperature Reactor Critical Assembly (VHTRC). Maintenance work for VHTRC and operations of other facilities were carried out as scheduled. Major activities of each facility of this fiscal year are summarized briefly below.

(1) The Heat Transfer Fluid Flow Test Facility was operated for various experiments such as Departure from Nucleate Boiling Test for Advanced Reactor, Measurement Test of Void Fraction Distribution by Neutron Radiography etc. And Thermal Fluid Safety Test (Ingress of Coolant Event/Loss of Vacuum event) for Fusion Reactor was carried out.

(2) The FCA was operated according to various purposes of experiments and recorded the operation time of 497hours. Maintenance activities, fuel management and physical protection were done, i.e., renewal of the exhaust equipment for the reactor room, repair for defects of coating on fuels etc. And the Physical Inventory Verification (PIV) of nuclear fuel materials was carried out.

(3) The TCA was operated for the nuclear constant experiments and the training courses of the Nuclear Technology and Education Center (NuTEC). And it was recorded 137 times operation in 54 days. Fuel management, Physical Protection and PIV were also carried out.

(4) Maintenance works were done for VHTRC such as the monthly and annual inspections according to the safety regulation. The Physical Inventory Taking (PIT) and PIV for VHTRC were also carried out.

The decommissioning of VHTRC reactor assembly and control panel was performed from Sep.2000 to Mar.2001.

10.1 Operation Report of Heat Transfer Fluid Flow Test Facility

T. Satoh, H. Watanabe, M. Shibata and K. Nakajima
(*E-mail* : taasato@popsvr.tokai.jaeri.go.jp)

In Fy-2002, operation and maintenance of Heat Transfer and Fluid Flow Test Facilities were carried out as scheduled.

As for the maintenance of test facilities, annual official inspections of the pressure vessels and the steam generator located at both Chemical/Mechanical Engineering Building and Two Phase Flow Test Facility buildings were carried out.

As for the operation of test Facilities, the following four tests were performed.

1) DNB test for Reduced-Moderation Water Reactors with a double flat core test Section
2) Low Pressure Experimental Test Facility
3) Measurement test of void fraction distribution by Neutron Radiography
4) Development test for measurement void fraction

As for the design and construction of test Facilities, the following two test Facilities were newly constructed.

1) Low Pressure Experimental Test Facility II
2) Tight-lattice large-scale thermal-hydraulic Test Facility for advanced nuclear power reactor

10.2 Operation Report of FCA

M. Saito, K. Satoh, K. Kurosawa, T. Ono, K. Hayasaka, and H. Sodeyama
(*E-mail*:saito@fca001.tokai.jaeri.go.jp)

Operation of Fast Critical Assembly (FCA) was carried out in accordance with the experimental schedule on the FCA XXI-1 and XXII-1 assembly. Operation of 113 times was carried out in 87 days. No scram was recorded during the operation. The total operation time was 497 hours and the integrated power was 0.37 kWh. A total number of 5565 criticality operations have been recorded at the end of this fiscal year since the first achievement of criticality on the 29 of April 1967. For the safety regulation of operation, two days were devoted to the monthly inspection and about 11 weeks from October 2002 to the annual inspection. Routine maintenance activities were done during the inspection to provide maximum operation days for the experiments.

As for fuel management, the defects of coating on uranium metallic fuel were repaired for about 7430 plates by spraying the surface in order to prevent the fuel from oxidation.

As for the physical protection (P/P), security control of the gate was done restrictively and the system was maintained properly.

In connection with safeguard, IAEA and JSGO* carried out monthly inspection under the international treaty. They performed the PIV (Physical Inventory Verification) from the 22th to the 24th of July. Prior to the PIV we performed item counting, weighing and non-destructive assay of the fuel from the 8th to the 19th of July.

* JSGO: Japan Safeguards Office

10.3 Operation Report of TCA

K. Murakami, Y. Hoshi, M. Kyoya and T. Ouchi
(*E-mail*:murakami@nucef.tokai.jaeri.go.jp)

Operation of Tank-type Critical Assembly(TCA) was carried out in accordance with the schedule on the experiments (the measurement of sub-criticality on the core by γ-ray detecting source multiplication method, the limit in the measurement of small reactivity at TCA, the noise measurement at TCA by neutron and γ-ray detecting) for the Research Group for Reactor Physics and on the experiments for the training courses of NuTEC(Nuclear Technology and Education Center). The total operation time was 171 hours and integrated power was 72.5Wh during 137 times operation in 54 days. A total number of 11,386 criticality operations had been recorded at the end of this fiscal year since the first achievement of criticality on the 23rd of August 1962.

As for the nuclear material physical protection(P/P), the management of the entrance and exit was done restrictively and the system was maintained properly.

In connection with safeguard the inspection of nuclear material, stored at TCA, was carried out by IAEA and NSB* under the international treaty. The Physical Inventory Taking (PIT) of the fuels was performed on the 18th of June and IAEA and NSB made the Physical Inventory Verification(PIV)on the 21st of June by means of item counting, and non-destructive assay

* NSB : Nuclear Safety Bureau

10.4 Maintenance Work Report of VHTRC

M.Takeuchi, N.Yabuuchi, N.Ohzeki, M.Kyoya, T.Ouchi and K.Nakajima
(*E-mail* : takeuchi@vhtrc01.tokai.jaeri.go.jp)

The decommissioning of reactor assembly and control panel which is the first step of the decommissioning of the VHTRC started on September 2000.
And it was finished in March 2001.

Maintenance and management of the other reactor equipment facilities such as reactor building and fuel storage room of the VHTRC will continue maintenance and management.

According to the safety regulation for maintenance, the 6 weeks were devoted to the annual inspection from July to August in 2002.

As for management, Physical Inventory Taking(PIT)was carried out from May 9 to 13 by means of item counting for fuel compact and fuel disk. IAEA and MEXT made the Physical Inventory Verification(PIV)under the international treaty on May14. No anomaly was confirmed. The maintenance activity was also taken on the physical protection(P/P)system.

The sensitivity calibration and function roundness of the system were examined.

11. Activities of the Research Committees

The Department of Nuclear Energy System serves as a secretariat of the following two research committees organized by JAERI: Japanese Nuclear Data Committee and Research Committee on Reactor Physics. The purpose and expected task of each committee are summarized here. The detailed activities of each committee are presented in the following sections.

Japanese Nuclear Data Committee

The Committee was organized to promote the evaluation of nuclear data and the utilization of nuclear data in application fields. The Committee also takes a task of cooperation with the activities of the International Nuclear Data Committee (INDC) and the Working Party on International Evaluation Cooperation under OECD/NEA Nuclear Science Committee (NSC). There are three subcommittees, six standing groups, an adhoc group and a steering committee.

Research Committee on Reactor Physics

The Committee reviews the research activities related to reactor physics in Japan and supports the reactor physics activities of OECD/NEA/NSC. The Committee consists of three working parties and a steering committee. The working parties deal with reactor physics of sub-critical systems, reactor physics of LWRs loaded with next generation fuels, and code systems for common usage of reactor physics calculations.

11.1 Activities of Japanese Nuclear Data Committee

A. Hasegawa

The Japanese Nuclear Data Committee (JNDC) consists of three subcommittees, six standing groups, a steering committee and an adhoc group. Each subcommittee consists of several working groups (WG). The Committee Meeting of JNDC was held on July 2002 to discuss the nuclear data activity in the previous fiscal year and plans for the fiscal year 2002. Discussions were made on several highlighted topics including JENDL-3.3 and a new WG set up in JNDC: Evaluation of Nuclear Data for Astrophysics.

The activities of subcommittees, standing groups and an adhoc group are briefly summarized below.

Subcommittee on Nuclear Data

1) High Energy Nuclear Data Evaluation WG

The evaluation works are progressing in parallel in two phases. In the phase-I, the data up to 50 MeV for IFMIF (International Fusion Material Irradiation Facility) project are targeted for neutron- and proton-induced reactions. In the phase-II, evaluations for high-energy neutron/proton induced reactions up to 3GeV are concerned. Data requests are very keen from the joint projects of JAERI and KEK (High Energy Accelerator Research Organizations) for a High Intensity Proton Accelerator of the Center for the Neutron Research. Following is the status of each Sub-working Group (SWG):

- High Energy File Compilation SWG: Compilation and evaluation of phase-II data are the main mission. Evaluations for the priority 2 nuclides (about 40 nuclides) have been finished. Evaluation has started for the priority 3 nuclides.
- IFMIF Neutron File Compilation SWG: Neutron file compilation is the main task of this SWG. Up to now, evaluation of 43 nuclides has been finished. The files are in the final reviewing stage after the format check.
- Photo Nuclear Data File Compilation SWG: All evaluations are finished. For important nuclides especially for FPs not available in JAERI's original evaluations, KAERI's data will be adopted.

2) Evaluation and Calculation Support System WG

Recommended parameters required in the nuclear model calculations such as OMP, level density, gamma strength functions, as well as advanced methodologies like multi-modal fission, essence from the latest frontiers of theoretical calculations were discussed. The results were reflected to RIPL-2 (Reference Input Parameter Library Version 2).

Discussions are started on a new JNDC original-code development for the statistical model.

3) Fission Product Nuclear Data Evaluation WG

This WG has been newly set-up due to the revision work for FP nuclides in the next generation JENDL general purpose file. Discussions on a new evaluation methodology to be taken were made based on the careful review of the evaluations adopted in the previous file. Needs for the new data evaluations are also investigated. Strong needs for Sr and Dy isotopes and other twelve nuclides were raised.

4) WG on Evaluation of Nuclear Data for Astrophysics

This group was also set up newly to provide consistent neutron capture cross-section data to be used in astrophysics especially for r-process nucleosynthesis in the Big-Bang model.

Subcommittee of Reactor Constants

1) Reactor Integral Test WG

Benchmark tests of JENDL-3.3 for fast and thermal reactors were made. Group constants based on JENDL-3.3 were produced and distributed to users for MVP, JFS, SRAC code systems.

2) Shielding Integral Test WG

For JENDL-3.3, benchmark tests were made for main shielding materials such as Al, Si, Na, Ti, V, Cr, Fe, Co, Ni, Cu, Nb, W, Hg. A summary of the results is available on the WEB of JAERI Nuclear Data Center.

3) Standard Group Constants WG

A report of the JSSTDL-300 is being prepared. Direction of group constants preparation for standardized libraries has been discussed.

3) Medium and High Energy Nuclear Data Integral Test WG

Benchmark problems to be calculated are selected and assigned to testers. Preparation of processing code NJOY99 and Monte Carlo code MCNPX were made.

Subcommittee on Nuclear Fuel Cycle

1) Decay Heat Evaluation WG

Calculation of β-ray and γ-ray emission energies for about 40 nuclides was made to compare with Greenwood's measured data using TAGS (Total Absorption Gamma-Ray Spectroscopy). In the estimated decay heat calculations including TAGS energies for ^{239}Pu, improvements in JEF-2.2 are remarkable mitigating the long standing discrepancy, while the JENDL results show too large compared with experiment. For JENDL side, a new methodology is required for bridging theoretical estimation and TAGS data base to give

consistent decay heat estimations. This group also contributes to the Standardization process for Decay Heat Calculation in the Atomic Energy Society of Japan (AESJ).

2) WG on Evaluation of Nuclide Generation and Depletion

ORIGEN-2 libraries based on JENDL-3.3 were produced for LWRs, including PWR and BWR-MOX. PIE analyses for high burn-up UO_2 fuels (41GWd/t) of PWR as well as for FBR JOYO MK-II fuels (58GWd/t) were made. From the latter study it is concluded that initial inventory and PIE experimental accuracy should be carefully re-checked. Sensitivity studies using different nuclear data libraries were made for 600MWe FBR at the end of equilibrium cycle.

3) FP Mass Yield Evaluation WG

The systematics of 5 Gaussian fitting model developed by Moriyama and Ohnishi was applied and analyzed. From the study, the applicability of the method was confirmed for the incident energies from thermal to 100 MeV.

Standing Groups

1) CINDA Group

Papers on neutron induced reaction data published in Japanese journals and reports are surveyed. A total of 3,545 entries (Journals: 711, ND2001: 534, JENDL3.3: 2,278) were sent to the NEA Data Bank in the last one year to update the CINDA master database.

2) ENSDF Group

Re-evaluation work has been made on the nuclear structure data for A= 120 and 126 nuclei.

3) Group on Atomic, Molecular and Nuclear Data for Medical Use

Survey work has been continued for the radiopharmaceutical data needed in the field of nuclear medicine. Home page of this group was updated to promote and encourage the WG missions.

4) JENDL Compilation Group

JENDL-3.3 was released on the 10th of May 2002 with Press Release Materials. A CD-ROM and some auxiliary booklets about JENDL-3.3 were published.

5) Editorial Group of "Nuclear Data News"

Three issues of "Nuclear Data News" (No.72-74) which is a periodic informal journal circulated in nuclear data communities of Japan (written in Japanese) were published. All articles of this News published up to now have been scanned and uploaded in our homepage.

6) High Priority Request List (HPRL) Group

A new file structure has been suggested (consisting of 4 parts: Request List, Satisfied List, Check List, Reference List) for the latest version of HPRL. This group is a

coordination group to set up a Japanese Requests List from domestic data users and a world-wide request list HPRL that is maintained at OECD/NEA/WPEC (Working Party on International Evaluation Cooperation).

Adhoc Group

Advisory Group for Next Generation of JENDL (JENDL-4)

A five-year project of JENDL-4 is going to start in 2003. Prior to the start of JENDL-4 project, an adhoc group for making the road map of JENDL-4 development was set up at March 2002 in JNDC. After one year discussions among nuclear data evaluators, users from various fields especially in advanced/innovative reactors, astrophysics group, BNCT (Boron neutron capture therapy) medical application etc, a report was released on May 2003.

In the report, the main objective of JENDL-4 is a file to solve current concerns on nuclear energy development such as high burn up, MOX fuels utilization, evaluations of burn-up credit and their safety assessments as well as innovative/advanced reactors seeking ultimate reliability in safety with reducing cost of fabrication. In the scope, included are also medical or fundamental scientific applications such as BNCT, medical use of accelerators, and nucleosynthesis in astrophysics. In JENDL-4 project, the outcome is to provide a whole system composed of not only JENDL-4 itself but also application libraries such as point Monte Carlo libraries and/or group constants libraries produced from JENDL-4. Quality assurance (QA) is a key issue for JENDL-4.

The 2002 Symposium on Nuclear Data

The 2002 Symposium on Nuclear Data was held at Tokai Research Establishment, Japan Atomic Energy Research Institute (JAERI), on 21st and 22nd of November 2002. Japanese Nuclear Data Committee and Nuclear Data Center, JAERI organized this symposium. In the oral sessions, presented were 17 papers on the release of JENDL3.3: outline of JENDL3.3, its benchmark test for LWR/FBR reactors and shielding applications, requests and discussions about JENDL utilizations among developers and Japanese nuclear industrial user groups, together with an international session and other topics like neutrino physics. In the poster session, presented were 33 papers concerning experiments, evaluations, benchmark tests and software on nuclear data. Those presented papers were compiled in the proceedings and published as JAERI-Conf 2003-006 (2003) report. A total of 133 scientists including 8 foreigners attended the symposium.

11.2 Activities of the Research Committee on Reactor Physics

M. Nakagawa and T. Osugi

The committee reviews research activities related to reactor physics in Japan and supports the activities of Nuclear Science Committee (NSC) of OECD/NEA. The committee consists of three working parties and a steering committee.

The 72nd meeting of the Research Committee on Reactor Physics (RCRP) was held on July 5th, 2002. In the meeting, the following topic was discussed: Conceptual design study of operator-free fast reactor RAPID-L (Refueling by All Pins Integrated Design for a Lunar base power system), which was equipped with innovative Li-6 reactivity control systems LEM and LIM. The meeting was also devoted to the distribution of documents discussed at the 13th meeting of NEA/NSC held at OECD Headquarters, Paris, June 3rd – 5th 2002.

Working Parties

Three working parties, as shown below, were established in FY-2001. The interval of their activities was limited in two years: FY-2002 was the second year. The meeting in each working party was held twice in FY-2002. The following topics were focused on and were discussed in the meetings.

1) Working Party on Reactor Physics of Sub-Critical Systems,
   - Review and definition of "Sub-Criticality" used in Accelerator Driven Systems (ADS)
   - Proposal of benchmark problems for sub-critical system such as ADS
   - Discussion of sub-critical condition in design study of ADS.
2) Working Party on Reactor Physics of LWRs Loaded with Next Generation Fuels,
   - Benchmark problems for calculation accuracy evaluation on LWRs loaded with next generation fuels.
3) Working Party on Code Systems for Common Usage of Reactor Physics Calculations,
   - Discussion of scope of common code systems
   - Review of code systems used in Japan.

Publication List

1. Energy System Analysis and Assessment

1) M. Yamaguchi and O. Sato: "An Investigation on Experience Curves of Solar Photovoltaic Power Systems", JAERI-Review 2002- 013 (2002) [in Japanese].

2. Advanced Reactor System Studies

1) T. Okubo, et al.: "Design of Small Reduced-Moderation Water Reactor (RMWR) with Natural Circulation Cooling", Proc. of International Conference on the New Frontiers of Nuclear Technology; Reactor Physics, Safety and High-Performance Computing (PHYSOR 2002), Seoul, Korea (2002).

2) T. Okubo, et al.: "Design Study on Reduced-Moderation Water Reactor (RMWR)", Proc. of 8th National Symposium on Power and Energy Systems (2002) [in Japanese].

3) T. Iwamura, et al.: "Core and System Design of Reduced-Moderation Water Reactor with Passive Safety Features", Proc. of ICAPP 2002, No. 1030, Hollywood, Florida (2002).

4) T. Iwamura, et al.: "Development of Reduced-Moderation Water Reactor (RMWR) for Sustainable Energy Supply", Proc. of The 13th Pacific Basin Nuclear Conference (PBNC 2002), Shenzhen, China (2002).

5) (Eds.) Y. Nakano, et al.: "Summary of the 5th Workshop on the Reduced-Moderation Water Reactor", JAERI-Conf 2002-012 (2002) [in Japanese].

6) S. Shimada, et al.: "Design Study on PWR-Type Reduced-Moderation Light Water Core –Investigation of Core Adopting Seed-blanket Fuel Assemblies-", JAERI-Research 2003-003 (2002) [in Japanese].

7) N. Ishikawa and K. Abe: "An Approximate Design Method of Discrete-time 2DOF Controller and its Parameter Tuning", IEEJ Trans. on Electronics, Information and Systems, Vol.123, No.2 (2003) [in Japanese].

8) K. Nabeshima, et al.: "Nuclear Reactor Monitoring with the Combination of Neural Network and Expert System", Mathematics and Computers in Simulation, Vol.60 (2002)

9) T. Suzudo: "Diversity of Complex Systems Produced by a Class of Cellular Automata", Proc. of 6th International Conference on Complex Systems, Tokyo, Japan (2002).

3. Research on Small Reactor for Dispersive Energy Supply System

1) T. Yoritsune, T. Ishida and S. Imayoshi: "In Vessel Type Control Rod Drive Mechanism Using Magnetic Force Latching for a Very Small Reactor", J. Nucl. Sci. Technol., 39[8],

913 (2002)

2) T. Yoritsune and T. Ishida: "Development of In-vessel Type Control Rod Drive Mechanism for a Innovative Small Reactor (Contract Research) ", JAERI-Tech 2003-022 (2003) [in Japanese].

3) H. Takahashi, N. Nakajima and T. Kusunoki: "Study on the Thermal Output Scale of a Very Small Reactor for District-Heat-and-Cooling System", JAERI-Tech 2003-052 (2003) [in Japanese].

4. Reactor Physics

1) H. Tsunoda, O. Satoh, S. Okajima, T. Yamane, S. Iijima and M. Kambe: "RAPID-L Highly Automated Fast Reactor Concept Without Any Control Rods Critical Experiment of Lithium-6 as a Liquid Poison of LEM and LIM", in session 6.04 of Proc. Int. Conf. of Advanced Nuclear Power Plants(ICAPP), Florida (2002).

2) S. Okajima, T. Sakurai, J. F. Lebrat, V. Z. Averlant and M. Martini: "Summary on International Benchmark Experiments for Effective Delayed Neutron Fraction (β eff)", Prog. in Nucl. Energy, 41, No.1-4, pp.285-301 (2002).

3) K. Okumura, H. Unesaki, T. Kitada and E. Saji: "Benchmark Results of Burn-up Calculation for LWR Next Generation Fuels", Proc. of Int. Conf. on the New Frontiers of Nuclear Technology: Reactor Physics, Safety and High-Performance Computing (PHYSOR 2002), 9A-03, Seoul, Korea, 7-10 October (2002).

4) Y. Nagaya, K. Okumura and T. Mori: "Analysis of VENUS-2 MOX Core Measurements with A Monte Carlo Code MVP", Proc. of Int. Conf. on the New Frontiers of Nuclear Technology: Reactor Physics, Safety and High-Performance Computing (PHYSOR 2002), 4A-04, Seoul, Korea, 7-10 October (2002).

5) T. Sakurai and S. Okajima: "Adjustment of Total Delayed Neutron Yields of U-235, U-238 and Pu-239 by Using Results of In-pile Measurements of Effective Delayed Neutron Fraction", Proc. of Int. Conf. on the New Frontiers of Nuclear Technology: Reactor Physics, Safety and High-Performance Computing (PHYSOR 2002), 10C-04, Seoul, Korea, 7-10 October (2002).

6) S. Okajima, H. Tsunoda, M. Kambe, T. Yamane, S. Iijima and O. Satoh: "Critical Experiment and Analyses for the Conceptual Design Study of Fast Reactor Equipped with Li-6 Reactivity Control Systems LEM and LIM", Proc. of Int. Conf. on the New Frontiers of Nuclear Technology: Reactor Physics, Safety and High-Performance Computing (PHYSOR 2002), 7E-07, Seoul, Korea, 7-10 October (2002).

7) S. Iijima, M. Ando and H. Oigawa: "Benchmark Experiment for Physics Parameters of

Advanced Fuel LMFBR at FCA", Proc. of Int. Conf. on the New Frontiers of Nuclear Technology: Reactor Physics, Safety and High-Performance Computing (PHYSOR 2002), 8C-02, Seoul, Korea, 7-10 October (2002).

8) Y. Nauchi, T. Kameyama, T. Matsumura, T. Suzaki and Y. Miyoshi: "Measurement and Analysis of High Energy Gamma Ray and Neutron in MOX Fuel Lattices For Subcriticality Estimation", Proc. of Int. Conf. on the New Frontiers of Nuclear Technology: Reactor Physics, Safety and High-Performance Computing (PHYSOR 2002), 1C-03, Seoul, Korea, 7-10 October (2002).

9) K. Tsujimoto, N. Kohno, N. Shinohara, T. Sakurai, Y. Nakahara: T. Mukaiyama and S. Raman : "Validation of Minor Actinide Cross Sections by Studying Samples Irradiated for 492 Days at the Dounreay Prototype Fast Reactor", Proc. of Int. Conf. on the New Frontiers of Nuclear Technology: Reactor Physics, Safety and High-Performance Computing (PHYSOR 2002), 14C-04, Seoul, Korea, 7-10 October (2002).

10) F. B. Brown and Y. Nagaya: "The MCNP5 Random Number Generator," Trans. Am. Nucl. Soc. 87, pp.230-232 (2002).

11) T. Fujimura and K. Okumura: "Analysis of the Applicability of Acceleration Method for a Triangular Prism Geometry Nodal Diffusion Code, JAERI-Research 2002-024 (2002) [in Japanese].

12) S. Iijima and S. Okajima: "Multi-group Diffusion Perturbation Calculation Code PERKY (2002) ", JAERI-Data/Code 2002-023 (2002) [in Japanese].

13) M. Haruyama, M. Takase, S. Iwasaki and H.Tobita: "Reconstruction of CT Images by the Bayes-back Projection Method", JAERI-Research 2002-022 (2002) [in Japanese].

14) M. Haruyama, H. Shitomi and K. Nakamura: "Modification of Fuel Failure Detection System at Multi-purpose Reactor RSG-GAS, BATAN", JAERI-Tech 2003-025 (2003) [in Japanese].

15) K. Okumura and T. Mori: "Integral Test of JENDL-3.3 for Thermal Reactors", Proc. of 2002 Symposium on Nuclear Data, Tokai, Japan, Nov. 21-22, JAERI-Conf 2003-006, pp.15-21 (2003).

16) M. Rahman, T. Suzaki and T. Mori: "Analytical Study of Two-Region TCA Critical Experiments with PWR-Type MOX Fuel by Using Monte Carlo Code MVP", JAERI-Research 2003-007 (2003).

17) Y. Matsuo, N. Morishima and Y. Nagaya: "Neutronic Study of Spherical Cold-neutron Sources Composed of Liquid Hydrogen and Liquid Deuterium", Nuclear Instruments and Method A, 496, pp.446-451 (2003).

18) Y. Nagaya and F. B. Brown: "Implementation of a Method to Estimate Change in

Eigenvalue due to Perturbed Fission Source Distribution into MCNP", LA-UR-03-1387 (2003).

19) T. Yoshida, S. Okajima, T. Sakurai, K. Nakajima, T. Yamane, J. Katakura,Y. Tahara, A. Zukeran, K. Oyamatsu, T. Ohsawa, T. Nakagawa and T. Tachibana: "Evaluation of Delayed Neutron Data for JENDL-3.3", J. Nucl. Sci. Technol. Supplement 2, pp.136-139 (2002).

5. Thermal and Fluid Engineering

1) K. Takase and H. Akimoto: "Depressurization Behavior of Vacuum Vessel Pressure Suppression Systems in Fusion Reactors at Multiple First Wall Pipe Break Events", Int. J. of Applied Electromagnetics and Mechanics, Vol.13, pp.365-372 (2001/2002).

2) K. Takase, Y. Ose and T. Kunugi: "Numerical Study on Direct-Contact Condensation of Vapor in Cold Water", Fusion Engineering and Design, Vol. 63-64, pp.421-428 (2002).

3) K. Takase, Y. Ose and H. Akimoto: "Three-Dimensional Analysis of Water-Vapor Void Fraction in a Fusion Experimental Reactor under Water Ingress", Fusion Engineering and Design, Vol. 63-64, pp.429-436 (2002).

4) K. Takase: "Effects of Breach Size and Dust density on Activated Dust Mobilization in ITER During a Loss-of-Vacuum Event", Fusion Engineering and Design, Vol. 63-64, pp.205-210 (2002).

5) Y. Ose, K. Takase, H. Yoshida and H. Akimoto: "Numerical Visualization of Water-Vapor Flow Configurations in Fusion Reactors during Ingress of Coolant Events", 10th International Conference on Nuclear Engineering, ICONE10-22376, Washington, USA (2002).

6) H. Yoshida, A. Ohnuki and H. Akimoto: "A Feasibility Study on Core Cooling of Reduced-Moderation PWR For the Large Break LOCA", 10th International Conference on Nuclear Engineering, Arlington, ICONE10-22509, Washington, USA (2002)

7) K. Takase, Y. Ose, E. Kume, T. Kitamura and H. Akimoto: "Numerical Evaluation of Chemical Reaction and Dust Mobilization Behavior at Transient Events", 4th Fusion Energy Combined Conference, I141 (2002).

8) Y. Ose, K. Takase, M. Shibata and T. Kunugi: "Direct Numerical Analysis on Condensation of Vapor under Low Pressure", 4th Fusion Energy Combined Conference, I142 (2002).

9) K. Takase, Y. Ose, H. Yoshida and T. Kunugi: "Experiments and Analyses on Direct-Contact Condensation of Vapor under Low Pressure", 39th National Heat Transfer Symposium of Japan, Vol.1, A114 (2002).

10) K. Takase, M. Shibata, Y. Ose, H. Yoshida and T. Kunugi: "Condensation Behavior of Vapor Injected into Cold Water under Low Pressure", 10th International Symposium on Flow Visualization, F0235, Kyoto (2002).

11) K. Takase, Y. Ose, S. Fijii and K. Watanabe: "Numerical Simulations on Chemical Reaction Behavior of Injected Vapor and Carbon Material under High Temperature Environment", The 2002 Annual Conference of the Japan Society for Industrial and Applied Mathematics, G12-2 (2002).

12) K. Takase and H. Akimoto: "Experimental and Analytical Studies on Thermal-Hydraulic Performance of a Vacuum Vessel Pressure Suppression System in ITER", 19th IAEA Fusion Energy Conference, SE/P-02, Lyon, France (2002).

13) Y. Ose, T. Suzuki, H. Yoshida, K. Takase and T. Kunugi: "Direct Numerical Simulation on Condensation Behavior between Water and Vapor", 2002 Yamanashi District Conference of JSME, No.020-4, 208 (2002).

14) H. Yoshida, Y. Ose, K. Takase and H. Akimoto: " Numerical Investigation on Phase Change Analysis by Surface Tracking Method", 2002 Yamanashi District Conference of JSME, 209 (2002).

15) K. Takase, Y. Ose, H. Yoshida, H. Tamai, E. Kume and T. Kitamura: "Numerical Analysis of Two Phase Flow in a Narrow Channel with a Three-Dimensional Rectangular Rib", 16th Symposium on the Japan Society of CFD, D11-2, Tokyo (2002).

16) H. Yoshida, Y. Ose, K. Takase, H. Tamai and H. Akimoto: "Numerical Simulation of the Void Drift Using Interface Tracking Method", 16th Symposium on the Japan Society of CFD, D11-1, Tokyo (2002).

17) K. Takase: "Post-test (Cases P1-P8) Analysis Results by TRAC-PF1", IEA-ESE/FP Task 2 Meeting, Cadarache, France (2002).

18) K. Takase: "Numerical Modeling of Phase Change Analysis for Multiphase Flows", IEA-ESE/FP Task 2 Meeting, Cadarache, France (2002).

19) M. Kureta, H. Akimoto, K. Yamamoto and H. Okada: "Critical Heat Flux Experiment for Reduced-Moderation Water Reactor (RMWR)", Proc. International Congress on Advanced Nuclear Power Plants (ICAPP), No.1129, Florida, USA (2002).

20) M. Kureta, F. Araya, A. Ohnuki, T. Okubo, T. Iwamura, H. Akimoto, K. Yamamoto and Y. Okada: "Critical Heat Flux in Tight Lattice Core of Reduced-Moderation Water Reactor (RMWR)", 8th Symposium of Power and Energy Systems, P21-6, Tokyo (2002).

21) M. Kureta and H. Akimoto: "Critical Heat Flux Correlation for Subcooled Boiling Flow in Narrow Channels", Int. J. of Heat and Mass Transfer, 45, 4107-4115 (2002).

22) M. Kureta and H. Akimoto: "Measurement and Visualization of Void Fraction in a Tight Lattice Bundle by High-Frame-Rate Neutron Radiography", Proceedings of the 10th Int. Symp. On Flow Visualization (ISFV-10), Kyoto, Japan, F0231 (2002).

23) M. Kureta, H. Akimoto: "3D Measurement of Void Fraction in Tight Bundles Using Neutron", Mechanical Engineering Congress, 2002 Japan, Tokyo, Japan, T12-1 (2002).

24) H. Yoshida, A. Ohnuki, K. Takase and H. Akimoto: "Numerical Simulation of the Slug Flow Using Interface Tracking Method", Mechanical Engineering Congress, 2002 Japan, Tokyo, Japan, S34-1 (2002).

25) M. Kureta, T. Hibiki, M. Mishima and H. Akimoto: "Study on Point of Net Vapor Generation by Neutron Radiography in Subcooled Boiling Flow along Narrow Rectangular Channels with Short Heated Length", Int. J. Heat and Mass Transfer, 46, 1171 (2003).

26) M. Kureta, W. Liu, T. Iwamura and H. Akimoto: "Critical Heat Flux in Tight Lattice Bundles [1] (Effect of Power Distributions and Flow Parameters)", JSME Thermal Engineering Division Meeting 2002, A254 (2002).

27) W. Liu, M. Kureta, T. Iwamura and H. Akimoto: "Critical Heat Flux in Tight Lattice Bundles [1] (Verification of Correlation for Tight Lattice Bundle)", JSME Thermal Engineering Division Meeting 2002, A255 (2002).

6. Reactor Structural Materials

1) Y. Kaji, Y. Matsui, S. Kita, H. Ide, T. Tsukada and H. Tsuji: "Application of a Fiber Optic Grating Strain Sensor for the Measurement of Strain under Irradiation Environment", Nuclear Engineering and Design, 217, pp.283-288 (2002).

2) Y. Kaji, H. Tsuji, H. Nishi, Y. Muto, H. J. Penkalla and F. Schubert: "Multiaxial Creep Behavior of Nickel-Base Heat-Resistant Alloys Hastelloy XR and Ni-Cr-W Superalloy at Elevated Temperatures", Journal of Nuclear Science and Technology, Vol.39, No.8, pp.923-928 (2002).

3) Y. Kaji, K. Yoshida, S. Mashiko, M. Fujita, K. Shimura, J. Kinugawa, H. Tsuji, S. Miyakawa and S. Iwata: "Development of Knowledge Base System Linked to Material Database", Trans. Atomic Energy Society of Japan, Vol.1, No.4, pp.412-418 (2002) [in Japanese].

4) Y. Kaji, Y. Miwa, T. Tsukada, M. Kikuchi, S. Kita, M. Yonekawa, J. Nakano, H. Tsuji and H. Nakajima: "Evaluation of In-pile and Out-of-pile Stress Relaxation in 316L Stainless Steel under Uniaxial Loading", Journal of Nuclear Materials, 307-311, pp.331-334 (2002).

5) Y. Kaji, H. Tsuji, M. Fujita, J. Kinugawa, K. Yoshida, S. Mashiko, K. Shimura, S. Miyakawa and S. Iwata: "Development of Knowledge Base System Linked to Material Database", Proc. of 18th International CODATA Conference, Motreal, Canada (2002).

6) Y. Kaji, T. Tsukada, M. Fujita, J. Kinugawa, K. Yoshida, S. Mashiko, S. Onose and S. Iwata: "Development of Distributed Material Knowledge Base System Based on XML", Proc. of the 20th Symposium on Informatics (Informatics 2003), Tokyo, Japan (2003).

7) Y. Miwa, T. Tsukada, H. Tsuji, S. Jitsukawa: "Irradiation-assisted SCC Susceptibility of HIPed 316LN-IG Stainless Steel Irradiated at 473K to 1dpa", J. Nucl. Mater., 307-311 (2002) 347-351.

8) M. Yonekawa, T. Ishii, M. Ohmi, F. Takada, T. Hoshiya, M. Niimi, I. Ioka, Y. Miwa, H. Tsuji: "Development of a Remote-controlled Fatigue Test Machine using a Laserextensometer for Investigation of Irradiation Effect on Fatigue Properties", J. nucl. Mater., 307-311, 1613-1618(2002).

9) J. Nakano, T. Tsukada, M. Kikuchi, Y. Kaji, H. Ugachi, Y. Miwa and H. Tsuji: "Development of In-situ Observation Technique during SCC Test in High Temperature Water for Irradiated Materials" Proceedings of the 3rd International Symposium on Material Chemistry in Nuclear Environment 2002.

10) J. Nakano, T. Kohya, S. Endo, H. Tsuji and T. Tsukada: "PIE Facility for In-Situ Observation of Specimen Surface during SSRT in High Temperature Water", Minutes of IASCC Review Meeting 2002.

11) Y. Nemoto, Y. Miwa, M. Kikuchi, Y. Kaji, T. Tsukada and H. Tsuji: "Development of Analytical Method and Study about Microstructure of Oxide Film on Stainless Steel" Journal of Nuclear Science and Technology, Vol.39, No.9, 996-1001 (2002)

12) Y. Nemoto, Y. Miwa, T. Tsukada and H. Tsuji: "AFM Evaluation for Grain Boundary Corrosion Behavior of Ion Irradiated Stainless Steel" JAERI-Conf 2003-001 / Proceedings of International Symposium on Material Chemistry in Nuclear Environment (Material Chemistry '02), 397-404 (2003).

13) Y. Nemoto, Y. Miwa, T. Tsukada and H. Tsuji: "AFM Evaluation for Corrosion Behavior of Ion Irradiated Stainless Steel" Proceedings of 11th International Conference On Nuclear Engineering (ICONE11), JSME/ASME, 36093 (2003) [CD-ROM].

14) Y. Nemoto, Y. Miwa, H. Tsuji and T. Tsukada: "Evaluation of Corrosion Behavior of Ion Irradiated Stainless Steel using Atomic Force Microscope" Journal of JSAEM (now printing).

7. Development of New Cladding Materials Applied to the Advanced Nuclear Reactors

1) T. Wakui, M. Futakawa, Y. Tanabe and I. Ioka: "Identification of Material Constants in Constitutive Equation by Indentation Test with Different Indenters", J. Soc. Mater. Sci. Japan, Vol. 51, 681-687 (2002) [in Japanese].

2) H. Date, M. Futakawa and S. Ishikura: "Impact Behavior of Mercury Droplet", Jikkenn Rikigaku, Vol. 2, 103-108 (2002) [in Japanese].

3) H. Kogawa, S. Ishikura, M. Futakawa and R. Hino: "Coupled Behavior between Structural Body and Liquid under Impact Loading", Jikkenn Rikigaku, Vol. 2, 122-127 (2002) [in Japanese].

4) S. Ishikura, H. Kogawa, M. Futakawa, R. Hino and H. Date: "Thermal Shock Analysis of Liquid Mercury Spallation Target", J. High Temperat. Soc. Japan, Vol. 28, 329-335 (2002) [in Japanese].

5) M. Futakawa, T. Wakui, H. Kogawa and H. Date: "Mechanical Property Evaluation of Nanoscale Zone by Indentation Technique", JSME/ASME International Conference on Materials and Processing, Honolulu, Oct. 15-18 (2002).

6) M. Futakawa, H. Kogawa, R. Hino, H. Date and H. Takeishi: "Erosion Damage on Solid Boundaries in Contact with Liquid Metals by Impulsive Pressure Injection", International Journal of Impact Engineering, Vol. 28, 123-135 (2003).

7) M. Futakawa, H. Kogawa, C.C. Tsai, S. Ishikura and Y. Ikeda: "Off-line Tests on Pitting Damage in Mercury Target", JAERI-Research 2003-005 (2003).

8) I. Ioka, M. Futakawa, Y. Nanjyo, K. Kiuchi, Y. Kuroda and T. Anegawa: "Effect of Triple Ion Beam Irradiation on Mechanical Properties of High Chromium Austenitic Stainless Steel", JAERI Conf 2003-001, 445-451 (2002).

9) K. Kiuchi, H. Ogawa, I. Ioka, Y. Kuroda and T. Anegawa: "Development of New Cladding Materials Applied for Advanced LWR Aiming at Ultra-high Burn-up and Fast Neutron Spectrum", International Congress on Advanced Nuclear Power Plants, June 9-13, Florida (2002).

10) I. Ioka, K. Kiuchi, Y. Kuroda and T. Anegawa: "Evaluation of New Fe-Cr-Ni Alloy for Ultra High Burnup Fuel Cladding Tube", International Congress on Advanced Nuclear Power Plants, June 9-13, Florida (2002).

11) F. Isozaki, T. Kikuchi, I. Ioka, K. Ishikawa and Y. Hitata: "Production of Pressurized Cladding Tube Specimen for Neutron Irradiation", JAERI-Tech 2002-074 (2002).

12) C. Kato, M. Yano, K. Kiuchi and K. Sugimoto: "Effect of a Heat-transfer on Corrosion of Zirconium in a Boiling Nitric Acid Solution", Zairyo to Kankyo, Vol. 52, 35-43 (2003) [in Japanese].

13) C. Kato, M. Yano, K. Kiuchi and K. Sugimoto: "Thermodynamic Study on Redox

Reactions of Boiling Nitric Acid Solutions", Zairyo to Kankyo, Vol. 52, 44-52 (2003) [in Japanese].

14) H. Nishi, M. Eto, K. Tachibana, K. Koizumi, M. Nakahira and H. Takahashi: "Fatigue Behavior on Weldment of Austenitic Stainless Steel for ITER Vacuum Vessel", Fusion Eng. Des., Vol. 58-59, 869-873 (2002).

8. Research on Advanced Transuranium Bearing Fuels

1) O. Shirai, K. Uozumi, T. Iwai, Y. Arai: "Electrode reaction of the U^{3+}/U Couple at Liquid Cd and Bi Electrodes in LiCl-KCl Eutectic Melts", Analytical Science 2001, Vol. 17 Supplement pp. i959-i962 (2002).

2) S. Nakayama, Y. Morita, K. Nishihara, H. Hayashi, O. Shirai: "Wastes Generated by Application of JAERI Partitioning-transmutation System to High Level Radioactive Waste", JAERI-Conf 2002-004 p.p. 309-314 (2002).

3) Y. Arai, T. Iwai, O. Shirai, H. Hayashi, K. Minato: "Research on Pyrochemical Process for Nitride Fuel at JAERI", JAERI-Conf 2002-004 p.p. 589-596 (2002).

4) K. Minato, Y. Arai, M. Akabori: "Research on Nitride Fuel for Transmutation of Minor Actinides", Proc. Nuclear Applications in the New Millennium (AccApp/ADTTA'01), November 11-15, 2001, Reno, USA (2002) (CD-ROM).

5) K. Nakajima, T. Ohmichi, Y. Arai: "Mass-spectrometric Determination of Oxygen Potential of Hypostoichiometric Urania-yttria Solid Solution", J. Nucl. Mater., 304 (2-3) pp. 176-181 (2002).

6) K. Arie, T. Abe, Y. Arai: "Present Status and Approach on Advanced Technologies of Nuclear Fuel -Research and Development of an Advanced Recycle Technology-", J. At. Energy. Soc. Jpn., Vol. 44, No. 8 (2002) pp.593-599 [Japanese].

7) Y. Arai, T. Iwai, K. Nakajima, O. Shirai, H. Kikuchi, H. Amezawa, H. Hayashi, K. Minato: "Irradiation Test of U-Free Nitride Fuel and Recent Progress of Pyrochemistry in JAERI", Proc. Seventh Information Exchange Meeting on Actinide and Fission Product Partitioning and Transmutation, 14-16 October 2002, Jeju (2002) (CD-ROM).

8) Y. Arai: "Nuclear Fuel Cycle Technology-Molten Salt Electrorefining Process (Nitride Fuel)-", J. At. Energy. Soc. Jpn. pp.119-126 (2002) [in Japanese].

9) T. Iwai, K. Nakajima, H. Kikuchi, H. Nagashima, Y. Kimura, H. Matui, Y. Arai: "Post Irradiation Examination of (U, Pu)C and (U, Pu)N Fuels for Fast Reactors", JAERI-Research 2002-038 (2003).

10) K. Nakajima, Y. Arai: "Heat Capacity of Neptunium Mononitride", J. Nucl. Sci. Technol., Supplement 3, 620-623 (2002).

11) O. Shirai, K. Uozumi, T. Iwai, Y. Arai: "Electrochemical Behavior of UN in LiCl-KCl Eutectic Melts", J. Nucl. Sci. Technol., Supplement 3, 745-748 (2002).

12) T. Ohmichi, Y. Arai: "Empirical Evaluation of the Thermodynamic and Magnetic Properties from the Atomic Distances of NaCl-type Actinide Compounds", J. Nucl. Sci. Technol., Supplement 3, 156-159 (2002).

13) T. Albiol, H. Serizawa, Y. Arai: "Studies in the PuO_2-ZrO_2 Pseudo-binary Phase Diagram", J. Nucl. Sci. Technol., Supplement 3, 834-837 (2002).

14) K. Uozumi, T. Kato, M.Iizuka, T. Inoue, T. Iwai, O. Shirai, and Y. Arai: "Development of an U and Pu Recovery Processby Molten Salt Electrorefinig -Behavior of U and Pu at Simultaneous Recoveriesinto Liquid Cadmium Cathodes-", Komae Research Laboratory Rep. No.T02004 (2003).

15) K. Minato, Y. Arai: "Kakuhenkan kennkyu kaihatu no genzyo (B) Kakuhenkan senyo nenryo to syori", Genshikaku Kenkyu, 47 (6), 31-38 (2003).

16) T. Yamashita, K. Kuramoto, M. Nakada, S. Yamazaki, T. Sato and T. Matsui: "Phase Relations between a Fluorite and a Pyrochlore Structure in the System of Actinides and Zirconium Oxides", J. Nucl. Sci. Technol. Suppl. 3, pp. 585-591 (2002).

17) T. Yamashita, S. Yamazaki, T. Sato and T. Matsui: "Phase Study and Thermal Expansion of Yttria Stabilized Zirconia Doped with PuO_{2-x}", J. Nucl. Sci. Technol. Suppl. 3, pp. 585-591, pp. 656-659 (2002).

18) T. Yamashita, K. Kuramoto, H. Akie, Y. Nakano, N. Nitani, T. Nakamura, K. Kusagaya and T. Ohmichi: "Rock-like Oxide Fuels and Their Burning in LWRs", J. Nucl. Sci. Technol. 39(8), pp. 865-871 (2002).

19) T. Nakamura, K. Kusagaya, H. Sasajima, T. Yamashita and H. Uetsuka: "Behavior of YSZ Based Rock-like Oxide Fuels under Simulated RIA Conditions", J. Nucl. Sci. Technol. 40(1), pp. 30-38 (2002).

20) K. Sawa, T. Yamashita, K. Minato, Y. Arai and K. Konashi: "Advances in Nuclear Fuel Technology - (4) Development of Advanced Nuclear Fuel Technology, J. At. Energy Soc. Japan, 44(9), pp. 6579662 (2002) [in Japanese].

21) T. Yamashita: "Development of an Advanced Nuclear Fuel - Plutonium Rock-like Oxide Fuel-", Sci. Technol. J., 11(11), pp.54-55 (2002) [in Japanese].

9. Nuclear Data

1) K. Shibata, T. Kawano, T. Nakagawa, O. Iwamoto, J. Katakura, T. Fukahori, S. Chiba, A. Hasegawa, T. Murata, H. Matsunobu, T. Ohsawa, Y. Nakajima, T. Yoshida, A. Zukeran, M. Kawai, M. Baba, M. Ishikawa, T. Asami, T. Watanabe, Y. Watanabe, M. Igashira, N.

Yamamuro, H. Kitazawa, N. Yamano, H. Takano: "Japanese Evaluated Nuclear Data Library Version 3 Revision-3: JENDL-3.3", J. Nucl. Sci. Technol., 39, 1125(2002).

2) T. Kawano and K. Shibata: "Uncertainty Analyses in the Resolved Resonance Region of ^{235}U, ^{238}U, and ^{239}Pu with the Reich-Moore R-Matrix Theory for JENDL-3.2", J. Nucl. Sci. Technol., 39, 807 (2002).

3) K. Shibata: "Evaluation of Neutron Nuclear Data for Sodium-23", J. Nucl. Sci. Technol., 39, 1065 (2002).

4) E. Sukhovitskii, S. Chiba, J.-Y. Lee, Y.-O. Lee, J. Chang, T. Maruyama and O. Iwamoto: "Nuclear Level Structure, B(E2) Gamma-transitions and Nucleon Interaction Data for ^{56}Fe by a Unified Soft-rotator Model and Coupled-channels Framework", J. Nucl. Sci. Technol., 39, 816 (2002).

5) J. Katakura and K. Kitao: "Nuclear Data Sheets for A=126", Nucl. Data Sheets 97, 765 (2002).

6) T. Fukahori, Y. Watanabe, N. Yoshizawa, F. Maekawa, S. Meigo, C. Konno, N. Yamano, A.Yu. Konobeyev and S. Chiba: "JENDL High Energy File", J. Nucl. Sci. Technol., Suppl. 2, 25 (2002).

7) K. Shibata, A. Hasegawa, O. Iwamoto, S. Chiba, M. Sugimoto, N. Odano, T. Kawano, Y. Nakajima, T, Murata, H. Matsunobu, S.Y. Oh, K. Yokoyama, K. Sugino, M. Ishikawa, K. Kosako, N. Yamano and Y. Kanda: "JENDL-3.2 Covariance File", J. Nucl. Sci. Technol., Suppl. 2, 40 (2002).

8) N. Kishida, T. Murata, T. Asami, K. Maki and T. Fukahori: "Present Status of JENDL Photonuclear Data File", J. Nucl. Sci. Technol., Suppl. 2, 56 (2002).

9) T. Murata and K. Shibata: "Evaluation of the (α,n) Reaction Nuclear Data for Light Nuclei", J. Nucl. Sci. Technol., Suppl. 2, 76 (2002).

10) V. Maslov, Y. Porodzinskij, M. Baba and A. Hasegawa: "Actinide Neutron-induced Fission up to 200 MeV", J. Nucl. Sci. Technol., Suppl. 2, 80 (2002).

11) W. Sun, Y. Watanabe, E. Suokhovitski, O. Iwamoto and S. Chiba: "Evaluation of Cross Sections for Neutrons and Protons up to 200 MeV on Silicon Isotopes", J. Nucl. Sci. Technol., Suppl. 2, 120 (2002).

12) T. Kawano, H. Matsunobu, T. Murata, A. Zukeran et al.: "New Evaluations of Heavy Nuclide Data for JENDL-3.3", J. Nucl. Sci. Technol., Suppl. 2, 108 (2002).

13) O. Iwamoto, Rong Jian, T. Fukahori, S. Chiba: "Calculation of Fission Reaction in the Framework of QMD+SDM", J. Nucl. Sci. Technol., Suppl. 2, 128 (2002).

14) T. Yoshida, S. Okajima, T. Sakurai, K. Nakajima, T. Yamane, J. Katakura, Y. Tahara, A. Zukeran, K. Oyamatsu, T. Ohsawa, T. Nakagawa and T. Tachibana: "Evaluation of

Delayed Neutron Data for JENDL-3.3", J. Nucl. Sci. Technol., Suppl. 2, 136 (2002).

15) V. Maslov, Y. Porodzinskij, M. Baba, A. Hasegawa, A. Kagalenko and N. Kornilov: "Neutron Scattering on ^{238}U and ^{232}Th", J. Nucl. Sci. Technol., Suppl. 2, 148 (2002).

16) O. Shcherbakov, A. Donets, A. Evdokimov, A. Fomichev, T. Fukahori, A. Hasegawa, A. Laptev, V. Maslov, G. Petrov, S. Soloview, Y. Tuboltsev and A. Vorobyev: "Neutron-induced Fission of ^{233}U, ^{238}U, ^{232}Th, ^{239}Pu, ^{237}Np, ^{nat}Pb and ^{209}Bi Relative to 235U in the Energy Range 1-200 MeV", J. Nucl. Sci. Technol., Suppl. 2, 230 (2002).

17) N. Shinohara, Y. Hatsukawa, M. Oshima, Y. Toh, J. Katakura, O. Iwamoto, K. Nishio, H. Haba, Y. Nagame, K. Tsukada and I. Nishinaka: "Measurement of Mass Yield Distributions in Proton-induced Fission of Minor Actinides", J. Nucl. Sci. Technol., Suppl. 2, 266 (2002).

18) A. Chtchetkovski, A. Goverdovski, E. Ivanov, A. Kotov, G. Ryabov, T. Fukahori, L. Vaisnene and V. Vovchenko: "Measurement of Cross Sections of Heavy Nuclei Fission Induced by Intermediate Energy Protons in the Energy Range 200-1000 MeV", J. Nucl. Sci. Technol., Suppl. 2, 323 (2002).

19) M. Harada, Y. Watanabe, Y. Tanaka, Y. Matsuoka, K. Shin, S. Meigo, H. Nakashima, H. Takada, T. Sasa, O. Iwamoto, T. Fukahori, S. Chiba and Su. Tanaka: "Light Charged-particle Production in Proton-induced Reactions on ^{12}C, ^{27}Al, ^{58}Ni, ^{90}Zr, ^{197}Au and ^{209}Bi at 42 and 68 MeV", J. Nucl. Sci. Technol., Suppl. 2, 393 (2002).

20) J. Katakura, T. Yoshida, K. Oyamatsu, T. Tachibana: "Development of JEND FP Decay Data File 2000", J. Nucl. Sci. Technol., Suppl. 2, 444 (2002).

21) Y. Toh, T. Czosnyka, M. Oshima, T. Hayakawa, Y. Hatsukawa, M. Matsuda, J. Katakura, N. Shinohara, M. Sugawara, H. Kusakari: "Shape Coexistence in Even-even Ge Isotopes – Complete Spectroscopy with Coulomb Excitation – ", J. Nucl. Sci. Technol., Suppl. 2, 497 (2002).

22) Y. Fujii, A. Iwamoto, T. Fukahori, T. Ohnuki, M. Nakagawa, H. Hidaka, Y. Oura and P. Moeller: "Nuclear Data in Oklo and Time-variability of Fundamental Coupling Constants", J. Nucl. Sci. Technol., Suppl. 2, 592 (2002).

23) N. Yamano, K. Ueki, F. Maekawa, C. Konno, C. Ichihara, Y. Hoshiai, Y. Matsumoto and A. Hasegawa: "Integral Test of JENDL-3.3 with Shielding Benchmarks", J. Nucl. Sci. Technol., Suppl. 2, 841 (2002).

24) H. Takano, T. Nakagawa and K. Kaneko: "Validation of JENDL-3.3 by Criticality Benchmark Testing", J. Nucl. Sci. Technol., Suppl. 2, 847 (2002).

25) M. Kawai, T. Watanabe, A. Zukeran, H. Matsunobu, S. Chiba, T. Nakagawa, Y. Nakajima, T. Sugi and K. Dietze: "Interpretation of Integral Test of FP Cross Sections in

JENDL-3.2 by Analyzing the STEK Experiments", J. Nucl. Sci. Technol., Suppl. 2, 982 (2002).

26) A. Zukeran, M. Ishikawa, T. Nakagawa, K. Shibata and T. Hino: "Doppler Reactivity Worth Uncertainties due to Errors of Resolved Resonance Paramters", J. Nucl. Sci. Technol, Suppl. 2, 1097 (2002).

27) A.Yu. Konobeyev, Yu.A. Korovin and M. Vecchi: "Nuclide Composition Calculation for Pb-Bi Coolant of 80 MW Sub-Critical Reactor. Comparison of Different Data Library", J. Nucl. Sci. Technol., Suppl. 2, 1256 (2002).

28) C. Dunford, A. Hasegawa, R. Jacqmin and C. Nordborg: "International Co-operation in Nuclear Data Evaluation", J. Nucl. Sci. Technol., Suppl. 2, 1449 (2002).

29) T.V. Golashivili, V.M. Kupriyanov, A.A. Labov, A.P. Demidov, V.P. Chechev, Z. Zhao, Y. Zhuang, C. Zhou, X. Huang, M.S. Antony, A. Hasegawa and J. Katakura: "International Chart of the Nuclides – 2001", J. Nucl. Sci. Technol., Suppl. 2, 1484 (2002).

30) V. Maslov, Yu. Porodzinskij, M. Baba and A. Hasegawa: "Neutron Capture Cross Section of Th-232", Nucl. Sci. Eng., 143, 177 (2003).

31) H. Sakane, Y. Kasugai, M. Shibata, T. Iida, A. Takahashi, T. Fukahori and K. Kawade: "Measurement of Activation Cross Sections of (n,np+d) Reactions Producing Short-lived Nuclei in the Energy Range between 13.4 and 14.9 MeV Using an Intense Neutron Source OKTAVIAN", Ann. Nucl. Energy, 29, 53 (2002).

32) K. Kawade, H. Sakane, Y. Kasugai, M. Shibata, T. Iida, A. Takahashi and T. Fukahori: "Measurement Method of Activation Cross Sections Producing Short-lived Nuclei with 14 MeV Neutrons", Nucl. Inst. Meth. In Phys. Research, A496, 183 (2003).

33) S. Raman, C.W. Nestor Jr., A. Ichihara and M.B. Trzhaskovskaya: "How good are the internal conversion coefficients now ?", Phys. Rev. C66, 044312 (2002).

34) J. Eichler and A. Ichihara: "Polarization of photons emitted in radiative electron capture by bare high-Z ions", Phys. Rev. A65, 052716 (2002).

35) T. Nakagawa, H. Kawasaki and K. Shibata: "Curves and Tables of Neutron Cross Sections in JENDL-3.3", JAERI-Data/Code 2002-020 (2002).

36) J. Katakura and H. Yanagisawa: "Photon and Decay Data Libraries for ORIGEN2 Code Based on JENDL FP Decay Data File 2000", JAERI-Data/Code 2002-021 (2002).

37) O. Iwamoto and T. Nakagawa: "Evaluation of Neutron-Induced Reactions on ^{236}Pu for JENDL-3.3", JAERI-Research 2002-013 (2002).

38) A. Konobeyev, T. Fukahori and O. Iwamoto: "Neutron and Proton Nuclear Data Evaluation for ^{235}U and ^{238}U at Energies up to 250 MeV", JAERI-Research 2002-028

(2002).

39) A. Konobeyev, T. Fukahori and O. Iwamoto: "Nuclear Data Evaluation for ^{238}Pu, ^{239}Pu, ^{240}Pu, ^{241}Pu and ^{242}Pu Irradiated by Neutrons and Protons at the Energies up to 250 MeV", JAERI-Research 2002-029 (2002).

40) A. Konobeyev, T. Fukahori and O. Iwamoto: "Nuclear Data Evaluation for ^{237}Np, ^{241}Am, ^{242g}Am and ^{242m}Am Irradiated by Neutrons and Protons at the Energies up to 250 MeV", JAERI- Research 2002-032 (2002).

41) T. Nakagawa, O. Iwamoto and A. Hasegawa: "Re-evaluation of Neutron Nuclear Data for ^{242m}Am, ^{243}Am, ^{99}Tc and ^{140}Ce", JAERI-Research 2002-035 (2002).

42) T. Nakagawa and O. Iwamoto: "Comparison of Fission and Capture Cross Sections of Minor Actinides", JAERI-Data/Code 2002-025 (2002).

43) (Ed.) K. Shibata: "Descriptive Data of JENDL-3.3", JAERI-Data/Code 2002-026 (2002).

44) T. Kawano and K. Shibata: "Evaluation of Covariances for Resolved Resonance Parameters of ^{235}U, ^{238}U, and ^{239}Pu in JENDL-3.2", JAERI-Research 2003-001 (2003).

45) J. Katakura: "A Systematics of Fission Product Mass Yields with 5 Gaussian Functions", JAERI- Research 2003-004 (2003).

Appendix I

March 2003

Department of Nuclear Energy System Organization Chart

Department of Nuclear Energy System

Director : T. Iwamura

Deputy Director : H. Nakajima

K. Fukuda S. Fujisaki S. Hamada M. Mizumoto[(2)]
Y. Anoda[(1)] H. Oigawa[(2)]

Administrative Service

T. Kaneko (Administrative Manager)
T. Mitadera C. Kawawa T. Ikejima

Reactor Engineering Facility Operation Division

K. Nakajima (Head)

K. Satoh	N. Yabuuchi	H. Watanabe	K. Murakami
M. Takeuchi	T. Ono	M. Kyoya	T. Satoh
M. Shibata	K. Hayasaka	H. Sodeyama	M. Ozeki
T. Ouchi	M. Saitoh	Y. Hoshi	Y. Miyoshi[(3)]
K. Nakajima[(3)]	H. Shitobe[(4)]	Y. Funayama[(5)]	M. Fumisawa[(4)]

Nuclear Data Center

A. Hasegawa (Head)

T. Nakagawa	J. Katakura	K. Shibata	T. Fukahori
A. Ichihara	O. Iwamoto	S. Chiba[(6)]	H. Iimura[(7)]

Research Group for Energy System Assessment

O. Sato (Head)

K. Kunii	K. Tatematsu	K. Otaki	T. Suzuki

Research Group for Advanced Reactor Systems

S. Uchikawa (Head)

Y. Asahi	T. Okubo	T. Suzudo	S. Fujiwara
H. Akie	K. Nabeshima	Y. Nakano	N. Ishikawa
T. Nakatsuka	H. Tamai	A. Shelley	W. Liu
M. Katagiri[(6)]	M. Suzuki[(8)]	T. Yonomoto[(8)]	H. Mineo[(3)]

Research Group for Reactor Physics

T. Mori (Head)

S. Okajima	M. Haruyama	K. Okumura	T. Yamane
T. Suzaki	T. Sakurai	M. Kurosawa	Y. Nagaya
M. Andoh	M. Takase	M. Fukushima	K. Kawasaki
Y. Shimada	K. Nishihara[(2)]		

Research Group for Thermal and Fluid Engineering

H. Akimoto (Head)

A. Ohnuki	K. Takase	H. Yoshida	M. Kureta

Research Group for Reactor Structural Materials

T. Tsukada (Head)

Y. Kaji	M. Kikuchi	F. Ueno	H. Ugachi
J. Nakano	Y. Miwa	Y. Sawai[(7)]	M. Omi[(9)]
Y. Matsui[(9)]			

Research Group for Compatible Materials

K. Kiuchi (Head)

T. Saito	I. Ioka	H. Nishi	K. Tachibana
T. Suzuki	R. Onishi	T. Motooka	C. Kato
N. Maruyama	T. Yanagihara	M. Tanabe	I. Tsukatani
Y. Nemoto	Y. Nakahara	Y. Kurata[(2)]	S. Ishiyama[(10)]
S. Baba[(10)]	T. Ishiyama[(11)]	A. Naito[(7)]	M. Futakawa[(2)]

Research Group for Advanced Fuel

Y. Arai (Head)

T. Yamashita	H. Serizawa	O. Shirai	K. Kikuchi
A. Inoue	T. Iwai	K. Kuramoto	N. Shirasu
K. Nakajima	H. Kimura[(3)]	H. Otsuka[(7)]	

Research Group of Small Reactor for Dispersive Energy Supply System

T. Ishida (Head)

N. Nakajima	H. Takahashi	T. Yoritsune	K. Sawada

Research Committee

Japanese Nuclear Data Committee

Research Committee on Reactor Physics

(No.) Original Organization of the Shared-Time Members
(1) Nuclear Safety Research Center
(2) Center for Proton Accelerator Facilities
(3) Dept. of Fuel Cycle Safety Research
(4) Nuclear Technology and Education Center
(5) Dept. of Research Reactor
(6) Advanced Science Research Center
(7) Dept. of Materials Science
(8) Dept. of Reactor Safety Research
(9) Dept. of JMTR
(10) Dept. of Advanced Nuclear Heat Technology
(11) Dept. of Environmental Science

Appendix II Engineering Facilities Related to the Department

FCA : Fast Critical Assembly

The FCA is a split-table type facility of horizontal matrix structure designed for studying nuclear characteristics of fast reactor. The construction of the FCA was started in 1965 and the first core went critical on the 29th of April 1967. The main features of facility are summarized as follows:

Type:	Split-table type of horizontal matrix structure
Size:	2.8m×2.8m×1.3m (each half assembly)
Fuel:	Enriched uranium and plutonium (Plate type)
Other material:	Sodium, stainless steel, aluminum oxide, polystyrene etc. (Plate type)
Maximum power:	2kW
Assembly name:	FCA-1～FCA-XXI

Critical experiments using enriched uranium cores were made in 1960s investing basic characteristics of fast reactor cores. Mock-up experiments were extensively made in 1970s for the Fast Experimental Reactor JOYO and the Prototype Fast Breeder Reactor MONJU. In 1980s, the main subjects of experiments were the investigation of the core characteristics of an axially heterogeneous large fast breeder reactor and the core physics study on a high conversion light water reactor. In early 1990s, the reactor physics experiment of metallic-fueled LMFBR was carried out. Since 1995, international benchmark experiments for β_{eff} were carried out. Since 2000, the reactor physics experiments for RMWR and ADS have been conducted by using uranium fueled core.

VHTRC : Very High Temperature Reactor Critical Assembly

The VHTRC is a low-enriched uranium fueled and graphite moderated / reflected critical assembly. At VHTRC, reactor physics experiments have been carried out mainly for the verification of the neutronics design of the HTTR.

Main features of VHTRC

Type:	Split table of hexagonal prism (prismatic block structure)
Size:	2.4m across the flats and 2.4m long
Fuel:	2.4 and 6wt% enriched UO_2
	Coated particle fuel compact, Pin-in-block type
Moderator/reflector:	Graphite
Core temperature:	Room temperature to 210 °C by electric heaters

Maximum power:	10W
Auxiliary equipments:	① Sample heating device (up to 800 °C)
	② Pulsed neutron source

TCA: Tank-type Critical Assembly

The TCA is a light-water-moderated critical facility to provide the experimental data on light water reactor physics. The construction of the TCA was started in 1961 and the first criticality was attained on the 23rd of August 1962.

Main features of TCA

Type:	Light water moderated Tank-type
Size:	Typically 0.5m×0.5m×1m
	(Core Tank 1.8m diam.×2.1m height)
Fuel:	Low-enriched UO_2 and PuO_2-UO_2 fuel rod
Moderator:	Light Water
Maximum Power:	200W
Auxiliary equipments:	Pulsed neutron source
	Neutron absorbing materials (soluble or solid state)

国際単位系 (SI) と換算表

表 1　SI基本単位および補助単位

量	名称	記号
長さ	メートル	m
質量	キログラム	kg
時間	秒	s
電流	アンペア	A
熱力学温度	ケルビン	K
物質量	モル	mol
光度	カンデラ	cd
平面角	ラジアン	rad
立体角	ステラジアン	sr

表 2　SIと併用される単位

名称	記号
分，時，日	min，h，d
度，分，秒	°，′，″
リットル	l，L
トン	t
電子ボルト	eV
原子質量単位	u

1 eV = 1.60218 × 10^{-19} J

1 u = 1.66054 × 10^{-27} kg

表 5　SI接頭語

倍数	接頭語	記号
10^{18}	エクサ	E
10^{15}	ペタ	P
10^{12}	テラ	T
10^{9}	ギガ	G
10^{6}	メガ	M
10^{3}	キロ	k
10^{2}	ヘクト	h
10^{1}	デカ	da
10^{-1}	デシ	d
10^{-2}	センチ	c
10^{-3}	ミリ	m
10^{-6}	マイクロ	μ
10^{-9}	ナノ	n
10^{-12}	ピコ	p
10^{-15}	フェムト	f
10^{-18}	アト	a

表 3　固有の名称をもつSI組立単位

量	名称	記号	他のSI単位による表現
周波数	ヘルツ	Hz	s^{-1}
力	ニュートン	N	$m \cdot kg/s^2$
圧力，応力	パスカル	Pa	N/m^2
エネルギー，仕事，熱量	ジュール	J	N·m
工率，放射束	ワット	W	J/s
電気量，電荷	クーロン	C	A·s
電位，電圧，起電力	ボルト	V	W/A
静電容量	ファラド	F	C/V
電気抵抗	オーム	Ω	V/A
コンダクタンス	ジーメンス	S	A/V
磁束	ウェーバ	Wb	V·s
磁束密度	テスラ	T	Wb/m^2
インダクタンス	ヘンリー	H	Wb/A
セルシウス温度	セルシウス度	℃	
光束	ルーメン	lm	cd·sr
照度	ルクス	lx	lm/m^2
放射能	ベクレル	Bq	s^{-1}
吸収線量	グレイ	Gy	J/kg
線量当量	シーベルト	Sv	J/kg

表 4　SIと共に暫定的に維持される単位

名称	記号
オングストローム	Å
バーン	b
バール	bar
ガル	Gal
キュリー	Ci
レントゲン	R
ラド	rad
レム	rem

1 Å = 0.1 nm = 10^{-10} m

1 b = 100 fm^2 = 10^{-28} m^2

1 bar = 0.1 MPa = 10^5 Pa

1 Gal = 1 cm/s^2 = 10^{-2} m/s^2

1 Ci = 3.7 × 10^{10} Bq

1 R = 2.58 × 10^{-4} C/kg

1 rad = 1 cGy = 10^{-2} Gy

1 rem = 1 cSv = 10^{-2} Sv

（注）

1. 表1－5は「国際単位系」第5版，国際度量衡局 1985年刊行による。ただし，1 eVおよび1 uの値はCODATAの1986年推奨値によった。
2. 表4には海里，ノット，アール，ヘクタールも含まれているが日常の単位なのでここでは省略した。
3. barは，JISでは流体の圧力を表わす場合に限り表2のカテゴリーに分類されている。
4. EC閣僚理事会指令ではbar，barnおよび「血圧の単位」mmHgを表2のカテゴリーに入れている。

換算表

力	N(=10^5 dyn)	kgf	lbf
	1	0.101972	0.224809
	9.80665	1	2.20462
	4.44822	0.453592	1

粘度　1 Pa·s(N·s/m^2) = 10 P(ポアズ)(g/(cm·s))

動粘度　1 m^2/s = 10^4 St(ストークス)(cm^2/s)

圧力	MPa(=10 bar)	kgf/cm^2	atm	mmHg(Torr)	lbf/in^2(psi)
	1	10.1972	9.86923	7.50062 × 10^3	145.038
	0.0980665	1	0.967841	735.559	14.2233
	0.101325	1.03323	1	760	14.6959
	1.33322 × 10^{-4}	1.35951 × 10^{-3}	1.31579 × 10^{-3}	1	1.93368 × 10^{-2}
	6.89476 × 10^{-3}	7.03070 × 10^{-2}	6.80460 × 10^{-2}	51.7149	1

エネルギー・仕事・熱量	J(=10^7 erg)	kgf·m	kW·h	cal(計量法)	Btu	ft·lbf	eV
	1	0.101972	2.77778 × 10^{-7}	0.238889	9.47813 × 10^{-4}	0.737562	6.24150 × 10^{18}
	9.80665	1	2.72407 × 10^{-6}	2.34270	9.29487 × 10^{-3}	7.23301	6.12082 × 10^{19}
	3.6 × 10^6	3.67098 × 10^5	1	8.59999 × 10^5	3412.13	2.65522 × 10^6	2.24694 × 10^{25}
	4.18605	0.426858	1.16279 × 10^{-6}	1	3.96759 × 10^{-3}	3.08747	2.61272 × 10^{19}
	1055.06	107.586	2.93072 × 10^{-4}	252.042	1	778.172	6.58515 × 10^{21}
	1.35582	0.138255	3.76616 × 10^{-7}	0.323890	1.28506 × 10^{-3}	1	8.46233 × 10^{18}
	1.60218 × 10^{-19}	1.63377 × 10^{-20}	4.45050 × 10^{-26}	3.82743 × 10^{-20}	1.51857 × 10^{-22}	1.18171 × 10^{-19}	1

1 cal = 4.18605 J（計量法）

= 4.184 J （熱化学）

= 4.1855 J （15 °C）

= 4.1868 J（国際蒸気表）

仕事率　1 PS（仏馬力）

= 75 kgf·m/s

= 735.499 W

放射能	Bq	Ci
	1	2.70270 × 10^{-11}
	3.7 × 10^{10}	1

吸収線量	Gy	rad
	1	100
	0.01	1

照射線量	C/kg	R
	1	3876
	2.58 × 10^{-4}	1

線量当量	Sv	rem
	1	100
	0.01	1

（86年12月26日現在）

Nuclear Energy System Department Annual Report (April 1, 2002–March 31, 2003)